TD

Metallodendrimers as HIV Antiviral and Anticancer Agents

DOCTORAL THESIS

Dina Maria Sousa Maciel
DOCTORATE IN CHEMISTRY

UNIVERSIDADE da MADEIRA
A Nossa Universidade
www.uma.pt

July | 2020

Metallodendrimers as HIV Antiviral and Anticancer Agents

DOCTORAL THESIS

Dina Maria Sousa Maciel
DOCTORATE IN CHEMISTRY

ORIENTATION
João Manuel Cunha Rodrigues

CO-ORIENTATION
Maria Ángeles Muñoz-Fernández

METALLODENDRIMERS AS HIV ANTIVIRAL AND ANTICANCER AGENTS

A thesis presented to Madeira University with the aim of obtaining a Doctoral degree in Chemistry

Dina Maria Sousa Maciel

Under the supervision of:
Doctor (PhD) João Manuel Cunha Rodrigues
Doctor (PhD, MD) Maria Ángeles Muñoz-Fernández

Faculdade de Ciências Exatas e da Engenharia,
Centro de Química da Madeira
Funchal – Portugal

July 2020

This doctoral thesis was carried out in the Molecular Materials Research Group (MMRG) of the *Centro de Química da Madeira* (CQM), University of Madeira, and in the *Laboratorio de Inmunobiología Molecular*, at the *Hospital General Universitario Gregorio Marañón*, Madrid, Spain.

This work was financially supported by the *Fundação para a Ciência e Tecnologia* (*FCT*) through the PhD Grant SFRH/BD/102123/2014, and partially with Portuguese Government funds through the CQM different Strategic Projects (UID/QUI/00674/2013, UID/QUI/00674/2015, Pest-OE/QUI/UI0674/2019, and the CQM Base Fund - UIDB/00674/2020, Programmatic Fund - UIDP/00674/2020). The Madeira 14-20 Program and ARDITI - *Agência Regional para o Desenvolvimento da Investigação Tecnologia e Inovação*, respectively through the projects PROEQUIPRAM - *Reforço do Investimento em Equipamentos e Infraestruturas Científicas na RAM* (M1420-01-0145-FEDER-000008) and M1420-01-0145-FEDER-000005 - *Centro de Química da Madeira - CQM*$^{+}$ (Madeira 14-20 Program), and CYTED 214RT0482.

Acknowledgments

I am grateful to everyone that helped and contributed in any way to the accomplishment of this project. Without their generous and critical support, the achievements of this doctoral thesis were impossible.

Particularly I would like to thank my supervisor, Prof. Dr. João Rodrigues, for the support, motivation, the share of knowledge, guidance, and enlightening during the development of this project.

I also show my appreciation to the *Centro de Química da Madeira* (CQM) for its support and for providing the facilities to carry out this project.

To my co-supervisor Prof. Dr. María Ángeles Muñoz-Fernández for the warm welcome at the *Laboratorio de Inmunobiología Molecular*, at the *Hospital General Universitario Gregorio Marañón*, in Madrid (Spain). And for all the generosity, support, and readiness. I am very grateful.

Also, I am grateful to Prof. Dr. Helena Tomás, CQM senior Member, for all the support, encouragement, suggestions, and understanding of some uncertainties and queries.

The support of the laboratory technicians of the Chemistry Department (University of Madeira, Portugal), Paula Andrade and Paula Vieira. They cannot be forgotten for their friendship and for helping me with the lab materials, reagents, and anything else that I needed during my work.

To Dr. Rosa Perestrelo (CQM, University of Madeira, Portugal) for the Mass Spectrometry analysis. And to Dr. Marijana Petkovic (CQM, University of Madeira, Portugal) for the MALDI TOF/TOF analysis.

To Prof. Xiangyang Shi and his group (Donghua University, China) for the *in vivo* assays of the ruthenium metallodendrimers.

I want to acknowledge everyone in the *Laboratorio de Inmunobiología Molecular* (in Madrid, Spain), especially Carlos, Nacho, Alba, Rafa, José, and Coral, for making me feel welcome. I really appreciate the kindness and support given to me. A special thanks to Carlos, who was patient in instructing and helping me in this project.

To my colleagues at CQM, and especially to the Molecular Materials Research Group (MMRG), for all the support and enthusiasm.

To my friends and colleagues Carla Alves, Cláudia Camacho, Nádia Nunes, Tomásia Fernandes, Igor Fernandes, Mara Gonçalves, Rita Castro, and Nilsa Oliveira for their friendship, motivation, and support. A special thanks to Cláudia Camacho, Nádia Nunes, and Francisco Santos for their precious help throughout the project. I really appreciate all the support and friendship.

Furthermore, finally, I want to express my sincere and special thanks to my parents for their endless love, support, understanding, and concern. To my brother Francisco, for all the comprehension and always encouraging me to move forward.

A great and sincere appreciation to all who, directly or indirectly, contributed to this project and my training. Thank you very much!

Resumo

O vírus da imunodeficiência humana / síndrome da imunodeficiência adquirida (VIH/SIDA) é responsável por infectar cerca de 75 milhões de pessoas e de causar 32 milhões de mortes desde o início da epidemia. O cancro, por sua vez, é uma das principais causas de morte em todo o mundo, com uma estimativa de mortalidade de 9,6 milhões em 2018. Em ambos os casos, há uma necessidade urgente de novos medicamentos e terapias, uma vez que o desenvolvimento de vacinas eficazes está longe de ser alcançado e a resistência aos medicamentos é um desafio. Estudos recentes mostraram que os dendrímeros e metalodendrímeros são potenciais fármacos antivirais e anticancerígenos. Os dendrímeros são nanomateriais versáteis com características excecionais, o que os torna atrativos para aplicações biomédicas. A combinação de metalofármacos com dendrímeros demonstrou melhorar a sua capacidade anticancerígena. No entanto, este campo permanece muito pouco explorado.

Neste trabalho de doutoramento descreve-se a preparação de uma nova família de dendrímeros e metalodendrímeros de poli(alquilidenamina) coordenados com complexos de ruténio e cisplatina e, a sua avaliação como possíveis antivirais e anticancerígenos, na infeção pelo VIH-1 e, em diferentes linhas celulares cancerígenas. Foram preparados dendrímeros com quatro grupos terminais diferentes: nitrilo, amina, carboxilato e sulfonato. O primeiro capítulo deste trabalho é dedicado ao estado da arte dos dendrímeros e metalodendrimeros, especialmente na sua aplicação no combate ao VIH/SIDA e no cancro. No segundo capítulo, foram sintetizados os dendrímeros aniónicos com gerações de 1 a 3, e a sua aptidão antiviral foi comprovada em duas variantes de HIV-1, R5-HIV-1_{NLAD8} e X4-HIV-$1_{NL4.3}$. Estudou-se o seu mecanismo de ação e toxicidade *in vivo*. No terceiro capítulo, é apresentada a preparação de dendrímeros com terminação nitrilo (G0 a G2) e metalodendrímeros de ruténio (G0 e G1), e avaliado o seu potencial como agentes antivirais. No quarto capítulo, apresenta-se a preparação da segunda geração de metalodendrímeros de ruténio e estuda-se, em várias linhas celulares cancerígenas, o potencial anticancerígeno dos metalodendrímeros preparados. Foi igualmente avaliada a apoptose, a produção de espécies reativas de oxigénio, o potencial da membrana mitocondrial e a análise do ciclo celular dos compostos preparados. No quinto capítulo, os dendrímeros de G1 e G2 carboxilato e sulfonato foram coordenados com a cisplatina na forma “bis-aquada”. Após a caracterização, a citotoxicidade foi testada em duas linhas de células cancerígenas. Por último, no sexto capítulo, são destacadas as conclusões e as futuras perspetivas do trabalho desenvolvido.

Palavras-chave: dendrímeros de poli(alquilidenamina); metalodendrímeros; ruténio; cisplatina; antiviral; anticancerígeno

Abstract

The human immunodeficiency virus / acquired immunodeficiency syndrome (HIV/AIDS) is responsible for infecting an estimated 75 million people and 32 million deaths since the beginning of the epidemic. On the other hand, cancer is one of the leading causes of death worldwide, with an estimated 9.6 million deaths in 2018. In both cases, there is an urgent need for new drugs and therapies since the development of effective vaccines is far from being accomplished, and drug resistance is a significant challenge.

Recent studies have shown that dendrimers and/or metallodendrimers present potential as antiviral and anticancer drugs. Dendrimers are versatile nanomaterials with exceptional characteristics, which makes them attractive for biomedicine applications. The combination of metallodrugs with dendrimers has been demonstrated improved anticancer activity. However, this field remains scarcely investigated.

In this PhD project, we describe the development of a new family of poly(alkylidenamine) dendrimers and ruthenium and *cisplatin* metallodendrimers, and their antiviral and anticancer potential were evaluated against HIV-1 infection and different cancer cell lines. Four different terminal groups were prepared, nitrile, amine, carboxylate, and sulfonate. The first chapter is dedicated to the state of the art of dendrimers and metallodendrimers, mainly in their application in the fight against HIV/AIDS and cancer. In the second chapter, the anionic poly(alkylidenamine) dendrimers generations 1 to 3 of each dendrimer were synthesized, and their antiviral ability was evaluated against two HIV-1 strains, R5-HIV-$1_{NLAD8,}$ and X4-HIV-$1_{NL4.3}$. The mechanism of action and the toxicity *in vivo* were also assessed. In the third chapter, we present the preparation of nitrile-terminated dendrimers (generation 0 to generation 2) and ruthenium metallodendrimers (G0 and G1), and their potential as antiviral agents was evaluated. In the fourth chapter, the generation 2 of the ruthenium metallodendrimers was prepared and characterized. The metallodendrimers were tested against several cancer cell lines to evaluate their anticancer potential. Their apoptosis, reactive oxygen species (ROS) accumulation, mitochondrial membrane potential, and cell cycle analysis were also verified. Furthermore, in the fifth chapter, generation 1 and 2 of the carboxylate and sulfonate dendrimers were coordinated with *bis*-aquated cisplatin. After characterization, their anticancer activity was tested against two cancer cell lines. Lastly, the sixth chapter the conclusions and future perspectives of the accomplished work are highlighted.

Keywords: poly(alkylidenamine) dendrimers; metallodendrimers; ruthenium; *cisplatin*; antiviral; anticancer

List of Publications

Journal papers

Associated with this thesis

- Maciel, D.; Nunes, N.; Santos, F.; Muñoz-Fernández, M.A.; Tomás, H.; Rodrigues, J.
  Design of a new metallodrug based in ruthenium metallodendrimers as a promising anticancer agent. (Manuscript under preparation)
- Maciel, D.; Guerero-Beltrán, C.; Ceña-Diez, R.; Tomás, H.; Muñoz-Fernández, M.A.; Rodrigues, J.
  New poly(alkylideneamine) dendrimers as a microbicide against HIV-1 infection.
  Nanoscale **2019**, 11, 9679-9690. doi: 10.1039/C9NR00303G. (IF: 7.233).

Complementary work

- Nunes, N.; Popović, I.; Abreu, E.; Maciel, D.; Rodrigues, J.; Soto, J.; Algarra, M.; Petković, M.
  Detection of Ru potential metallodrug in human urine by using MALDI-TOF mass spectrometry: validation and options to enhance the sensitivity.
  Talanta **2021**, 222, 121551. doi: 10.1016/j.talanta.2020.121551. (IF 5.339)
- Xiao, S.; Castro, R.; Maciel, D.; Gonçalves, M.; Shi, X.; Rodrigues, J.; Tomás, H.
  Fine tuning of the pH-sensitivity of Laponite-doxorubicin nanohybrids by polyelectrolyte multilayer coating.
  Materials Science and Engineering C **2016**, 60, 348-356. doi: 10.1016/j.msec.2015.11.051. (IF 4.164)
- Li, Y.; Maciel, D.; Rodrigues, J.; Shi, X.; Tomás, H.
  Biodegradable Polymer Nanogels for Drug/Nucleic Acid Delivery.
  Chemical Reviews **2015**, 115, 8564-8608. doi: 10.1021/cr500131f. (IF 37.369)

Proceedings

- Nunes, N.; Maciel, D.; Tomás, H.; Rodrigues, J.
  Synthesis and Characterization of Novel Ruthenium(II)-based G0/G1/G2-PAMAM Metallodendrimers,
  International Seminar on Advanced Materials Research - ISAMR 2018, Donghua University, Shanghai, China; August 2-5, **2018**. Editor: Beijing Institute of Technology. Advanced Fiber and Functional Textile Materials Section, Proceedings book, page. 254-257.

Oral presentations

Associated with this thesis

Oral Communications – International conferences

- Maciel, D.; Guerrero-Beltrán, C.; Ceña-Diez, R.; Tomás, H.; Muñoz-Fernández, M.A.; Rodrigues, J. New anionic poly(alkylidenamine) dendrimers as a potential microbicide: the behavior against HIV-1 infection. IDS11 – International Dendrimer Symposium. Funchal, Madeira Island: July 14 – 18, **2019**.
- Maciel, D.; Tomás, H.; Muñoz-Fernández, M.A.; Rodrigues, J. Low generation of ruthenium metallodendrimers: a promising metallodrug to fight cancer. MAD-Nano18: Madeira International Conference on Emerging Trends and Future of Nanomaterials for Human Health. Funchal, Madeira Island: November 30 – December 02, **2018**.
- Maciel, D.; Guerrero-Beltrán, C.; Ceña-Diez, R.; Tomás, H.; Muñoz-Fernández, M.A.; Rodrigues, J. Exploring the Antiviral Behaviour of Anionic Poly(alkylidenamine) Dendrimers as Potential Agents Against HIV-1 Infection. 6th International Symposium on Biomedical Applications of Dendrimers – Biodendrimer 2018, Urbino, Italy: June 4 – 7, **2018**.
- Maciel, D.; Camacho, C.; Nunes, N.; Muñoz-Fernández, M.A.; Tomás, H.; Rodrigues, J. Metallodendrimers as Anticancer and Antiviral Drug Candidates. The 10th International Dendrimer Symposium (IDS10), Weihai, China: August 5 – 9, **2017** (invited talk) (Biological medicine/Nanodrug Section, Abstract book, page 32).
- Maciel, D.; Muñoz-Fernández, M.A.; Tomás, H.; Rodrigues, J. Ruthenium Poly(alkylidenamine)-based Dendrimers: Synthesis, Characterization, and Cytotoxicity Studies. MAD-Nano16: Madeira International Conference on Emerging Trends and Future of Nanomaterials for Human Health. Funchal, Madeira Island: November 17 – 20, **2016**.
- Rodrigues, J.; Gouveia, M.; Maciel, D.; Camacho, C.; Nunes, N.; Tomás, H. The Need for New Approach to Fight Cancer – the use of metallodendrimer as anticancer drug. Emerging Trends of Nanotechnology in Chemistry and Biology (INCB). New Delhi, India: February 12 – 13, **2016.**
- Maciel, D.; Muñoz-Fernández, M.A.; Tomás, H.; Rodrigues, J. Poly(alkylidenamine)s dendrimers with nitrile and amine terminal groups as a platform to deliver metallodrugs. International School of Inorganic Chemistry (ISOC). Camerino, Italy: September 5 – 9, **2015**. (Flash presentation)

Oral Communications – National conferences

- Maciel, D.; Santos, F.; Tomás, H.; Muñoz-Fernández, M.A.; Rodrigues, J. Poly(alkylidenamine) dendrimers as drug delivery vehicles for ruthenium anticancer drugs. 6th CQM Annual Meeting, organized by Centro de Química da Madeira (CQM), at Ciência Viva, Porto Moniz, Madeira Island: April 26 – 27, **2019**.
- Maciel, D.; Guerrero-Beltrán, C.; Tomás, H.; Muñoz-Fernández, M.A.; Rodrigues, J. Anionic poly(alkylidenamine)s dendrimers as a potential antiviral agent against HIV-1. 5th CQM Annual

Meeting, organized by Centro de Química da Madeira (CQM), at University of Madeira, Funchal, Madeira Island: February 1 – 3, **2018**.

- Maciel, D.; Muñoz-Fernández, M.A.; Tomás, H.; Rodrigues, J. Synthesis and Anticancer Activity of Ruthenium-based Metallodendrimers. 4th CQM Annual Meeting, organized by Centro de Química da Madeira (CQM), at University of Madeira, Funchal, Madeira Island: February 3 – 4, **2017**.
- Maciel, D.; Muñoz-Fernández, M.A.; Tomás, H.; Rodrigues, J. A new family of poly(alkylidenamine)s metallodendrimers ruthenium based: synthesis, characterization and cytotoxicity studies. 11th Inorganic Chemistry Conference 1st Meeting of the Inorganic and Bioinorganic Chemistry Division of SPQ. Sintra, Portugal: October 7 – 8, **2016**.
- Maciel, D.; Muñoz-Fernández, M.A.; Tomás, H.; Rodrigues, J. Preparation of a New Family of Poly(alkylidenamine)s Dendrimers with Different Functional Groups. 3rd CQM Annual Meeting, organized by Centro de Química da Madeira (CQM), at the University of Madeira, April 1 – 2, **2016**.

Complementary work

- Nunes, N.; Maciel, D.; Tomás, H.; Rodrigues, J. [Ru(η^5-C_5H_5)(PPh_3)$_2$]-PAMAM Metallodendrimers as Promising Anticancer Drugs. IDS11 – International Dendrimer Symposium. Funchal, Madeira Island: July 14 – 18, **2019**.
- Nunes, N.; Maciel, D.; Tomás, H.; Rodrigues, J. Novel low generation ruthenium (II)-based PAMAM dendrimers: synthesis and cytotoxicity studies. MAD-Nano18: Madeira International Conference on Emerging Trends and Future of Nanomaterials for Human Health. Funchal, Madeira Island: November 30 – December 02, **2018**.
- Nunes, N.; Maciel, D.; Tomás, H.; Rodrigues, J. Synthesis and characterization of novel ruthenium (II)-based G0/G1/G2-PAMAM metallodendrimers, International Seminar on Advanced Materials Research (2018 ISAMR), Donghua University, Shanghai, China; August 2 – 5, **2018**. (Invited lecture)
- Nunes, N.; Maciel, D.; Tomás, H.; Rodrigues, J. Novel nitrile based PAMAM dendrimers functionalized with the [Ru(η^5-C_5H_5)(PPh_3)$_2$]$^+$ moiety: synthesis and cytotoxicity studies. 6th International Symposium on Biomedical Applications of Dendrimers – Biodendrimer 2018, Urbino, Italy: June 4 – 7, **2018**.

Poster presentations

Associated with this thesis

- Maciel, D.; Santos, F.; Muñoz-Fernández, M.A.; Tomás, H.; Rodrigues, J. Anticancer activity of ruthenium-based metallodendrimers: a hopeful metallodrug against cancer. 2nd International Workshop on Advanced Materials for Healthcare Applications. Funchal, Madeira Island: October 8 – 9, **2019**.

- Maciel, D.; Santos, F.; Muñoz-Fernández, M.A.; Tomás, H.; Rodrigues, J. Ruthenium-based metallodendrimers: synthesis, cytotoxicity and hematotoxicity studies. IDS11 – International Dendrimer Symposium. Funchal, Madeira Island: July 14 – 18, **2019**.
- Maciel, D.; Guerrero-Beltrán, C.; Ceña-Diez, R.; Tomás, H.; Muñoz-Fernández, M.A.; Rodrigues, J. Poly(alkylidenamine) dendrimers with anionic terminal groups as a potential microbicide against HIV-1 infection. MAD-Nano18: Madeira International Conference on Emerging Trends and Future of Nanomaterials for Human Health. Funchal, Madeira Island: November 30 – December 02, **2018**.
- Maciel, D.; Guerrero-Beltrán, C.; Ceña-Diez, R.; Tomás, H.; Muñoz-Fernández, M.A.; Rodrigues, J. HIV-1 inhibition using carboxylate and sulfonate poly(alkylidenamine) dendrimers. Encontro com a Ciência e a Tecnologia em Portugal - Ciência 2018, Lisbon, Portugal: July 2 – 4, **2018**.
- Maciel, D.; Camacho, C.S.; Muñoz-Fernández, M.A.; Tomás, H.; Rodrigues, J. Synthesis and Characterization of a New Family of Poly(alkylidenamine)s Dendrimers with Different Terminal Groups. Emerging Trends of Nanotechnology in Chemistry and Biology (INCB). New Delhi, India: February 12 – 13, **2016**.
- Maciel, D.; Munóz-Fernández, M.A.; Tomás, H.; Rodrigues, J. Poly(alkylidenamine)s dendrimers with nitrile and amine terminal groups as a platform to deliver metallodrugs. International School of Inorganic Chemistry (ISOC). Camerino, Italy: September 5 – 9, **2015**.

Complementary work

- Nunes, N.; Maciel, D.; Tomás, H.; Rodrigues, J. G0 to G3-[Ru(η^5-C_5H_5)(PPh_3)$_2$]-PAMAM metallodendrimers as novel anticancer drugs candidates. 2nd International Workshop on Advanced Materials for Healthcare Applications. Funchal, Madeira Island: October 8 – 9, **2019**.
- Santos, F.; Maciel, D.; Rodrigues, J. Synthesis and Characterization of Low Generation of Sulfonated and Carboxylated Poly(alkylidenamine) Dendrimers. IDS11 – International Dendrimer Symposium. Funchal, Madeira Island: July 14 – 18, **2019**.
- Santos, F.; Maciel, D.; Rodrigues, J. Copper (II) complexes formed in the presence of low generation poly(alkylidenamine) dendrimers: a UV-Vis study. MAD-Nano18: Madeira International Conference on Emerging Trends and Future of Nanomaterials for Human Health. Funchal, Madeira Island: November 30 – December 02, **2018**.
- Camacho, C.S.; Maciel, D.; Tomás, H.; Rodrigues, J. Different Generations of Fluorescent PAMAM Dendrimers for Biomedical Applications. International School of Inorganic Chemistry (ISOC). Camerino, Italy: September 5 – 9, **2015**.

Other duties

- During the PhD period, from 2015 to present Dina Maciel was responsible for the management and acquisitions for the projects developed at Coordination Chemistry and Molecular Materials

Laboratory (*Laboratório de Química de Coordenação e Materiais Moleculares – LQCMM*) of CQM.

List of Abbreviations

AA	Antibiotic-antimycotic
ADME	Absorption, distribution, metabolism, and elimination
ALD	Adrenoleukodystrophy
ART	Antiretroviral therapy
bis-HMPA	2,2-bis-(hydroxymethyl)-propanoic acid
BSA	Bovine serum albumin
BV	Bacterial vaginosis
(CAR)-T	Chimeric antigen receptor T cell therapy
CART	Combination antiretroviral therapy
CBMSO	*Centro de Bíologia Molecular Severo Ochoa*
CBS	Cystathionine β-synthase
CCR5	C-C chemokine receptor type 5
CDKs	Cyclin-dependent kinases
cDNA	Complementary deoxyribonucleic acid
CD8	Cluster of differentiation 8
CD4	Cluster of differentiation 4
CEEA	Committee for European Education in Anesthesiology
CI	Control of infection
cisPt	Cisplatin
CNT	Control
CT-DNA	Calf thymus deoxyribonucleic acid
CXCR4	C-X-C chemokine receptor type 4
Da	dalton (unified atomic mass unit)
DAB	Diaminobutane
DMSO	Dimethyl sulfoxide
DNA	Deoxyribonucleic acid
DO3A	1,4,7,10-tetraazacyclododecane-*N,N',N'',N'''*-triacetic acid
DPX	Dibutylphthalate Polystyrene Xylene
EA	Elemental analysis
EDA	Ethylenediamine
env	Envelope
EPR	Enhanced permeability and retention
ER	Endoplasmic reticulum

ESI-TOF-MS	Electrospray ionization time-of-flight mass spectrometry
FBS	Fetal bovine serum
FDA	Food and Drug Administration
FT-IR	Fourier-transform infrared
G	Generation
gag	Group-specific antigen
GHRH	Growth hormone-releasing hormone
gp41	Glycoprotein 41
gp120	Glycoprotein 120
HAART	Highly active antiretroviral therapy
HEC	Hydroxyethylcellulose
HIV	Human immunodeficiency virus
HIV/AIDS	Human immunodeficiency virus / acquired immunodeficiency syndrome
HIV-1 / HIV-2	Human immunodeficiency virus type 1 / type 2
hMSC	Human mesenchymal stem cells
HSA	Human serum albumin
HST	HIV-1 sexual transmission
HSV	Herpes simplex virus
IC_{50}	Half maximal inhibitory concentration
MALDI	Matrix-assisted laser desorption/ionization
MS	Mass spectrometry
MTT	3-(4,5-dimethylthiazol-2-yl)-2,5-diphenyl-2H-tetrazolium bromide
MWCO	Molecular weight cutoff
NAMI	“NA” is from the symbol for sodium and “MI” is from the word imidazole
NMR	Nuclear magnetic resonance
PAMAM	Polyamidoamine
PBS	Phosphate-buffered saline
PEG	Polyethylene glycol
PPI	Poly(propyleneimine)
PLGA	Poly(lactic-*co*-glycolic acid)
PLL	Poly-L-lysine
pol	Polymerase
PrEP	Pre-Exposure prophylaxis
PS	Phosphatidylserine
PURE	Polyurea
p6	Protein 6
p7	Protein 7
p17	Protein 17

p24	Protein 24
RAL	Raltegravir
RNA	Ribonucleic acid
ROS	Reactive oxygen species
RSV	Respiratory syncytial virus
RuCp	$[Ru(\eta^5\text{-}C_5H_5)(PPh_3)_2Cl]$
SARS	Severe acute respiratory syndrome
SD	Standard deviation
SeChrys	Selenium-chrysin
siRNA	Small interfering ribonucleic acid
TDF	Tenofovir disoproxil fumarate
T-20	Enfuvirtide
UNAIDS	Joint United Nations Program on HIV/AIDS
USA	United States of America
VIP	Vasoactive intestinal peptide

Contents

Figures Index

Scheme Index

Table Index

Chapter 1.

Introduction

Chapter 1. Introduction

1. Dendrimers

Nanotechnology has developed as a great science in discovering new materials with particular and special characteristics that can be applied in various fields. Nanotechnology can be explained as the field that handles atoms, molecules, or compounds into structures to create materials and devices with unique properties.[1,2] To create small structure molecules, by reducing the size of large to smaller structures is named top-down, and bottom-up is described by taking individual atoms and molecules and changing them into nanostructures.[1] Nanotechnology works at nanometer dimensions dealing with materials in the nanometer scale range (1 – 100 nm) and can be applied in a wide variety of applications in the design of different types of nanomaterials and nanodevices.[1,2] This nanoscale size range is ideal when considering biological systems, such as entering cells, circulation in the bloodstream, and crossing tissues.[2] Nanobiotechnology has emerged from nanotechnology and its relationship with biomedicine. The use of nanomaterials has become known for their application in nanobiotechnology in particular as therapeutics (on drug delivery systems) and diagnosis.[3,4] Therefore, nanotechnology has developed several materials in the nanoscale range namely nanoparticles, including liposomes, carbon nanotubes, metallic particles, polymers, and in particular dendrimers.[3,5]

In 1833, Jöns Jacob Berzelius, a Swedish chemist, introduced the term “polymer” when he firstly described “isomerism” as substances that possess similar composition; but the difference in properties and the total number of atoms was assigned to “polymerism”.[6,7] A few years later, in 1920, Hermann Staudinger described the modern concept of polymers as macromolecular structures covalently bonded.[8] Staudinger received in 1953 the Nobel Prize in Chemistry for his discoveries in macromolecular chemistry.[9] Paul J. Flory also contributed to polymer chemistry for over 50 years. In the early 1940s, Paul J. Flory published several papers related to his work in crosslinked polymers networks,[10–13] and later in 1974 he received a Nobel Prize in Chemistry due to his theoretical and experimental contribution to the physical chemistry of macromolecules.[14] Indeed, all this development in polymer chemistry contributed to the breakthrough of different types of polymers, linear and/or branched. Among the classified branched polymers, we will highlight a specific class of polymers, dendrimers, that are mainly related to the scope of this project. As such, the synthesis, structure, properties, and some types of dendrimers families will be discussed in the following sections.

Dendrimers are a class of synthetic monodispersed polymers, highly branched, three dimensional, and nanoscale macromolecules, where their size and shape can be controlled.[15] Their compact structure and molecular weight can be predictable.[16] They were initially prepared by Fritz Vögtle[17] in 1978 and in the 1980s by two different groups, namely Donald Tomalia[18,19] and by George R. Newkome.[20,21] The word dendrimer comes from the two Greek words “dendron”, which means tree, and “meros”, which means part.[22,23] The capacity to conjugate or complex guest molecules with a dendrimer makes it an exceptional candidate for nanomedicine diagnostic and therapeutic applications.[16,24]

Dendrimers have several different applications due to their multivalency and structure, making them excellent scaffolds with high potential for biomedical applications,[25,26] electronics,[27] and environmental applications such as in pest control[28] and water treatment.[29,30]

1.1. Synthesis

Dendrimers are prepared in a controlled manner and a step-by-step technique. There are two conventional methods to prepare dendrimers. The divergent method (starting from an initial core and extended layers or generations are added) was proposed by Fritz Vögtle[31] and later by Donald Tomalia,[18] while the convergent method (reactions go from the exterior to the interior, from the branching units until the core is reached) was suggested by Jean Fréchet.[32] Dendrimers are synthesized through a sequence of reactions named Michael addition reactions, and the choice of the synthesis method depends on the final application.[33,34] Also, dendrimers can be prepared using different cores, and thus the synthesis strategy can be different.[35] Yet, there are other synthetic strategies for the preparation of dendrimers including lego chemistry[36] and click chemistry.[37]

1.1.1. Divergent method

The divergent technique is an ascending method. It is characterized by building the dendrimer from the core and constructing the molecule by adding layers (Figure 1a). The addition of each new layer of branching units to the molecule will increase by one number, the dendrimer generation.[38,39] There are a few drawbacks of using this method to synthesize dendrimers. For each increasing number of reaction sites, there is an increase in the reaction points. Consequently, an increase in the molecular weight, which will lead to a prolonged reaction kinetics, and the purification of the final product will also be more complicated, particularly in the case of higher molecular weight dendrimers.[33,38] In the divergent synthesis method, an excessive amount of monomer is required, which leads to extended purification steps, mainly in higher generations.[40] In fact, higher generations of dendrimers produced by this method present more imperfection sites, which takes to a low yield of the desired dendrimer.[41] Poly(amidoamine) (PAMAM), poly(propylene imine) (PPI), and phosphorus-based dendrimers are some examples of dendrimers that can be created by the divergent technique.[33,38]

1.1.2. Convergent method

In the convergent synthesis method, by opposition to the divergent technique, the construction of the dendrimers begins from the periphery and continues in direction of the core (Figure 1b). As such, this method is a descending technique. Synthesis by this method starts by connecting the surface groups to a branching unit, and branching units are added until the desired size (generations) is accomplished. In the end, the core is connected to the dendritic segments to form the dendrimer.[34,38] This synthetic method

can produce dendrimers with a core with different functionalities, providing diverse structural characteristics to the dendrimer.[33] Indeed, the convergent method presents a monodispersed and symmetric compound with fewer impurities.[33,34] Furthermore, the molecular weight and the reactive positions and numbers can be rigorously controlled in each synthesis step.[40] Anyway, this technique presents a limitation related to the size of the dendrimers, and the steric hindrance between dendrons when connected to the core.[33] Usually, dendrimers synthesized by this method have fewer defects in their structure.[41]

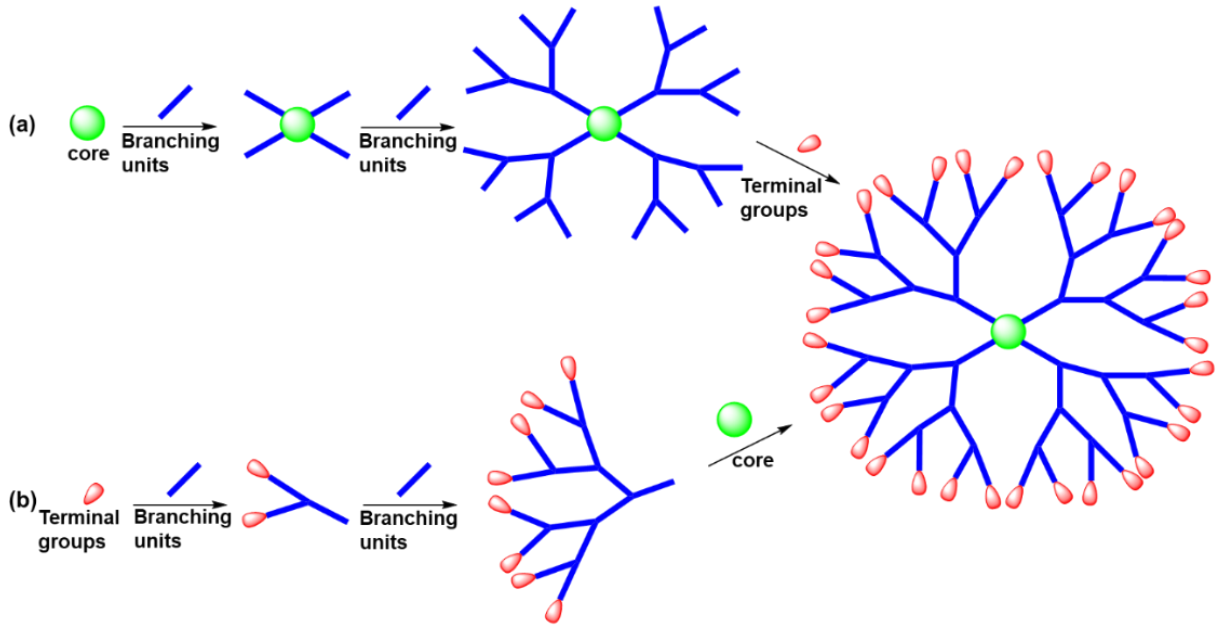

Figure 1. Schematic representation of the synthesis of dendrimers: (a) Divergent method and (b) Convergent method.

1.2. Structures

The dendrimer structure can be divided into a central core, interior layers (generations), and terminal groups (functionalization).[15,42] Each component has its own purpose: the core determines the shape, size, multiplicity, and direction in which the functional groups are connected; the generations correspond to the connected branched units, which control the type and the size of the internal spaces; and the terminal groups give function and reactive sites to the dendrimer.[33] The extent and nature of the guest-host properties of the dendrimer can be controlled and reached by the internal spaces of the dendrimer family.[33] The interior layers are made of repeating branch units, where each repeating branch is referred to as a generation (represented as G0, G1, G2, G3, …) (Figure 2). The size of these molecules can be fabricated in a controllable manner, defining them with a globular shape, monodispersity, and with a great number of groups at the edge.[38,43]

Low generation dendrimers present more flexibility than higher generations.[15] Additionally, low generation dendrimers have more open structures and present an asymmetric shape, whereas higher

generation dendrimers have a globular structure and are more densely packed.[44,45] Increased flexibility in dendrimers has also been shown to be involved in the release properties of drugs encapsulated within dendrimers.[46]

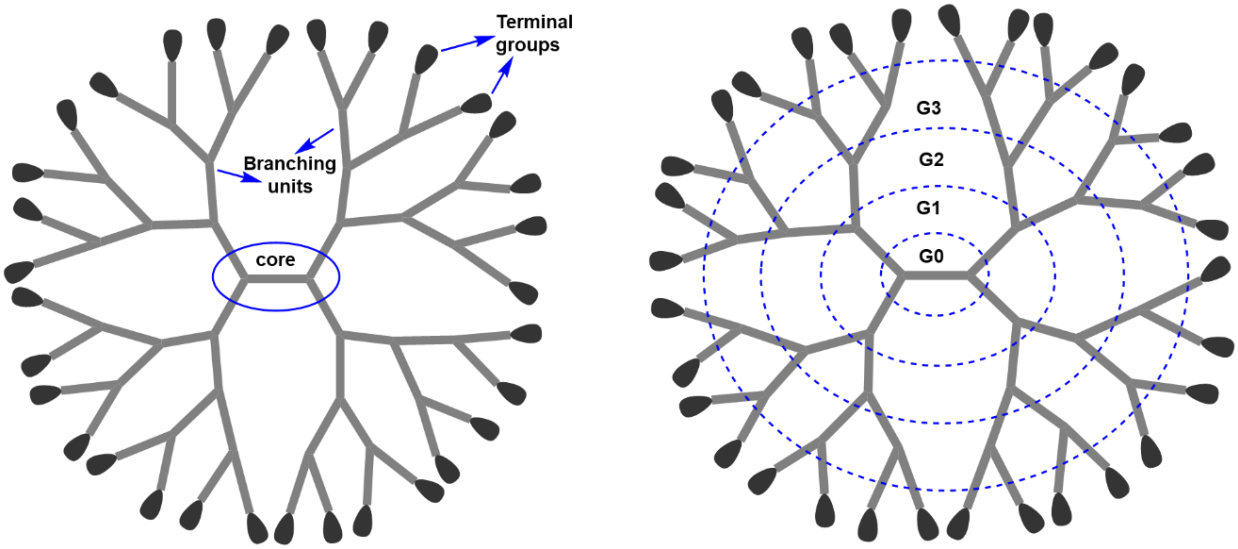

Figure 2. Schematic representation of the dendrimer structure with the main components.

1.3. Properties

Dendrimers have several physicochemical properties, which makes them ideal candidates for biomedical and pharmaceutical applications.[47] The physicochemical properties are important when designing a dendrimer, and depending on the ultimate purpose, these properties can be tuned to obtain the desired molecule. In the next segment, some important dendrimer properties will be discussed like monodispersity, size, solubility, functionalization, and multivalency.

1.3.1. Monodispersity

Monodispersity is an important feature of materials that are used in biological applications. It is a desirable characteristic for synthetic reproducibility, decreasing experimental and therapeutic unpredictability.[48] Monodispersity in dendrimers is one of the main aspects that make this particular class of polymers so attractive for biomedical research.[49] As a result of their controllable synthesis, dendrimers present a unique architecture with a defined size, globular structure, and are monodisperse in size, as opposed to conventional polymer syntheses that produce polydisperse products due to chain growth.[48,50,51] A monodisperse compound is basically achieved when a low generation of dendrimer is prepared, but when the generation increases some defects in the structure can occur which can affect the dispersity, deviating from absolute monodispersity.[48]

1.3.2. Size

The size of a dendrimer is important, and it depends on the final aim. Depending on the dendrimer's family, generation, and surface modification, their size is usually between 2 to 10 nm.[5] Although a smaller size can enhance the efficacy of dendrimers and lead to deeper penetration in tumors, a drawback lies in their rapid clearance through the kidney and space availability to encapsulate or complex drugs.[52] The size of the nanoparticle determines the half-life and distribution: the kidney filters particles smaller than 10 nm, and particles larger than 200 nm are phagocytosed and eliminated by the spleen.[4] In fact, the particle size and shape dictates the clearance rate and circulation time in the bloodstream.[53] For instance, if the size of the dendrimer transporting a drug is higher than 5 nm, it will be less capable of being cleared out of the bloodstream *via* the kidneys.[49] The dendrimer size also has an impact on the drug cell uptake and on the interactions with specific tissues, as well as in the drug stability, drug loading, and release.[54] Moreover, the nanoscale size gives them suitable characteristics to interact with cell components, such as cytotoxicity, lipid bilayer interactions, internalization, biodistribution, and retention time, making them perfect for different routes of administration.[15,53,55] According to the type and number of terminal groups low generation dendrimers (up to generation 3) are more biocompatible and less immunogenic when compared to higher generations.[56]

1.3.3. Solubility

The solubility of dendrimers is one of the most important properties to take into consideration. To begin with, solubility issues can complicate drug delivery. Low solubility is a crucial obstacle for *in vitro*/*in vivo* experiments with the decrease in bioavailability, partial release, and poor correlation absorption.[56] What confers dendrimers their solubility are the surface groups. But the generation, the nature of the branching units, and the core also play an important role in this aspect.[57] A dendrimer with hydrophilic terminal groups and a hydrophobic core usually is soluble in water. In contrast, a dendrimer with hydrophobic end groups and a hydrophilic core is usually soluble in organic solvents.[48] One parameter that also contributes to the solubility of a dendrimer is the generation number; the higher the generation, the hydrophobicity increases.[56,58] However, other factors such as pH, generation, type of surface groups, dendritic core properties, concentration, nature of the solvent, presence of salts, and temperature also affect the dendrimers solubility.[58] Ideally, the design of a dendrimer should take into account its solubility in an aqueous solution and should avoid the use of organic solvents that could contribute to the increase of the dendrimer cytotoxicity.

1.3.4. Functionalization

Dendrimers present unique properties due to their architecture and the terminal groups. The incorporation of multiple active sites in dendrimers, such as drugs, antibodies, nucleic acids, fluorophores, targeting ligands, polysaccharides, to produce macromolecules with a multifunctional structural design is

a process known as functionalization (Figure 3).[33] The terminal groups, such as amine or carboxyl, can be easily modified to other groups, for example, hydroxyl, acetyl, and methoxy.[5] Effectively, dendrimer peripheral groups can be modified, giving them different specific physicochemical and biological properties, increasing in that manner, their reactivity for different applications in nanomedicine.[15,55] The terminal groups on dendrimers can be anionic, cationic, or neutral. The number and nature of terminal groups affect the cytotoxicity of dendrimers.[16] Anionic and neutral dendrimers present minor or no toxicity behavior, and cationic dendrimers usually show higher toxicity.[16,59] This higher toxicity of cationic dendrimers can be due to the damage and formation of nanopores in the cell membrane, because of the interaction of the positively charged dendrimers with the negatively charged cell membrane.[16] These give different properties to the dendrimers. For instance, anionic dendrimers have been used against human immunodeficiency virus (HIV)[60–62] while cationic dendrimers have been used as carriers for drugs or nucleic acids.[63–66] The amine terminal groups on the dendrimer surface can limit the use of these dendrimers in cancer therapy due to the fast clearance from the blood circulation and increased toxicity.[67] However, the number of amine terminal groups can improve the functionalization process and thus overcome the toxicity of the cationic dendrimers.[68] Therefore, the functionalization of dendrimers with biocompatible terminal groups such as peptides, carbohydrates, amino acids, or surface modification by PEGylation or acetylation, can improve the blood circulation time to prolong its effectiveness in interacting with the cell components.[67,69] This may be important because of the nanometric size of dendrimers to bind and interact with cells and cellular components.[67,70] To conclude, the surface functionalization of dendrimers can cause modification and enhance important properties, such as toxicity, solubility, biodistribution and pharmacokinetics, drug release efficiency, stability profile, among others.[71]

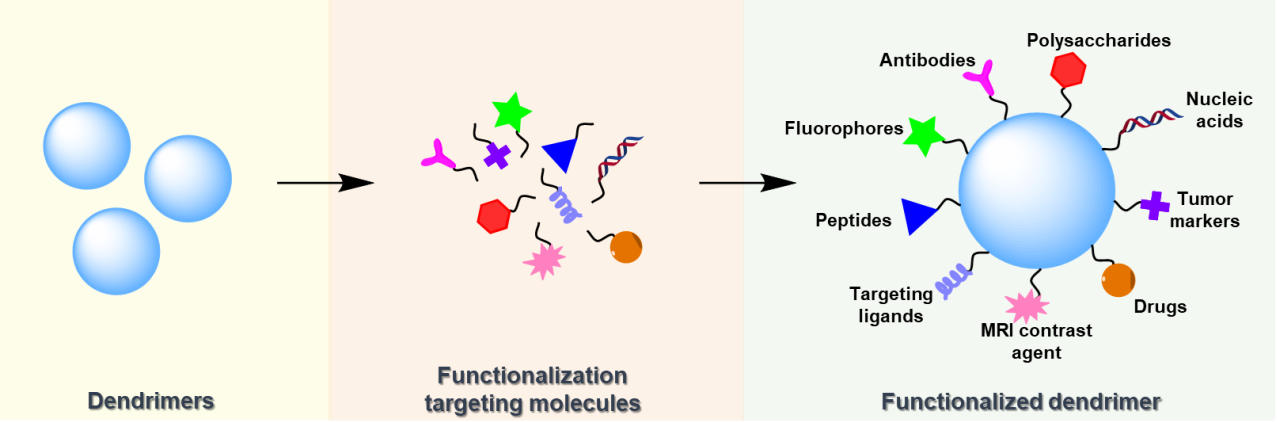

Figure 3. Illustration of dendrimer surface functionalization: dendrimer surface functionalization allows the connection of a variety of target molecules, including fluorophores, drugs, nucleic acids, and targeting ligands (adapted from reference 72).

1.3.5. Multivalency

The multivalent concept specifies that several functionalities of one entity interact with the complementary functionalities of another, in more detail the number of reactive sites on the surface that

can link with the target of interest.[57,73] When designing a multivalent platform, it is essential to know your target. As such, it is imperative to consider the ligand valency, linker length, density, steric hindrance and spatial arrangement, solubility, and capacity to match the binding sites of biomolecules.[74] On the cell surface, some receptors can interact with multivalent ligands, binding with a first and second location on the same receptor.[75] This is possible due to the “chelate” effect, which means that the first binding favors the next and additional bindings.[75]

For instance, dendrimers display multivalency, which is convenient to functionalize ligands to the surface of the molecule.[48] For biological processes, such as viral infection or cell to cell communication, dendrimers are considered a useful platform, as multivalency plays a central role, since it can enhance through multiple interactions the binding strength to biomolecules.[43,73,74] Dendrimers can present several recognition elements, and this is because of their architecture, such as shape, size, flexibility, and valency.[75] The multivalency of dendrimers given by the terminal groups can be used to link drugs, targeting molecules, or solubilizing groups.[76] However, to design a good delivery system, it is important to keep in mind what the ultimate purpose is. The importance of multivalency in drug delivery and how to prepare a successful multivalent system was recently explored in a fascinating review paper from K. C. Tjandra *et al*.[77]

1.4. Dendrimer families

Dendrimers such as PAMAM, PPI, and carbosilane, have been extensively used for several applications, including for drug/gene delivery. They can be classified into two main groups: organic dendrimers having in their composition amines at all the branching points (*e.g.*, PAMAM and PPI dendrimers) or inorganic dendrimers that have inorganic atom-like phosphorus or silicon.[78] In the following section, the most common types of dendrimers are presented, namely the PAMAM and the PPI dendrimers, silicon-based dendrimers, glycodendrimers, phosphorus-based dendrimers, polyester dendrimers, polyurea dendrimers and metallodendrimers (Figure 4).

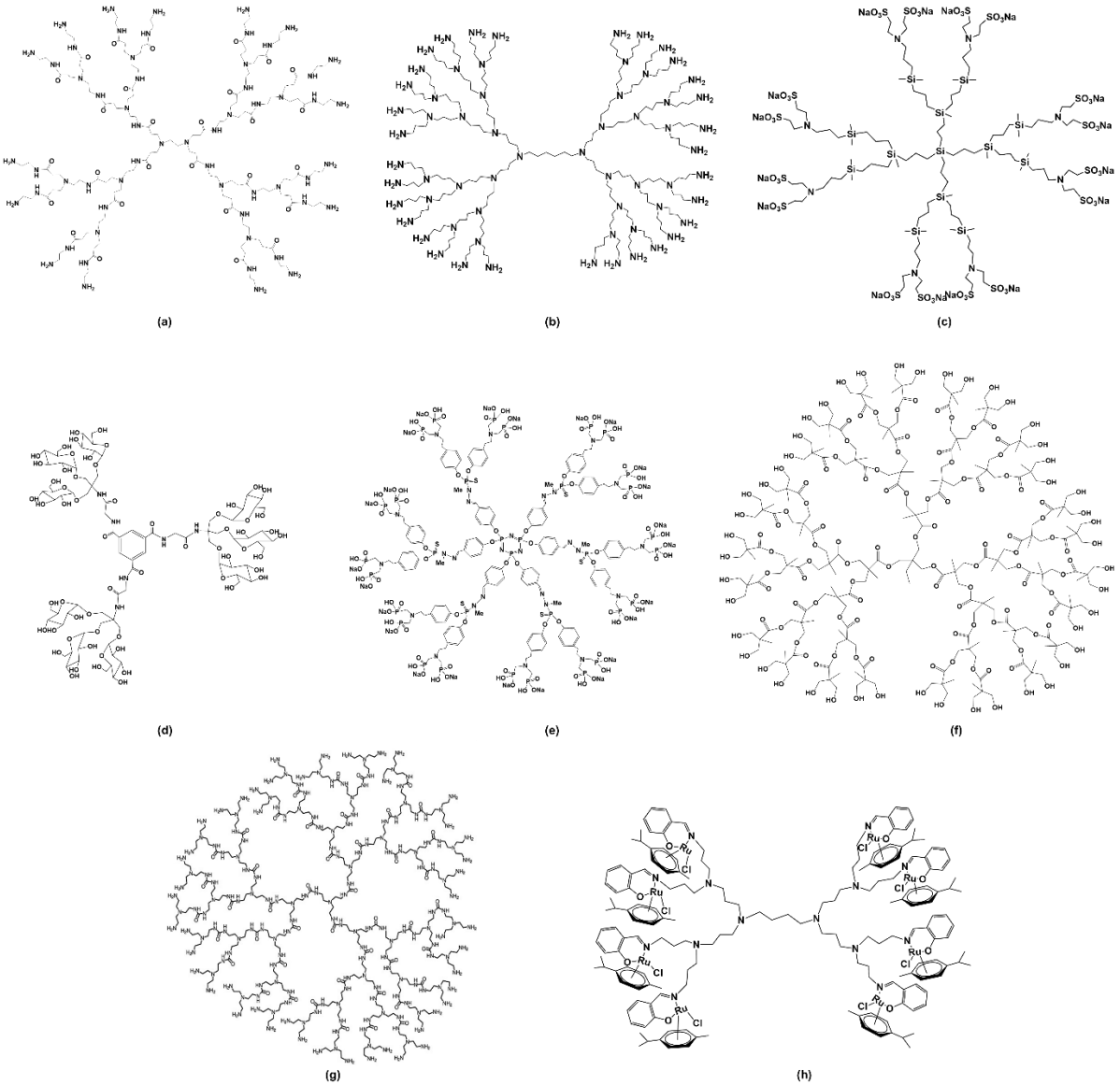

Figure 4. Structures of the different families of dendrimers: (a) PAMAM;[79] (b) PPI (this work); (c) silicon-based dendrimer;[80,81] (d) glycodendrimer;[82] (e) phosphorus-based dendrimer;[78] (f) polyester dendrimer;[83] (g) polyurea dendrimer;[84] (h) metallodendrimer.[85]

1.4.1. PAMAM dendrimers

PAMAM dendrimers are globally the most well-known dendrimer family due to their high use, for instance, as drug delivery systems. They are commercially available from different suppliers and, also for that reason are one of the most extensively used types of dendrimers.[58] PAMAM was developed by Donald Tomalia and co-workers, prepared by divergent methods that are composed of polyamide branches and tertiary amines as branching units and ethylenediamine (EDA) core.[18] PAMAM dendrimers are classified by full generation, with amino or hydroxyl terminal groups, or half-generation with carboxylic acid terminal groups.[86] PAMAM dendrimers present several attractive characteristics such as their unique architecture, the ability to deliver therapeutic agents, high aqueous solubility, and a large number of surface groups.[87] Cytotoxicity of PAMAM dendrimers is dependent on the generation, concentration, and

charge.[79] PAMAM dendrimers are widely used for biological applications, due to their properties such as solubility in water and biocompatibility. For instance, our group prepared PAMAM dendrimer/pDNA complexes immobilized in electrospun fibers for gene delivery.[88] Biodegradable and biocompatible fibers were prepared using poly(lactic-*co*-glycolic acid) (PLGA), chitosan, and alginate through the layer-by-layer technique, and were used to immobilize the dendrimer/pDNA complexes. Results showed that the prepared fibers allowed the attachment and growth of hMSCs and the delivery of pDNA to promote cell differentiation. Gunes Esendagli and coworkers have prepared PAMAM dendrimers functionalized with anti-Flt1 antibody and loaded with gemcitabine to eradicate tumor-induced myeloid cells.[89] The results proved that these dendrimers could reduce the tumor mass and eliminate tumor-induced myeloid cells in several compartments, demonstrating to be a promising approach to decrease pancreatic cancer growth. Hamid R. Moghimi and coworkers synthesized a G3 and G5 PAMAM dendrimer with vancomycin to act as an antibacterial against Gram-negative bacteria.[90] These dendrimer complexes presented an antibacterial effect against Gram-negative bacteria relative to a vancomycin solution that showed to be non-effective against these bacteria.

1.4.2. PPI dendrimers

Fritz Vögtle *et al.* in 1978 were the first to describe the preparation of dendrimers.[17] In 1993, E. M. M. Brabander-van den Berg and E. W. Meijer described the preparation of PPI dendrimers with an adjustment to the Vögtle method.[91] PPI dendrimers are as well, extensively used for drug delivery. These dendrimers normally incorporate an interior of tertiary tris-propyleneamines and contain poly(alkylamines) with primary amines.[38,86] The most common cores used to prepare PPI dendrimers have been EDA or diaminobutane (DAB).[92] They can be prepared by repetitive reactions of Michael addition of amines with acrylonitrile followed by the reduction of the nitrile groups into primary amines.[93] Compared to the PAMAM dendrimers, PPI dendrimers present smaller sizes with three bonds (PAMAM have seven bonds), the same globular shape, and are more hydrophobic.[92] As such, PPI dendrimers present advantageous characteristics for biological applications. Barbara Klajnert-Maculewicz and coworkers previously developed PPI dendrimers modified with sugar molecules (maltose) and with a nucleoside analog drug as a treatment for leukemia to overcome drug resistance.[94] The results showed that these dendrimers are good candidates as an anticancer drug against resistant acute lymphoblastic leukemia cells, which presented increased cytotoxicity and uptake in these cells. Ivo Grabchev and collaborators prepared a new modified PPI dendrimer with acridine and copper complexes as potential antimicrobial agents.[95] These modified dendrimers were tested against pathogenic microorganisms and proved to inhibit bacterial growth and prevent biofilm formation.

1.4.3. Silicon-based dendrimers

Silicon-based star-branched polymers, more specifically, carbosilane dendrimers, were first introduced by L. J. Fetters and his collaborators in 1978.[96] Later, Satoru Masamune in 1990 and Masa-aki Kakimoto in 1991 presented the silicon-based dendrimers.[97,98] Silicon-based dendrimers have silicon (Si) atoms between generations as branching points.[99] These silicon-based dendrimers can be subclassified in carbosilane, siloxane, silane, silazane, and silatrane dendrimers (Figure 5).[99] They are characterized by their high flexibility, synthesized by the divergent method, and the presence of Si as branching points gives their multiplicity some variety.[99] Carbosilane dendrimers have gathered much attention due to the synthesis procedure that can modify their structures, and they are kinetically and thermodynamically stable molecules.[99] As mentioned above, the Si atoms give these dendrimers special characteristics, including their anionic and cationic functionalization, which are ideal for biological applications. Jan Maly and coworkers prepared several carbosilane dendrimers modified with phosphonium groups as nonviral transfection vectors for siRNA delivery.[100] The results showed that these dendrimers presented less toxicity *in vivo* compared with the ammonium-based carbosilane dendrimers with equivalent transfection efficiency. Francisco J. de la Mata and collaborators developed cationic carbosilane dendrimers with neuropeptides (VIP or GHRH) to form dendriplexes to act against prostate cancer.[101] The results showed that the dendriplexes increased cell adhesion to the matrix and decreased the metastatic ability in the PC-3 cell line.

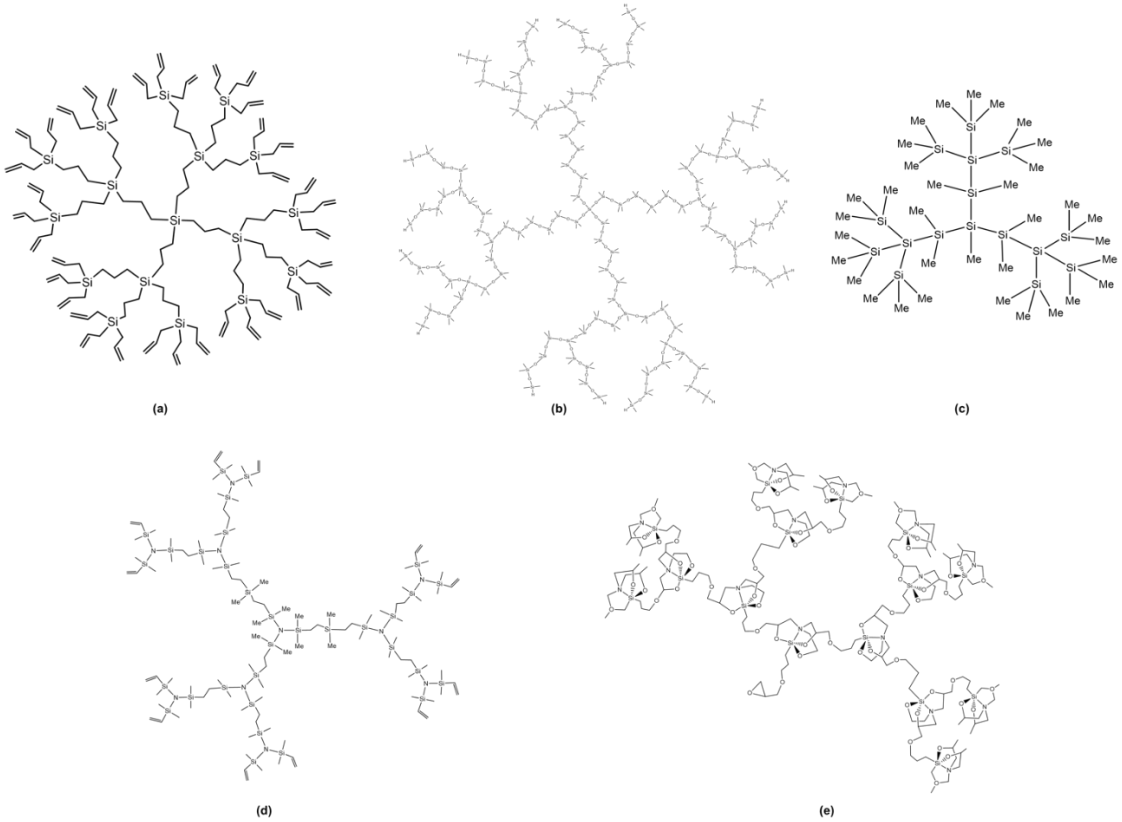

Figure 5. Structure of the different type of silicon-based dendrimers: (a) carbosilane;[99] (b) siloxane;[97] (c) silane;[102] (d) silazane;[103] (e) silatrane.[104]

1.4.4. Glycodendrimers

Glycodendrimers are dendrimers that have carbohydrate molecules in their structure, either at the surface or inserted into the dendritic structure. René Roy first introduced them in 1993, and since then, they have been developed and optimized as potential therapeutics by different research groups.[105] According to the sites where the carbohydrate molecules are located in the dendritic structures, glycodendrimers can be categorized into three families: carbohydrate-coated dendrimers, carbohydrate-centered dendrimers, and carbohydrate-branched dendrimers.[106,107] The most common dendrimers used as scaffolds to bear carbohydrate molecules are the PAMAM, PPI, polyesters, polylysine, and carbosilane dendrimers.[82] There are various advantages in coating dendrimers with carbohydrates, neutralizing the positive charges of the cationic surface groups, such as reducing cytotoxicity, hemolytic toxicity, immunogenicity, and antigenicity.[107] Moreover, this type of dendrimer has proven to have crucial functions in signal transduction and receptor crosslinking.[108,109]

Glycodendrimers can be used in cancer therapy to stimulate the immune response against cancer cells, in vaccines, and screening antigens.[87,109] Other applications for glycodendrimers include immune-modulating, cancer prevention, targeting or therapy, biomimicry, and photoaffinity labeling.[106] Therefore, glycodendrimers present excellent properties to be used for biomedical applications. Takashi Yoshida *et al.* previously synthesized a G3 glycodendrimer with HIV activity and low cytotoxicity.[110] Yvette van Kooyk and coworkers prepared an antitumor vaccine based on glycodendrimers for targeting skin dendritic cell subsets improving the antitumor $CD8^+$ T cell responses.[111]

1.4.5. Phosphorus-based dendrimers

Phosphorus-based dendrimers were firstly prepared by the groups of Kasthuri Rengan and Robert Engel and by Jean-Pierre Majoral and Anne-Marie Caminade in the early 90s.[112,113] These dendrimers have a phosphorus atom at the branching point, which allows them to strictly control their structure and purity by ^{31}P-NMR.[114] Phosphorus dendrimers can interact with the lipid membrane and be integrated into the cells due to the hydrophilic surface and hydrophobic internal skeleton.[114] From all the advantages of phosphorus dendrimers, the high solubility and reactivity make them ideal for biomedical applications.[115] In the last years, innumerous phosphorus dendrimers have been prepared for nanomedicine, and evaluated *in vitro* and *in vivo,* and used as anti-prion agents, as drug carriers for anti-inflammatory and anticancer applications, and as fluorescent bioimaging markers.[78,115,116] As shown next, the functionalization of these dendrimers with positively or negatively charged groups confers ideal properties for use in biomedical applications.[93] Dzmitry Shcharbin and coworkers prepared phosphorus dendrimers with piperidine terminal groups for cancer cell inhibition using siRNA cocktails and 5-Fluorouracil.[117] They discovered that these dendrimers could deliver 80-100% of siRNA to HeLa cells, and the cytotoxicity of 5-Fluorouracil increased when the dendrimers and siRNA cocktail complexes were added. Xiangyang Shi and coworkers prepared a phosphorus dendrimer functionalized with a morpholino molecule for stem cell osteogenic differentiation.[118] The results showed that this modified phosphorus

dendrimer revealed osteogenic differentiation and stimulated the transformation of the stem cells into osteoblasts.

1.4.6. Polyester dendrimers

Polyester dendrimers are known for their biodegradability and biocompatibility. They were first prepared by Craig J. Hawker and Jean M. J. Fréchet in 1992.[119] The 2,2-bis(hydroxymethyl)propionic acid (bis-HMPA) was initially synthesized in 1996 by Anders Hult and Erik Söderlind.[120] Bis-HMPA dendrimers belong to a family of degradable polyester dendrimers, and among several qualities, they are non-toxic, biodegradable, and non-immunogenic.[121] To achieve biodegradable labile bonds that are easy to cleave and that are capable of being broken with a specific biological stimulus, chemical groups such as esters, anhydrides, phosphoesters, ethers, amides, and carbamates can be incorporated.[122] Currently, they are commercially available from Polymer Factory. The presence of ester groups in the dendritic structure allows for cleavage by chemical hydrolysis or by enzymes present in physiological media.[87] As such, these dendrimers are ideal molecules to be used as carriers for biomedical applications. Michael Malkoch and coworkers prepared several generations (G1-G4) of the bis-MPA polyester dendrimer as nonviral vectors for siRNA delivery.[123] The results showed that the low generation dendrimers presented no toxicity, and the G3 and G4 toxicity were concentration-dependent, and G2-G4 dendrimers were able to complex and protect siRNA from degradation. Silvana Alfei and Sara Castellaro prepared polyester dendrimers G4 and G5 decorated with amino acid residues (arginine, lysine, and *O*-methyltyrosine, and or arginine-glycine dipeptide) with good characteristics to be used as nontoxic carriers for gene and drug delivery.[124] Ana Paula Pêgo and coworkers prepared a biodegradable PEG-dendritic structure as delivery vectors for siRNA.[125] These compounds were successfully obtained and the degradation points of the dendrimer near the complexed siRNA revealed to be important for nucleic acid release, improving the transfection efficiency.

1.4.7. Polyurea dendrimers

Polyurea (PURE) dendrimers present interesting characteristics that classify them as green dendrimers since their synthesis are done in supercritical carbon dioxide with a clean approach.[84] With two functional groups, these dendrimers have a solubility in water, are biocompatible, biodegradable, and have blue photoluminescence.[84,126] Due to the exceptional characteristics these PURE dendrimers have been explored to be used in the biomedical field. Vasco D. N. Bonifácio and coworkers demonstrated the use of PURE dendrimers for the delivery of siRNA.[127] The same group also used PURE dendrimers with selenium-chrysin (SeChry) to target glutathione (GSH) and cystathionine β-synthase (CBS) in ovarian cancer.[128] This seChry@PURE$_{G4}$-FA compound revealed promising results against ovarian cancer and two mechanisms of action of SeChry were unraveled: the enhanced oxidative stress triggering GSH depletion and the inhibition of the H_2S-generation enzyme CBS.

1.4.8. Metallodendrimers

The incorporation of metal centers in the architecture of the dendrimer's structure gives a new family of dendrimers called metallodendrimers. The teams of Vincenzo Balzani[129,130] and George R. Newkome[131,132] in the early 1990s developed the first supramolecular metallodendrimers. This pioneering work expanded within dendrimer chemistry as one of the most interesting fields to be explored.[133] Also, in 1999, Didier Astruc and coworkers prepared a polycationic iron-based metallodendrimer for the recognition of chloride and bromide anions.[134]

Metallodendrimers like dendrimers can be prepared by divergent or convergent methods,[135] and by "click" chemistry, as firstly reported by the Astruc group in 2007.[136] Different types of metallodendrimers can be obtained depending on how the metal ion is integrated into the dendrimer structure or coordinate/complexed in chelating sites (Figure 6).[137] Indeed, there are three main different classes of metallodendrimers: where dendrimers have the metal as a core, the metal as branching units, and the metal as building block connectors.[138] Among the many advantages of metallodendrimers, there are two main features such as the controlled structure for reproducible biocompatibility and pharmacokinetics, and the multivalency will increase their reaction sites and rates permitting several copies of metal-based drugs linked to the dendrimer, which present distinct behaviors from the inorganic molecule itself.[139–141] Dendrimers provide exceptional benefits for tuning metal centers because they offer a well-controlled positioning of the metallic moiety into the dendrimer architecture.[141,142] The conjugation of dendrimers with metallodrugs can improve the metallodrug solubility and increase the metallodrug sensitivity against the resistance of tumor cell lines.[143] Metallodendrimers that transport metallodrugs appear to be novel candidates as chemotherapeutic agents since they seem to work through a distinct mechanism of action from the native metallodrug.[144] Due to their properties and significant structural diversity[145] metallodendrimers present several applications such as catalysts,[146,147] biosensors,[148] molecular switches,[149,150] and therapeutic agents.[151–153]

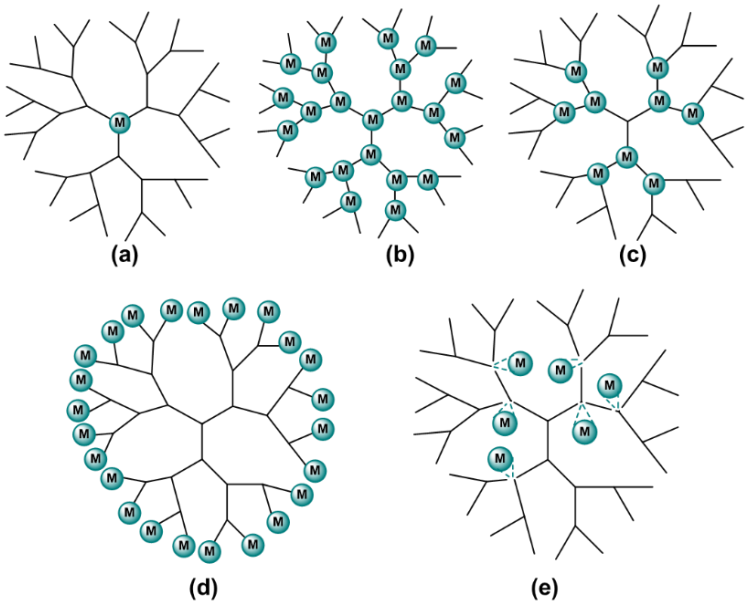

Figure 6. The different types of metallodendrimers: (a) metal as a core; (b) metal as branching points; (c) metal as connectors; (d) metal as terminal groups; (d) metal complexation (adapted from reference 137).

2. Dendrimers and their biomedical applications

Nanotechnology has been helping to solve most of the issues of nanomedicine associated with insoluble drugs by improving their solubility, crossing the biological, biophysical, and biomedical barriers of the human body.[154] In this context, conjugation of a drug to a dendrimer may increase its solubility and the circulation half-life of drugs.[34]

To achieve biomedical applications, dendrimers like other systems must take into account the pharmacokinetic properties, such as absorption, distribution, metabolism, and elimination (ADME).[155–157] One important aspect of biodistribution and pharmacokinetic studies is to classify if the new drug is safe and efficient but also to estimate the clinical doses.[158] Besides, when free medicine is administrated, it is necessary to increase the dose to achieve the therapeutic drug concentration.[51] However, this high dose can lead to severe toxicity. The pharmacokinetics of the dendrimer itself and a dendrimer conjugated with a drug will change the properties of the dendrimers, and as consequence, the biodistribution will also be different.[159] The ADME parameters can define the dendrimer pharmacokinetics such as clearance, the volume of distribution, the dose concentration, and the half-life of the drug.[46,155,159] Some characteristics of dendrimers that influence their biodistribution and pharmacokinetics are the size and generation, the terminal functionalization (such as charge and target ligands), and the administration routes.[71,158–161] Indeed, a dendrimer can be designed to present desirable characteristics such as biocompatibility, pharmacokinetics, and bioavailability, that contribute to a successful material for biomedical applications.[162,163] On this basis, dendrimers have been described in a wide range of biomedical applications including drug/gene delivery, transfection, antimicrobials, and tissue engineering.[93,163]

In the following sections, the application of dendrimers will be discussed in the context of their use for antiviral therapy. The use of metallodendrimers and metallodrugs for cancer therapy will also be presented.

2.1. Drug delivery

Dendrimers are an excellent platform for drug delivery, protecting the drug molecules from the biological environment, reducing toxicity, and maintaining the accumulation into tumor tissue.[24] The functionality of dendrimers can allow several interactions of drug molecules per dendrimer, which also increases the loading and stability of the dendrimer-drug conjugate.[164] Dendrimer interactions with a molecule are mostly with the external terminal groups of the dendrimer. Nevertheless, there are five approaches of interaction between a dendrimer and a drug molecule: (a) electrostatic interactions with the surface groups; (b) encapsulation in the interior cavities of the dendrimer; (c) conjugation of the dendrimer to a drug with a covalent bond or by (d) a cleavable bond; (e) interaction of the drug and associated dendrimers[165,166] (Figure 7).

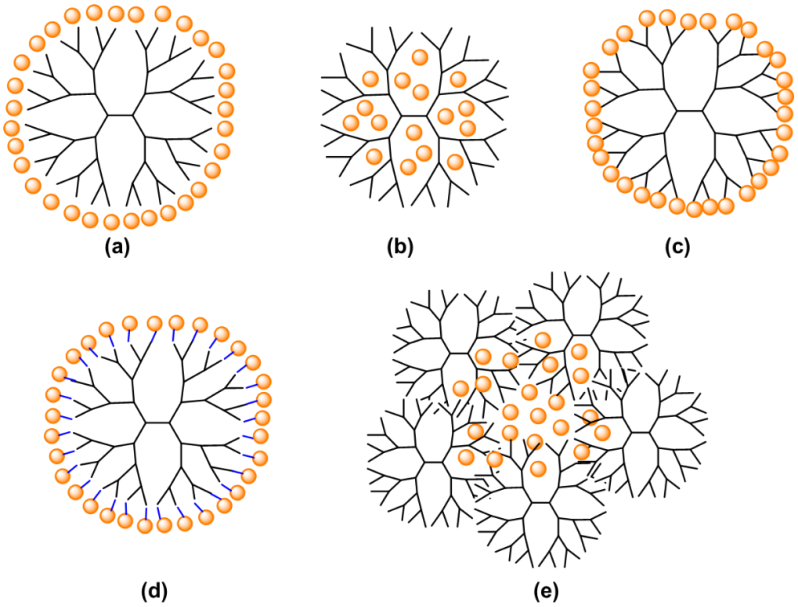

Figure 7. Types of drug interactions using dendrimers: (a) electrostatic interactions; (b) encapsulation; (c) conjugation with a covalent bond (c) or by (d) a cleavable bond; (e) interaction of the drug and associated dendrimers (adapted from reference 165).

The mechanisms for drug delivery can be summarized into two main aspects: the degradation by enzymes of the covalent bond between the drug and the dendrimer, and the drug release from the dendrimer due to physical variations or stimulus such as pH or temperature.[166]

To be valid in nanomedicine, drug delivery systems have to accomplish certain requirements, such as a nanometric size, improve the solubility of hydrophobic drugs, the ability to deliver drugs or biomolecules to specific locations in the human body, and due to its nanosize can avoid fast clearance thus extending the time in the bloodstream.[154] Nanocarriers can be found using different types of nanomaterials, including liposomes, nanocapsules, dendrimers, polymeric nanoparticles, nanotubes, micelles, and metal nanoparticles.[24,154] Dendrimers offer several advantages such as increased drug stability, solubility, protection, and extend the drug's circulation time.[92,167,168] However, it is crucial to know the safety of using dendrimers *in vivo*. It is important to take into consideration the cytotoxicity of dendrimers, through the interaction with blood proteins and cells, animal toxicity, and biodistribution.[163] Dendrimers have been used as nanoplatforms as drug delivery systems, mostly as a vehicle for therapeutic drugs in cancer therapy.[169] The functionalization of targeting molecules to the dendrimer can enhance cancer treatment efficiency by attaching to the tumor cells, and the side effects may be controlled.[68]

2.2. Antiviral therapy

Infectious diseases are one of the leading causes of death worldwide. Mainly viral infections have a significant impact on health and socioeconomic development, infecting millions of people.[170,171] There are several diseases caused by viruses, including human immunodeficiency virus/acquired

immunodeficiency syndrome (HIV/AIDS), hepatitis B and C, influenza, and severe acute respiratory syndrome (SARS) more specifically respiratory syncytial virus (RSV) and the novel coronavirus SARS-Cov-2 (COVID-19).[171,172] To date, COVID-19 infection has shown to be extremely contagious, with more than 16.8 million confirmed cases and over 662 thousand deaths worldwide.[173]

HIV/AIDS remains a major problematic subject with millions of new infections every year. The most recent data from the Joint United Nations Program on HIV/AIDS (UNAIDS) show that 38 million people are living with HIV and 1.7 million people were newly infected worldwide in 2019.[174]

Member of the *Retroviridae* family and genus *Lentivirus*, HIV is a retrovirus, and its genome has two identical copies of single-strand RNA molecules.[175,176] AIDS/HIV is characterized as a disorder of the immune system with a decrease in the number of helper T-cells responsible for the stimulation of B-cells to produce antibodies.[177] HIV can infect a diversity of cells such as $CD4^+$ T cells, macrophages, and microglial cells, and present a spherical shape with around 120 nm diameter.[176] HIV was initially detected in 1981 in the United States, and the virus was first isolated in 1983 by Luc Montagnier[178], and Robert Gallo[179,180] assigned it to the cause of AIDS.[181–183]

HIV infection can be categorized into two types of HIV isolates, HIV-type 1 (HIV-1) which is the most prevalent and infectious globally, and HIV-type 2 (HIV-2) more common in Africa, in particular in some regions of Western and Central Africa.[175–177] These two types of HIV isolates present similar basic structural viral genes (*gag*, *pol*, and *env*) with other complex combinations of regulatory or accessory genes.[175] In Figure 8 can be observed the basic structure of HIV-1. The gag gene encodes the core proteins (p24, p6, p7) and matrix (p17). The viral envelope glycoproteins (gp120 and gp41) are encoded by the *env* viral gene responsible for cell surface receptor recognition.[175] The *pol* gene encodes the viral reverse transcriptase (responsible for the conversion of viral RNA into DNA), the integrase (assimilates viral DNA into host chromosomal DNA), and the protease (responsible for the cleavage of the gag and pol protein precursors into their active forms).[175]

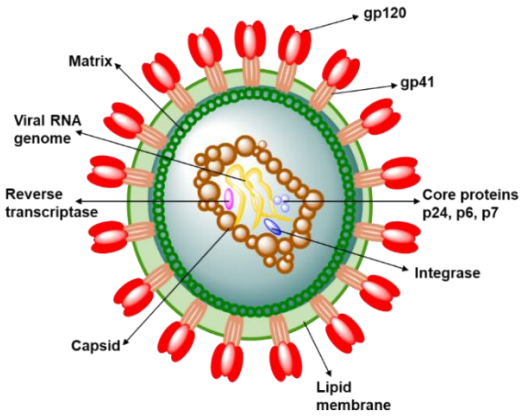

Figure 8. The fundamental structure of HIV-1.

Nowadays, there is no cure for HIV, the primary cause of AIDS, and the main problem to overcome is viral reservoirs.[184] These reservoirs are the primary cause that turns the cure of HIV

problematic since they are responsible for the drug-resistant virus.[185] Viral reservoirs are the cellular locations and the anatomical sites where the virus replication is halted in infected cells.[184] HIV can be transmitted by contact with contaminated blood and body fluids, *via* sexual intercourse, mother-to-child transmission, and the sharing of intravenous syringes.[176,186]

HIV-1 infection begins with the entry of the virus through the binding of the viral envelope proteins gp120 to the cell surface receptors CD4, and then to the coreceptors, CCR5 and CXCR4.[187–190] There are two types of HIV-1 isolates, R5 and X4, R5 isolates require CCR5 coreceptor for entry, the X4 isolates require CXCR4 coreceptors, and there are double R5X4 isolates that can use either CCR5 or CXCR4 coreceptors.[188]

In more detail, HIV-1 infection occurs with 6 phases:

a) entry of the virus into immune cells by the absorption and fusion of glycoprotein (gp120) to the CD4 receptor on the cell surface, and the viral envelope releases the HIV RNA;

b) the replication of the single-stranded RNA genome and transcription into complementary DNA (cDNA);

c) integration of the cDNA into the cell nucleus DNA (such as leukocytes);

d) recombination between the two RNA genomes of the HIV particle;

e) the two HIV envelope glycoproteins (gp41 and gp120) are assembled, and the gp41 enters into the host cell and anchors gp120 to the membrane of the infected cell;

f) spread and infection of HIV between $CD4^+$ T cells.[176,191]

Figure 9 is a schematic representation of the HIV infection/replication process.

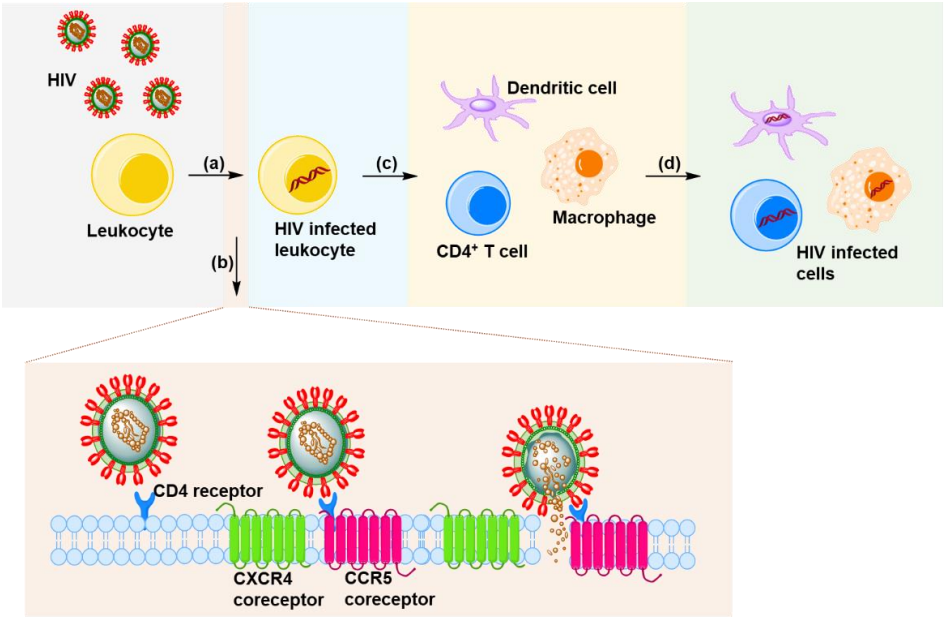

Figure 9. Schematic representation of the HIV infection/replication process: (a) HIV gets in contact with leukocytes, and the leukocytes are infected with HIV; (b) the infection/replication occurs by the virus binding to the CD4 receptor and coreceptors CXCR4 or CCR5, the fusion of the virus to the cell membrane, and release of the viral proteins and particles into the cell; (c) the infected leukocytes, after the replication/amplification of the virus, reach other target cells, such as $CD4^+$ T cells, dendritic cells, and macrophages; (d) and infect these target cells with the HIV to then proliferate.

2.2.1. Dendrimers as antivirals

Nanomaterials, due to their high reactivity and extensive terminal surface volume, gave researchers innovative methodologies to develop new treatment and prevention approaches for HIV-1.[192] Dendrimers are excellent candidates as antivirals due to their functionality, multivalency, controllable toxicity, increased specificity, and improved bioavailability.[170,186,193] The multivalency of dendrimers can be harnessed as inhibitors since viruses also use multivalent interactions to bind to receptors.[193] Multivalency is a great assistance in using dendrimers as nanotherapeutics because multivalent interactions are significantly stronger than monovalent interactions.[193,194] Indeed, it is important to take into consideration the generation as well as the number of end-groups in dendrimers since this number increases exponentially with generations, and with that also the steric hindrance of the end-groups.[193] Therefore, dendrimers with low generations are less toxic, present more flexibility, and the structure tends to be more open and amorphous than the higher generation dendrimers that can have spherical conformation, the opposite of lower generation dendrimers.[193] Dendrimers have shown excellent activity against several viruses such as HIV,[195–198] herpes simplex virus (HSV),[199,200] RSV,[201] Ebola,[202–204] and influenza virus.[203,205,206] The dendrimers most used as antivirals have been functionalized with carbohydrates, anionic species, and peptides.[207] Glycodendrimers are the most common to be tested as antivirals against infection by influenza and HIV.[207] Polyanionic dendrimers have also been studied as inhibitors to HSV and HIV because of their negative charge surface.[193,207] The *in vitro* studies show that dendrimers first act in the early stages of viral infection by preventing viral fusion to target cells and also play a role as entry inhibitors.[197,198] Although VivaGel® failed to reach the clinical phase against HIV infection, recent news from Starpharma revealed that the SPL7013 dendrimer, the active compound in VivaGel®, presented promising results against SARS-CoV-2, responsible for COVID-19 infection, with significant antiviral activity.[208]

Generally speaking, dendrimers can act as transporters of antiretroviral agents and can also act as antiretrovirals themselves.

2.2.2. Current therapies targeting HIV infection

Nanotechnology has been taking several efforts to discover new strategies to find and decrease HIV reservoirs.[184] Although all efforts have been directed to find a cure for HIV/AIDS, until now it has remained a challenge to find. Treatment through antiretroviral therapy (ART) is still the best option to control this disease. The ART involves six classes of medicines including, nucleoside reverse transcriptase inhibitors, non-nucleoside reverse transcriptase inhibitors, protease inhibitors, entry and fusion inhibitors, CCR5 antagonists, and integrase inhibitors.[170,209] However, HIV/AIDS infection entails an eternal treatment that can lead to the progress of drug resistance because they are not able to eradicate viral reservoirs.[170,185]

An effective therapy that has improved the quality of life of HIV-infected individuals is the combination therapy of two or more drugs.[170] Combination therapy can be more efficient and have a

synergetic effect relative to monotherapy that often leads to drug resistance, and thus to treatment failure.[210,211] The combination of two or more drugs may reduce the amount of drug needed without compromising the required effect.[210,212] Combination antiretroviral therapy (cART) through targeting multiple steps in viral infection, can be obtained by highly active antiretroviral therapy (HAART).[191] However, HAART presents some restrictions, even if it can suppress viral infection, unfortunately, it cannot avoid the eradication of HIV.[191] For this reason it is less and less used in the clinic, and as such the main focus will be on cART. The differences between the most important therapies under clinical use for HIV treatment can be explained as cART, as mentioned above, which is characterized by the combination of at least two drugs from two different classes, while ART is the current term used to define HIV antiretroviral therapy (Figure 10).[213]

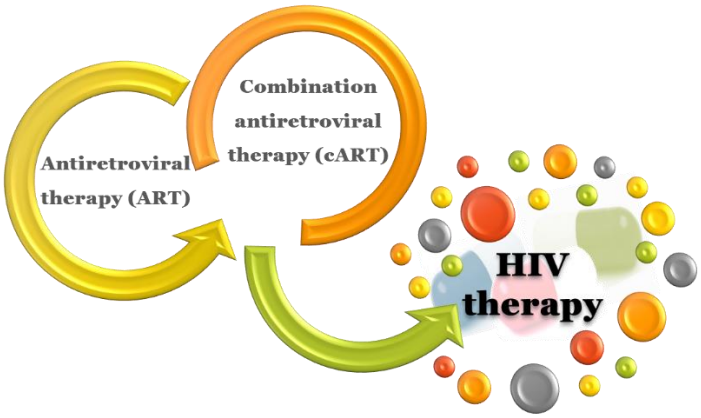

Figure 10. Therapies used to treat HIV infection.

Since none of the drugs currently available can cure HIV infections, antiviral therapy through effective viral suppression is the goal to improve the lives of HIV-infected individuals. Nevertheless, there are some issues to overcome with drug toxicity, drug interactions, drug-resistant mutations, and non-adherence drugs.[185,192] The use of delivery systems or new drugs with improved solubility and new mechanisms of action could answer some of these concerns.[185]

2.2.3. Dendrimers as anti-HIV drugs

Several ARV drugs are in different clinical phases with different mechanisms of action, from entry or fusion inhibitors to maturation inhibitors.[191] Despite that VivaGel® developed by Starpharma, was initially prepared to be used as a microbicide against HIV and HSV infections, this dendrimer-based gel is currently commercially available (VivaGel® BV) for the treatment of bacterial vaginosis and is already in the market in Europe and Australia.[214]

Presently, there are several dendrimer-based nanomaterials in research to act as antivirals agents. Muriel Blanzat and coworkers prepared a phosphorus-containing dendrimer with cinnamic acid

as a terminal with aminolactitol 3 to form a catanionic dendrimer.[215] The prepared glycodendrimers were designed to take into consideration the influence of the multivalency of the dendrimer and the virus particles.

Maria Ángeles Muñoz-Fernández and collaborators developed an anionic carbosilane dendrimer with promising results to be used as a topical microbicide against HIV-1 infection.[81,197] This carbosilane dendrimer (G2-S16) has excellent biocompatibility *in vivo* and can prevent HIV-1 infection in the presence of semen. The same group also developed carbosilane dendrons functionalized with DO3A ligand with a copper complex and carbosilane dendrons containing fatty acids with high inhibitory capacity against HIV-1 infection and HSV-2/HIV-1 co-infection, respectively.[216,217]

The group of Francisco J. de la Mata and Rafael Gómez prepared anionic PPI copper metallodendrimers as antiviral agents against HIV-1 infection.[218] They demonstrated that the copper complex improved the antiviral activity when compared with the free copper dendrimer.

Ana San-Félix and coworkers prepared a tryptophan-based dendrimer with the ability to inhibiting HIV replication.[219] These tryptophan dendrimers were effective in halting HIV entry by binding to the envelope glycoproteins gp120 and gp41.

Our group prepared a series of low generation anionic poly(alkylidenamine)-based dendrimers with high antiviral activity against HIV-1 infection.[198] These dendrimers of generation 1 with carboxylate and sulfonate terminal groups could block the entry of the viral particles into the cells and presented no inflammation or irritation on vaginal tissue using BALB/c mice.

Development of novel formulations, such as new microbicides, whether as carriers for drugs or new nanomaterials capable of acting as antiretrovirals, gives a new hope to find an efficient treatment against HIV infection. Meanwhile, prevention is still the better choice to overcome this pandemic disease. HIV prevention can be done through Pre-Exposure Prophylaxis (PrEP) since the hope of an HIV vaccine continues elusive regardless of all the efforts to develop one.[191] PrEP is a strategy developed for HIV-negative individuals as a prevention approach for viral dissemination as oral, topical, or inject compounds.[191]

2.3. Cancer Therapy

Cancer is one of the leading causes of death in the world. In 2018, cancer was responsible for around 9.6 million deaths worldwide, with lung, breast, colorectal, prostate, skin, and stomach cancers being the most common tumors.[220] In Europe, the most common cancers were prostate, breast, colorectal, and lung, with lung cancer responsible for about 56 000 deaths per 100 000 cases.[221] Nevertheless, the number of cancer survivors in the United States of America (USA) continues to increase.[222] The estimated new cancer cases for the USA is 1.8 million, and an estimated 606 thousand deaths for this year of 2020.[223]

Solid tumors start with uncontrolled cell division and spread to adjacent tissues, causing a group of associated diseases (Figure 11).[224] Cancer can be classified according to the tissue which is formed, such as:

a) carcinoma, which is the most common type of cancer formed by epithelial cells;

b) sarcoma, that form in bone and soft tissues;

c) leukemia, formed in blood tissue in the bone marrow;

d) lymphoma, starts in the lymphocytes;

e) multiple myeloma, starts in plasma cells;

f) melanoma, starts in cells that will become melanocytes;

g) brain and spinal cord tumors, based on the kind of cell in which they are formed.[224]

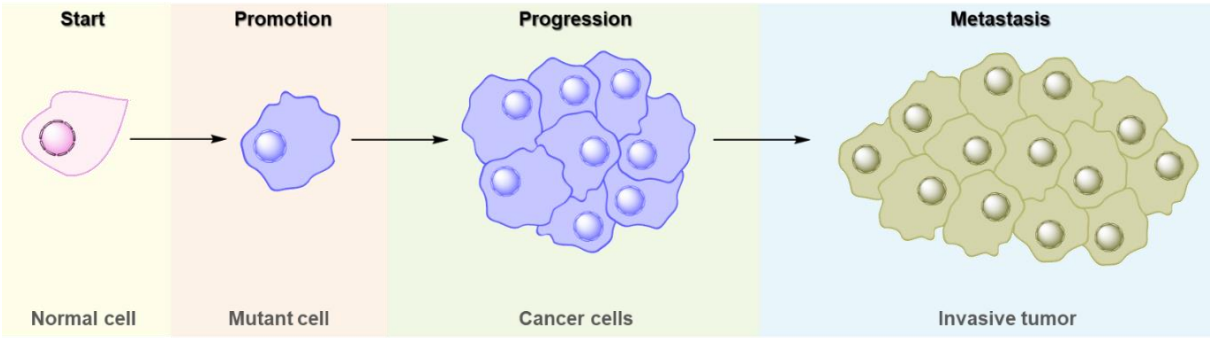

Figure 11. Schematic representation of the stages of cancer formation.

Combination chemotherapy was firstly used to overcome drug resistance. As a result, combination therapy has been applied as a new treatment for cancer therapy, with the administration of combined chemotherapeutics that present different mechanisms of action.[225]

Nanomedicine, more specifically through the use of nanotechnological approaches, is prevailing over the drawbacks of the conventional procedures of diagnosis and treatment by presuming more precision to the existing methods [226]. Dendrimers have been used as delivery systems since they improve the therapeutic efficiency and reduce the negative aspects of the drug.[227]

Theranostics,early cancer diagnosis and therapy, has been developed as a new approach for cancer treatment.[227] Theranostic biomaterials can offer a new strategy to drug progress by improving the therapeutic efficiency and avoiding unwanted side effects leading to an increase on the practicability of precision medicine.[228] In cancer, chemotherapy is important to eliminate the residual tumor that can spread metastatically after removal/reduction by surgery or radiotherapy.[229] A chemotherapy drug is specifically related if it is effective against tumor metastases.[229]

2.3.1. New methodologies for cancer treatment

The therapeutics method is to target the typical characteristics of cancer, with the aim specific to inhibit tumor angiogenesis and thus preventumor progression.[160,230] Angiogenesis has an important contribution to tumor growth, progression, metastasis, and survival.[231] Nanotechnology can support antiangiogenic therapy to overcome some limitations of cancer treatment.[230] In particular, nanomedicine using antiangiogenic treatment still needs to improve its anticancer efficiency.[231] The mostlty used cancer treatment approaches combine an extensive variety of chemotherapy drugs, with radiotherapy and surgery.[52,160]

Cancer immunotherapies have progressed immensely revealing promising clinical responses, more precisely cancer vaccines, chimeric antigen receptor (CAR)-T cell therapy, immune checkpoint blockade (ICB) therapy, and cytokine therapy.[232] The purpose of cancer immunotherapy is to communicate to the immune cells in the lymphoid tissues and in the tumor microenvironment to explore and destroy tumor cells.[233] The antitumor immune responses can contribute to systemic immune surveillance and eradicate local and dispersed metastatic tumors.[233]

The use of nanomaterials for drug delivery improves the protection and circulation time of the drug, and in this way decreases the toxicity towards the healthy cells.[160] The accumulation of the drug at the tumor site can induce the enhanced permeability and retention (EPR) effect, which will improve the therapeutic effectiveness and reduce the side effects on healthy tissue.[234,235] Dendrimers have several benefits in cancer diagnosis and therapy:

(1) well-defined structure with surface multifunctionality for various purposes;

(2) reproducible pharmacokinetics due to the monodispersity of dendrimers;

(3) the multivalency or synergistic effects improve the biological, chemical, and physical properties of the compounds linked to the surface of the dendrimers;

(4) exceptional cellular uptake efficacy and bioavailability for anticancer drugs;

(5) controllable and variable sizes make them good candidates to use as protein mimetics for cancer therapy lacking immunogenicity;

(6) excellent drug/gene delivery efficiency which can prevent some complications in cancer therapy.[236]

2.3.2. Metallodrugs

In the last years, there has been a breakthrough with the emergence of different types of metallodrugs, surpassing the predominance of cisplatin-based metallodrugs. Metallodrugs can be designed based on the choice of metal, oxidation state, coordination geometry, types, and the number of coordinated ligands (Figure 12).[237]

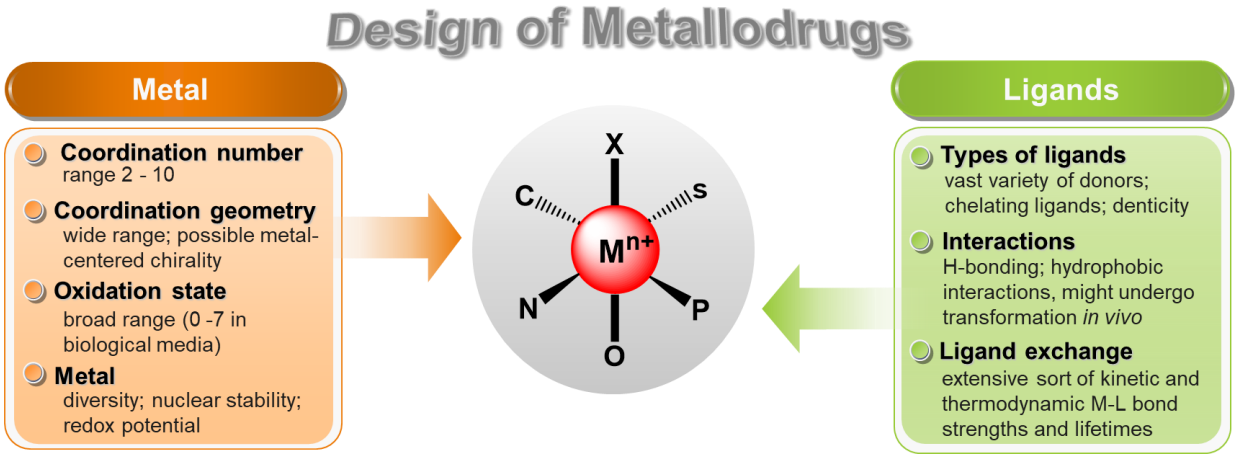

Figure 12. Characteristics to take into consideration on how to create a metallodrug, the metal, and ligand aspects to design a metal complex (adapted from reference 237).

Coordination chemistry is characterized by the bond of a central atom, generally a metal ion, and a ligand, such as organic or inorganic molecules.[238] Metal ions have natural properties, including favorable oxidation states and ligand geometries; however, the metal complex reactivity can differ in the number and type of ligands but also the surrounding environment.[237] These metal complexes are coordination compounds, where the metal ion acts as a Lewis acid by receiving electron pairs from ligands, the Lewis bases.[239] Some chemical and physical properties of metal complexes can be modified by potential reactions such as reduction and oxidation of the metal ion, or the linked or the substituted ligands, and the reactions on the ligands that are distant from the metal ion.[237] Therefore, different types of metal can coordinate in different kinds of geometry. For example, ruthenium (Ru) can present two different types of coordination; ruthenium(II) can form both penta- or hexacoordinated complexes, but ruthenium(III) can only form hexacoordinated complexes, while cisplatin ((*SP*-4-2)-diamminedichloroplatinum(II), cis-[$Pt(NH_3)_2Cl_2$]) has a square planar geometry.[240] This structural diversity provides one of the desirable characteristics in coordination compounds.[239]

Metallodrugs have an interesting biological activity and, as a result, have been applied in several applications such as antibacterials, antimalarials, or as neuro-protector agents, against arthritis, among others.[241] Of particular interest is their application in anticancer therapies. In this context, these metallotherapeutics offer exceptional and alternative mechanisms of action *via* conventional pure organic medicines, where they play a role in the prevention of cancer cell division and the activation of cancer cell apoptosis through the induction of DNA damage and the disruption of the DNA repair process.[242,243] However, due to the low efficacy of transportation of the active species to the target, new technologies have been developed based on nanostructured materials to overcome some problems related to the delivery of drugs to the desired location.[154] In fact, nanomaterials can prevail over some of the disadvantages of metallodrugs. Furthermore, for that reason, they have been considered to improve their delivery and efficacy. Among the possible nanomaterials, due to their characteristics, dendrimers assume a significant role since they can address the limitations of conventional drugs such as solubility, stability,

specificity, and efficiency, and overcome biological issues (like cell penetration, clearance, and off-target interactions), offering an improved position of the metallic species by tuning metal centers.[141,144] Their characteristics make them desirable nanomaterials to be used for drug delivery since the size and molecular weight can be controlled to enhance drug properties.[139] Therefore, metal complexes with therapeutic qualities, including cisplatin and ruthenium complexes, can be transported by dendrimers as metal-based drugs. In the next sections, we will present these two metals, their complexes with biological activities, and mechanism of action since they are related to the scope of this thesis.

2.3.2.1. Platinum

The most well-known coordination compounds for anticancer chemotherapeutics involving platinum metal are cisplatin [cis-diaminedichloroplatinum(II)] and its derivatives, as can be seen in Figure 13.[241] Cisplatin was firstly prepared in 1844 by Michele Peyrone, and only in 1965 Barnett Rosenberg and coworkers discovered its biological activity, including its action against sarcoma cancer in rats and inhibition of *Escherichia coli* (*E. coli*) bacterial cell growth.[244–246] At the end of 1978, cisplatin was approved as the first Food and Drug Administration (FDA) platinum drug for testicular and ovarian cancers treatment.[247–250]

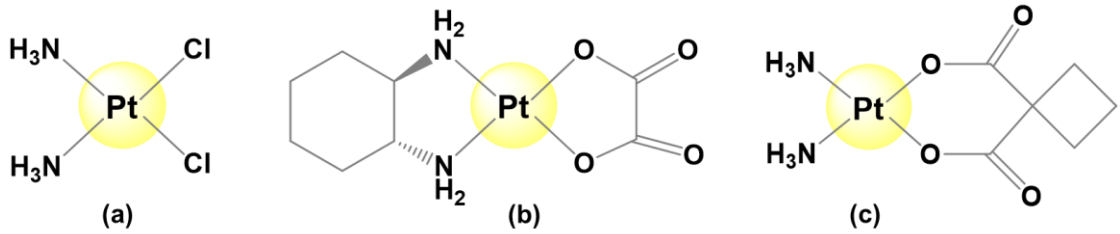

Figure 13. Structures of platinum anticancer derivatives: (a) cisplatin, (b) oxaliplatin, (c) carboplatin.

Equally important, in the last decades, researchers developed several analogs of cisplatin to improve its therapeutic index, such as oxaliplatin and carboplatin.[247,251] These two cisplatin analogs present different effectiveness in cancer treatment compared to cisplatin. Oxaliplatin is efficient against colon cancer and other cancers where cisplatin is not effective, and carboplatin is not active in treating germ cell tumors like cisplatin.[251,252]

In the following subsections, side effects, drug resistance, mechanism of action, and DNA interaction of cisplatin will be discussed.

2.3.2.1.1. Cisplatin: side effects and drug resistance

Currently, cisplatin is extensively used in several cancer treatments, including ovarian, testicular, bladder, head, and neck tumors.[243,247,248,251,253] The use of cisplatin, however, presents side effects due

to drug resistance, and several cytotoxicities such as nephrotoxicity (damage in the kidneys), hepatotoxicity (liver damage), cardiotoxicity (damage in the cardiac muscle), neurotoxicity (decrease in response due to infection damage in the neurons), ototoxicity (hearing loss), myelosuppression (reduction in the bone marrow activity), nausea and vomiting.[247,254–257] These toxicities are dose-dependent.[258] Cisplatin has been used in combination therapy with other anticancer drugs due to significant side effects and drug resistance.[247] Clinical platinum resistance is a major concern since it is the most used anticancer drug in chemotherapy.[259] Drug resistance can be categorized as intrinsic resistance and acquired resistance. Intrinsic resistance is when a drug reveals to be ineffective from the beginning of the treatment, and acquired resistance is when a drug is efficient but over time becomes ineffective.[258] In light of the drug resistance, several mechanisms in the cisplatin resistance can be involved, such as drug inactivation, changes in the drug target, reduction of intracellular drug accumulation, and avoiding of apoptosis.[260]

2.3.2.1.2. Cisplatin: mechanism of action and DNA interaction

The intracellular uptake of cisplatin has been assumed to occur by passive diffusion.[261] It was found that copper transporter 1 (CTR1), a transmembrane protein implicated in copper homeostasis, has a central role in this uptake.[251,262] This may result in a reduced accumulation of cisplatin by cancer cells since it induces degradation in the CRT1 concentration.[248] Cisplatin can present at least two mechanisms of action towards cancer cells namely, binding to DNA and cytoplasmic targets such as proteins *e.g.* a deficient accumulation of cisplatin in the cell and the binding of cisplatin to proteins like glutathione.[263] After intravenously administrated into the bloodstream, cisplatin comes into contact with a high concentration of chloride (~100 mM), which prevents the aquation process, the substitution of the chloride ligands by water molecules.[264,265] Once in the interior of the cell, hydrolysis occurs forming aquated species, due to the low chloride ion concentration (~4 mM).[266] Studies performed by Trevor W. Hambley and collaborators showed that monoaquated cisplatin is more reactive to DNA binding than the diaquated species.[267] To activate its anticancer potential, cisplatin may enter the cell and be activated *via* the substitution of the chloride ligands by water molecules. This substitution into hydroxyl species is influenced by the pH. In this case, 85% of the cisplatin complex will be in the dihydrate form at pH 7.4. However, at a lower pH (~6.0) about 80% of the monohydrate species are present.[266] Nevertheless, when in blood circulation, cisplatin is exposed and can reach and bind to proteins such as human serum albumin (HSA) and the amino acid cysteine, especially glutathione.[264,268,269] Glutathione may protect the cells through the capture of platinum compounds before their reaction with DNA, as well as support DNA repair.[269] Indeed, after administration a large amount of cisplatin binds to proteins in blood plasma, and this binding is responsible for the drug deactivation.[248,270]

Cisplatin interacts with DNA by coordinating to the N7 positions of the imidazole ring of two nearby guanines *via* an intrastrand crosslink.[265] This coordination, with two guanines, usually occurs to a higher extent, but it can also occur with adducts of one guanine and one adenine to a lower extent.[265] The

cytotoxicity effects between cisplatin and DNA are due to the changes in the intrastrand crosslinks leading to the distorted combination of DNA, which can be removed from DNA through repair pathways identified by damage-DNA binding proteins.[265,271] DNA damage caused by cisplatin leads to cell death through the signal transduction pathways of apoptosis.[261]

2.3.2.2. Ruthenium

Ruthenium, being a transition metal, can occur in several oxidation states (+2, +3, and +4) that are useful for biological systems by reducing it to a more biologically active form.[272–274] The different oxidation states confer to ruthenium complexes several benefits. For example, the Ru(II) complexes can kill cancer cells directly through various mechanisms, have good photophysical and chemical properties; while Ru(III) complexes can be used as prodrugs in conditions of acidic pH, hypoxia, they also have good thermodynamic stability and kinetics, and when *in vivo* can be reduced to Ru(II).[240,272,273] Ru(II) and Ru(III) complexes are known for their potential as anticancer drugs. Ru(III) complexes are usually more inert, which can be assigned to the higher effective nuclear charge and they can be reduced to Ru(II), the more active form.[259] Ruthenium can mimic the behavior of iron by binding to biological molecules, such as the affinity for transferrin and albumin, which leads to its accumulation in cancer cells and a decrease of the free complex concentration in the bloodstream.[240,242,274] The capacity of ruthenium to mimic iron is probably related to the fact that it belongs to the same group as iron in the periodic table. The three-dimensional configuration of ruthenium permits ligand coordination and functionalization that can be tuned depending on the molecular target.[272]

Ruthenium complexes have been the alternative to platinum drugs due to their unusual antitumor activity, as well as their high possibilities of coordination geometries, and their ligand exchange kinetics are similar.[259,273] Therefore, these complexes are likely to turn into the next generation of clinical metal anticancer drugs, owing to the many advantages, such as less cytotoxicity and genotoxicity, diverse ligand exchange kinetics, activation mechanism, transport, less drug resistance, potent efficacy, when compared to platinum drugs.[242,273]

Organometallic ruthenium compounds containing cyclopentadienyl (η^5-C_5H_5) ligand have exceptional cytotoxicity in the nanomolar range against numerous human cancer cell lines, which makes them promising candidates for cancer therapy.[274] Several cyclopentadienyl ruthenium complexes have been developed as anticancer agents with promising outcomes to be used as novel chemotherapeutics.[153,275–278]

2.3.2.2.1. Ruthenium: cell cycle and DNA interactions

Although all efforts have been directed towards understanding the mechanism of action of ruthenium complexes, it still remains elusive. Understanding at what stage of the cell cycle the ruthenium complexes are acting is also crucial. In cancer, cell cycle deregulation is a predictable characteristic,

since cancer cells present spontaneous proliferation and an increase in DNA mutations.[279] The cell cycle is a process that guarantees the duplication of genetic information and cell division.[280] This well-organized and regulated process occurs in four different phases, Gap 1 (G1) phase, synthesis (S) phase, Gap 2 (G2) phase, and Mitosis (M) phase controlled by a family of cyclin-dependent kinases (CDKs).[280–282] The phases involved in the cell cycle are characterized by G1 phase with cell growth and metabolic changes (duplication of cellular contents) for cell division; S phase with DNA synthesis, each chromosome is replicated; G2 phase, the cell prepares for division (mitosis and cytokinesis); M phase, nuclear division followed by cell division (cytokinesis), leading to the formation of two identical cells (Figure 14).[281,282] In cancer, the cell cycle activity is atypical due to the changes in upstream signaling pathways or through genetic damage in genes encoding cell cycle proteins.[280,282] The design of anticancer drugs, more precisely synthetic inhibitors of CDKs could control the unusual activation of the CDKs in cancer.[279,280] Previous studies showed that Ru(II) polypyridyl complexes are capable of inhibiting cell growth at G0/G1 phase arrest.[283–285]

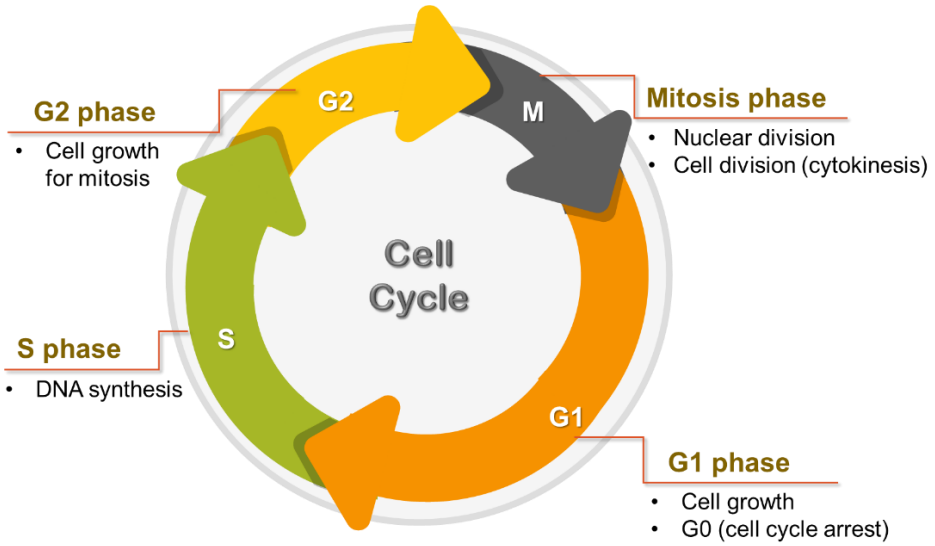

Figure 14. Stages of the cell cycle: G1 phase (preparation for cell division); S phase (the genetic material is replicated); G2 phase (the cell is prepared for mitosis); Mitosis phase (nuclear and cell division occurs to form two identical cells).

Findings achieved along the years have demonstrated the abilities of ruthenium complexes to prevent DNA replication, present mutagenic activity, induce the SOS repair mechanism, bind to nuclear DNA by reducing RNA synthesis, and atypical DNA structures.[286] In particular, ruthenium compounds can bind to DNA in several ways, including covalent, intercalative, electrostatic, and major or minor groove binding.[274,286] Ru(II) and Ru(III) complexes are recognized to target the N7 binding site of guanine, which is the most electron-rich location on DNA.[287] Arene ruthenium complexes were suggested to have different mechanisms of action, such as the interactions between complexes that have reactive Ru-Cl bonds with nuclear DNA that can happen due to hydrolysis, leading to the formation of intermediary aqua complexes.[237] These Ru(II) complexes can ruthenate DNA by binding to the guanine residues through

covalent or π-stacking, and the arene attaches to DNA non-covalently by intercalation and minor groove binding.[237,259,274] It seems that ruthenium complexes do not selectively interact with nucleobases and can bind to more than one reactive coordination site, acting as intra- or interstrand crosslink agents.[287,288] However, it is still necessary to recognize how these ruthenium complexes act in the cell cycle and their interaction with DNA. Therefore, our goal is to understand the mechanism of action of ruthenium complexes that currently remains unknown.

2.3.2.2.2. Ruthenium complexes under development

As mentioned above, ruthenium complexes have a high potential to be used as anticancer agents. Several complexes have been developed, offering promising outcomes as chemotherapeutics. Pedro R. Florindo and collaborators synthesized eight cyclopentadienyl-ruthenium(II) complexes and evaluated their anticancer properties against the HCT116 cell line through glucose transporters (GLUTs).[289] Two of the eight ruthenium compounds were checked for the role of GLUTs in cellular internalization, and competition experiments using glucose. These ruthenium complexes were capable of internalizing *via* GLUT transmembrane proteins.

Christian Gaiddon and coworkers prepared an organoruthenium compound (RDC11) (Figure 15a) with anticancer activity and studied the interaction of this ruthenium compound with histones and the impact on death pathways.[290] The results indicated that RDC11 strongly interacts with several histones and triggers the ribosomal biogenesis response and the regulation of p53 and endoplasmic reticulum (ER) stress pathways.

Alzir A. Batista and coworkers synthesized five ruthenium complexes (Figure 15b) and evaluated their antitumor efficacy and their interaction with calf thymus deoxyribonucleic acid (CT-DNA) and HSA.[291] All five compounds revealed their antitumor capacity against several cancer cell lines. The interaction studies with CT-DNA showed that the ruthenium compounds have a weak interaction with DNA. However, the binding studies with HSA demonstrated that the compounds were able to bind to HSA, suggesting that it can be transported in the body by this protein.

Riccardo Pettinari and collaborators prepared seven Ru(II) arene complexes (Figure 15c) to assess their anticancer and apoptosis induction efficiency and their capacity to bind to DNA and bovine serum albumin (BSA).[292] These compounds demonstrated cytotoxicity and pro-apoptotic effect and were able to interact with DNA *via* electrostatic interactions with an affinity for the DNA minor groove.

Jesús J. Fernández and coworkers prepared two ruthenium complexes (Figure 15d) with anticancer activity that presented no toxicity *in vivo.*[293] They performed several biological studies that proved that these two ruthenium (*p*-cymene) complexes presented a strong interaction with DNA, and their antiproliferative capacity was related to the joint mechanism of autophagy and apoptosis. Zebrafish embryo was used as an *in vivo* model, and the ruthenium complexes did not present any significant effect of lethal toxicity.

G. Bernal and coworkers developed two Ru(II) complexes and determined their anticancer activity through cytotoxicity studies, gene expression analysis, and caspase activation assays.[294] The cytotoxicity studies were compared with cisplatin, and the ruthenium complex (Ru-UCN3) was more toxic, and the other ruthenium complex (Ru-UCN1) was more active when compared with cisplatin (Figure 15e). Both complexes induced apoptosis, and the Ru-UCN1 complex presented a solid caspase activation, which suggests being an attractive anticancer drug.

Despite the promising results presented by ruthenium complexes, several obstacles need to be overcome to understand what their mechanism of action is and to maintain their anticancer activity.

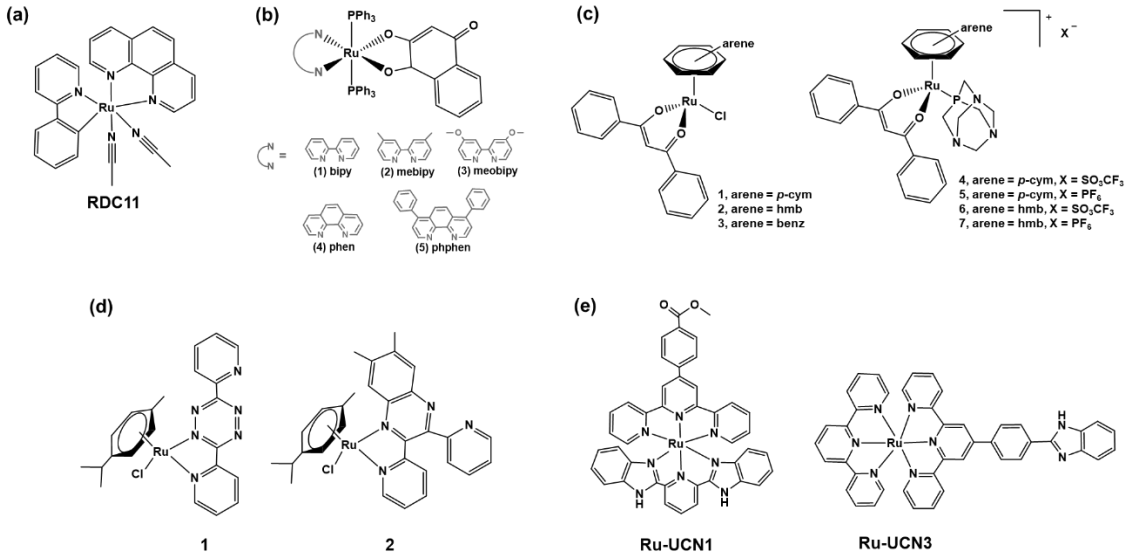

Figure 15. Ruthenium complexes structures under development: (a) RDC11 complex synthesized by Gaiddon *et al.*,[290] (b) five ruthenium complexes derivatives prepared by Batista *et al.*,[291] (c) seven ruthenium arene complexes prepared by Pettinari *et al.*,[292] (d) two ruthenium complexes synthesized by Fernández *et al.*,[293] (e) Ru-UCN1 and Ru-UCN3 complexes prepared by Bernal *et al*.[294]

2.3.2.2.3. Ruthenium complexes in the clinical and preclinical phase

In the early 1990s the anticancer activity of NAMI-A ((ImH)[*trans*-$RuCl_4$(DMSO-S(Im)], Im = imidazole), a Ru(III) coordination compound was discovered.[229] NAMI-A and KP1019/1339 ((IndH)[*trans*-$RuCl_4(Ind)_2$], KP1019; Na[*trans*-$RuCl_4(Ind)_2$], KP1339/IT-139, Ind = indazole) were the first Ru(III) complexes that reached the clinical phase (structures in Figure 16).[295]

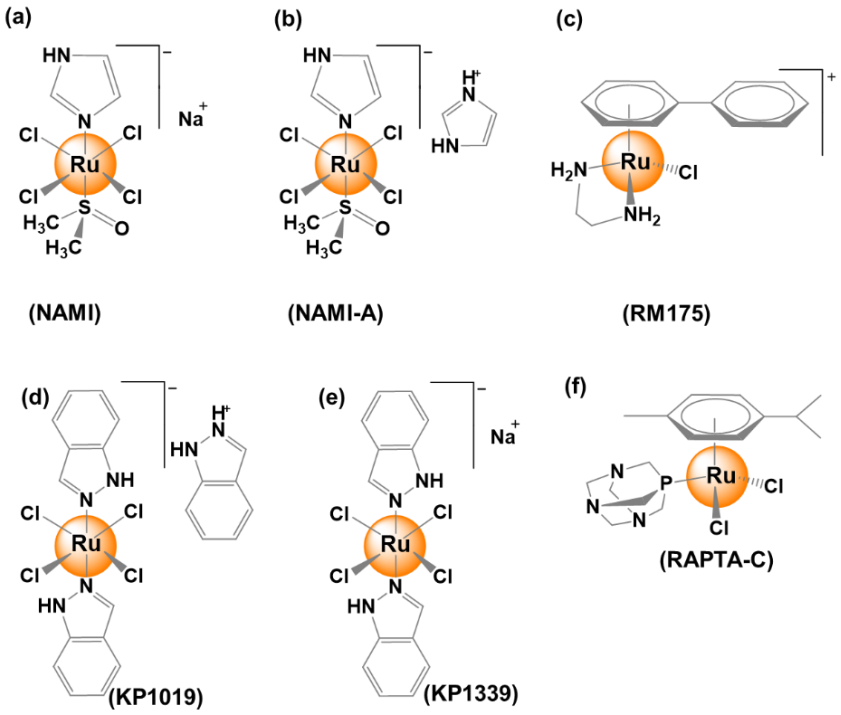

Figure 16. Ruthenium complexes most explored as anticancer metallodrugs candidates: (a) NAMI, (b) NAMI-A, (c) RM175, (d) KP1019, (e) KP1339 (also known as IT139), and (f) RAPTA-C.

NAMI-A complex is an antimetastatic compound with low cytotoxicity that when replaced with imidazolium salt presents excellent water solubility, an improved synthesis, and better stability in the solid state because when in solution it suffers aquation that is deeply dependent on pH.[229,295] The *in vitro* and *in vivo* studies of NAMI-A showed it to be less cytotoxic than cisplatin against several cancer cell lines with IC_{50} values at a millimolar range.[296,297] However, NAMI-A presented high toxicity in several leukemia cell lines, both myeloid and lymphoid, at low micromolar concentrations.[298] NAMI-A was also able to reduce the growth of lung metastases and tumor growth.[299,300] To improve its therapeutic effect, NAMI-A can have a synergistic behavior when used with anticancer drugs such as cisplatin, doxorubicin, 5-fluorouracil, and gemcitabine.[229,301,302] Clinical studies using NAMI-A showed that in some patients the disease was stabilized, with low to moderate adverse effects.[302,303] Despite all good expectations, NAMI-A did not proceed to clinical phase 2 due to low treatment efficacy and to side effects like nausea, vomiting, and diarrhea with patients claiming that the treatment was exhausting.[295,304] KP1019 was also evaluated against several chemosensitive and chemoresistant cell lines and presented IC_{50} values of 56 µM to 179 µM.[305] Results showed that a fast KP1019 resistance was unlikely because the resistance levels of KP1019 were considered low. Other *in vitro* studies show that the KP1019 complex was moderately cytotoxic, even compared to the sodium salt KP1339/IT-139, and *in vivo* models presented a tumor volume reduction of up to 95%, exhibiting to be an extremely active compound.[295,304] But KP1019 also failed clinical studies due to its deficient water solubility, acute side effects, and reduced efficacy. As a result, to improve the solubility of KP1019, KP1339/IT-139 (Figure 16d and Figure 16e) was developed, a sodium salt complex recently assessed in clinical trial phase 1 with controllable side effects.[304,306,307]

Other ruthenium complexes well-known for their anticancer properties are RM175 ([Ru(biphenyl)Cl(en)]$^+$, en=1,2-ethylenediamine) and RAPTA-C (1,3,5-triaza-7-phosphaadamantane (PTA)) (Figure 16c and 15f, respectively).[259] The RM175 complex was developed in 2001 by Peter J. Sadler and collaborators.[308] This ruthenium compound, being a Ru(II) complex, binds to the guanines in the DNA thus increasing the DNA binding affinity to the complex, as well as inhibits the matrix metalloproteinase-2 (MMP-2).[259] The RM175 complex acts by leading cells to apoptosis, preventing progression of the cell cycle and interfering with DNA replication.[259] *In vitro* studies showed that RM175 presented anticancer activity and reduced metastasis against MCa mammary carcinoma.[309] On the other hand, RM175 increased the resistance of the MDA-MB-231 cell line. Other studies, displayed that RM175 had IC_{50} values similar or higher than cisplatin in non-small-cell lung cancer cell lines and in the A2780 cell line, and was active in *in vivo* studies.[310,311] Initial studies of RAPTA-C showed that the damage in pBR322 DNA was pH-dependent, which may be used for selective targeting in cancer cells, but *in vivo* studies displayed a 50-75% tumor growth inhibition.[259] *In vitro* and *in vivo* experiments showed that even when IC_{50} values werehigher than cisplatin, RAPTA-C was able to reduce tumor growth.[312,313]

Despite all the potential that ruthenium compounds have demonstrated as anticancer drugs and the possibility of them becoming an alternative to platinum compounds, as far as we know, none of the ruthenium complexes have been approved until now for clinical use by any of the official drug regulatory authorities.

2.3.2.2.4. Ruthenium metallodendrimers under development

Additionally, ruthenium complexes have been coordinated to dendrimers as carriers, which can enhance the delivery of the metallodrug to aspecific location, reduce side effects, and improve therapeutic efficiency. Our group previuosly prepared two cyclopentadienyl ruthenium poly(alkylidenimine)-based metallodendrimers and evaluated them against several cancer cell lines and human mesenchymal stem cells (hMSCs).[314] The two metallodendrimers showed high anticancer activity against the tumor cell lines, specifically to the cisplatin-resistant cancer cell line (A2780cisR).

Gregory S. Smith and collaborators prepared PPI dendrimers functionalized with mono- and multinuclear Ru(II) arene complexes and tested them against ovarian cancer cell lines.[85] The DNA binding studies indicated that the Ru(II) complexes increased DNA binding with the multinuclear complexes relative to the mononuclear complexes. Moreover, the antiproliferative activity of the multinuclear metallodendrimers was more effective than cisplatin. The same group developed four different generations of *N,N*-ruthenium(II)-ethylene-glycol-derived metallodendrimers.[315] The prepared metallodendrimers were evaluated against cancer cell lines, and the results demonstrated that the lowest generations presented no activity. However, the higher generations were active in the cancer cell lines.

Francisco J. de la Mata and collaborators developed carbosilane metallodendrimers bearing Ru(II) arene complexes and evaluated their ability to inhibit Cathepsin-B, a marker for numerous types of tumors and implicated in metastasis and tumor progression.[316] The results showed that these

metallocompounds interacted with HSA and that they were able to inhibit Cathepsin-B with an IC_{50} in the same range of RAPTA-C and RAPTA-T ($Ru(\eta^6\text{-}C_6H_5Me)(PTA)Cl_2$). This group also prepared another family of ruthenium metallodendrimers using carbosilane dendrons with N-, NH_2-donor monodentate and N,N-chelating ruthenium complexes with potential as anticancer agents against a leukemia cell line (HL60).[317] In this study, generation 0 of these metallodendrimers was most effective, while generation 1 was more active towards the cancer cell line with similar IC_{50} values between the cell lines relative to generation 0 that presented a higher IC_{50} for the non-cancer cell line. The same group also used ruthenium metallodendrimers as a transporter to deliver anticancer siRNA.[318] The results displayed that the ruthenium metallodendrimers were able to transfect cancer cells with the siRNA and protect the siRNA from nuclease degradation. Recently, they published an article where ruthenium cyclopentadienyl metallodendrimers were prepared for the treatment of advanced prostate cancer.[319] The prepared metallodendrimers showed an unusual anticancer activity towards several cancer cell lines and induced apoptosis on an advanced prostate cancer cell line. Moreover, the ruthenium cyclopentadienyl metallodendrimers inhibited tumor growth with nontoxic effects.

Table 1 summarizes the IC_{50} values of the metallodendrimers previously described for each group. The IC_{50} concentrations of the ruthenium metallodendrimers in the A2780 and A2780cisR cell lines showed that the metallodendrimers developed by our group[314] were more effective than the metallodendrimers prepared by Gregory S. Smith[85,315] with concentrations at the nanomolar range. The same was observed with the metallodendrimers prepared by our group and the ones prepared by Francisco J. de la Mata's group. More than the generation and the number of ruthenium complexes functionalized into the dendrimer, the type of ruthenium complexes seems to play an essential role in the anticancer potential of these macromolecules.

Table 1. Summary of the metallodendrimers, ruthenium complex, type of dendrimer used for coordination, metal centers per dendrimers, cell lines tested, and IC_{50} values of each group mentioned.

Metallodendrimer reference	Ruthenium complex/type of dendrimer	Metal centers	Cell line	IC_{50}, μM	Reference
3	Ru(II)-cyclopentadienyl PPI	4	Caco-2 CAL-72 MCF-7 A2780 A2780cisR	3.4 0.6 2.5 0.1 0.3	Rodrigues *et al.*[314]
4		4	Caco-2 CAL-72 MCF-7 A2780 A2780cisR	3.2 1.4 3.0 0.2 0.3	
5	Ru(II) *p*-cym PPI	4	A2780 A2780cisR	>200 >200	Smith *et al.*[85]
6	Ru(II) HMB PPI	4	A2780 A2780cisR	32 42	
7	Ru(II) *p*-cym PPI	8	A2780 A2780cisR	23 76	
8	Ru(II) HMB PPI	8	A2780 A2780cisR	4 4	

Table 1. (*Cont.*) Summary of the metallodendrimers, ruthenium complex and type of dendrimer used for coordination, metal centers per dendrimers, cell lines tested, and IC_{50} values of each group mentioned.

Metallodendrimer reference	Ruthenium complex/type of dendrimer	Metal centers	Cell line	IC_{50}, μM	Reference
5	Ru(II) *p*-cym PPI	4	A2780 A2780cisR	>200 >200	Smith *et al.*[85]
6	Ru(II) HMB PPI	4	A2780 A2780cisR	32 42	
7	Ru(II) *p*-cym PPI	8	A2780 A2780cisR	23 76	
8	Ru(II) HMB PPI	8	A2780 A2780cisR	4 4	
1	Ru(II) arene PPI	4	A2780 A2780cisR	25.8 50.0	Smith *et al.*[315]
2		8	A2780 A2780cisR	>100 >100	
3		16	A2780 A2780cisR	16.7 19.0	
4		32	A2780 A2780cisR	5.0 17.3	
14	Ru(II) *p*-cym carbosilane	4	HeLa MCF-7 HT-29 MDA-MB-231	4.4 2.5 3.3 4.9	de la Mata *et al.*[316]
15		8	HeLa MCF-7 HT-29 MDA-MB-231	9.1 3.4 7.0 6.7	
17		4	HeLa MCF-7 HT-29 MDA-MB-231	8.1 6.9 5.6 6.1	
18		8	HeLa MCF-7 HT-29 MDA-MB-231	6.9 8.5 13.4 10.1	
CRD13	Ru(II) *p*-cym carbosilane	4	HL-60	11.57	de la Mata *et al.*[317]
CRD14		4		12.05	
CRD32		4		12.01	
CRD27		8		12.94	
CRD28		8		29.81	
7	Ru(II)-cyclopentadienyl carbosilane	1	HeLa HCC1806 MCF-7 PC-3 HT-29	18.3 23.7 26.4 57.3 59.3	de la Mata *et al.*[319]
8		4	HeLa HCC1806 MCF-7 PC-3 HT-29	6.3 2.2 10.3 8.3 11.4	
9		8	HeLa HCC1806 MCF-7 PC-3 HT-29	4.5 2.3 14.9 6.6 9.1	

2.4. Dendrimers and metallodendrimers in preclinical and clinical trials

Several dendrimer-based materials have been patented in recent years. Ana Paula Pêgo and collaborators developed a biodegradable and biocompatible dendrimer to be used as a delivery system for nucleic acids.[320] Jean-Pierre Majoral and Anne-Marie Caminade have submitted several dendrimer-related patents. They have developed different families of phosphorous dendrimers for the treatment of inflammatory diseases,[321] as transfection agents,[322] for immobilizing molecules of interest (such as nucleic acids, polypeptides, lipids, and proteins),[323] to stimulate cell growth or to activate cells in culture.[324] They have also developed new dendritic compounds for ocular drug delivery.[325] In this case, preclinical studies showed no irritation when drops of the dendrimers solution were added into the rabbit eye.

The dendrimers and metallodendrimers presently in the clinical phase are used as nanocarriers, as detection agents or as therapeutic agents. Most of the therapeutic agents that reach clinical trials often fail, even if they are shown to be effective in *in vitro* tests and animal models.[326] These failures can be due to the biodistribution of the drug, where insufficient drug concentration reaches the target site, as well as the dose-limit toxicity.[326] As mentioned before, VivaGel®, a naphthalene disulfonic acid conjugated to a poly-L-lysine (PLL) dendrimer, used for the treatment and prevention of bacterial vaginosis, has already been approved in Europe, Asia, and Australia. However, it is still awaiting approval by the US FDA.[327,328] At present, there are several dendrimer-based materials for research purposes in the pharmaceutical industry, mainly with PAMAM and PLL dendrimers.[329] Stratus® CS 200 Acute Care™ developed by Dade Behring, a Siemens Healthineers Global company, is a PAMAM dendrimer-based immunoassay for the diagnosis of myocardial infarction in patients with acute chest pain.[330,331] Qiagen company developed a gene transfection reagent for gene delivery (SuperFect®) based on PAMAM dendrimers.[332] Priofect® (now NanoJuice®) is a PAMAM dendrimer-based DNA transfection kit developed by Starpharma for gene transfection.[333] Bayer Schering Pharma AG developed a PLL dendrimer with 24 Gd-DOTA complexes (Gadomer-17) as a promising contrast-enhanced MRI agent.[334,335] Alert Ticket™ is a dendron-based compound developed by the US Army Research Laboratory for anthrax detection.[329,336,337]

Currently, in the clinical phase, there are quite a few dendrimer-based nanomaterials in study. OP-101 is a dendrimer-based drug for the treatment of adrenoleukodystrophy (ALD) developed by Orpheris that finished phase I clinical trials and will start phase 2 and 3.[338–340] Starpharma has now three dendrimer-based anticancer drugs in clinical trials, DEP™ docetaxel in clinical phase 2, DEP® cabazitaxel showed positive results in clinical phase 1 and now progressed to phase 2, and DEP® irinotecan is in clinical phase 1/2.[341–343] The conjugated PLL-based dendrimers, DEP™ docetaxel, presented a higher anticancer activity compared to free docetaxel (about 40-fold when compared to the free drug).[344]

To the best of our knowledge, the first metallodendrimer in the clinical stage is a rhenium complex associated with a dendrimer for the treatment of liver cancer, which is currently in clinical phase 1.[345] The treatment is performed by *in situ* and intratumoral injection of inoperable liver cancers. This rhenium metallodendrimer known as "[^{188}Re]rhenium-ImDendrim" (rhenium-nitro-imidazolemethyl-1,2,3-triazol-

methyl-di-(2-pycolyl)amine)) is based on a generation 5 poly-L-lysine dendrimer with a radioactive nitro-imidazole derived ligand *(*Figure 17).[346]

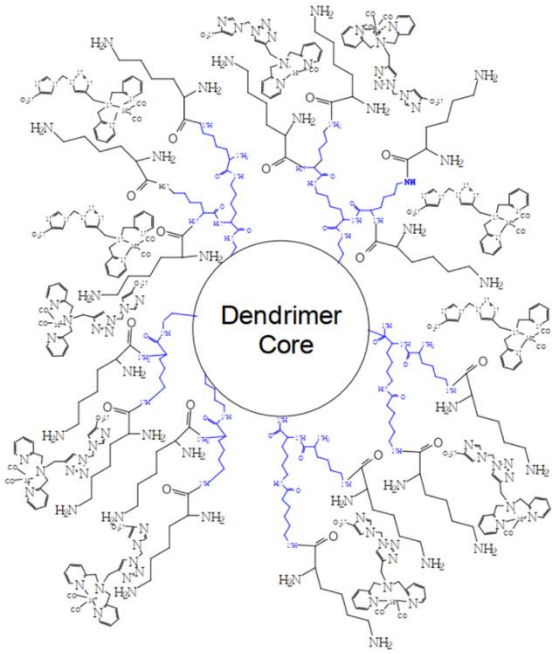

Figure 17. Structure of the rhenium metallodendrimer, ^{188}Re-ImDendrim (adapted from reference 346).

3. General objectives of the thesis

The fundamental goal of this thesis was to prepare and characterize poly(alkylidenamine)-based dendrimers and metallodendrimers against HIV infection and for anticancer applications. For this, we focused on the development of a nanocarrier, such as the poly(alkylidenamine)-based dendrimer family, able to be negatively charged or capable of transporting metal complexes.

Four different terminal groups of the dendrimers were synthesized: nitrile, amine, carboxylate, and sulfonate. The dendrimers were coordinated with either a ruthenium cyclopentadienyl complex ($[Ru(\eta^5\text{-}C_5H_5)(PPh_3)_2]^+$) or cisplatin ($[Pt(NH_3)_2(Cl)_2]$), avoiding by using this approach the concerns associated with metallodrugs and also improving the delivery efficiency for anticancer therapy. Their anticancer efficacy was evaluated against a representative set of cancer cell lines (A2780, A2780cisR, MCF-7, CAL-72, Caco-2, U-87 MG, and hMSC cells). The antiviral behavior of the anionic dendrimers with carboxylate and sulfonate terminal groups was assessed against HIV-1 infection using R5-HIV-1 and X4-HIV-1. Their mechanism of action and the antiviral potential were also determined.

The experimental part of this thesis is divided into three chapters, according to the final application and metal complex used. In more detail:

a) The first goal (Chapter 2) was to prepare low generation (1 to 3) anionic poly(alkylidenamine) dendrimers as potential antiviral agents. The generation 1, 2, and 3 dendrimers with carboxylate and sulfonate terminal groups were characterized by Nuclear Magnetic Resonance (NMR), Fourier Transformed Infrared Spectroscopy (FT-IR), Mass Spectrometry (MS), and Zeta potential measurements. Furthermore, degradation studies of the first generation of each dendrimer at 25°C were evaluated by ^{1}H-NMR. Their biocompatibility was studied using TZM.bl cells, and their antiviral efficacy was assessed using R5-HIV-1 and X4-HIV-1 isolates. The mechanism of action as well as the *in vivo* biocompatibility was evaluated using BALB/c mice.

b) The second goal (Chapter 3) was to prepare low generations of the nitrile terminated poly(alkylidenamine) dendrimers (G0 to G2) and to functionalize the generation 0 and 1 with $[Ru(\eta^5\text{-}C_5H_5)(PPh_3)_2]^+$ moieties and to evaluate their behavior against HIV-1 infection. The generation 0 and 1 dendrimers with nitrile terminal groups were used to coordinate the ruthenium moiety. All dendrimers and metallodendrimers were characterized by NMR, FT-IR, MS, and Elemental Analysis (EA). Afterwards, their biocompatibility was assessed with the TZM.bl cell line to obtain non-toxic concentrations and to test their anti-HIV-1 activity.

c) Chapter 4, generation 2 ruthenium poly(alkylidenamine)-based metallodendrimer was prepared and characterized. The G2Ru metallodendrimer was characterized by NMR, FT-IR, Ultraviolet-visible spectroscopy (UV-Vis), and MS. In this chapter, generation 0, 1, and 2 metallodendrimers were evaluated as potential anticancer metallodrugs. Additionally, in Chapter 4, stability studies were performed using ^{1}H- and ^{31}P-NMR at three different temperatures (4, 25, and 37°C). Subsequently, the antitumor activity of each metallodendrimer was quantitatively analyzed against several cancer cell lines (A2780, A2780cisR, MCF-7, CAL-72, Caco-2, U-87 MG) and a non-cancerogenic cell line hMSCs using a cell metabolic activity assay. DNA binding assays were

performed with the metallodendrimers and CT-DNA. The hemolytic activity was also evaluated using human blood. The reactive oxygen species (ROS), the mitochondrial membrane potential, the cell cycle, and apoptosis were assessed by flow cytometry.

d) The fourth aim (Chapter 5) was to prepare low generations (1 and 2) of the anionic poly(alkylidenamine) dendrimers and their functionalization with cisplatin to improve its anticancer efficacy. All metallodendrimers were characterized by NMR, FT-IR, MS. The preliminary results of their potential anticancer activity were evaluated against A2780 and MCF-7 cancer cell lines.

Chapter 2.

New poly(alkylidenamine) dendrimers as a microbicide against HIV-1 infection

*This Chapter is based on the following publication:

Maciel, D.; Guerero-Beltrán, C.; Ceña-Diez, R.; Tomás, H.; Muñoz-Fernández, M.A.; Rodrigues, J. New poly(alkylideneamine) dendrimers as a microbicide against HIV-1 infection. *Nanoscale* **2019**,11, 9679-9690. doi: 10.1039/C9NR00303G.

Chapter 2. New poly(alkylidenamine) dendrimers as a microbicide against HIV-1 infection

1. Introduction

Although the advent of combined antiretroviral therapy has been crucial for controlling the human immunodeficiency virus type-1 (HIV-1) infection and reducing morbidity and mortality worldwide, a cure for HIV/AIDS is still elusive, and prevention remains crucial.[347] The Joint United Nations Program on HIV/AIDS (UNAIDS) estimates that 38 million people were living with HIV-1 worldwide at the end of 2019.[174] Moreover, HIV-1 sexual transmission (HST) is responsible for around 80% of all infection cases, with women being a group particularly affected due to their more vulnerable socio-economic situation (they correspond to more than 50% of infected individuals).[348] In the last years, the use of long-lasting, female-controlled, and efficacious topical microbicides to decrease and control the HIV-1 epidemic among women has strongly emerged.[349,350] In this scope, microbicides have been developed to target viral surface proteins, such as gp120, for the direct binding and inactivation of HIV-1. Interestingly enough, the most researched systems in this kind of microbicides have been dendrimers.[197,351–355]

Nanomaterials, such as dendrimers, present characteristics that make them very attractive to the biomedical field. The number of peripheral chemical groups in dendrimers is usually relatively high (multivalency) and this is maybe one of their most valuable properties having in view possible biomedical applications, mainly when recognition processes are involved.[75] Indeed, the use of multiple ligands may compensate for a low binding activity of the ligand towards the receptor (low affinity), leading to an improved avidity (the combined effect of multiple ligands). Anionic dendrimers, specifically with sulfonate groups in the periphery, have shown promising results as antiviral agents.[218,356,357] The SPL7013, a fourth-generation dendrimer, is composed of a benzhydrylamine amide core linked to PLL branches capped with 32 anionic naphthalene disulfonate groups (BHA.$lys_{15}lys_{16}$($NHCOCH_2O$)1-(3,6-naphth(SO_3Na)$_{32}$ (BHA = benzhydrylamine)) (Figure 18).[358–360] The anionic groups are responsible for interacting with gp120.[188,357,360] This SPL7013 dendrimer has been developed commercially as a gel (VivaGel®) by Starpharma (Australia). However, the use of this microbicide was halted in early clinical trials due to safety issues.[361,362] As stated before, Starpharma gel (VivaGel® BV), is under FDA regulatory evaluation to obtain approval for the treatment and prevention of bacterial vaginosis (BV).[327,328]

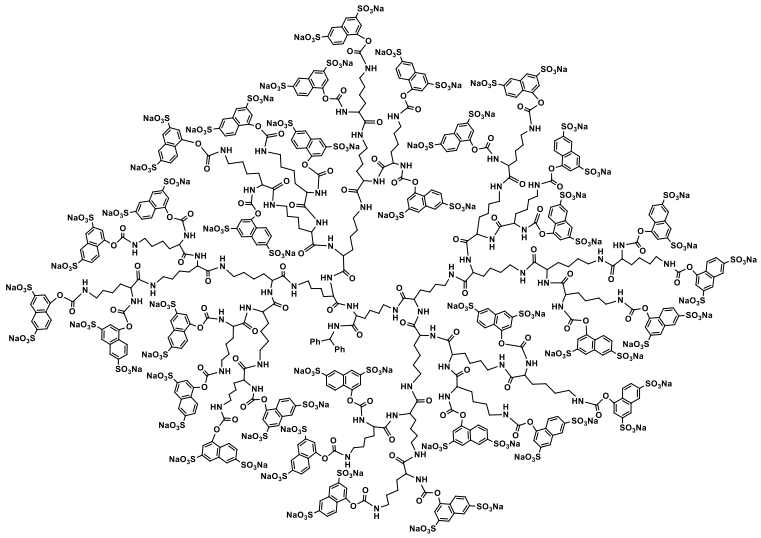

Figure 18. Structure of the SPL7013 dendrimer used in the preparation of VivaGel® (adapted from reference 360).

Other microbicide dendrimers sharing similar gp120 targeting ability have been developed, such as G2-S16, a second-generation carbosilane dendrimer capped with 16 sulfonate groups.[81] Promising results were obtained in a humanized mice model by treatment with a vaginal gel containing 3% w/v of G2-S16 dendrimer before intravaginal exposure to HIV-1. This vaginal gel loaded with G2-S16 dendrimer provided 84% of HIV-1 protection in comparison with no protection in the placebo gel group of humanized mice.[193,197,363]

Based on our previous teamwork[217,364–366] and on the fact that dendrimers having a long core carbon chain (in our case the 1,6-diaminohexane/Hexamethylenediamine) as a starting molecule present more flexibility, these molecules can be potentially used *in vitro* and *in vivo* to target proteins more efficiently at the nanometer scale.[367] We have now synthesized novel poly(alkylidenamine) dendrimers with carboxylate and sulfonate terminal groups, from the first to the third generation, aimed at evaluating their potential as inhibitors of HIV-1 activity. In this scope, studies were done with the variants R5-HIV-1 and X4-HIV-1 and the mechanism of action of the developed dendrimers was investigated (Figure 19).

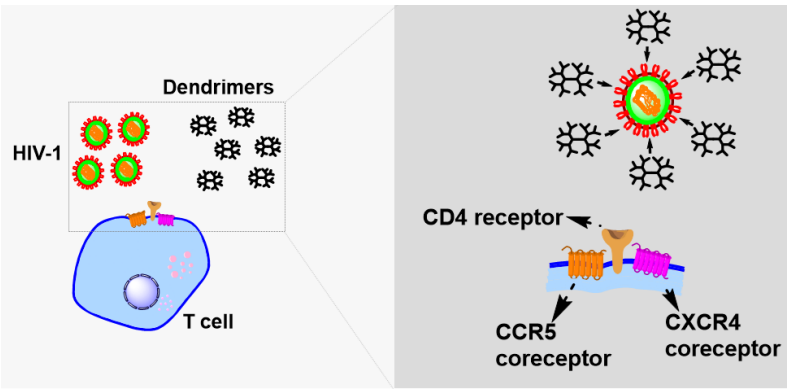

Figure 19. Schematic representation of the hypothetic mechanism of action of the anionic poly(alkylidenamine) dendrimers: in the left, a representation of the interaction of HIV-1 and the dendrimers with a T cell; on the right, an enlarged representation of the interaction (dendrimers go to the virus blocking the attachment of HIV-1 to the cell).

2. Materials and methods

2.1. Materials

All reagents were used as received unless otherwise reported. Sodium vinyl sulfonate was purchased from TCI. Methyl acrylate was bought from Acros Organics. Sodium hydroxide was obtained from Fisher Scientific. Methanol was bought from Fisher Chemical. Dialysis membranes (MWCO 100-500 Da, 500-1000 Da, and 3500 Da) were purchased from SpectrumLabs. The epithelial Hela-derived cell line TZM.bl (Cat# 8129, AIDS Reagent Program, Germantown, MD, USA), expressing CD4, CCR5, and CXCR4 co-receptors, and containing HIV-1 Tat-regulated reporter genes for firefly luciferase and β-galactosidase (β-gal) were used. These TZM.bl cells were modified to be extremely permissive to infection by most strains of HIV, such as primary or molecularly cloned viral isolates.[368] Virus stocks of R5-HIV-1_{NLAD8} and X4-HIV-$1_{NL4.3}$ were obtained by transient transfection of pNL(AD8) and pNL(4.3) plasmids (NIH AIDS Research and Reference Reagent Program), respectively, into 293T cells (American Type Culture Collection [ATCC], Manassas, VA, USA) as previously described.[356] Viral stocks were purified by centrifugation, and the viral titer was obtained using an HIV p24gag ELISA kit (Innotest® HIV, antigen mAb, Innogenetic, Ghent, Belgium).[217]

All the biological studies performed in this chapter were carried out at the Section of Immunology, *Laboratorio de Inmunobiología Molecular* at the *Hospital General Universitario Gregorio Marañón* (Madrid, Spain), under the support of the FCT Ph.D. grant and the project CYTED.

2.2. Dendrimer synthesis and characterization

As presented below (Scheme 2 and Figure 20), and detailed ahead, the preparation of the carboxylate and sulfonate dendrimers can be divided into three steps. First, we started by preparing the nitrile poly(alkylidenamine) dendrimers using a methodology previously developed by our team.[364] Next, the amine-terminated dendrimers were prepared through the reduction of the nitrile groups into primary amines by following the method developed by Marie-Christine Daniel *et al.* (Scheme 1) and described in section A.1.2.[369] Finally, in the last step, the carboxylate and sulfonate dendrimers were obtained using Michael addition according to the procedure described by Francisco J. de la Mata *et al*.[366] All dendrimers were characterized by NMR and FT-IR spectroscopies, mass spectrometry (ESI-TOF-MS), and zeta potential analysis.

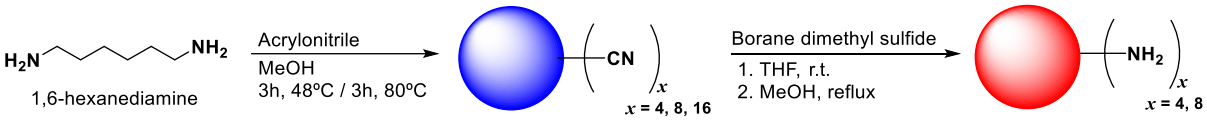

Scheme 1. Reaction scheme of the preparation of the nitrile and amine-terminated dendrimers.

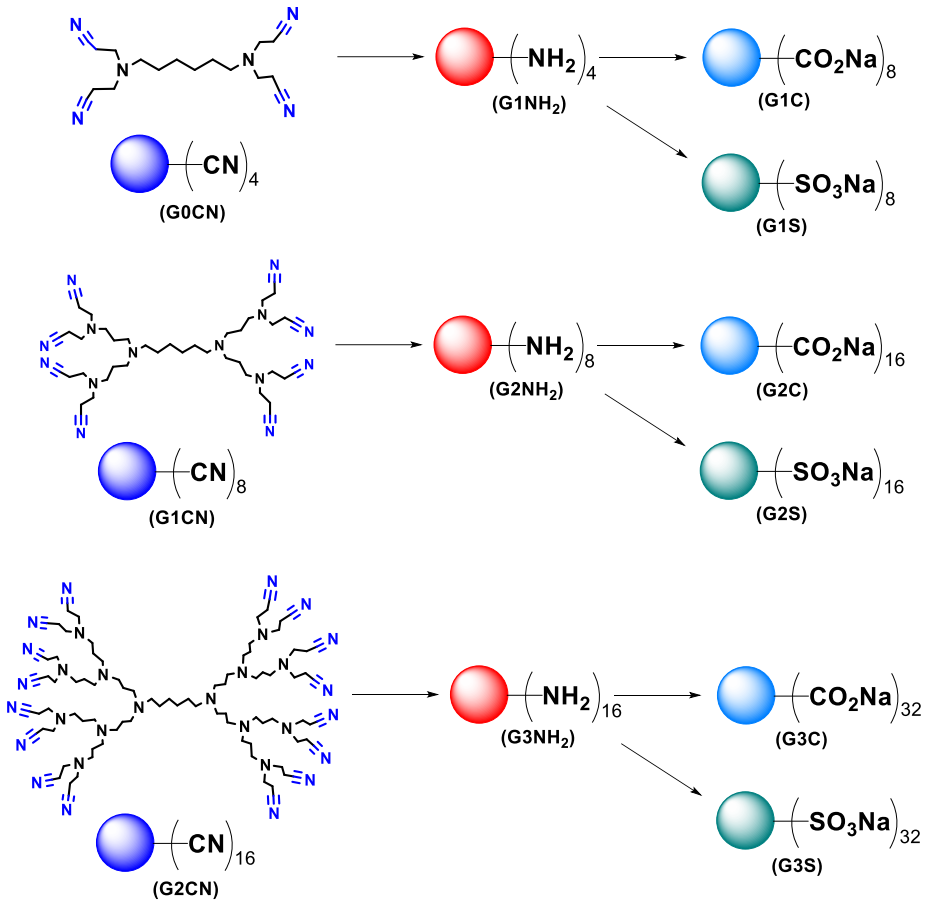

Scheme 2. General procedure for the synthesis of the carboxylate and sulfonate dendrimers.

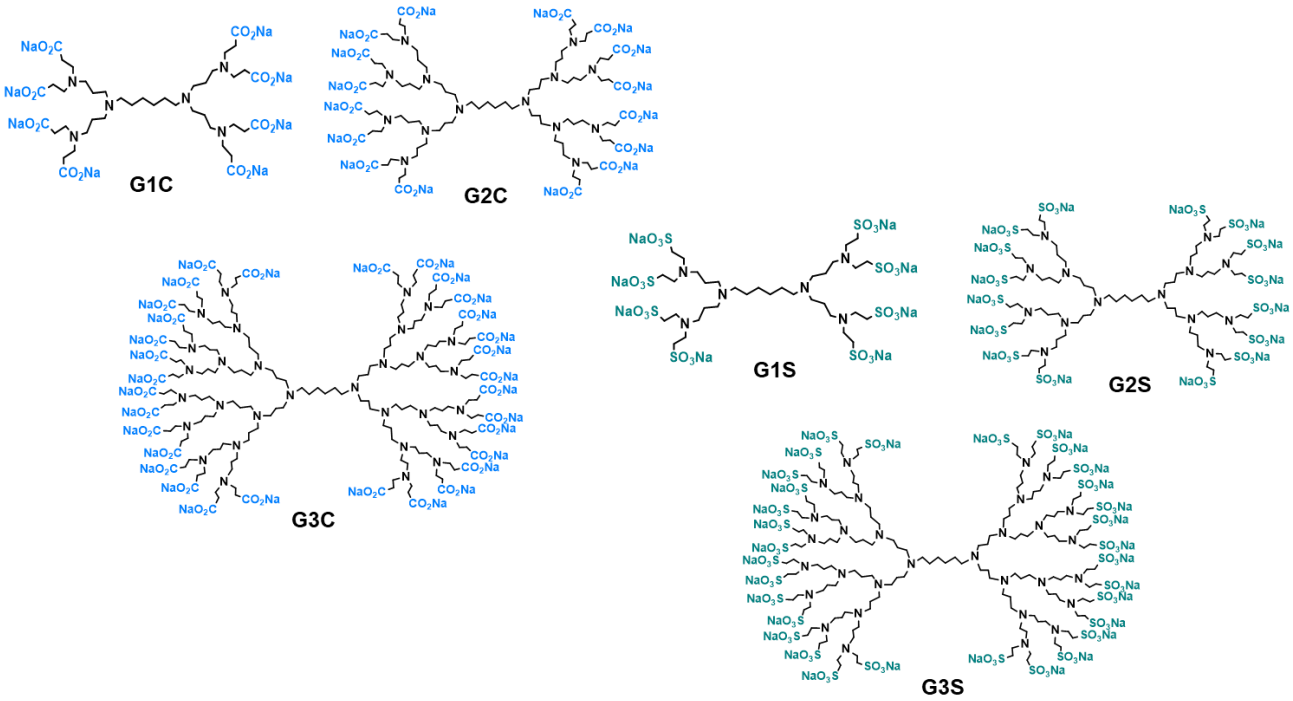

Figure 20. Structures of the carboxylate (G1C, G2C, and G3C) and the sulfonate (G1S, G2S, and G3S) poly(alkylidenamine) dendrimers.

2.2.1. Synthesis and characterization of GxCO$_2$Na dendrimers.

2.2.1.1. G1C dendrimer

At room temperature, the amine-terminated dendrimer G0NH$_2$ (1.3 g, 3.7 mmol) prepared as described before[369] (for the synthesis see annex section A.1.2.1), was dissolved in 8 mL of methanol. Methyl acrylate (3.7 mL, 41.5 mmol; 2.8 equiv. per amine group) was then added to the previous solution. The reaction mixture was then stirred overnight at 80°C under a nitrogen atmosphere. The solvent was removed under vacuum to obtain the methyl ester dendrimer as a clear oil with a yield of 71% (2.7 g). ^{1}H-NMR (400 MHz, D$_2$O) δ = 3. 63 (–CO$_2$**Me**), 2.99, 2.75 – 2.71 (–C**H**$_2$CO$_2$Me), 2.42 – 2.35, 1.54 – 1.24 ppm. ^{13}C-NMR (100 MHz, D$_2$O) δ = 173.10 (–**C**O$_2$Me), 54.14, 52.05 (–CO$_2$**Me**), 51.90, 51.57, 49.33, 32.56, 25.89, 24.58, 23.65 ppm. Only the relevant signals are presented.

To prepare the carboxylate dendrimers, a solution of sodium hydroxide (0.6 g, 14.6 mmol; 1.1 equiv. per carboxylate group) in 4 mL of methanol was added to the methyl ester dendrimer (1.7 g, 1.7 mmol) dissolved in 3 mL of methanol and this was stirred for 48 h at room temperature. The solvent was removed under reduced pressure, dissolved in distilled water, and purified with a dialysis membrane (MWCO 100-500 Da) for 1 day. The carboxylate dendrimers were obtained as white solids after lyophilization, washed with diethyl ether, and dried under vacuum with a yield of 87% (1.6 g). ^{1}H-NMR (400 MHz, D$_2$O) δ = 2.82 – 2.55, 2.36 (–C**H**$_2$CO$_2$Na), 1.95 – 1.32 ppm. ^{13}C-NMR (100 MHz, D$_2$O) δ = 180.47/180.45* (–**C**O$_2$Na, protonated*), 52.44, 50.53, 49.66, 49.06, 33.12, 25.84, 24.07, 22.77 ppm. FT-IR: ν = 2946.48 cm^{-1} (ν_{O-H}). TOF-MS (ESI-): *m/z* = 941.51 [M – 7Na + 6H]$^{-1}$, 919.52 [M – 8Na + 7H]$^{-1}$. Only the relevant signals are presented.

2.2.1.2. G2C dendrimer

The generation 1 of amine-terminated dendrimer G1NH$_2$ (0.5 g, 0.7 mmol) (prepared as described before;[369] for the synthesis see annex section A.1.2.2) was dissolved in 8 mL of methanol. Methyl acrylate (1.3 mL, 14.8 mmol; 2.8 equiv. per amine group) was then added to the previous solution at room temperature. The solution mixture was then stirred overnight at 80°C under a nitrogen atmosphere. The solvent was removed under vacuum to obtain the methyl ester dendrimer as a clear oil with a yield of 84% (1.2 g). ^{1}H-NMR (400 MHz, D$_2$O) δ = 3.63 (–CO$_2$**Me**), 2.95, 2.74 – 2.70 (–C**H**$_2$CO$_2$Me), 2.42 – 2.39, 1.57 – 1.24 ppm. ^{13}C-NMR (100 MHz, D$_2$O) δ = 173.10 (–**C**O$_2$Me), 51.80 (–CO$_2$**Me**), 51.63, 50.67, 49.21, 32.44, 26.39, 24.07, 23.27 ppm. Only the relevant signals are presented.

The carboxylate dendrimers were prepared using a solution of sodium hydroxide (0.3 g, 6.6 mmol; 1.1 equiv. per carboxylate group) in 4 mL of methanol that were added to the methyl ester dendrimer (0.8 g, 0.4 mmol) dissolved in 3 mL of methanol and stirred for 48 h at room temperature. The solvent was removed under reduced pressure, dissolved in distilled water, and purified with a dialysis membrane (MWCO 500-1000 Da) for 1 day. The carboxylate dendrimers were obtained as white solids after lyophilization, washed with diethyl ether, and dried under vacuum with a yield of 60% (0.5 g). ^{1}H-NMR (400 MHz, D$_2$O) δ = 3.11 – 2.51, 2.37 (–C**H**$_2$CO$_2$Na), 1.97 – 1.18 ppm. ^{13}C-NMR (100 MHz,

D_2O) δ = 178.68 (–**C**O_2Na), 51.92, 50.55, 49.53, 49.27, 31.68, 25.55, 23.28, 20.31 ppm. FT-IR: ν = 2953.63 cm^{-1} (ν_{O-H}), 1727.23 cm^{-1} ($\nu_{C=O}$). TOF-MS (ESI-): *m/z* = 939.57 [M – $C_3H_5O_2$ – 16Na + 13H]$^{-2}$. Only the relevant signals are presented.

2.2.1.3. G3C dendrimer

At room temperature, the G2 amine-terminated dendrimer $G2NH_2$ (0.5 g, 0.3 mmol) was dissolved in 8 mL of methanol.Methyl acrylate (1.3 mL, 13.9 mmol; 2.8 equiv. per amine group) was then added to the previous solution. The reaction mixture was then stirred overnight at 80°C under a nitrogen atmosphere. The solvent was removed under vacuum to obtain the methyl ester dendrimer as a clear oil with a yield of 78% (1.1 g). ^{1}H-NMR (400 MHz, D_2O) δ = 3.64 (–CO_2**Me**), 2.76 – 2.72 (–C**H**$_2$$CO_2$Me), 2.44 – 2.38, 1.55 – 1.23 ppm. ^{13}C-NMR (100 MHz, D_2O) δ = 173.13 (–**C**O_2Me), 51.91 (–CO_2**Me**), 51.64, 50.80, 49.28, 32.51, 24.49 ppm. Only the relevant signals are presented.

To prepare the carboxylate dendrimers, a solution of sodium hydroxide (0.2 g, 4.6 mmol; 1.1 equiv. per carboxylate group) in 4 mL of methanol was added to the methyl ester dendrimer (0.6 g, 0.1 mmol) dissolved in 3 mL of methanol and this was stirred for 48 h at room temperature. The solvent was removed under reduced pressure, and the product was dissolved in distilled water and purified with a dialysis membrane (MWCO 3500 Da) for 1 day. The carboxylate dendrimers were obtained as white solids after lyophilization, washed with diethyl ether, and dried under vacuum with a yield of 47% (0.3 g). ^{1}H-NMR (400 MHz, D_2O) δ = 3.35 – 2.53, 2.46 (–C**H**$_2$$CO_2$Na), 1.98 – 1.16 ppm. ^{13}C-NMR (100 MHz, D_2O) δ = 179.53/178.31* (–**C**O_2Na, protonated*), 49.94, 49.29, 45.64, 44.20, 32.32, 25.87, 22.54, 20.70 ppm. FT-IR: ν = 2954.49 cm^{-1} (ν_{O-H}). TOF-MS (ESI-): *m/z* = 1146.74 [M – $C_{93}H_{154}N_{15}Na_{16}O_3$ – 3Na + 1H]$^{-2}$. Only the relevant signals are presented.

2.2.2. Synthesis and characterization of GxSO$_3$Na dendrimers

2.2.2.1. G1S dendrimer

G0 amine-terminated dendrimer (1.4 g, 4.0 mmol) was dissolved in 3 mL methanol and sodium vinyl sulfonate (13.8 mL, 31.7 mmol; 2 equiv. per amine group) was added to the previous solution at room temperature. The reaction was stirred for 48 h at 120°C under nitrogen. The solvent was removed and the final product was purified using a dialysis membrane (MWCO 100-500 Da) for 1 day. The sulfonate dendrimers were obtained after lyophilization as white solids in gram scale 37% (2.0 g). ^{1}H-NMR (400 MHz, D_2O) δ = 3.22 – 3.04, 2.98 (–C**H**$_2$$SO_3$Na), 2.74, 2.62, 1.90 – 1.38 ppm. ^{13}C-NMR (100 MHz, D_2O) δ = 52.45, 50.72, 49.13, 46.76, 43.19 (–**C**H_2SO_3Na), 25.39, 25.17, 21.48, 20.50 ppm. FT-IR: ν = 1194.75 cm^{-1} ($\nu_{S=O}$), 1045.45 cm^{-1} ($\nu_{S=O}$). TOF-MS (ESI-): *m/z* = 622.76 [M – 8Na + 5H + K]$^{-2}$. Only the relevant signals are presented.

2.2.2.2. G2S dendrimer

At room temperature, the G1 amine-terminated dendrimer (0.5 g, 0.7 mmol) was dissolved in 3 mL methanol and sodium vinyl sulfonate (2.8 mL, 6.5 mmol; 2 equiv. per amine group) was added to the solution. The reaction mixture was stirred for 48 h at 120°C under nitrogen. The solvent was removed and the final product was purified using a dialysis membrane (MWCO 500-1000 Da) for 1 day. The sulfonate dendrimers were obtained after lyophilization as white solids in gram scale 48% (0.9 g). ^{1}H-NMR (400 MHz, D_2O) δ = 3.11 – 3.09, 2.99 (–C**H**$_2$SO$_3$Na), 2.71 – 2.58, 1.85 – 1.40 ppm. ^{13}C-NMR (100 MHz, D_2O) δ = 52.45, 50.53, 47.25, 46.64, 43.06 (–**C**H$_2$SO$_3$Na), 25.55, 23.44, 22.36, 20.44 ppm. FT-IR: ν = 1188.10 cm^{-1} ($\nu_{S=O}$), 1043.79 cm^{-1} ($\nu_{S=O}$). TOF-MS (ESI-): m/z = 441.79 [M – $C_{37}H_{74}N_7Na_8O_{24}S_8$ – 5Na + 2H]$^{-3}$, 691.75 [M – $C_{37}H_{74}N_7Na_8O_{24}S_8$ – 4Na + 2H + CH_3OH]$^{-2}$. Only the relevant signals are presented.

2.2.2.3. G3S dendrimer

At room temperature, the G2 amine-terminated dendrimer (0.3 g, 0.2 mmol) was dissolved in 3 mL methanol and sodium vinyl sulfonate (2.8 mL, 6.5 mmol; 2 equiv. per amine group) was added to the previous solution. The reaction was stirred for 48 h at 120°C under nitrogen. The solvent was removed and the final product was purified using a dialysis membrane (MWCO 3500 Da) for 1 day. The sulfonate dendrimers were obtained after lyophilization as white solids in gram scale 76% (0.9 g). ^{1}H-NMR (400 MHz, D_2O) δ = 3.25 – 3.11, 3.04 (–C**H**$_2$SO$_3$Na), 2.66, 1.88 – 1.31 ppm. ^{13}C-NMR (100 MHz, D_2O) δ = 52.61, 50.13, 47.51, 46.90, 43.12 (–**C**H$_2$SO$_3$Na), 25.72, 23.29, 21.34, 20.36 ppm. FT-IR: ν = 1186.19 cm^{-1} ($\nu_{S=O}$), 1042.64 cm^{-1} ($\nu_{S=O}$). TOF-MS (ESI-): *m/z* = 1333. 97 [M – $C_{77}H_{154}N_{15}Na_{16}O_{48}S_{16}$ – 12Na + 10H + CH_3OH + 2H_2O]$^{-2}$, 1369.93 [M – $C_{77}H_{154}N_{15}Na_{16}O_{48}S_{16}$ – 13Na + 11H + H_2O]$^{-2}$, 1571.98 [M – $C_{77}H_{154}N_{15}Na_{16}O_{48}S_{16}$ – 8($C_2H_4NaO_3S$) – 3Na + 5H]. Only the relevant signals are presented.

2.3. Dendrimer stability studies

Stability studies for the carboxylate and sulfonate dendrimers were performed using NMR spectroscopy. The ^{1}H-NMR spectra were obtained by dissolving the prepared dendrimers in D_2O. Initial spectra were done at 25°C. Then, the NMR tube solutions were incubated at 4°C and NMR spectra were acquired at different periods at the probe temperature (25°C).

2.4. Dendrimer zeta potential measurements

The zeta potential of the carboxylate and sulfonate dendrimers was measured using Zetasizer Nano ZS equipment. All dendrimers were dispersed in nuclease-free water at a concentration of 1 mg/mL. The measurements were done for three independent experiments corresponding to 20 runs each. Disposable folded capillary cells were used for the zeta potential analysis.

2.5. Biological assays

2.5.1. Cell viability assays

TZM.bl cells were seeded in 96-well plates at a density of 15 x 10^3 cells/well. After that, cells were treated with G1C, G2C, G3C, G1S, G2S and G3S dendrimers, each prepared at a stock concentration of 250 μM in nuclease-free water and diluted to a range concentration of 0.01 μM to 25 μM. After 48 h of incubation, TZM.bl cell viability was quantified by the measurement of the metabolic activity of the cells in culture through the (3-(4,5-dimethylthiazol-2-yl)-2,5-diphenyl-2H-tetrazolium bromide) (MTT) assay (Sigma-Aldrich). Briefly, the cell culture medium was replaced with OPTI-MEM containing MTT (0.5 mg/mL). The formazan crystals obtained were dissolved in DMSO, and the absorbance was measured at 570 nm with a reference of 690 nm in a microplate reader (Synergy 2 Multi-Detection Microplate Reader, BioTek Instruments, Inc.).

2.5.2. Anti-HIV-1 activity of dendrimers

TZM.bl cells were seeded in 96-well plates (15 x 10^3 cells/well). After 24 h, the cells were pre-treated with the dendrimers at maximum non-toxic concentrations for 1 h at 37 °C. Next, cells were infected with R5-HIV-1_{NLAD8} or X4-HIV-$1_{NL4.3}$ isolates (15 ng/10^6 cells). After 2 h post-infection, the cells were washed twice with sterile PBS to remove unbound viruses and compounds. Luciferase activity was measured after 48 h post-infection to quantify the extension of HIV-1 infection (Luciferase Assay System kit, Promega Corporation, Fitchburg, WI, USA).

2.5.3. Time-of-addition experiment

TZM.bl cells were infected with 15 ng/10^6 cells of the R5-HIV-1_{NLAD8} strain for 2 h at 37°C. The dendrimer solutions at 25 μM and the controls, T-20 (20 μM), TDF (1 μM), and RAL (1 μM), were added at different time points post-infection. HIV-1 infection was quantified after 48h by measuring luciferase activity.

2.5.4. Inhibition of virus-cell attachment assay

TZM.bl cells were cultured as mentioned above. The cells were cooled at 4°C for 30 min before being treated with the dendrimers for 1 h at 4°C. The cells were then infected with the R5-HIV-1_{NLAD8} and X4-HIV-$1_{NL4.3}$ viruses (15 ng/10^6 cells) for 2 h at 4°C. Thereafter the cells were washed twice with sterile PBS and fresh medium was added to the wells. After 48 h of incubation at 37°C, HIV-1 infection on TZM.bl cells was evaluated as mentioned above.

2.5.5. Evaluation of the direct effect of the dendrimer on viral particles

In order to assess the direct effect of the dendrimers on the HIV-1 particles, cell-free virus (15 ng/10^6 cells) was incubated with the G1C and G1S dendrimers for 1 h at 4 °C. Afterwards, the cells were infected with dendrimer-virus solutions. At 2 h post-infection, they were washed twice with PBS and fresh medium was then added. The luciferase assay was performed 48 h post-infection to quantify the extent of HIV-1 infection.

2.5.6. Dendrimer-cell binding assay

TZM.bl cells were treated with the G1C and G1S dendrimers for 1 h. Then, cells were washed twice with sterile PBS and infected with R5-HIV-1_{NLAD8} or X4-HIV-$1_{NL4.3}$ isolates (15 ng/10^6 cells). After 2 h, the cells were washed to remove unbound viruses. After 48 h, HIV-1 infection of the TZM.bl cells was quantified by the luciferase assay.

2.5.7. pH effect on dendrimer anti-HIV-1 activity

The G1C and G1S dendrimers were incubated at room temperature in various pH solutions prepared in sterilized distilled water (ranging from 3.0 to 8.0 values) for 1 h. TZM.bl cells were pre-treated for 1 h with the G1C and G1S dendrimers, and subsequently, the cells were infected with R5-HIV-1_{NLAD8} isolates (15 ng/10^6 cells) for 2 h. After 48 h, the HIV-1 infection on TZM.bl cells was measured using the luciferase assay.

2.5.8. Vaginal irritation assay in BALB/c mice

To know if the dendrimers could cause vaginal irritation, a vaginal irritation assay was performed in BALB/c mice for 7 days with the daily application of the dendrimers. Twelve female, 7 week old BALB/c mice with a weight of 20±3 g were used in the assay. G1C or G1S was added to 1% hydroxyethylcellulose (HEC) placebo gel to a final dendrimer concentration of 3% w/v. BALB/c mice were randomized into 4 groups of 3 mice per group. Group A (control) was treated vaginally only with 30 µl of 1% HEC gel, group B (irritation group) was treated vaginally with 4.5% nonoxynol-9 (N9) a nonionic surfactant in PBS, group C was treated with 1% HEC gel with G1C and group D was treated with 1% HEC gel with G1S. The four conditions were applied intravaginally in female BALB/c mice previously anesthetized with isoflurane. After 20h, the BALB/c mice were sacrificed and the vaginas were extracted and conserved in 4% (w/v) formaldehyde.

The presence of histological lesions in the mice vaginas was evaluated with hematoxylin-eosin staining. Samples were embedded in paraffin by passage through increasing degree alcohols, two baths of xylene, and then paraffin, before being placed in the paraffin mold. Subsequently, they were cut by using a semi-motorized microtome (RM2145 Leica) and processed for staining. For dewaxing, samples

were submitted to two baths of xylene (10 min) and three baths of descending order of alcohols (100%, 90%, and 70%) (5 min), before being stained with hematoxylin (Merck, Madrid, Spain) for 5 min and eosin (Merck, Madrid, Spain) for another 5 min. Post-eosin staining dehydration was performed with passage through increasing degree alcohols (70%, 90%, and 100%) and bath of xylene solution. Finally, they were mounted with DPX (Prolabo, Obregón, Mexico). The existence of an injury in the vaginal epithelium, inflammatory infiltrate, vascular congestion, and/or edema in the submucosa was evaluated in each histological sample. The scores assigned for each of these lesions were: 0 (no change) when no injury or the observed changes were within the normal range; 1 (minimum) when changes were sparse but exceeded those considered normal; 2 (light) when injuries were identifiable but with no severity; 3 (moderate) for a significant injury that could increase in severity; 4 (very serious) for injuries that occupy most of the analyzed tissue. These values were added up and determined the level of vaginal irritation as a minimum of 1-4, average 5-6, moderate 7-9, and severe 9+.[81] These animal studies were conducted and approved by the CBMSO Institutional Animal Care and Use Committee (CEEA-CBMSO, Madrid, Spain). All experiments were carried out following CEEA-CBMSO, National (Royal Decree 1201/2005), and the Directive 2010/63/EU of the European Parliament guidelines and regulations.

2.5.9. Statistical analysis

Statistical analysis was performed with GraphPad software Prism v.5.0 (GraphPad Software, San Diego, CA, USA). Calculation of the mean, standard deviation, standard error of the mean, and p-values was performed using Mann–Whitney U nonparametric test. A *p*-value ≤0.05 was considered statistically significant.

3. Results and discussion

3.1. Synthesis and characterization of the carboxylate and sulfonate dendrimers

The development of a microbicide able to protect against HIV-1 and capable of fighting its dissemination is still a huge necessity and a challenge for the scientific community. In the last years, nanomaterials based on dendrimers have been proposed as a viable strategy to reach the UNAIDS objective of zero infections.[193,370,371] Inspired by these promising works, we have prepared three generations of new dendrimers with carboxylate (G1C-G3C) and sulfonate (G1S-G3S) terminal groups based on nitrile-terminated poly(alkylidenamine) dendrimers and aimed at their use as potential microbicides against HIV-1 infection. The G1C, G2C, and G3C carboxylate dendrimers were successfully prepared with good to reasonable yields of 87%, 60%, and 47%, respectively. The same happened for the G1S, G2S, G3S sulfonate dendrimers, with yields of 37%, 48%, and 76%, respectively. The carboxylate and sulfonate dendrimers were characterized by ^{1}H- and ^{13}C-NMR and FT-IR spectroscopies, MS, and zeta potential techniques. Despite our efforts to remove all signals of solvents used in the purification (done by solvent-solvent extraction), they are still visible in the spectra. The

carboxylate and sulfonate dendrimers presented the expected characteristic signals of each compound. Characteristic signals at 2.36, 2.37, and 2.46 ppm, for the G1C (Figure 21), G2C (see annex Figure A9), and G3C (annex Figure A11) carboxylate dendrimers correspond to the protons near the carboxylate group. The signal around 180 ppm in the ^{13}C-NMR spectra of the G1C (Figure 22), G2C, and G3C carboxylate dendrimers correspond to the carbon of the carboxylate group (annex Figure A10 and Figure A12, respectively). G1S (Figure 23), G2S, and G3S sulfonate dendrimers show expected proton signals, respectively, at 2.98, 2.99, and 3.04 ppm (see annex Figure A13 and Figure A15, respectively). In Figure 24, the ^{13}C-NMR spectra for G1S, G2S and G3S (annex Figure A14 and Figure A16), the carbon nearest to the sulfonate group is shown at 43.19, 43.06, and 43.12 ppm, respectively.

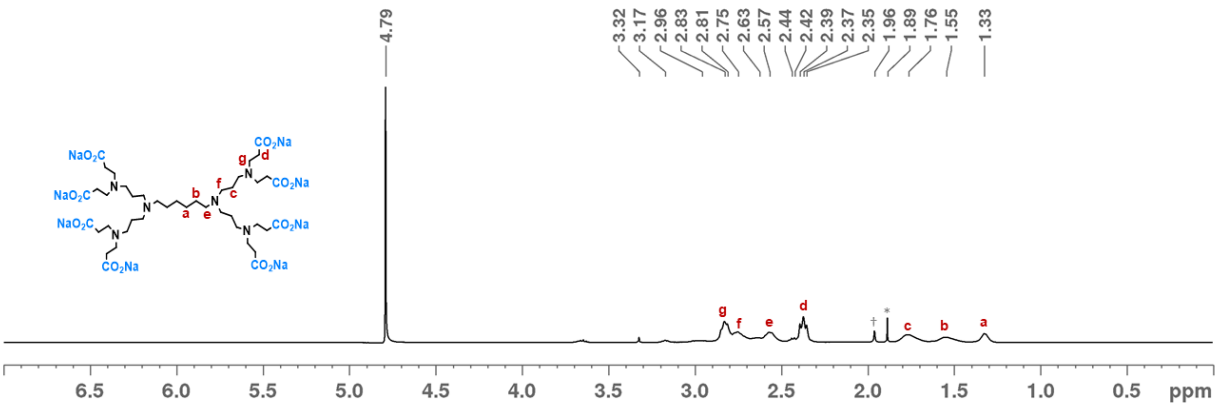

Figure 21. ^{1}H-NMR spectrum of the carboxylate dendrimer G1C in D_2O. (Abbreviation: * = tetrahydrofuran, † = ethyl acetate).

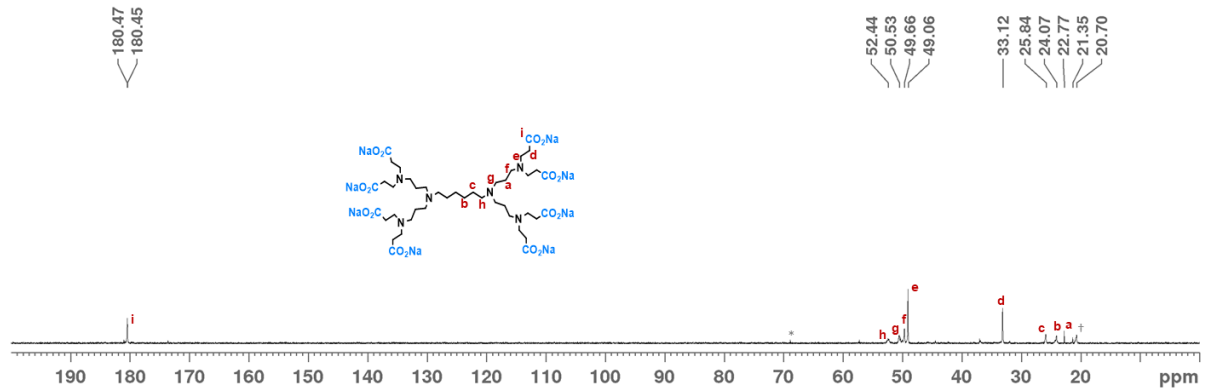

Figure 22. ^{13}C-NMR spectrum of the carboxylate dendrimer G1C in D_2O. (Abbreviation: † = ethyl acetate, * = tetrahydrofuran).

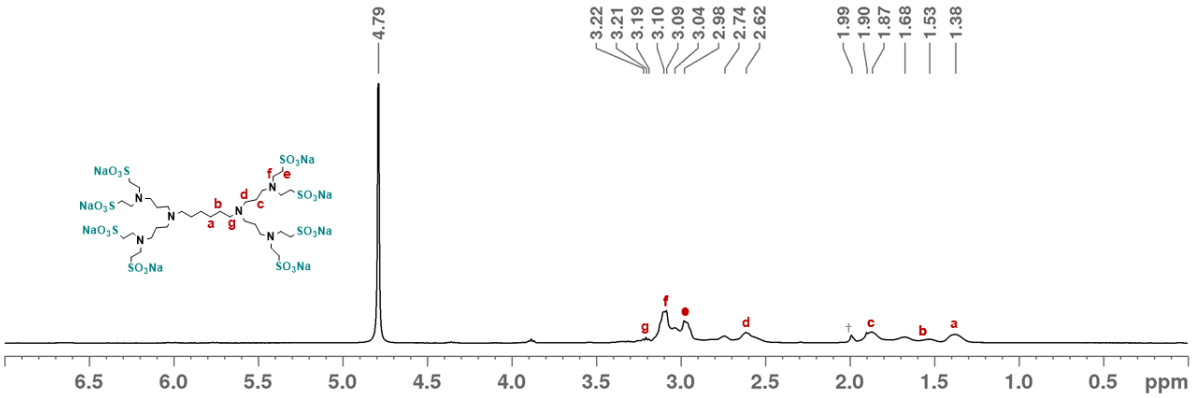

Figure 23. ^{1}H-NMR spectrum of the sulfonate dendrimer G1S in D_2O. (Abbreviation: † = ethyl acetate).

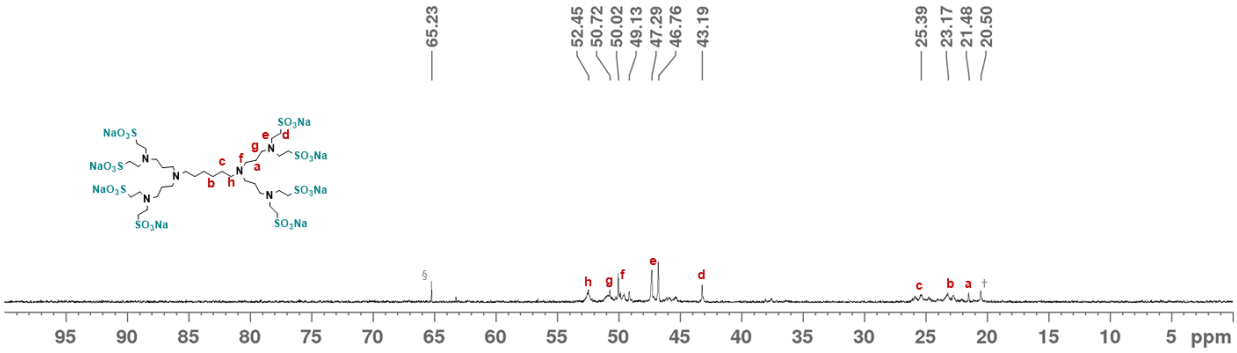

Figure 24. ^{13}C-NMR spectrum of the sulfonate dendrimer G1S in D_2O. (Abbreviation: † = ethyl acetate, § = diethyl ether).

The FT-IR analysis of the sulfonate and carboxylate dendrimers was also performed. The carboxylate dendrimers (Figure 25), generation 1 to 3, presented the expected characteristic bands for these dendrimers. The bands corresponding to the O-H stretch are observed at 2946.48, 2953.63, and 2954.49 cm^{-1}, for the G1C, G2C, and G3C, respectively. A stretch band due to the C=O of the carboxylic acid was, as well, detected at 1727.23 cm^{-1} for the G2C dendrimer. In the case of the sulfonate dendrimers, the bands for G1S, G2S, and G3S at 1194.75, 1188.10, and 1186.19 cm^{-1}, respectively, correspond to the sulfonate region of the FT-IR spectrum (Figure 26). The stretch bands of the sulfoxides (S=O) at 1045.45, 1043.79, and 1042.64 cm^{-1} were also detected for the G1S, G2S, and G3S dendrimers, respectively.

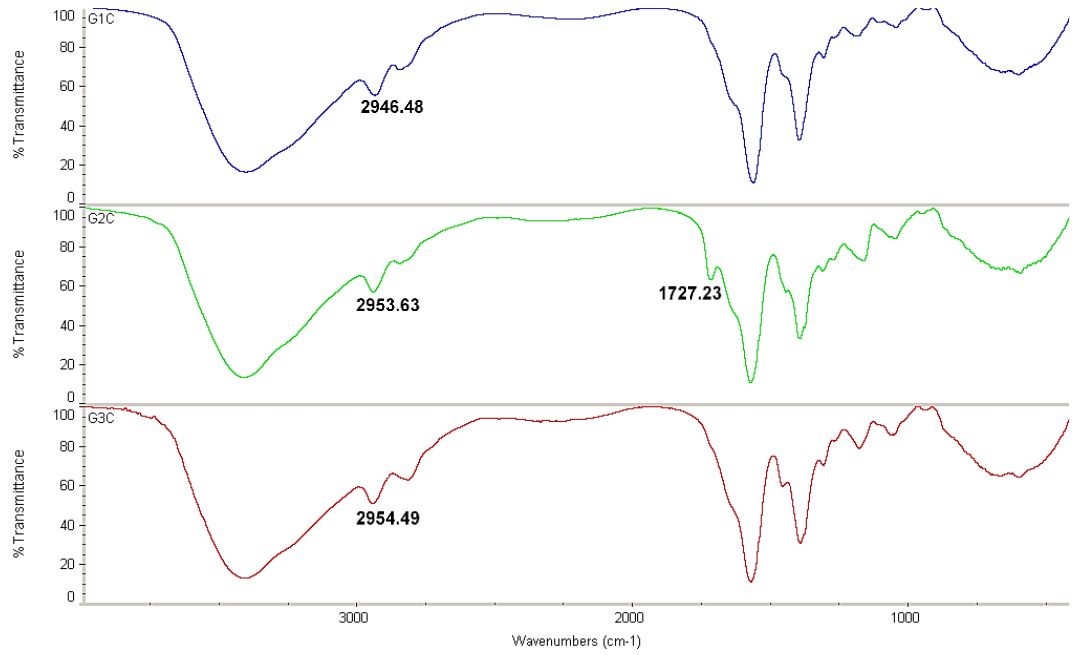

Figure 25. FT-IR spectra of the carboxylate dendrimers from generation 1 to 3, G1C, G2C, and G3C (KBr pellets).

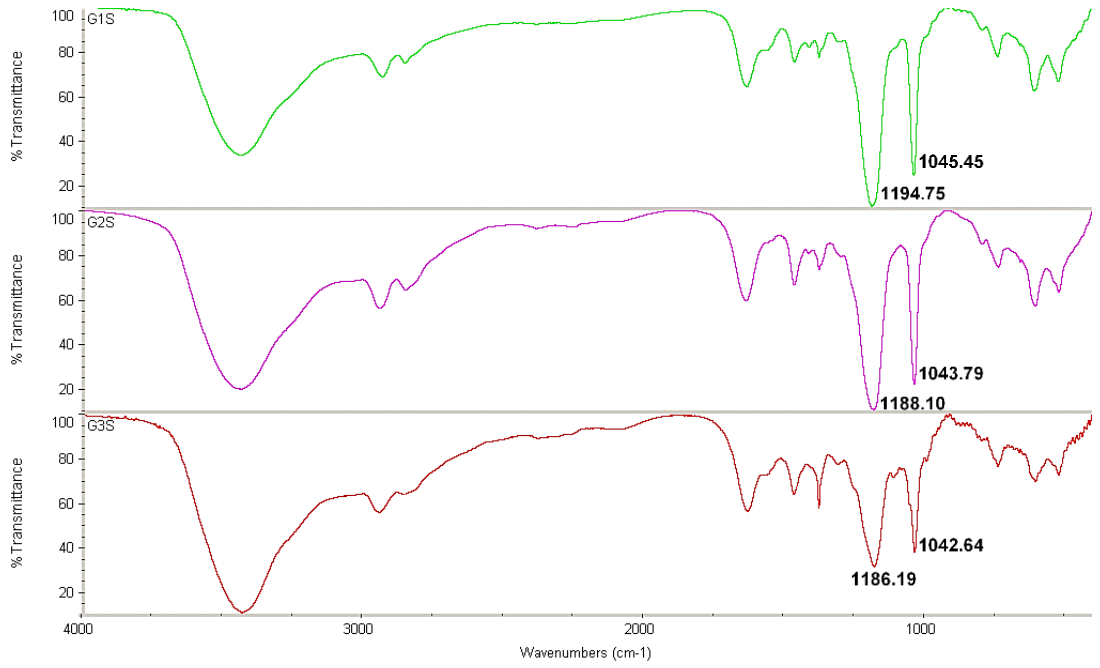

Figure 26. FT-IR spectra of the sulfonate dendrimers from generation 1 to 3, G1S, G2S, and G3S. (KBr pellets).

The synthesis of the carboxylate and sulfonate dendrimers was confirmed by TOF-MS (ESI-) negative mode analysis as can be seen summarized in Table 2. Peaks at *m/z* = 941.51 $[M - 7Na + 6H]^{-1}$ and at *m/z* = 919.52 $[M - 8Na + 7H]^{-1}$ were observed for the G1C dendrimer (Figure 27). The G2C dendrimer presented a peak at *m/z* = 939.57 $[M - C_3H_5O_2 - 16Na + 13H]^{-2}$ (see annex Figure A17). In

the case of the G3C dendrimer, only half a molecule was found with *m/z* = 1146.74 [M – $C_{93}H_{154}N_{15}Na_{16}O_3$ – 3Na + 1H]$^{-2}$ (annex Figure A18). The G1S dendrimer (Figure 28) showed a peak at *m/z* = 622.76 [M – 8Na + 5H + K]$^{-2}$. For the G2S and G3S dendrimers, since they are large molecules, just half dendrimers were found. For the G2S dendrimer, the two half molecules found were *m/z* = 441.79 [M – $C_{37}H_{74}N_7Na_8O_{24}S_8$ – 5Na + 2H]$^{-3}$ and 691.75 [M – $C_{37}H_{74}N_7Na_8O_{24}S_8$ – 4Na + 2H + CH_3OH]$^{-2}$ as can be seen in see annex Figure A19. In the G3S dendrimer (annex Figure A20) 3 partial molecules were also identified with *m/z* = 1333. 97 [M – $C_{77}H_{154}N_{15}Na_{16}O_{48}S_{16}$ – 12Na + 10H + CH_3OH + $2H_2O$]$^{-2}$, 1369.93 [M – $C_{77}H_{154}N_{15}Na_{16}O_{48}S_{16}$ – 13Na + 11H + H_2O]$^{-2}$ and 1571.98 [M – $C_{77}H_{154}N_{15}Na_{16}O_{48}S_{16}$ – 8($C_2H_4NaO_3S$) – 3Na + 5H].

Table 2. Molecular weight of the carboxylate and sulfonate dendrimers.

	G1C	**G2C**	**G3C**	**G1S**	**G2S**	**G3S**
Molecular weight	1096.95	2306.08	4724.33	1385.33	2882.84	5877.86
***m/z* calculated**	941.50 919.52	939.56	1146.98	622.10	441.74 691.13	1333.31 1369.32 1571.76
***m/z* found**	941.51 M – 7Na + 6H]$^{-1}$ 919.52 M – 8Na + 7H]$^{-1}$	939.57 [M – $C_3H_5O_2$ – 16Na +13H]$^{-2}$	1146.74 [M – $C_{93}H_{154}N_{15}Na_{16}O_3$ – 3Na + 1H]$^{-2}$	622.76 [M – 8Na + 5H + K]$^{-2}$	441.79 [M – $C_{37}H_{74}N_7Na_8O_{24}S_8$ – 5Na +2H]$^{-3}$ 691.75 [M – $C_{37}H_{74}N_7Na_8O_{24}S_8$ – 4Na + 2H + CH_3OH]$^{-2}$	1333.97 [M – $C_{77}H_{154}N_{15}Na_{16}O_{48}S_{16}$ – 12Na + 10H + CH_3OH + $2H_2O$]$^{-2}$ 1369.93 [M – $C_{77}H_{154}N_{15}Na_{16}O_{48}S_{16}$ – 13Na + 11H + H_2O]$^{-2}$ 1571.98 [M – $C_{77}H_{154}N_{15}Na_{16}O_{48}S_{16}$ – 8($C_2H_4NaO_3S$) - 3Na + 5H]

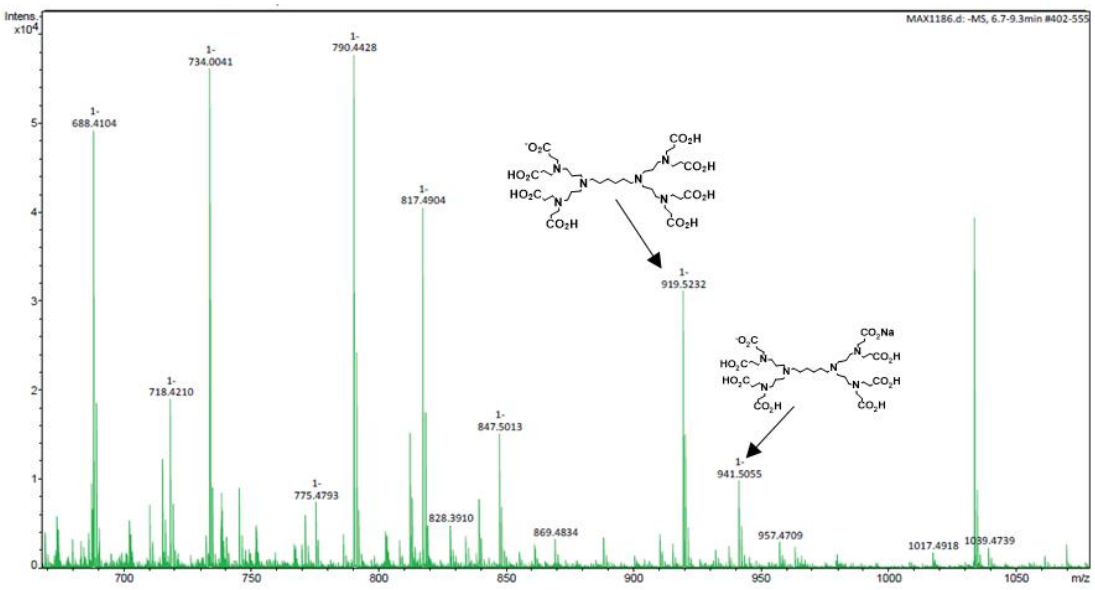

Figure 27. HRMS Q-TOF (ESI-) mass spectrum of the G1C dendrimer.

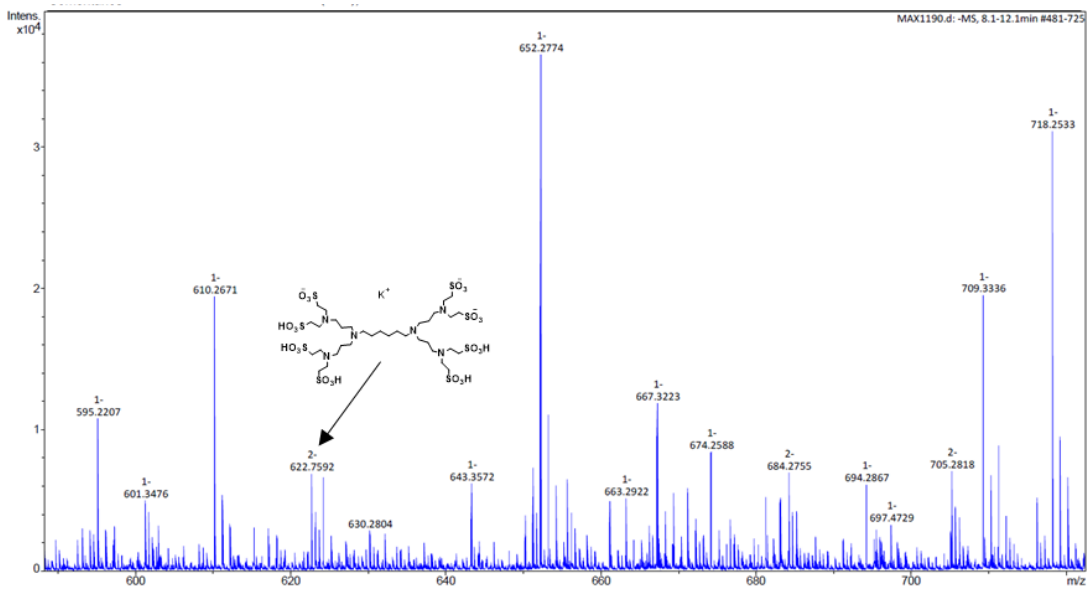

Figure 28. HRMS Q-TOF (ESI-) mass spectrum of the G1S dendrimer.

In particular, the G1C and G1S dendrimers, which were later shown to possess the best anti-HIV-1 activity and were selected to proceed to further biological and anti-infection studies, were fully functionalized at their surface. Their total functionalization was confirmed by the NMR spectra and by MS for both G1C and G1S dendrimers. Each dendrimer had 8 carboxylate (G1C) or 8 sulfonate (G1S) terminal groups that were responsible for their anionic character as indicated by zeta potential

measurements. One should notice that absolute values of zeta potential for G1C (–31.9 ± 1.2) and G1S (–45.1 ± 4.4) are quite high in absolute value, which should be good to keep them in a non-aggregated form in aqueous solutions for long periods (Table 3). Furthermore, the negative charge on the surface of the G1C and G1S dendrimers should be crucial to avoid interactions with the surface of epithelial cells, where there are plenty of glycoproteins and glycolipids (the glycocalyx) that confer them a negative surface charge too. The repulsion between anionic dendrimers and the cell membrane will contribute to their cytocompatibility. As expected, G1C, G2C, and G3C carboxylate dendrimers displayed a negative charge surface of –31.9 mV, –43.5 mV, and –50.4 mV, respectively. The zeta potential of the G1S and G2S sulfonate dendrimers was negative too, presenting values of –45.1 mV and –44.3 mV, respectively. The positive charge of the G3S dendrimer (19.5 mV) suggests that the dendrimer could be only partially functionalized with the sulfonate groups, as can be confirmed by the MS data where a half-molecule was found partially functionalized.

Table 3. Zeta potential data of the carboxylate and sulfonate dendrimers.

	G1C	**G2C**	**G3C**	**G1S**	**G2S**	**G3S**
Zeta potential (mV)[a]	–31.9 ± 1.2	–43.5 ± 1.4	–50.4 ± 2.9	–45.1 ± 4.4	–44.3 ± 2.8	19.5 ± 1.2

[a]Data represent the mean ± SD of three independent experiments.

3.2. Dendrimer stability studies

Stability studies were carried out with the G1C and G1S dendrimers using ^{1}H-NMR. The G1C and G1S dendrimers show to have chemical stability with time, which is a significant characteristic to be considered when long-term storage is required, as is the case of pharmaceutical formulations. Indeed, the stability studies made with the G1C and G1S dendrimers using ^{1}H-NMR clearly showed that they were stable in an aqueous solution at the temperature of 4ºC at least for one year and a half (Figure 29 and Figure 30).

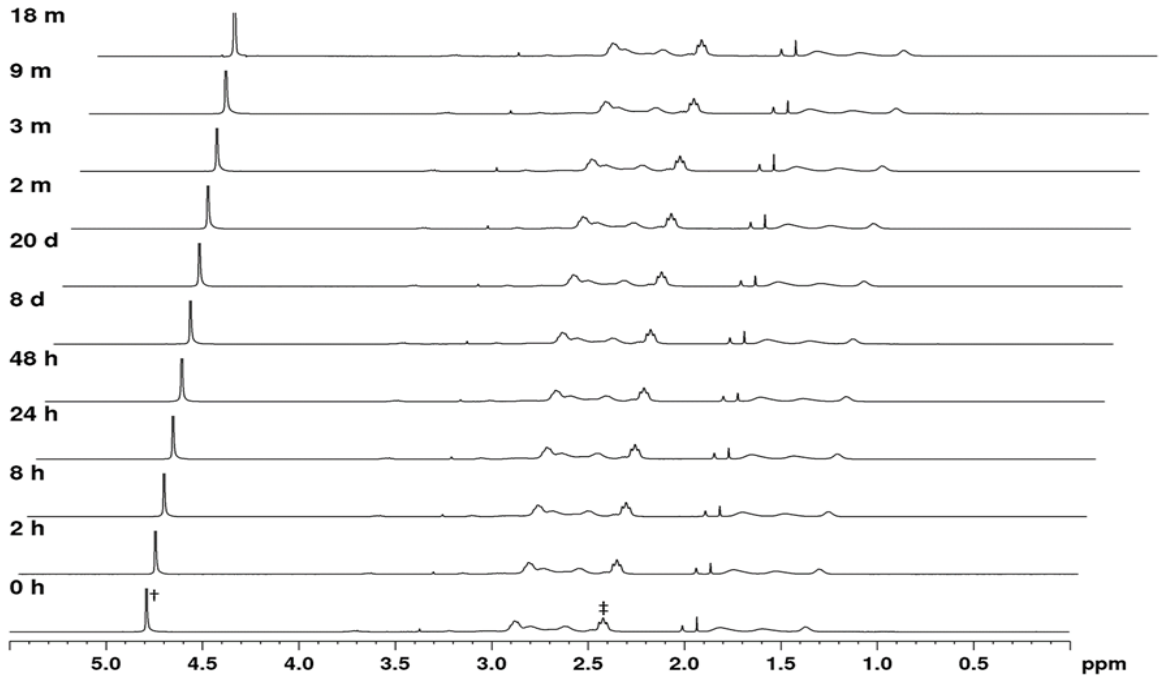

Figure 29. ^{1}H-NMR spectra of the G1C dendrimer. Stability studies were performed in D_2O (probe temperature: 25°C), and the dendrimer solutions were kept at 4°C for a long time. Abbreviations: h = hours, d = days, m = months, † = solvent signal, ‡ = carboxylate group (*–CH_2CO_2Na*).

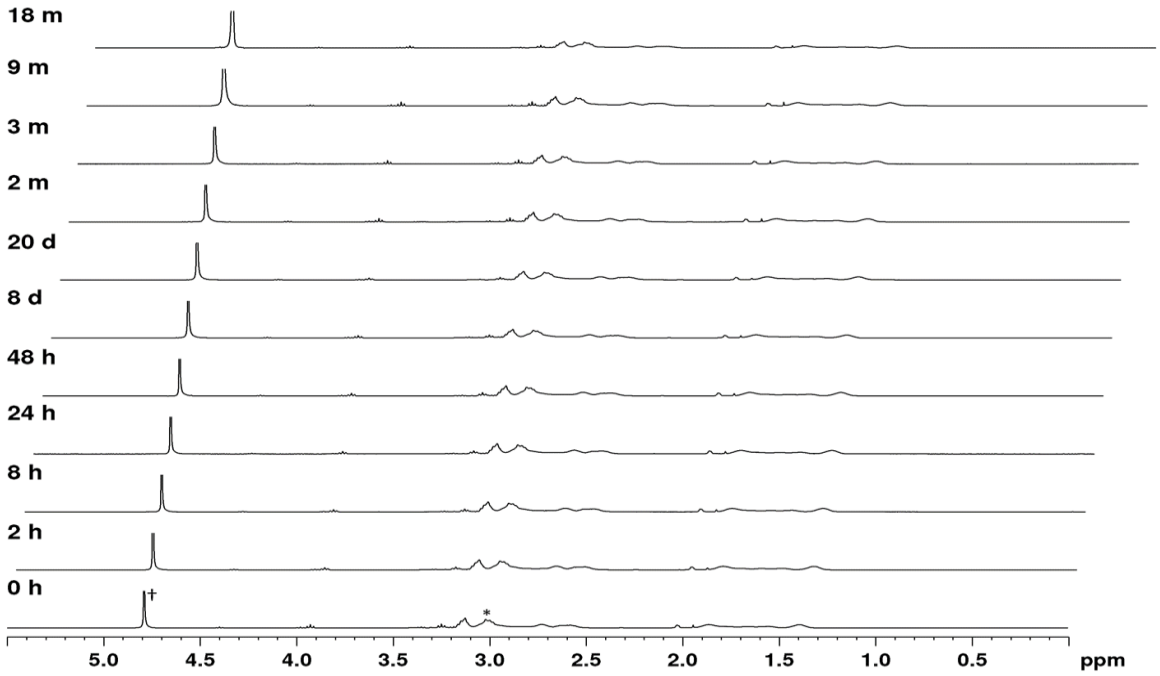

Figure 30. ^{1}H-NMR spectra of the G1S dendrimer after 18 months. Stability studies were performed in D_2O (probe temperature: 25°C), and the dendrimer solutions were kept at 4°C for a long time. Abbreviations: h = hours, d = days, m = months, † = solvent signal, * = sulfonate group (*–CH_2SO_3Na*).

3.3. Cell viability assays

As expected, and in accordance with their anionic charge surface, all carboxylate and sulfonate dendrimers exhibited a very good cytocompatibility (Figure 31). The *in vitro* cell viability of the G1C, G2C, and G3C carboxylate and G1S, G2S, G3S sulfonate dendrimers was evaluated on TZM.bl cells using the MTT assay. Cells were treated for 48 h with serial dilutions of both types of dendrimers. Adequate controls were established by exposing the cells only to cell culture medium (negative control) and to DMSO diluted in cell culture medium at 10% (v/v) (positive control). When the extension of cell survival was >80% compared to the negative control, compounds were considered to be non-toxic. Our results showed that the G1C, G2C, and G3C and the G1S and G2S dendrimers were non-toxic even for the maximum concentration tested of 25 µM. The G3S dendrimer was the only exception, reaching toxicity level at a concentration of 10 µM. This information concerning the effect of dendrimers on cell viability was very important to establish adequate concentrations to use in the anti-HIV-1 infection assays.

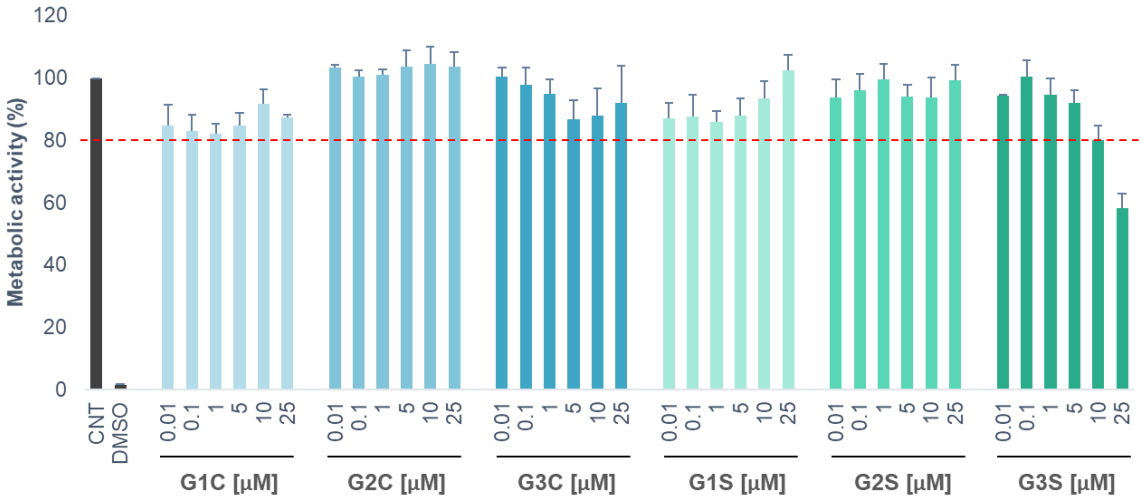

Figure 31. Viability of TZM.bl cells upon exposure to carboxylate and sulfonate dendrimers. TZM.bl cells were subjected for 48 h to carboxylate dendrimers (G1C, G2C, G3C), sulfonate dendrimers (G1S, G2S, G3S), within a concentration range of 0.01 µM to 25 µM. Negative (non-treated cells, CNT) and positive controls (DMSO at 10% v/v) are indicated. Data are represented as mean ± SD of three independent experiments performed in triplicate.

3.4. Dendrimer anti-HIV-1 activity using TZM.bl cells

TZM.bl cells were used to verify the anti-HIV-1 activity of the prepared compounds. This cell line is highly sensitive to HIV-1 infection, with CD4 receptors at the surface, and copies of luciferase and β-galactosidase genes that can be easily used to quantify the HIV-1 infection. Anti-HIV-1 activity assays were carried out using the carboxylate and sulfonate dendrimers (Figure 32). Therefore, to evaluate whether the activity of the dendrimers is dose-dependent, the anti-HIV-1 activity in TZM.bl cells was estimated for both families of carboxylate and sulfonate dendrimers at 10 µM and 25 µM which were the two highest concentrations tested in the cell viability assays – these concentrations were shown to be nontoxic. For the G3S dendrimer, 5 µM and 10 µM concentrations were tested since this particular dendrimer was more toxic than the others at 25 µM. TZM.bl cells were pre-treated for 1 h with the different

dendrimers and then infected with R5-HIV-1_{NLAD8} and X4-HIV-$1_{NL4.3}$ isolates for 2 h. The percentage of infection was determined at 48 h post-infection by the measurement of luciferase activity.

Very interesting results were obtained for the dendrimers with carboxylate terminal groups as they were able to diminish viral activity for both R5-HIV-1_{NLAD8} and X4-HIV-$1_{NL4.3}$ isolates significantly. As displayed in Figure 32a, results showed that the G1C carboxylate dendrimer prevented R5-HIV-1_{NLAD8} infection by an extent of 85% and 90% for concentrations of 10 µM and 25 µM, respectively. These values were 55% and 64% for the G2C dendrimer and 57% and 40% for the G3C dendrimer, respectively. The anti-HIV-1 activity, however, did not increase with dendrimer generation and the G1C dendrimer was, in general, the most promising one. In the case of the dendrimers with sulfonate terminal groups, only the lowest generation (G1S dendrimer) presented significant antiviral activity against both types of virus isolates. The G1S sulfonate dendrimer reached inhibition values of 75% (at 10 µM) and 85% (at 25 µM) regarding R5-HIV-1_{NLAD8} infection. However, the G2S and G3S dendrimers did not exert any activity against R5-HIV-1_{NLAD8} infection (Figure 32a).

The carboxylate and sulfonate dendrimers were also tested for anti-X4-HIV-$1_{NL4.3}$ activity. The G1C dendrimer prevented X4-HIV-$1_{NL4.3}$ infection by 59% and 50% for concentrations of 10 µM and 25 µM, respectively. The G2C dendrimer reached infection inhibition values of 63%, whereas the G3C dendrimer led to a reduction of X4-HIV-$1_{NL4.3}$ infection of 53% (at 10 µM) and 48% (at 25 µM). As regards the G1S dendrimer, the percentage of inhibition of X4-HIV-$1_{NL4.3}$ infection was between 52% (at 10 µM) and 72% (at 25 µM). Finally, it was observed that the G2S and G3S dendrimers did not inhibit X4-HIV-$1_{NL4.3}$ infection (Figure 32b).

This first set of experiments allowed for the selection of the G1C and G1S dendrimers as the best microbicide candidates from the group.

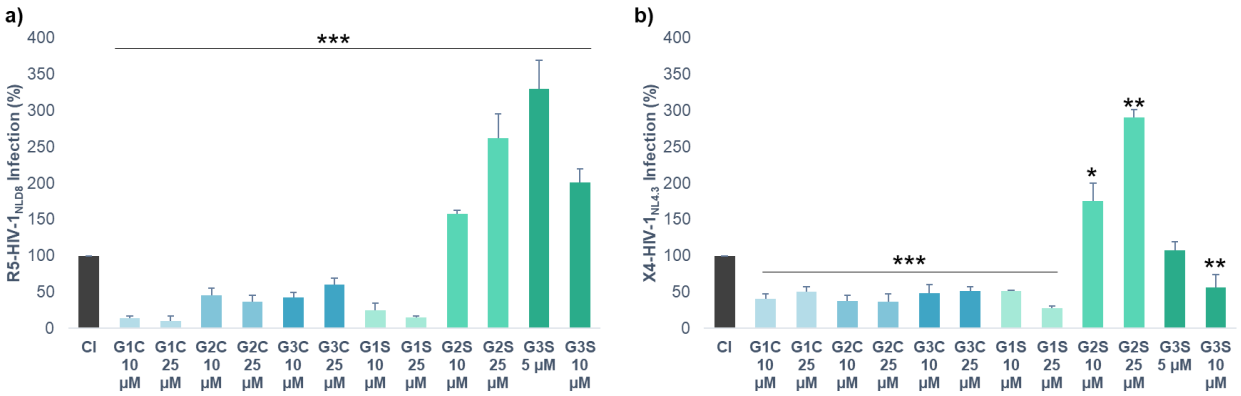

Figure 32. HIV-1 inhibition assays. TZM.bl cells were treated with the dendrimers G1C, G2C and G3C (10 µM and 25 µM); G1S and G2S (10 µM and 25 µM); G3S (5 µM and 10 µM) for 1 h and then infected with (a) R5-HIV-1_{NLAD8} or (b) X4-HIV-$1_{NL4.3}$ isolates for 2 h. Luciferase activity was measured after 48 h of infection. CI is the control of infection. The data represent the mean ± SD of three independent experiments performed in triplicate. *: p<0.05; **: p<0.001; ***: p<0.0001 *vs* CI.

3.5. Time-of-addition experiment

To determine at which time point the dendrimers act through an HIV-1 infection cycle, a time-of-addition assay was performed as can be seen in Figure 33. A non-toxic concentration (25 μM) was selected to evaluate the dendrimer mode of action and was added to R5-HIV-1_{NLAD8} infected cells at the different time of addition. The selected dendrimers, G1C, and G1S were evaluated against HIV-1 infection. As controls were used, Enfuvirtide (T-20) as a fusion inhibitor, Tenofovir Disoproxil Fumarate (TDF) as a transcriptase inhibitor, and Raltegravir (RAL) as an integrase inhibitor. Enfuvirtide (T-20), blocks the fusion of the gp41 subunit of HIV to the cell membrane, preventing cells of the immune system from infection, and reducing the amount of HIV in the human body.[372,373] Tenofovir Disoproxil Fumarate (TDF) inhibits the activity of HIV-1 transcriptase *via* competition with deoxyadenosine 5'-triphosphate in the DNA by initiating viral DNA chain termination.[374] TDF belongs to the nucleoside reverse transcriptase inhibitor drug class and is always combined with other HIV antiretroviral drugs for the treatment of HIV infection.[375] Raltegravir (RAL) hampers the insertion of HIV-1 DNA into the host cell genome by preventing the activity of HIV-1 integrase, and like TDF is always used in combination with other antiretroviral medicines.[376,377] Enfuvirtide (T-20) started to decline after 7h, Tenofovir Disoproxil Fumarate (TDF) sustained its activity for 8h, and RAL (Raltegravir) maintained its activity constant for 24h. The G1S and G1C dendrimers presented inhibition in the first hour of viral infection. In conclusion, our anionic dendrimers act in the first stage of the virus cycle, preventing the spread right from the entry/fusion of the HIV-1 in the host cell.[378]

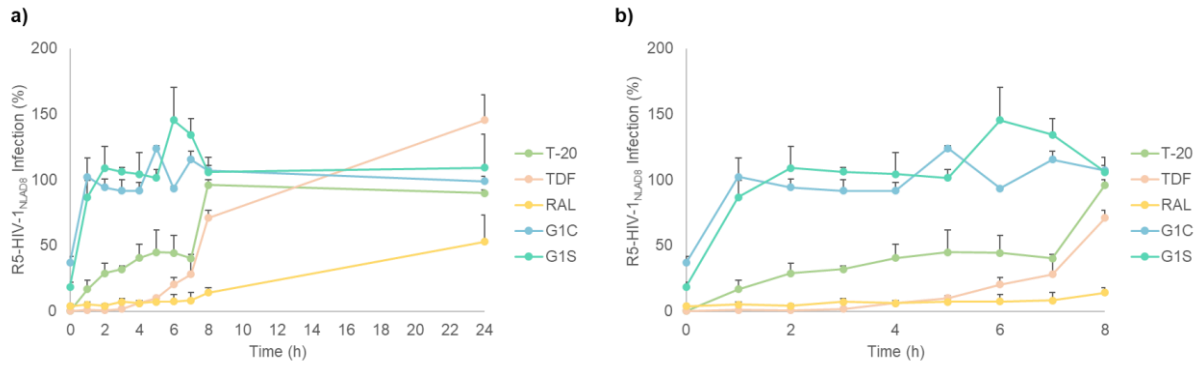

Figure 33. Time-of-addition experiment in the HIV-1 viral cycle. TZM.bl cells were infected with the R5-HIV-1_{NLAD8} isolate for 2 h. G1C and G1S dendrimers (25 μM), T-20 (20 μM), TDF (1 μM) or RAL (1 μM) were added at various time points: (a) results obtained over 24 h; (b) enlarged graph of the first 8 h of treatment. Data represent the mean ± SD of three independent experiments performed in triplicate. Abbreviations: T-20 = enfuvirtide; TDF = Tenofovir Disoproxil Fumarate; RAL = Raltegravir.

3.6. Inhibition of virus-cell attachment assay

To identify the possible mechanism of action of the G1C and G1S dendrimers against HIV-1 infection, time-of-drug-addition assays were performed where TZM.bl cells were infected with R5-HIV-1_{NLAD8} isolates for 2 h at 37°C, followed by dendrimer (at 25 μM) addition at different time points post-infection. These assays revealed that the dendrimers were acting in the first stages of the viral cycle

(Figure 33). Consequently, the next objective was to investigate whether the dendrimers were inhibiting virus-cell attachment. Thus, a first assay was carried out to evaluate whether the dendrimers were interfering with the binding of the virus to the host cells. For this assay, TZM.bl cells were pre-chilled at 4°C since, at this temperature, the overall fluidity of the cellular membrane decreases and becomes less permeable. Then, after being treated with the dendrimers for 1 h, cells were exposed to the R5-HIV-1_{NLAD8} and X4-HIV-$1_{NL4.3}$ isolates for 2 h. After washing (to remove unbound dendrimers and viruses) and cell incubation at 37°C (to allow the membrane to recover its permeability and the infection process to proceed) for 48 h, the extent of infection was quantified by measurement of luciferase activity. The results demonstrated that the carboxylate and sulfonate (G1C and G1S) dendrimers decreased the ability of both virus isolates to attach to the cell membrane. The G1C dendrimers prevented R5-HIV-1_{NLAD8} infection by 55% (at 10 µM, p<0.05) and 93% (at 25 µM, p<0.0001). The G1S dendrimers displayed 94% (at 10 µM, p<0.0001) and 87% (at 25 µM, p<0.001) of inhibition of R5-HIV-1_{NLAD8} infection (Figure 34a). In relation to X4-HIV-$1_{NL4.3}$ infection, inhibition by the G1C dendrimer was 60% (at 10 µM, p<0.05) and 49% (at 25 µM, p<0.05), whereas inhibition by the G1S dendrimer was 79% (at 10 µM, p<0.0001) and 77% (at 25 µM, p<0.001) (Figure 34b).

Indeed, our results demonstrated that the G1C carboxylate and G1S sulfonate dendrimers inhibited both viruses from attaching to the cell membrane to a great extent. At this point, the question to ask was if dendrimers were hampering the viruses from attaching to the cell membrane by directly interacting with them or if they were preventing virus uptake by binding to the virus receptors at the cell's membrane.

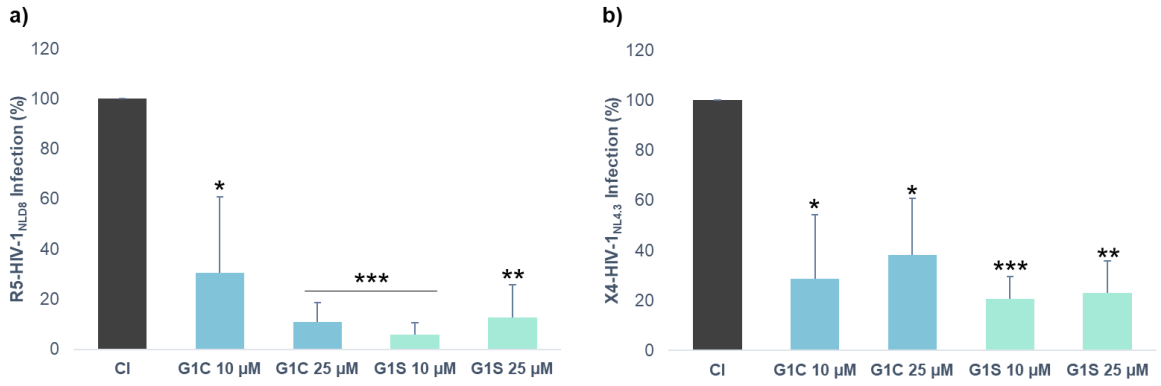

Figure 34. Inhibition of virus-cell attachment assay. TZM.bl cells were treated with the G1C and G1S dendrimers (10 µM and 25 µM) at 4°C for 1 h and infected with (a) R5-HIV-1_{NLAD8} and (b) X4-HIV-$1_{NL4.3}$ isolates. The data represent the mean ± SD of three independent experiments performed in triplicate. *: p<0.05; **: p<0.001; ***: p<0.0001 *vs* CI. Abbreviations: CI = control of infection.

3.7. The direct effect of the dendrimers on viral particles

Following the previous experiments, the direct effect of the dendrimers on the R5-HIV-1_{NLAD8} and X4-HIV-$1_{NL4.3}$ viral particles was studied. The G1 of the carboxylate and sulfonate dendrimers were used to prepare the dendrimer-virus solutions that were first pre-incubated for 1 h at 4°C, and only then TZM.bl

cells were infected for 2 h with these dendrimer-virus solutions. After infection using the virus/dendrimer mixture, the antiviral activity was measured, revealing a significant decrease in infection when compared with the control (Figure 35). This happened for both the G1C and G1S dendrimers, for both concentrations studied, and for both virus isolates (R5-HIV-1_{NLAD8} and X4-HIV-$1_{NL4.3}$). These results indicate that the dendrimers were acting directly on the viral particles, as already observed for other nanoparticles.[217,379] Results showed that the G1C and G1S dendrimers had activity directed against the R5-HIV-1_{NLAD8} and X4-HIV-$1_{NL4.3}$ isolates. For the R5-HIV-1_{NLAD8} isolate, the G1C dendrimers exhibited inhibition percentages of 78% (at 10 µM, p<0.0001) and 90% (at 25 µM, p<0.0001), while for the G1S dendrimers these values were 79% (at 10 µM, p<0.0001) and 84% (at 25 µM, p<0.0001) (Figure 35a). Furthermore, the G1C dendrimers inhibited X4-HIV-$1_{NL4.3}$ infection by 64% (at 10 µM, p<0.001) and 72% (at 25 µM, p<0.0001) and the G1S dendrimer by 71% (at 10 µM, p<0.0001) and 69% (at 25 µM, p<0.0001) (Figure 35b).

This mechanism could be due to the negative charges on the surface of the dendrimers that interact through electrostatic forces with the cationic residues of the viral glycoproteins that have an important role in infection like gp120 and/or gp41.[188] Since dendrimers of low generation are more flexible, probably they can better interact with their molecular target in the virus.[187,363]

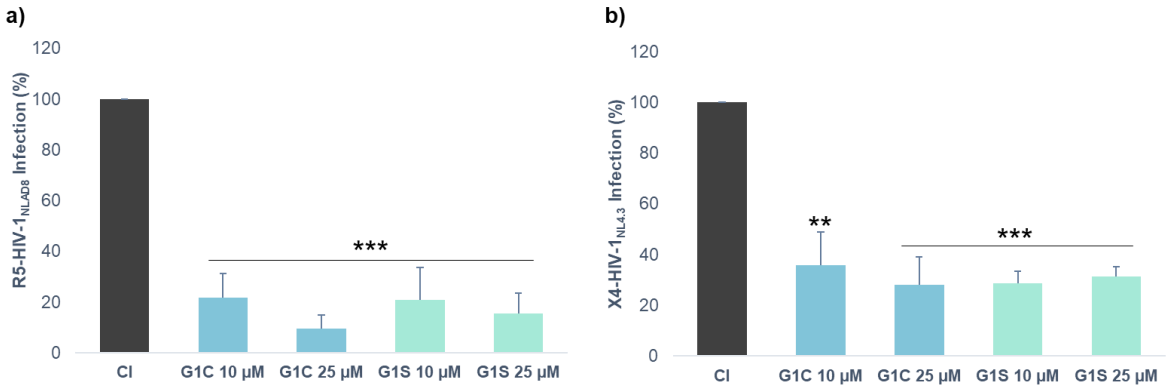

Figure 35.The direct effect of the dendrimers on the viral particles. TZM.bl cells were infected with (a) R5-HIV-1_{NLAD8} and (b) X4-HIV-$1_{NL4.3}$ strains previously co-incubated (at 4°C) with the G1C and G1S dendrimers (10 µM and 25 µM) for 2 h. The percentage of HIV-1 infection was measured as luciferase activity after 48 h of infection. The data correspond to the mean ± SD of three independent experiments performed in triplicate. **: p<0.001; ***: p<0.0001 *vs* CI. Abbreviations: CI = control of infection.

3.8. Dendrimer-cell binding assays

In order to determine whether dendrimers bind to host cells to protect them against HIV-1 infection by binding to specific cell surface proteins, dendrimer-cell binding assays were performed. Indeed, it is known that HIV-1 entry is mainly dependent on gp120 binding to the CD4 receptor and CCR5/CXCR4 co-receptors present in the target cells.[187,193] Briefly, TZM.bl cells were pre-treated with the G1C and G1S dendrimers for 1 h. Then, the cells were washed to remove the unbound dendrimers before R5-HIV-1_{NLAD8} and X4-HIV-$1_{NL4.3}$ infection. Results showed that both dendrimers at all concentrations tested did not significantly reduce the extent of HIV-1 infection (Figure 36). Therefore, it was concluded that the

dendrimers of these families did not interact with the proteins (cell receptors) at the cell surface to protect them against HIV-1 infection. So, clearly, the G1C or G1S dendrimer mechanism of action is through direct binding to the viral nanoparticles and not with the target cells.

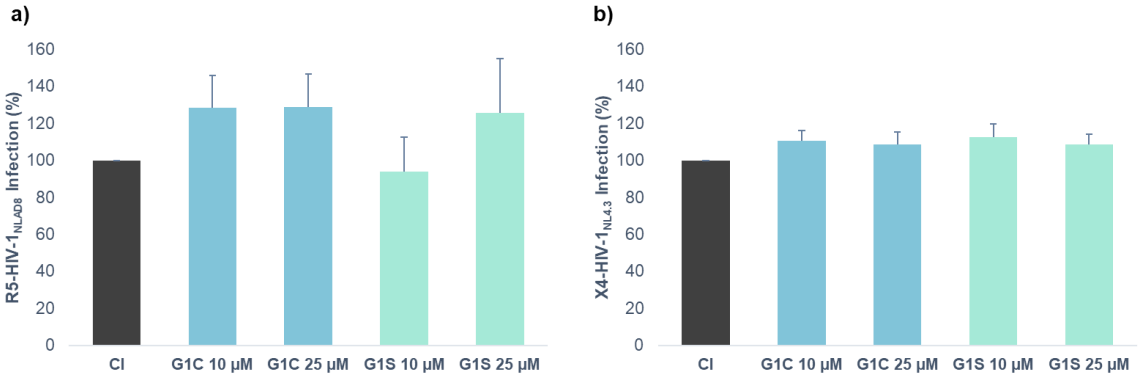

Figure 36. Dendrimer-cell binding assay. TZM.bl cells were pre-treated with the G1C and G1S dendrimers (10 µM and 25 µM) for 1 h and washed. After that, cells were infected with (a) R5-HIV-1_{NLAD8} and (b) X4-HIV-$1_{NL4.3}$ isolates for 2 h. The percentage of infection was determined 48 h post-infection. The data represent the mean ± SD of three independent experiments performed in triplicate. Abbreviations: CI = control of infection.

3.9. pH effect on dendrimers

Having in view the application of the G1C or G1S dendrimers as microbicides for woman vaginal use, experiments were further conducted to evaluate their stability and biological activity in the acidic environment of the vagina and basic pH of semen.[379] The effect of pH on the dendrimer anti-HIV-1 activity was studied using the G1C and G1S dendrimers, incubated for 1 h at room temperature at different pH values (3, 4, 5, 7.4 (pH value of PBS), and 8). After that, TZM.bl cells were pre-treated with these solutions for 1 h and infected with R5-HIV-1_{NLAD8} isolates for 2 h. Results showed that the G1C and G1S dendrimers maintained the anti-HIV-1 activity at basic and acid pH values (Figure 37) without significant differences when compared to the experiments done in PBS. The G1S dendrimer led to very high inhibition levels of HIV-1 activity independently of the tested pH value (around 90% when used at a 25 µM concentration).

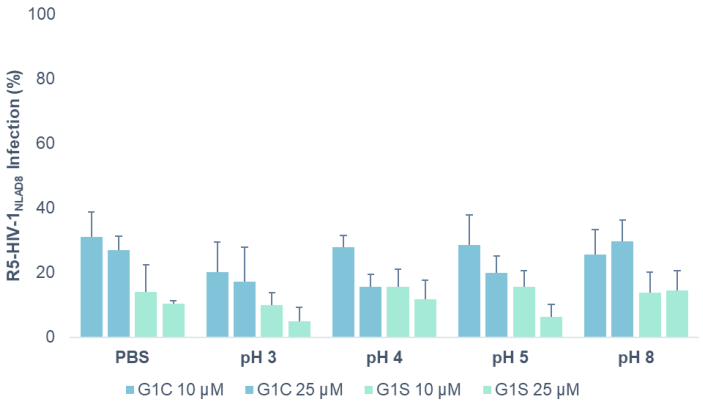

Figure 37. pH effect on the anti-HIV-1 activity of dendrimers. The G1C and G1S dendrimers were pre-incubated at 37 °C at different pH values for 1 h. Then, TZM.bl cells were treated with the dendrimer solutions for 1 h and infected with R5-HIV-1_{NLAD8} for 2 h. The percentage of infection was measured at 48 h of infection as luciferase activity. The data correspond to the mean ± SD of three independent experiments performed in triplicate.

3.10. Vaginal irritation assay in BALB/c mice

The possibility of using the G1C and G1S dendrimers as topical microbicides against HIV-1 infection was investigated by performing a vaginal irritation assay in BALB/c mice. This histological study in BALB/c vaginal tissue showed that when the mice were treated with G1C or with G1S dendrimers, after 7 consecutive days of exposure, all mice had a similar level of irritation and inflammation of their vaginal epithelium (total score < 4) as that of the non-irritation control (Table 4). The estrous cycle begins with sexual maturity and is defined by physiological changes in females that are induced by reproductive hormones. The estrous cycle is divided into four stages: proestrus (P, first stage characterized by the maturing of the endometrium and the ovarian follicles), estrus (E, second stage designated by receptivity to a male and mating), metestrus (M, third stage classified by sexual inactivity and the formation of the corpus luteum), and diestrus (D, fourth stage characterized by a functional corpus luteum and an increase of progesterone in the blood concentration).[380] Even though the all BALB/c mice were at the same age (7 weeks) they presented different stages of the estrous cycle, with the majority of the mice in the first stage of the estrous cycle, proestrus. Concluding, the G1C or G1S dendrimers did not damage or alter the vaginal epithelium, which reveals their safety and potential to be used *in vivo*.

Table 4. The existence of an injury in the vaginal epithelium was evaluated in each biological sample. **0** (no change) when no injury or the observed changes were within the normal range; **1** (minimum) when changes were sparse but exceeded those considered normal; **2** (light) when injuries were identifiable but with no severity; **3** (moderate) for a significant injury that could increase in severity; **4** (very serious) for severe injuries that occupy most of the analyzed tissue. These values were added up and determined the level of vaginal irritation as a minimum of **1-4**, average **5-6**, moderate **7-9**, and severe >**9+**.

	PBS			**Control N9 (4.5%)**			**G1C (3%)**			**G1S (3%)**		
Epithelial lesion	3	0	4	3	2	1	0	0	0	0	0	0
Inflammatory infiltrate	2	0	2	3	2	3	0	0	1	1	1	1
Vascular congestion	0	0	0	2	2	1	1	1	0	0	0	0
Edema/fibrosis	1	0	0	3	0	0	0	0	1	0	1	0
TOTAL SCORE	**6**	**0**	**6**	**11**	**6**	**5**	**1**	**1**	**2**	**1**	**2**	**1**
Estrous cycle moment	**P**	**P**	**M**	**D**	**D**	**E**	**P**	**E**	**P**	**P**	**P**	**P**

Many microbicide candidates have failed due to their high toxicity or irritation *in vivo*. As so, we decided to evaluate the possible vaginal irritation and inflammation caused by the G1C and G1S dendrimers using BALB/c mice. The experimental results (Figure 38) were very promising, showing that repeated intra-vaginal administration of the G1C and G1S dendrimers do not produce vaginal irritation and inflammation. Globally, our results are not only similar to those obtained with the previously published G2-S16 carbosilane dendrimers also tested *in vivo* in BALB/c mice, but we were also able to achieve this without the use of higher dendrimer generation.[197,363]

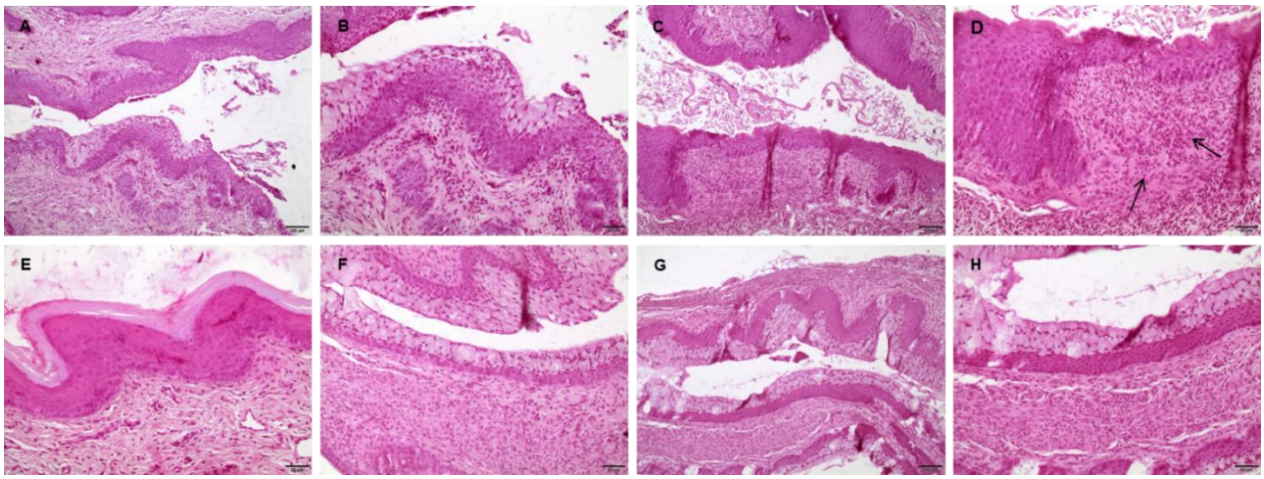

Figure 38. Hematoxylin-eosin staining of the vagina sample extracted after 7 days of daily application. A and B, vehicle control; C and D, N9 (4,5%); E and F, G1C 3%; and G and H, G1S 3%.

4. Conclusions

New and chemically stable anionic poly(alkylidenamine)-based dendrimers with carboxylate and sulfonate terminal groups were prepared, characterized, and tested against HIV-1 infection *in vitro*. Although all dendrimers presented good cytocompatibility independently of their generation (G1 to G3), only the ones pertaining to the lower generation (G1C and G1S dendrimers) showed antiviral activity against infection by R5-HIV-1_{NLAD8} and X4-HIV-$1_{NL4.3}$ isolates in TZM.bl cells. The investigation of the possible mechanism of action of these dendrimers against HIV-1 infection revealed that they could directly interact with the viruses hampering their entry into the cells. Additionally, the G1C and G1S dendrimers preserved their antiviral activity both at acidic and basic pH values with high inhibition of HIV-1 infection (~90%), as well as long-term chemical stability in aqueous solution at 4ºC. *In vivo* assays using BALB/c mice revealed that the G1C and G1S dendrimers did not cause noticeable irritation or inflammation in the vaginal epithelium. So, overall, when included in a gel matrix, the developed dendrimers should constitute good systems to be used as a physical barrier at the epithelial surface to protect against HIV-1 infection. Importantly, the results obtained with our poly(alkylidenamine) dendrimers are not only comparable to the well-studied carbosilane dendrimers, G2-S16, but they were also achieved using a distinct chemical structure and lower generation.[81,197,363] Also and not less important, our poly(alkylidenamine) dendrimers can prevent HIV-1 infection with no combination with other antiviral drugs.[212] To conclude, the present study supports further *in vivo* experiments, which, hopefully, will validate the use of these types of dendrimers as safe, efficient, and potent topical microbicides.

Chapter 3.

The behavior of low generation dendrimers coordinated with $[Ru(\eta^5\text{-}C_5H_5)(PPh_3)_2]^+$ moieties against HIV-1 infection

Chapter 3. The behavior of low generation dendrimers coordinated with [Ru(η^5-C_5H_5)(PPh_3)$_2$]$^+$ moieties against HIV-1 infection

1. Introduction

Metal complexes have been shown to have several pharmacological applications in medicine as metal-based drugs.[381] Metal ions have a variety of factors that contribute to their qualities as metallodrugs, including the oxidation state, types of geometry, and coordination ligands, which play essential roles in the recognition by transport, uptake, and delivery proteins.[382] Moreover, metals behave as catalysts in several intracellular processes, by interacting with intracellular proteins and enzymes.[383]

The research of metal compounds as antivirals remains scarce. For instance, ruthenium complexes have been explored as potential candidates in cancer treatment.[153,384–386] Metal complexes, such as platinum and ruthenium, have been shown to present antiviral activity against tuberculosis.[387,388] Recently, Salam J.J. Titinchi *et al.* published a review of platinum and ruthenium complexes with antimycobacterial and anti-HIV-1 potential activity.[389] However, only a few studies with ruthenium compounds have been investigated as antivirals and against HIV-1 infection.[390–394] Metal complexes or compounds containing metals have been shown to interact in the early stages of HIV infection.[395]

The combination of nanomaterials with metal complexes can improve their efficacy. Metallodendrimers present several advantages since they combine the unique characteristics of both dendrimers and metal complexes. However, their potential is lacking investigation. The teams of Francisco J. de la Mata and M. Ángeles Muñoz-Fernández have prepared and evaluated the HIV-1 potential of copper carbosilane dendrimers and anionic PPI metallodendrimers.[218,396]

Here we describe and, based on our previous work,[364] the preparation of low generation (0 to 2) poly(alkylidenamine) dendrimers with nitrile terminal groups and their coordination with [Ru(η^5-C_5H_5)(PPh_3)$_2$]$^+$ moieties. These dendrimers and metallodendrimers were fully characterized by ^{1}H-, ^{13}C- and ^{31}P-NMR, MS, FT-IR, and EA techniques. Subsequently, the HIV antiviral activity of the prepared metallodendrimers was assessed using the TZM.bl cell line and the two viruses R5-HIV-1 and X4-HIV-1.

2. Material and Methods

2.1. Materials

All the nitrile terminated dendrimers and the ruthenium-based metallodendrimers were prepared according to the strategy developed by our group.[364] The amine dendrimers were prepared following the method developed by Marie-Christine Daniel *et al*. through the reduction of the nitrile groups into primary amines (Scheme 1, chapter 2) and as described in section A.1.2.[369] The metallodendrimers (Scheme 3) were prepared through a dry argon atmosphere by Schlenk-tube techniques. Methanol, dry diethyl ether,

and dry dichloromethane were degassed before use. Methanol extra-dry was bought from Acros Organics. The ruthenium complex [Ru(η^5-C_5H_5)(PPh_3)$_2$Cl] (RuCp)[397,398] was synthesized based on adapted literature methods and as described in the annex section A.1.3. All other reagents were acquired from Acros Organics and Fisher Chemical and used as received.

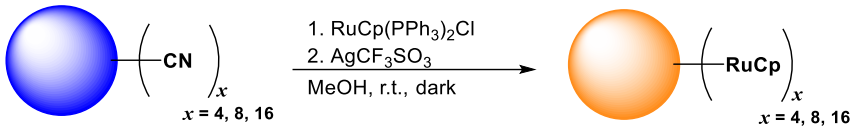

Scheme 3. Reaction scheme of the preparation of the metallodendrimers.

2.2. Synthesis of the nitrile dendrimers

2.2.1. Synthesis and characterization of G0CN

1,6-hexanediamine (16.9 g, 145.5 mmol) was dissolved in 60 mL of methanol, and acrylonitrile (36.2 mL, 552.9 mmol) was dropped into the previous solution at room temperature. The reaction mixture was stirred and warmed up to 48°C for 3 h. Acrylonitrile (36.2 mL, 552.9 mmol) was dropped into the mixture and the temperature was increased to 80°C for 3 h. After 3 h, the heating was stopped and the mixture was cooled down. The solvent was removed under reduced pressure, and the resulting oil was taken up in chloroform and washed by extraction using distilled water (3 x 15 mL). The chloroform was removed under reduced pressure to obtain the final product a golden oil with a 75% yield (35.9 g). ^{1}H-NMR (400 MHz, $CDCl_3$) δ = 2.84 (–C**H**$_2$CN), 2.54 – 2.45, 1.47, 1.34 ppm. ^{13}C-NMR (100 MHz, $CDCl_3$) δ = 118.82 (–CH_2**C**N), 49.71, 49.06, 27.04, 26.97, 17.12 ppm. FT-IR: ν = 2247 cm^{-1} ($\nu_{C\equiv N}$). TOF-MS (ESI+): *m/z* = 329.2 [M + H]$^+$.

2.2.2. Synthesis and characterization of G1CN

The G1NH_2 dendrimer (5.3 g, 15.4 mmol) was dissolved in 90 mL of methanol, and acrylonitrile (7.7 mL, 117.2 mmol) was dropped into the previous solution at room temperature. The reaction mixture was stirred and warmed up to 48°C for 3 h. Then, acrylonitrile (7.7 mL, 117.2 mmol) was dropped into the previous mixture and the temperature was increased to 80°C for 3 h. After 3 h, the heating was stopped and the mixture was allowed to cool down. The solvent was removed under vacuum and the final product was obtained as a golden oil with a 61% yield (7.2 g). ^{1}H-NMR (400 MHz, $CDCl_3$) δ = 2.85 (–C**H**$_2$CN), 2.66 – 2.46, 1.42, 1.28, 1.25 ppm. ^{13}C-NMR (100 MHz, $CDCl_3$) δ = 118.93 (–CH_2**C**N), 54.22, 52.13, 51.73, 49.79, 27,86, 27.23, 25.22, 17.12 ppm. FT-IR: ν = 2248 cm^{-1} ($\nu_{C\equiv N}$). TOF-MS (ESI+): *m/z* = 769.6 [M + H]$^+$.

2.2.3. Synthesis and characterization of G2CN

The $G2NH_2$ dendrimer (2.2 g, 2.8 mmol) was dissolved in 60 mL of methanol, and acrylonitrile (2.8 mL, 42.7 mmol) was dropped into the previous solution at room temperature. The reaction mixture was stirred and warmed up to 48°C for 3 h. Acrylonitrile (2.8 mL, 42.7 mmol) was dropped into the mixture and the temperature was increased to 80°C for 3 h. Then, the heating was stopped and the mixture was allowed to cool down. The solvent was removed under reduced pressure and the final product was obtained as a golden oil with a yield of 56% (2.6 g). ^{1}H-NMR (400 MHz, $CDCl_3$) δ = 2.85 (–C**H**$_2$CN), 2.57 – 2.41, 1.59, 1.43, 1.28 ppm. ^{13}C-NMR (100 MHz, $CDCl_3$) δ = 118.94 (–CH_2**C**N), 52.41, 51.73, 51.58, 49.76, 27,97, 27.22, 25.17, 17.11 ppm. FT-IR: ν = 2248 cm^{-1} ($\nu_{C\equiv N}$). TOF-MS (ESI+): *m/z* = 1650.2.

2.3. Synthesis of the metallodendrimers

2.3.1. Synthesis and characterization of G0Ru

[Ru(η^5-C_5H_5)(PPh_3)$_2$Cl] (0.8 g, 1.1 mmol) was added with 75 mL of degassed methanol into a Schlenk under argon and stirred for about 30 min. Silver trifluoromethanesulfonate, $AgCF_3SO_3$ (0.4 g, 1.4 mmol) and G0CN (0.08 g, 0.2 mmol) were added to the previous suspension. The solution was stirred in the dark and at room temperature (*ca.* 27°C) for 19 h. The suspension mixture was filtered and the solvent was removed to obtain a green solid. At this time, the product was quickly extracted with dichloromethane (DCM) by filtration to prevent decomposition and was then washed with diethyl ether. After several precipitations with DCM/hexane, the final product, the G0Ru metallodendrimer (Scheme 4) was obtained as a yellowish solid with a yield of 29% (0.265 g). ^{1}H-NMR (400 MHz, $CDCl_3$) δ = 7.50 – 7.00 (PPh_3), 4.48 (–C_5**H**$_5$), 2.65 – 1.17 ppm. ^{31}P-NMR (161 MHz, $CDCl_3$) δ = 41.88 (**P**Ph_3) ppm. FT-IR: ν = 2363 cm^{-1} ($\nu_{C\equiv N}$). TOF-MS (ESI+): *m/z* = 3538.61 [M + ($CF_3SO_3^-$)$_3$]$^+$, *m/z* = 1694.83 [M + ($CF_3SO_3^-$)$_2$]$^{2+}$. EA: G0Ru ($C_{186}H_{168}F_{12}N_6O_{12}P_8Ru_4S_4$) + 5 H_2O, calc. for %C: 59.14, %H: 4.75, %N: 2.22; found %C: 59.15, %H: 4.94, %N: 2.56.

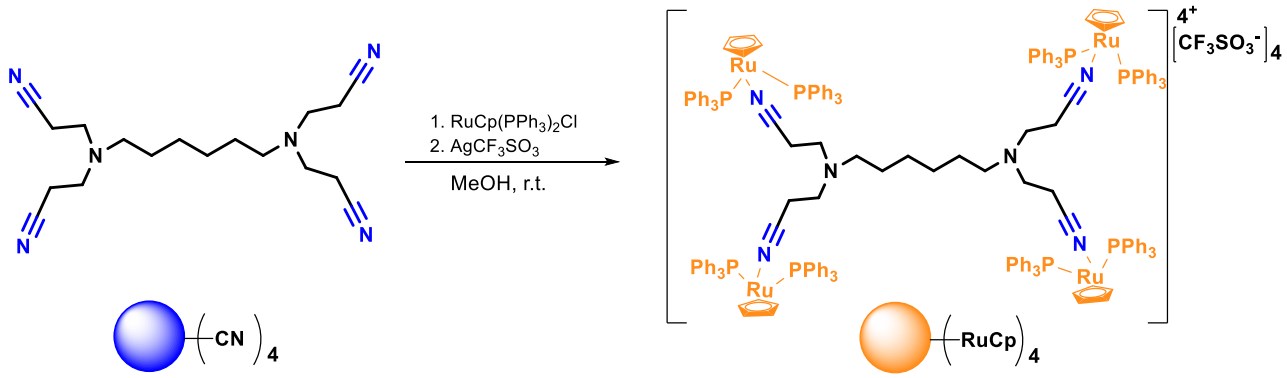

Scheme 4. Reaction scheme of the preparation of the G0Ru metallodendrimer.

2.3.2. Synthesis and characterization of G1Ru

$[Ru(\eta^5\text{-}C_5H_5)(PPh_3)_2Cl]$ (0.8 g, 1.1 mmol) was added with 80 mL of degassed methanol into a Schlenk under argon and stirred for about 30 min. Silver trifluoromethanesulfonate, $AgCF_3SO_3$ (0.4 g, 1.5 mmol) and G1CN (0.1 g, 0.1 mmol) were added to the previous suspension. The solution was stirred in the dark at room temperature (*ca.* 27°C) for 25 h. The suspension mixture was filtered and the solvent was removed to obtain a green solid. At this time, the product was quickly extracted with dichloromethane (DCM) by filtration to prevent decomposition. After several precipitations with DCM/hexane, the final product, the G1Ru metallodendrimer (Scheme 5), was obtained as a green olive solid with a yield of 33% (0.323 g). ^{1}H-NMR (400 MHz, $CDCl_3$) δ = 7.50 – 7.00 (PPh_3), 4.47 ($-C_5\mathbf{H}_5$), 2.35 – 1.25 ppm. ^{31}P-NMR (161 MHz, $CDCl_3$) δ = 41.56 (**P**Ph_3) ppm. FT-IR: ν = 2365 cm^{-1} ($\nu_{C\equiv N}$). TOF-MS (ESI+): *m/z* = 1007.03 [M + 7($CF_3SO_3^-$) – C_5H_5 – 3(C_6H_6)]$^+$, *m/z* = 1011.03 [M + 7($CF_3SO_3^-$) – 3(C_6H_6)]$^+$, *m/z* = 1036.04 [M + 7($CF_3SO_3^-$) – C_6H_6]$^+$.

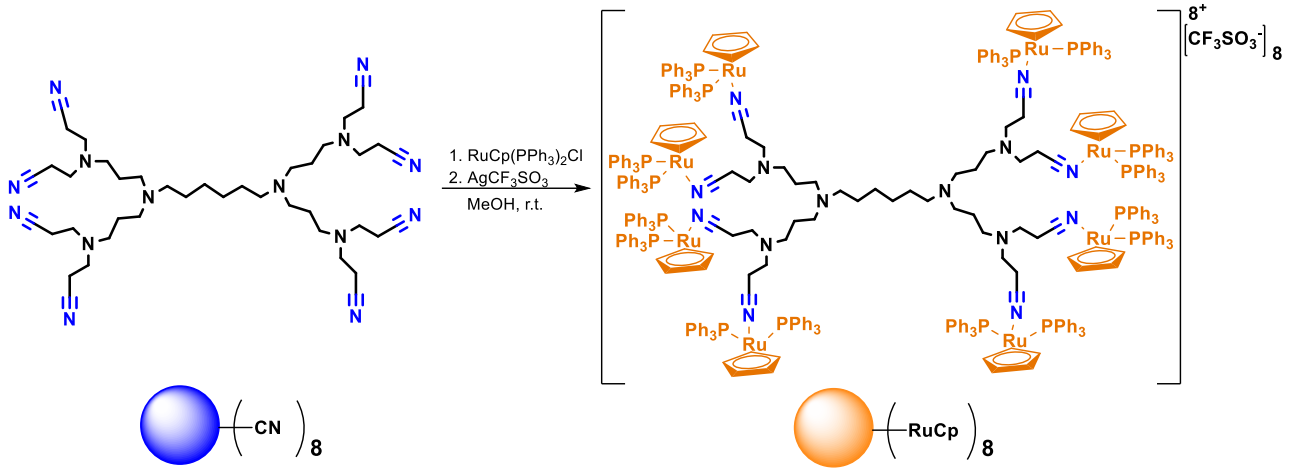

Scheme 5. Reaction scheme of the preparation of the G1Ru metallodendrimer.

2.4. Biological assays

2.4.1. Cell viability assays

The TZM.bl cells were seeded in 96-well plates at a density of 15 x 10^3 cells/well. After that, cells were treated with the G0CN, G1CN and G2CN nitrile dendrimers, the RuCp complex, and the G0Ru and G1Ru metallodendrimers each prepared at a stock concentration of 250 µM in 0.5% DMSO / nuclease-free water and diluted to a range concentration of 0.01 µM to 25 µM. After 48 h of incubation, the TZM.bl cell viability was quantified by the measurement of the metabolic activity of the cells in culture through the (3-(4,5-dimethylthiazol-2-yl)-2,5-diphenyl-2H-tetrazolium bromide) (MTT) assay (Sigma-Aldrich). Briefly, the cell culture medium was replaced with OPTI-MEM containing MTT (0.5 mg/mL). The formazan crystals obtained were dissolved in DMSO, and the absorbance was measured at 570 nm with a

reference of 690 nm in a microplate reader (Synergy 2 Multi-Detection Microplate Reader, BioTek Instruments, Inc.).

2.4.2. Anti-HIV-1 activity of the dendrimers and metallodendrimers

The TZM.bl cells were seeded in 96-well plates at a cell density of 15 x 10^3 cells/well for 24 h. The next day, the cells were pre-treated with the dendrimers and metallodendrimers at maximum non-toxic concentrations of each compound for 1 h at 37°C. Then, the cells were infected with the R5-HIV-1_{NLAD8} or X4-HIV-$1_{NL4.3}$ isolates (15 ng/10^6 cells). After 2 h post-infection, the cells were washed twice with sterile PBS to remove the unbound viruses and compounds. Luciferase activity was assessed after 48 h post-infection to quantify the extension of HIV-1 infection (Luciferase Assay System kit, Promega Corporation, Fitchburg, WI, USA).

3. Results and Discussion

3.1. Synthesis and characterization of the dendrimers and metallodendrimers

The G0CN, G1CN, and G2CN nitrile dendrimers were successfully prepared with good yields of 75%, 61% and 56%, respectively. They were characterized by ^{1}H-NMR and ^{13}C-NMR, FT-IR, MS and EA. The ^{1}H-NMR spectrum (Figure 39) of the G0CN dendrimer showed the expected signals of the nitrile compound, with signals at 1.33, 1.45, 2.46, 2.83 ppm. In Figure 40, the ^{13}C-NMR spectrum presents the characteristic signals of the compound, the signals at 17.04, 26.89, 27.02, 49.03, 49.65 ppm, and the characteristic signal around 118 ppm corresponding to the nitrile functional group. To proceed and to obtain higher generations of the dendrimers, the nitrile dendrimers were reduced to amine-terminated dendrimers. The ^{1}H-NMR and ^{13}C-NMR spectra of the G0NH_2 and G1NH_2 dendrimers presented the expected signals of the compound for the G0NH_2 dendrimer (see annex Figure A1 and Figure A2) and for the G1NH_2 dendrimer (see annex Figure A3 and Figure A4).

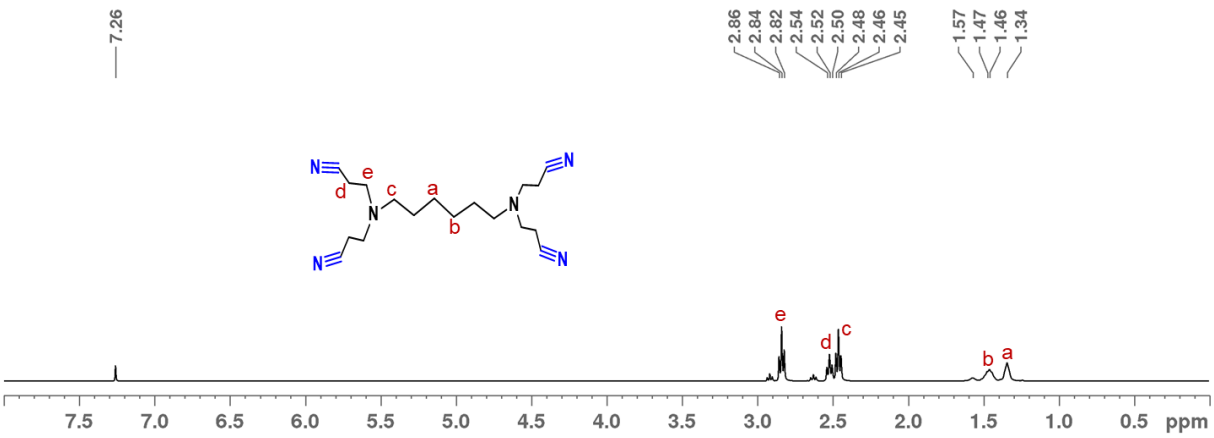

Figure 39. ^{1}H-NMR spectrum of compound G0CN in $CDCl_3$.

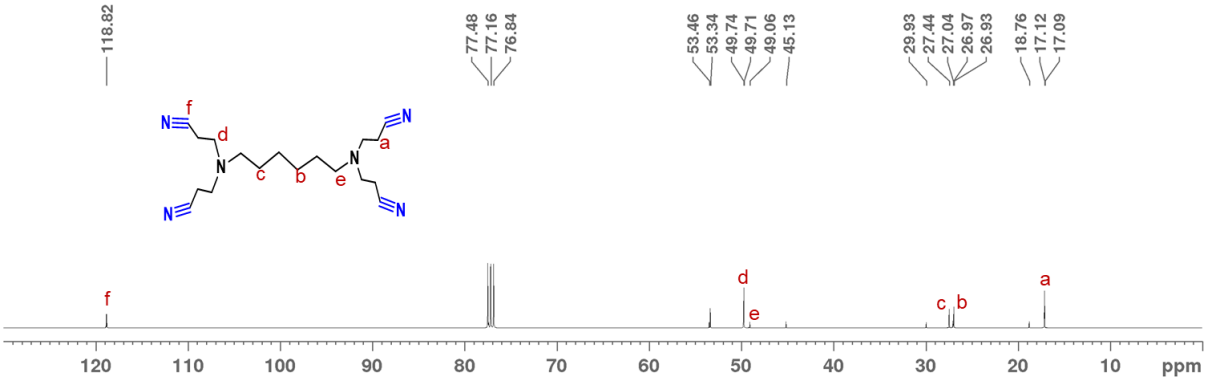

Figure 40. ^{13}C-NMR spectrum of compound G0CN in $CDCl_3$.

The G1CN and G2CN dendrimers displayed the expected proton signals at 1.25, 1.28, 1.42, 2.47, 2.59, 2.85 ppm and at 1.28, 1.43, 1.59, 2.41, 2.49, 2.85 ppm, respectively (Figure 41 and Figure 43). The carbon NMR of the G1CN and G2CN dendrimers (Figure 42 and Figure 44) presented the estimated signals of each dendrimer and the characteristic signal of the nitrile around 118 ppm, corresponding to the nitrile region on the carbon NMR spectrum.

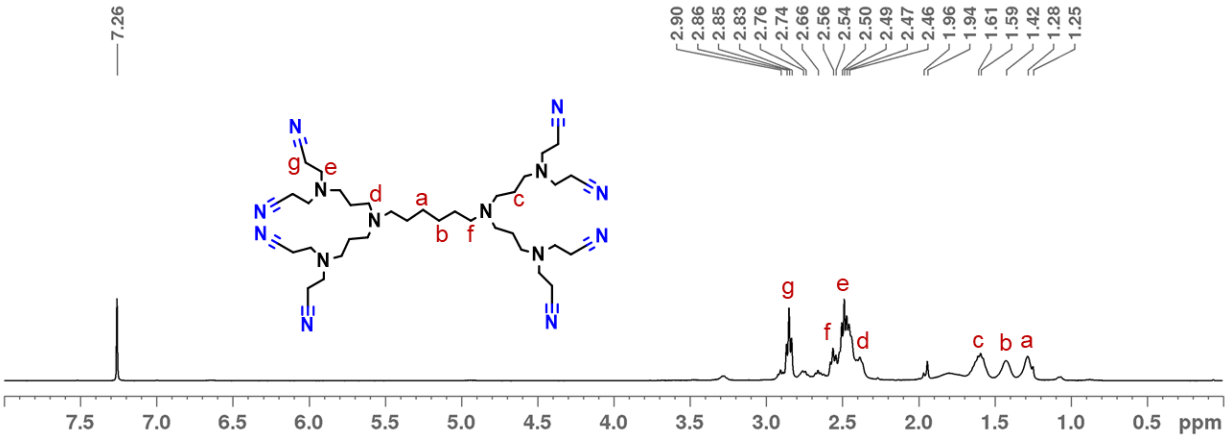

Figure 41. ^{1}H-NMR spectrum of compound G1CN in $CDCl_3$.

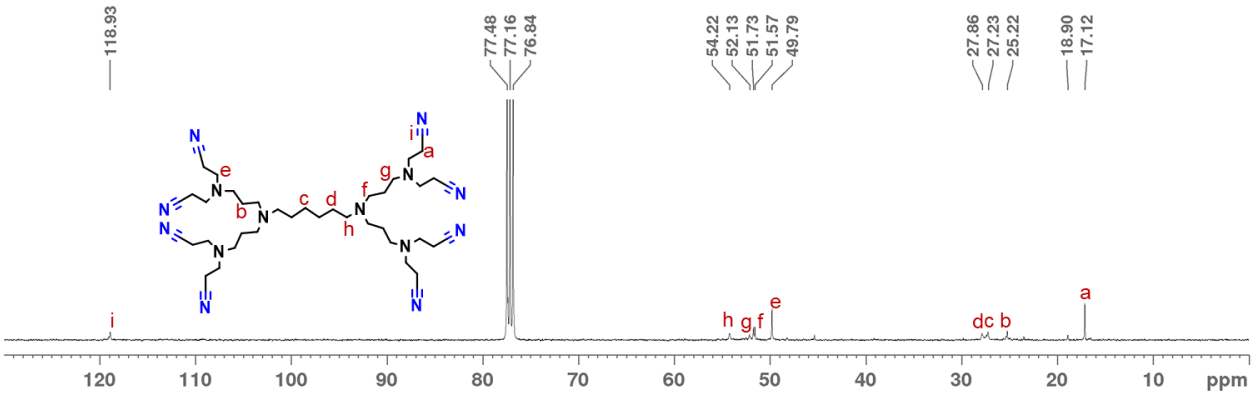

Figure 42. ^{13}C-NMR spectrum of compound G1CN in $CDCl_3$.

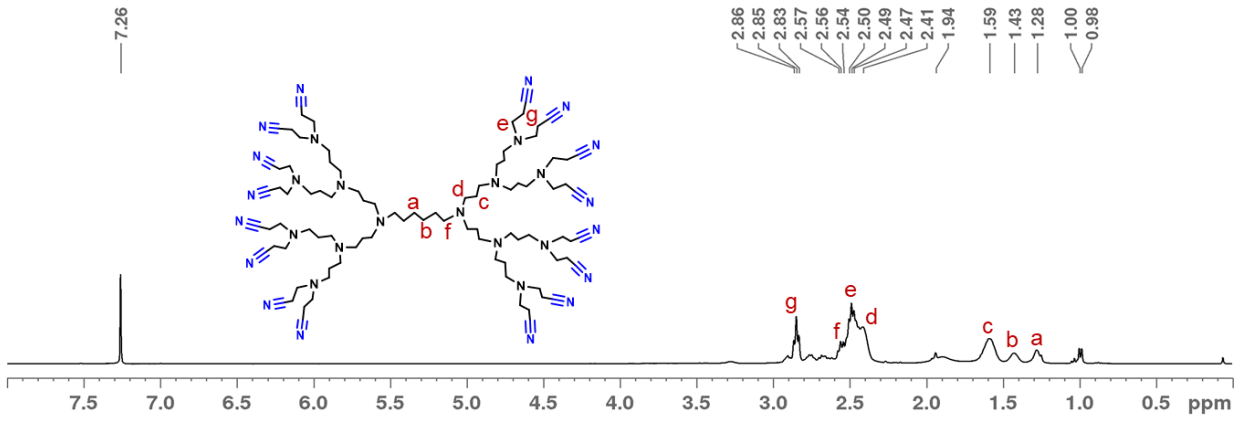

Figure 43. ^{1}H-NMR spectrum of compound G2CN in $CDCl_3$.

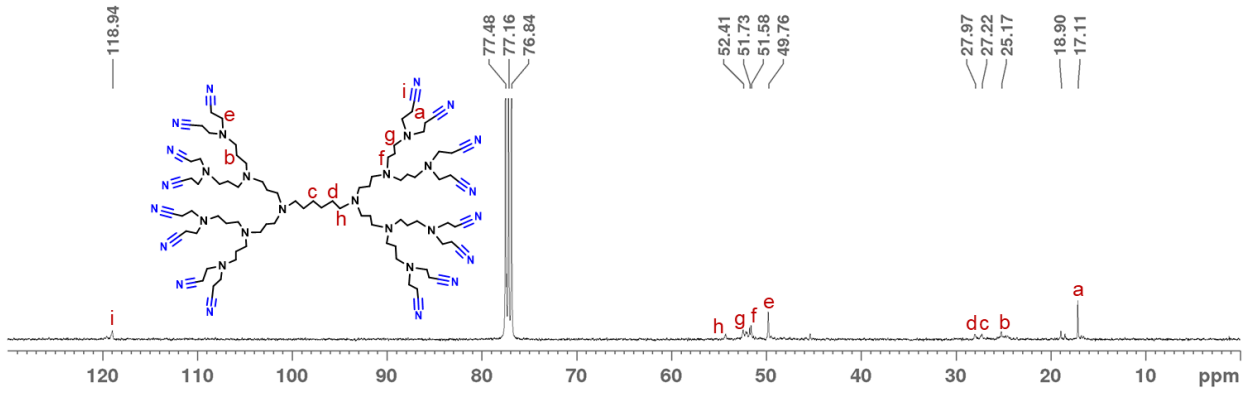

Figure 44. ^{13}C-NMR spectrum of compound G2CN in $CDCl_3$.

The nitrile dendrimers were confirmed by TOF-MS (ESI+) and MALDI analysis. In Figure 45, generation 0 of the nitrile terminated dendrimer presents the expected spectrum with a peak at *m/z* =

329.2 $[M + H]^+$. The generation 1 and 2 nitrile dendrimers were also confirmed by MALDI analysis. The G1CN dendrimer (annex Figure A21) was obtained with a matrix of α-cyano-4-hydroxycinnamic acid and it has a corresponding signal of the dendrimer structure at *m/z* = 769.6 $[M + H]^+$. The G2CN dendrimer presented a peak with low intensity at *m/z* = 1650.2 (annex Figure A22).

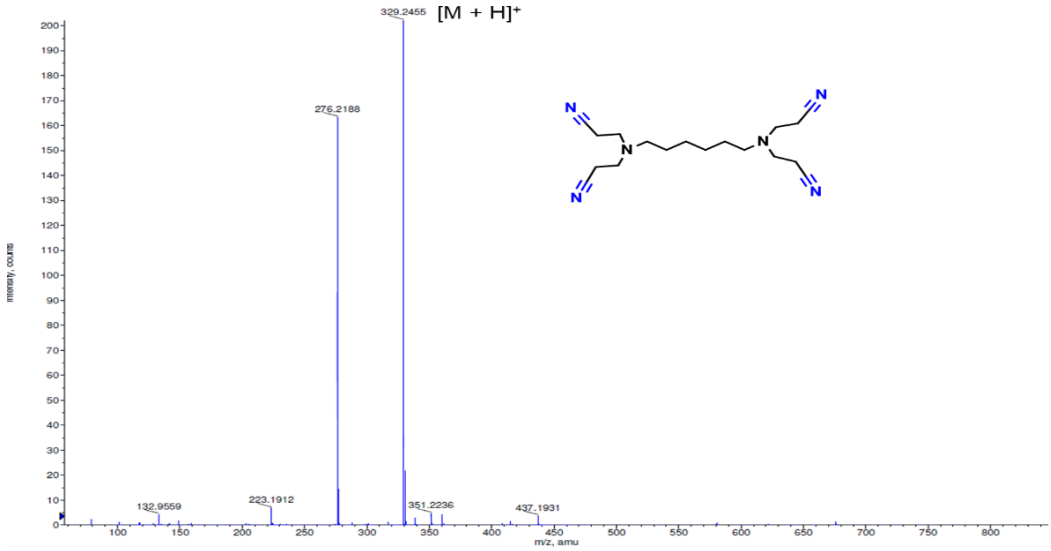

Figure 45. TOF-ESI spectrum of the compound G0CN. The sample was prepared with methanol + 0.1% of formic acid as an ionizing phase.

After preparing the nitrile terminated dendrimers they then served as an anchor to coordinate the ruthenium complex ($[Ru(\eta^5\text{-}C_5H_5)(PPh_3)_2Cl]$) to synthesize the metallodendrimers. The G0Ru and G1Ru metallodendrimers were obtained after precipitation with DCM and n-hexane and washing the product with n-hexane, with yields of 29% and 33%, respectively. The metallodendrimers were fully characterized by ^{1}H-, ^{13}C-, and ^{31}P-NMR, and FT-IR spectroscopies and MS. The elemental analysis (EA) on carbon (C), hydrogen (H), and nitrogen (N) of the G0 ruthenium metallodendrimer is presented in Table 5. For G0Ru metallodendrimer ($C_{186}H_{168}F_{12}N_6O_{12}P_8Ru_4S_4$), and since it is hygroscopic, the EA showed the expected water molecules (5) in its composition, confirming the successful synthesis of the metallocompound.

Table 5. Elemental analysis calculated and found percentages of C, H, and N obtained for the G0 ruthenium metallodendrimers.

		C	H	N
G0Ru	**Calculated**	59.14	4.75	2.22
	Found	59.15	4.94	2.56

The NMR characterization of all the metallodendrimers was performed in $CDCl_3$ and using proton and phosphorous techniques. The proton NMR spectrum of the G0Ru metallodendrimer displayed the expected signals around 7.0 and 7.3 ppm, characteristic of the aromatic protons from the phosphines present in the ruthenium complex (Figure 46). The singlet at 4.48 ppm corresponds to the cyclopentadienyl from the metallic complex. The signals at 1.17, 1.25 and 2.65 – 2.24 ppm are from the dendrimer.

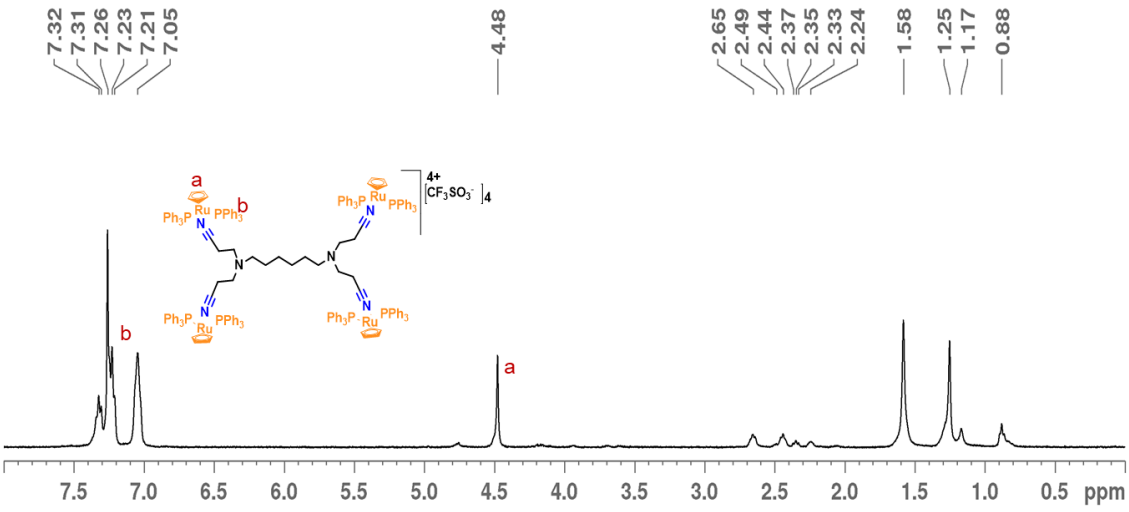

Figure 46. ^{1}H-NMR spectrum of the G0Ru metallodendrimer performed in $CDCl_3$.

The ^{31}P-NMR spectrum of the G0Ru metallodendrimer showed a singlet at 41.88 ppm corresponding to the phosphorous atoms from the phosphines of the ruthenium complex (Figure 47). This signal is different from the free RuCp complex, which presents a signal at 38.83 ppm (see annex Figure A8). The singlet also reveals that all phosphorus atoms are equivalent, suggesting the successful synthesis of generation 0 of the ruthenium metallodendrimer.

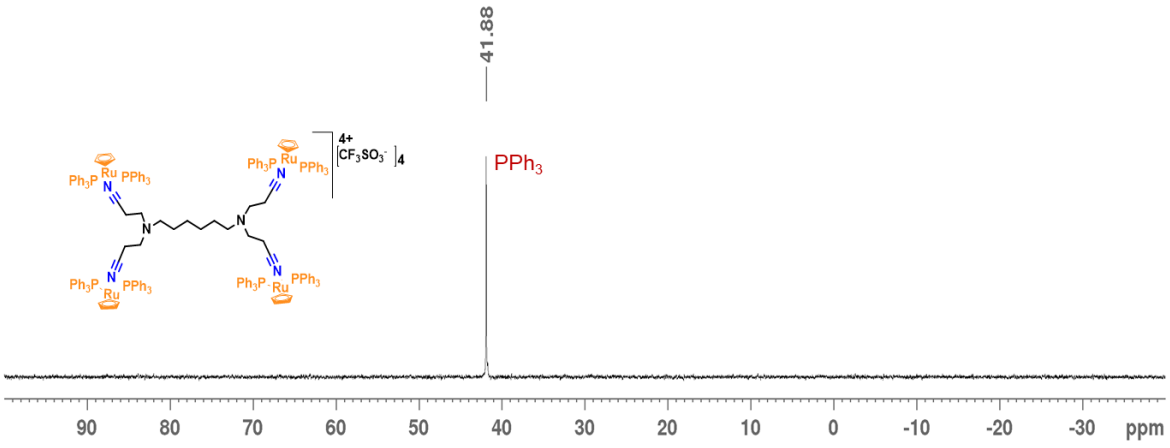

Figure 47. ^{31}P-NMR spectrum of the G0Ru metallodendrimer performed in $CDCl_3$.

The same behavior was also observed with the G1Ru metallodendrimer, with all the expected signals of the compound presented. The ^{1}H-NMR spectrum (Figure 48) displayed the signals around 7.0 and 7.5 ppm that are characteristic of the aromatic protons from the phosphines present in the ruthenium complex. The signal at 4.47 ppm corresponds to the cyclopentadienyl from the metallic complex. The signals at 1.25, 1.78, and 2.33 – 2.35 are attributed to the dendrimer structure.

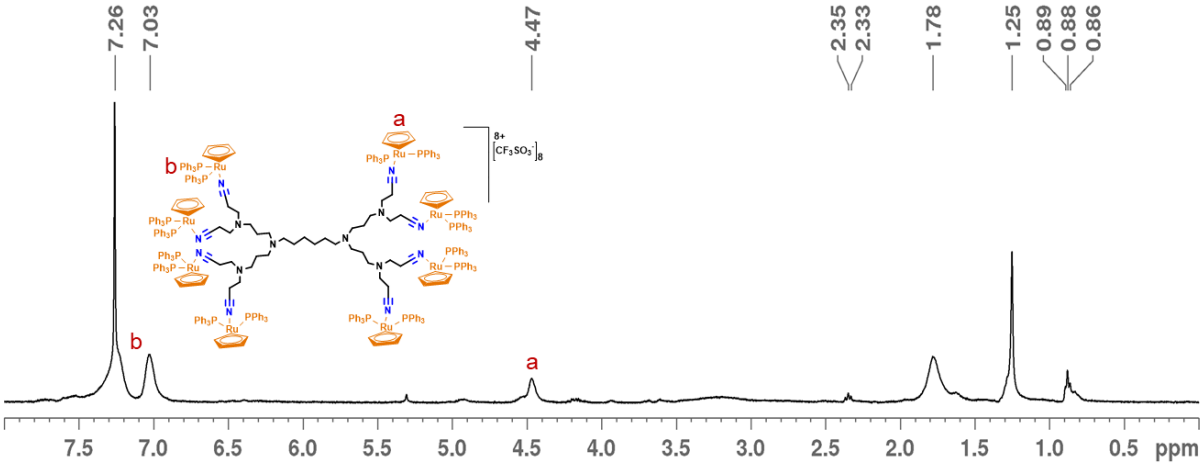

Figure 48. ^{1}H-NMR spectrum of the G1Ru metallodendrimer performed in $CDCl_3$.

In Figure 49, the ^{31}P-NMR spectrum of the metallodendrimer shows as a singlet at 41.56 ppm from the phosphorous from the ruthenium complex. This also suggests that the synthesis of the ruthenium metallodendrimer was successfully accomplished.

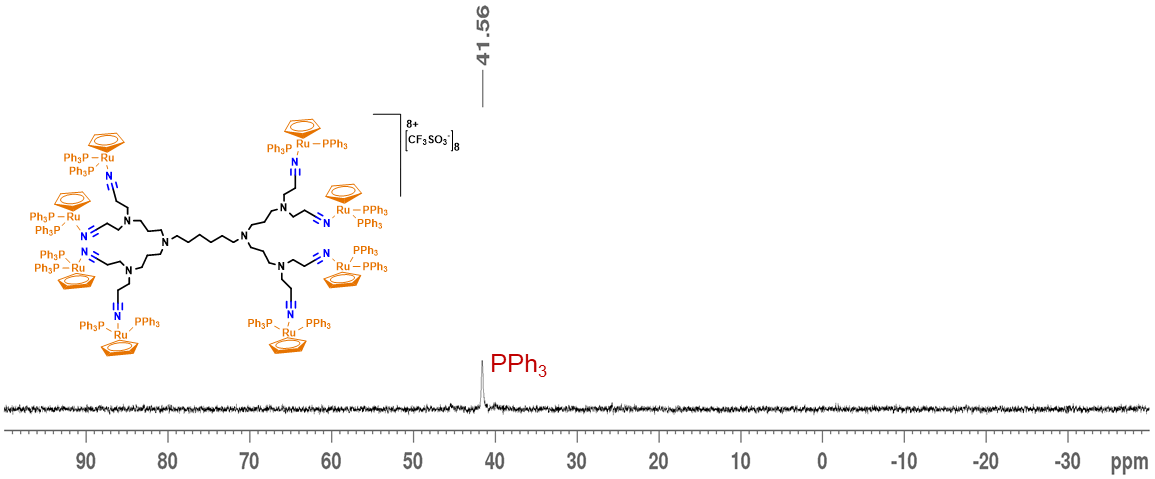

Figure 49. ^{31}P-NMR spectrum of the G1Ru metallodendrimer performed in $CDCl_3$.

The G0Ru and G1Ru metallodendrimers were characterized by FT-IR using KBr pellets, and the nitrile dendrimers (G0CN, G1CN, and G2CN) were characterized using NaCl cells. As can be seen in Figure A23 (see annex), a shift to higher wavelengths is noticed in the G0Ru metallodendrimer, from 2247 cm^{-1} to 2363 cm^{-1}, of the nitrile band correspondent to the C≡N stretch, confirming the successful coordination of the RuCp complex to the nitrile dendrimer (G0CN). The FT-IR spectrum of the G1Ru metallodendrimer (see annex Figure A24) is also shifted to higher wavelengths of the nitrile band C≡N stretch in the G1Ru metallodendrimer, from 2248 cm^{-1} to 2363 cm^{-1}. This data confirms the coordination of both nitrile dendrimers with the RuCp complex.

The formation of generation 0 to 2 ruthenium metallodendrimers were also confirmed by the ESI^+ TOF-MS technique. The G0Ru metallodendrimer has a corresponding signal of the metallodendrimer product with 2 triflate counterions in the structure at *m/z* = 1694.83 $[M + 2(CF_3SO_3^-)]^{2+}$ (see annex Figure A25) and with 3 triflate counterions at a lower portion at *m/z* = 3538.61 $[M + 3(CF_3SO_3^-)]^+$ (Figure 50). The G1Ru metallodendrimer presented a peak with ruthenium at *m/z* = 1007.03 $[M + 7(CF_3SO_3^-) - C_5H_5 - 3(C_6H_6)]^+$ and at *m/z* = 1011.03 $[M + 7(CF_3SO_3^-) - 3(C_6H_6)]^+$ (annex Figure A26). In annex Figure A27 a peak of the G1Ru metallodendrimer with ruthenium is also visible at *m/z* = 1036.04 $[M + 7(CF_3SO_3^-) - C_6H_6]^+$.

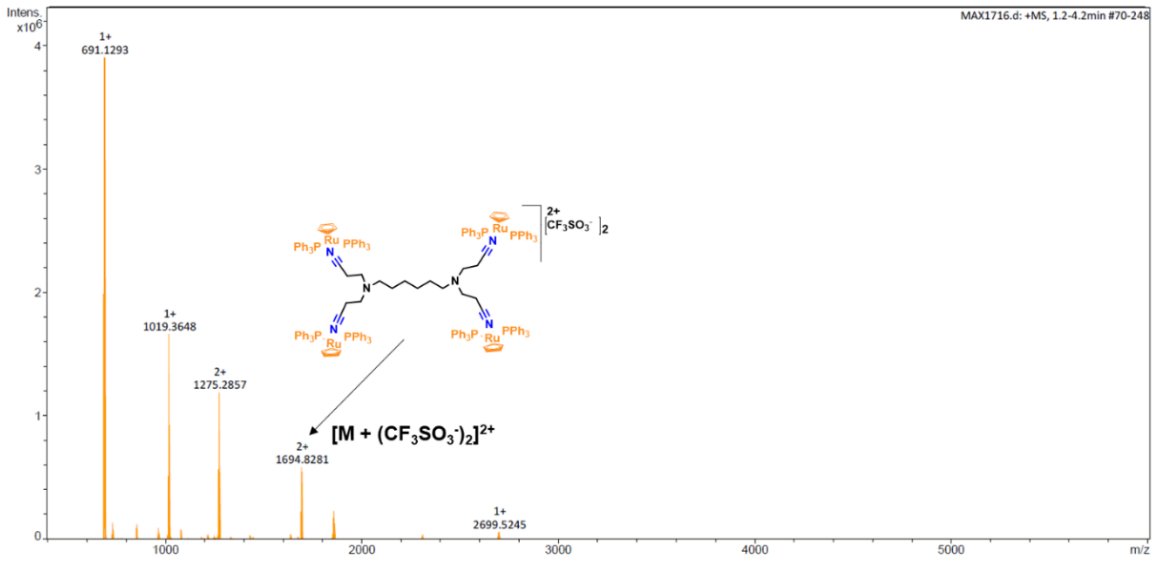

Figure 50. Mass spectrum of G0Ru metallodendrimer.

3.2. Cell viability assay

The generation 0 to 2 nitrile dendrimers (G0CN, G1CN, and G2CN), the cyclopentadienyl ruthenium complex $[Ru(\eta^5\text{-}C_5H_5)(PPh_3)_2Cl]$ (RuCp), and the generation 0 and 1 ruthenium metallodendrimers (G0Ru and G1Ru) were assessed on the TZM.bl cell line for their cytotoxicity using the MTT assay (Figure 51). TZM.bl cells were treated for 48 h with a range of concentrations between

0.01 to 25 µM of each compound. 0.5% DMSO (vehicle control) and 10% DMSO (v/v) were used as negative and positive controls, respectively. Compounds were considered to be non-toxic when cell survival was superior to 80% compared to the negative control. The cell viability of the nitrile dendrimers G0CN and G1CN presented to be non-toxic at all the tested concentrations. The G2CN dendrimer was nontoxic up to 10 µM. The RuCp complex presented toxicity at 1 µM, as did the G0Ru and G1Ru metallodendrimers. The effect of the G2CN dendrimer on cell viability was performed to determine the acceptable concentrations to use in the anti-HIV-1 infection assay and to evaluate their antiviral potential towards HIV-1 infection.

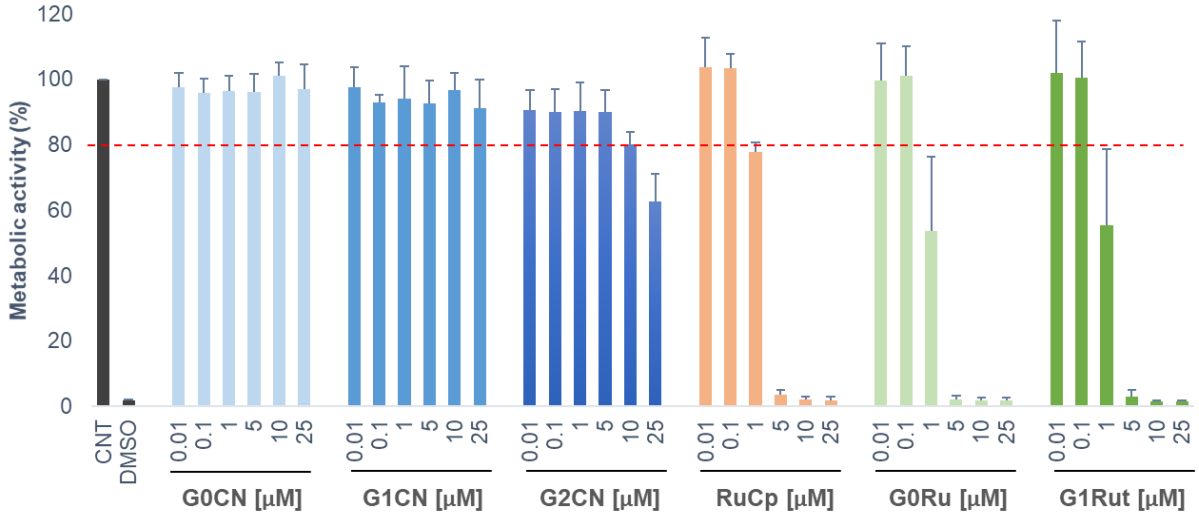

Figure 51. Viability of TZM.bl cells upon exposure to different compounds: nitrile dendrimers, RuCp complex, and G0 and G1 ruthenium metallodendrimers. TZM.bl cells were subjected for 48 h to nitrile dendrimers (G0CN, G1CN, G2CN), [Ru(η^5-C_5H_5)(PPh_3)$_2$Cl] (RuCp), and metallodendrimers (G0Ru and G1Ru) within a concentration range of 0.01 µM to 25 µM. Negative (CNT, 0.5%DMSO, vehicle control) and positive controls (DMSO at 10% v/v) are indicated. Data are represented as mean ± SD of three independent experiments performed in triplicate.

3.3. Anti-HIV-1 activity of the nitrile dendrimers and metallodendrimers

The anti-HIV-1 activity was evaluated using TZM.bl cells. The ability of other dendrimers to prevent HIV-1 infection was also assessed. For the nitrile dendrimers, the nontoxic concentrations tested were 0.1 µM (G0CN), G1CN (10 µM), and 1 and 5 µM (G2CN). The RuCp complex was used at 0.1 µM, and for G0Ru and G1Ru were also used at 0.1 µM. The anti-HIV-1 activity results obtained for the nitrile dendrimers, the RuCp complex and the G0Ru and, G1Ru metallodendrimers for the R5-HIV-1_{NLAD8} isolate showed that these compounds were unable to inhibit this HIV-1 strain (Figure 52a). The same happened with the X4-HIV-$1_{NL4.3}$ isolate (Figure 52b), where the compounds did not present any anti-HIV-1 activity. This can be justified due to the affinity of the gp120 V3 loop of HIV-1 that has a positive global charge.[399] As a result, compounds negatively charged compounds interact more efficiently with HIV-1 than those with neutral or positive charge.[400,401] Consequently, this may be the reason why the nitrile dendrimers,

neither the neutral ruthenium organometallic moiety RuCp or the cationic metallodendrimers (G0Ru, and G1Ru) were unable to prevent HIV-1 infection.

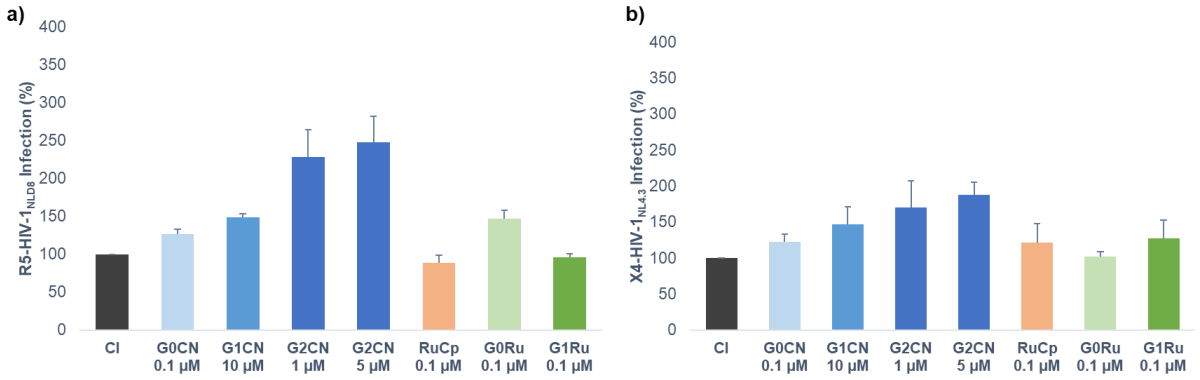

Figure 52. HIV-1 inhibition assays. TZM.bl cells were treated with G0CN (0.1 µM); G1CN (10 µM); G2CN (5 µM); RuCp (0.1 µM); G0Ru and G1Ru (0.1 µM) dendrimers for 1 h and then infected with (a) R5-HIV-1_{NLAD8} or (b) X4-HIV-$1_{NL4.3}$ isolates for 2 h. Luciferase activity was measured after 48 h of infection. CI is the control of infection. The data represent the mean ± SD of three independent experiments performed in triplicate.

4. Conclusions

We prepared low generation dendrimers from 0 to 2 with nitrile terminal groups (G0CN, G1CN, and G2CN), a ruthenium complex [Ru(η5-C_5H_5)(PPh_3)$_2$Cl] (RuCp), and generation 0 and 1 of ruthenium metallodendrimers (G0Ru and G1Ru). All these compounds were characterized by NMR, MS, FT-IR, and EA techniques, and their cytocompatibility and capacity as potential antivirals towards HIV-1 infection were assessed. The generation 0 and 1 nitrile terminated dendrimers presented to be non-toxic at the tested concentrations, and the G2CN dendrimer was biocompatible up to 10 µM. For the metallocompounds, the RuCp complex, and the G0Ru and G1Ru metallodendrimers, they presented to be toxic from 1 µM up to 25 µM. As such, the selected concentrations to proceed to the anti-HIV-1 assays were chosen from the nontoxic concentrations of each compound. The results showed that neither the nitrile dendrimers nor the metallocompounds presented any anti-HIV-1 activity towards the two HIV-1 strains, R5-HIV-$1_{NLAD8,}$ and X4-HIV-$1_{NL4.3}$. As it is known, compounds with negative charges interact with HIV-1 with more affinity than those with neutral or positive charges. Indeed, our neutral charged poly(alkylidenamine)-based dendrimers with nitrile terminal groups and the cationic metallodendrimers functionalized with the ruthenium moiety [Ru(η5-C_5H_5)(PPh_3)$_2$Cl] will not be able to interact with the gp120 V3 loop, and thus, will not prevent HIV-1 infection. To ensure the possibility of these cationic metallodendrimers to present some anti-HIV-1 activity, a modification of the system may be necessary to make them more attractive to interact with HIV-1.

Chapter 4.

Ruthenium-based metallodendrimers as promising anticancer drugs

Chapter 4. Ruthenium-based Metallodendrimers as Promising Anticancer Drugs

1. Introduction

Metal-based compounds are being explored as a result of their extraordinary outcomes as anticancer drugs due to their diversity and characteristics.[402,403] More precisely, ruthenium complexes are emerging as promising substitutes to platinum compounds due to their anticancer and antimetastatic properties.[273,289,404–406] Ruthenium-based drugs present significant advantages. Such as different oxidation states (II, III, IV) and the fact that the reduction to ruthenium (II) can occur because of the low pH in the interior of cancer cells, which can affect the cytotoxicity.[273,402,407,408] Ruthenium compounds present less toxicity than platinum compounds and can mimic the behavior of iron in living cells.[85,407,408] In addition to this behavior, ruthenium can bind to plasma proteins and can consequently be transported by proteins such as transferrin to tumor cells and internalized by endocytosis instead of iron.[317,409] NAMI-A was the first ruthenium compound to enter clinical trials, followed by two more ruthenium compounds, KP1019 and KP1339 (Chapter 1, Figure 16).[273,410] However, NAMI-A and KP1019 failed because of severe side effects and poor solubility.[273]

Nevertheless, several ruthenium complexes have been investigated as potential new metallodrugs.[314,317,411–413] One of the ruthenium complexes that displays promising results against several cancer cell lines is ruthenium(II)-cyclopentadienyl tested *in vitro* by our group in a set of cancer cell lines.[314] The ruthenium(II)-cyclopentadienyl complex presented IC_{50} values significantly inferior to cisplatin with high cytotoxicity in numerous tumors.[289,414] In 1969, G. Wilkinson and coworkers have discovered a ruthenium bis-phosphine complex, $[Ru(\eta^5\text{-}C_5H_5)(PPh_3)_2Cl]$, as a side product when reacting $[RuCl_2(PPh_3)_3]$ with cyclopentadiene.[415] Later in 1971, F. G. A. Stone and collaborators confirmed this ruthenium-cyclopentadienyl complex synthesis, presenting its characterization and reactivity.[416] And, in 1977, M. Bruce in the Australian Journal of Chemistry presented the preparation of several cyclopentadienyl ruthenium tertiary phosphine halide complexes with high-yield, including the synthesis of RuCp followed by us in this work.[398]

Nanotechnology has advanced exponentially in the last decades to discover new materials for the diagnosis and treatment of several diseases, including cancer. Nanomaterials such as dendrimers present desirable and attractive characteristics for the biomedical field.[166,417] As stated before, dendrimers are globular macromolecules, monodispersed and can be easily conjugated with targeting molecules, amino acids, ligands, among others due to the functional groups on their surface,.[166,417,418] On the other hand, metallodendrimers are nanomaterials that combine metal complexes into the dendrimer structure. The combination of metal complexes with dendrimers can improve the therapeutic advantages of these new nanomaterials for diagnosis and therapy.[419] Indeed, it can also improve the solubility, biocompatibility, and reproducible pharmacokinetics of the metal complexes.[139] Among all the advantages due to the size, metallodendrimers can be explored because of the “enhanced permeability

and retention (EPR) effect" which consists of the preferential accumulation of macromolecules at the tumor site compared to normal tissues.[365,420]

Based on our previous works,[314,364] we have prepared a second-generation poly(alkylidenamine)-based metallodendrimer with the $[Ru(\eta^5\text{-}C_5H_5)(PPh_3)_2]^+$ moieties. The G2Ru metallodendrimer was characterized by ^{1}H-, ^{13}C- and ^{31}P-NMR, mass spectrometry (MS), FT-IR, and UV-Vis techniques. Stability studies were as well performed using ^{1}H- and ^{31}P-NMR, at three different temperatures (4, 25, and 37°C) to evaluate the stability of these metallodendrimers in solution. After that, the dendrimers and metallodendrimers were tested against several cancer cell lines to evaluate their anticancer efficacy. The hemolytic assay was also evaluated using healthy human blood. Additionally, the induction of apoptosis, cell cycle analysis (which cell cycle phase the metallocomponds are arrested), the accumulation of reactive oxygen species (ROS, production of reactive chemical species), and the JC-1 assay to evaluate the mitochondrial membrane potential, were also performed with the prepared metallodendrimers using flow cytometry.

2. Material and Methods

2.1. Materials

The nitrile terminated reactions were prepared according to the strategy developed by our group and described in the previous chapter.[364] The G2Ru metallodendrimer was prepared through a dry argon atmosphere by Schlenk-tube techniques. Methanol, dry diethyl ether, and dry dichloromethane were degassed before use. Methanol extra-dry was bought from Acros Organics. Hydrogen peroxide 30% wt solution (H_2O_2) was obtained from Chem-Lab. Calf thymus DNA (CT-DNA) was bought from Sigma-Aldrich. 4' 6-diamidino-2-phenyindole dilactate (DAPI) was purchased from Sigma-Aldrich. The Annexin V Apoptosis Detection Kit eFluor™ 450 was obtained from Thermofisher Scientific. The CellROX® Green Reagent was bought from Thermofisher Scientific. The JC-1 Mitochondrial Membrane Potential Detection Kit was purchased by Biotium. All other reagents were acquired from Acros Organics and Fisher Chemical and were used as received.

2.2. Synthesis of the metallodendrimers

The generation 0 to 2 ruthenium metallodendrimers were prepared following a methodology previously reported by our group.[364] The synthesis and characterization of the generation 0 and 1 ruthenium metallodendrimers (G0Ru and G1Ru, Figure 53) are described and discussed in the previous chapter (chapter 3).

2.2.1. Synthesis and characterization of G2Ru

[Ru(η^5-C_5H_5)(PPh_3)$_2$Cl] (0.7 g, 1.0 mmol) was added with 70 mL of degassed methanol into a Schlenk under argon and stirred for about 30 min. Silver trifluoromethanesulfonate, $AgCF_3SO_3$ (0.3 g, 1.4 mmol) and G2CN (0.1 g, 0.06 mmol) were added to the previous suspension. The solution was stirred in the dark at room temperature (*ca.* 27°C) for 25 h. The suspension mixture was filtered and the solvent was removed under vacuum to obtain a green solid. The product was then quickly extracted with dichloromethane (DCM) by filtration to prevent decomposition. After several precipitations with DCM/hexane and several washes with hexane, the final G2Ru product (Figure 53) was obtained by removing the solvent under vacuum and a green olive solid with a yield of 26% (0.235 g). ^{1}H-NMR (400 MHz, $CDCl_3$) δ = 7.50 – 7.00 (PPh_3), 4.44 (–C_5**H**$_5$), 2.35 – 1.25 ppm. ^{31}P-NMR (161 MHz, $CDCl_3$) δ = 41.63 (**P**Ph_3) ppm. FT-IR: ν = 2370 cm^{-1} ($\nu_{C\equiv N}$). TOF-MS (ESI+): *m/z* = 1007.02 [M + 7($CF_3SO_3^-$) – 8(RuCp) – 5(C_5H_5) – 10(C_6H_6) + H]$^+$ and at *m/z* = 1009.03 [M + 7($CF_3SO_3^-$) – 8(RuCp) – 4(C_5H_5) – 2(C_6H_6) + 2(PPh_3)]$^+$.

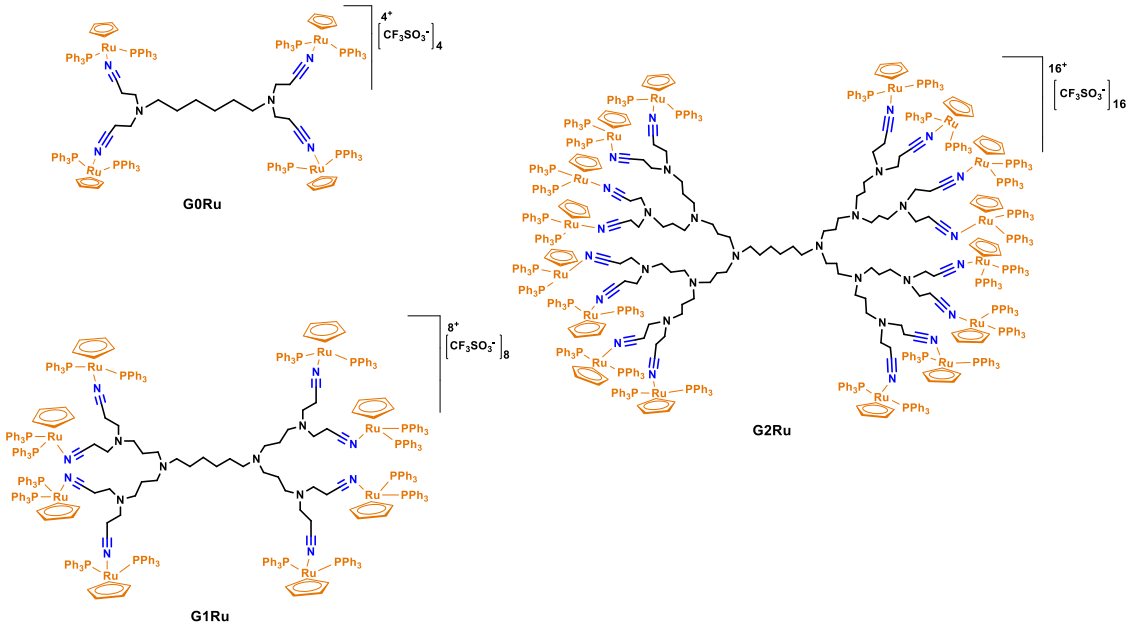

Figure 53. Schematic representation of the ruthenium metallodendrimers (G0Ru – G2Ru).

2.3. Stability studies

Stability studies with generations 0 to 2 of the ruthenium metallodendrimer were carried out using the ^{1}H- and ^{31}P- NMR techniques. A concentration of 0.015 mg/µL was prepared for the ruthenium metallodendrimers in DMSO-d_6. The NMR tubes were incubated at 25°C and 37°C and all studies were done at 25°C and 37°C (probe temperature) to obtain the ^{1}H- and ^{31}P-NMR spectra. The spectra were acquired at different periods. Stability studies of the G0Ru metallodendrimer at a low temperature was also performed using ^{31}P-NMR. The G0Ru metallodendrimer was prepared at a 0.011 mg/µL

concentration in $CDCl_3$. All studies were carried out at 4°C (probe temperature). The probe was cooled down using a liquid nitrogen circulator to maintain the desired temperature.

2.4. Biological assays

2.4.1. Cell viability assays

The dendrimers coordinated with the ruthenium complex were evaluated against several cancer cell lines (A2780, A2780cisR, CAL-72, MCF-7, Caco-2, U-87 MG) and a non-cancer cell line (hMSCs). Cells were seeded in 96-well plates at a density of 5 x 10^3 cells/well with respective culture media for each cell line, supplemented with 10% FBS and 1% antibiotic-antimycotic for 24 h, incubated at 37°C and 5% CO_2. Subsequently, cells were treated with the metallodendrimers, G0Ru, G1Ru, and G2Ru and the nitrile terminated dendrimers, G0CN, G1CN, and G2CN. Cisplatin (cisPt) and ruthenium complex (RuCp) were used as controls at a range concentration of 0.01 µM to 10 µM (prepared in a solution of 5% DMSO). After 72 h of incubation, cell viability was quantified by the measurement of the metabolic activity of the cells in culture through the MTT assay. Briefly, the cell culture medium was replaced with a cell culture medium containing MTT (0.5 mg/mL). The formazan crystals obtained were dissolved in DMSO and the absorbance was measured using a microplate reader.

2.4.2. DNA binding studies

All DNA binding experiments were performed at ambient temperature (~23 °C). The interaction of the G0Ru, G1Ru, and G2Ru metallodendrimers and RuCp complex with calf thymus DNA (CT-DNA) were evaluated by UV−Vis spectroscopy (200−800 nm). To perform the DNA interaction studies, a calibration curve was initially done for the metallodendrimers and the RuCp complex, and the determination of the CT-DNA concentration was calculated at 260 nm using a Molar extinction coefficient of 6600 $M^{-1}cm^{-1}$.[293] The UV-Vis spectra were obtained using 3 µM of the G0Ru and G1Ru metallodendrimers, 1.5 µM of the G2Ru metallodendrimer and 6 µM of the RuCp complex. Increasing concentrations of CT-DNA (0 and 50 µM) were added to the previous solutions. All the ruthenium-based compound solutions were firstly prepared in 5% DMSO in ultrapure water (Milli-Q) and then diluted in 5 mM Tris−HCl, 50 mM NaCl and pH 7.4 buffer. Subsequently, all DNA-metallocompound solutions were incubated at room temperature for 5 min before UV-Vis spectroscopy measurement. Buffer containing the same amounts of DNA were used as reference blanks. The binding constant (K_b) values for each metallocompound were determined by the following equations:[421,422]

$$\frac{\varepsilon_a - \varepsilon_f}{\varepsilon_b - \varepsilon_f} = \frac{b - \sqrt{b^2 - \frac{2K_b^2 C_t\,[DNA]}{s}}}{2K_b C_t}$$

$$b = 1 + K_b C_t + \frac{K_b[DNA]}{2s}$$

where $[DNA]$ is the DNA concentration in base pairs; ε_a, ε_f and ε_b are the apparent, free, and bound metallocompound Molar extinction coefficients, respectively; s is the binding site size in base pairs; and C_t is the total ruthenium compound concentration.

2.4.3. Hematotoxicty

Healthy human blood was obtained from Hospital Dr. Nélio Mendonça, in Funchal, Madeira. Briefly, the hematotoxicity assay was performed as follows: 10% of blood solution in phosphate buffer solution (PBS, Mg^{2+}/Ca^{2+} free) was prepared. Afterwards, a 10 µL volume of blood solution was added to the microtubes. Then, 70 µL of each metallocompound (G0Ru, G1Ru, G2Ru, RuCp, and cisPt) at four different concentrations (0.1, 0.5, 1 and 5 µM) was added to each tube. The solvent control (0.5% DMSO), distilled water and PBS were used for positive and negative controls, respectively. The microtubes were incubated at 37 °C for 3 h. Then, the tubes were centrifuged at 3800 rpm for 10 min. A 40 µL volume of each supernatant was transferred to a 96-well plate, and 160 µL of reagent C was added to each well. The absorbance was measured at 550 nm using a microplate reader.

2.4.4. Apoptosis induction by Annexin V staining

Apoptosis was assessed by the Annexin V Apoptosis Detection Kit eFluor™ 450. MCF-7 cells were cultured and seeded at a cell density of 8 x 10^5 cells per well in a 6-well plate and incubated at 37°C for 24 h. The culture medium was removed and replaced with fresh medium containing the IC_{50} concentration of each metallocompound (G2Ru, RuCp and cisPt) or 0.5% (v/v) DMSO as a control vehicle. After 72 h, the cells were trypsinized, and washed with PBS and then washed once with 1x Binding Buffer before staining with fluorochrome-conjugated Annexin V. After incubating for 15 min at room temperature, the cells were washed and resuspended with 1x Binding Buffer and then the 7-Aminoactinomycin D (7-AAD) viability staining solution was added to the cell suspension. Cells were analyzed and quantified by flow cytometry at 405 nm excitation and 450 nm emission for Annexin V and 488 nm excitation and 647 nm emission for 7-AAD.

2.4.5. Cell cycle assessment

MCF-7 cells were cultured in RPMI medium supplemented with 10% fetal bovine serum (FBS) and 1% antibiotic-antimycotic (AA). Cells were seeded into 6-well plates at a cell density of 8 x 10^5 cells per well and incubated for 24 h. The medium was removed and replaced with fresh medium containing the metallocompounds (G2Ru, RuCp, and cisPt) at their IC_{50} concentration or 0.5% (v/v) DMSO (vehicle control). After 72 h incubation, the cells were trypsinized and washed with PBS before fixation with cold 70% ethanol which was added dropwise while vortexing. Cells were allowed to fix for 30 min at 4°C. After

incubation, the cells were washed twice with PBS and centrifuged at 850 *g* to obtain the cell pellet. The cells were then treated with 100 µg/mL of RNase. Afterwards, 4' 6-diamidino-2-phenyindole (DAPI, 50 µg/mL) was added to label the DNA. Flow cytometry was used to assess the DNA content (DAPI: 358 nm excitation and 461 nm emission).

2.4.6. Analysis of Reactive oxygen species (ROS) accumulation

To evaluate the accumulation of mitochondrially produced by intracellular ROS, MCF-7 cells were plated at a density of 5 x 10^5 cells per well into 6-well plates. After 24 h, the medium was removed and replaced with a fresh medium containing the metallocompounds (G2Ru, RuCp and cisPt) at their IC_{50} concentration or 0.5% (v/v) DMSO (vehicle, control). Hydrogen peroxide 30% wt solution (H_2O_2, 50 µM) was used as a positive control and ascorbic acid (4 mM) as a negative control. After 72 h, the medium was removed and a fresh medium containing 5 µM of CellROX® Green Reagent was added and incubated for 30 min at 37°C. Cells were washed with PBS, collected and centrifuged at 850 *g* to get the cell pellet. The production of ROS was analyzed by flow cytometry at 485 nm excitation and 520 nm emission.

2.4.7. Mitochondrial membrane potential

MCF-7 cells were seeded in a 6-well plate with a density of 8 x 10^5 cells/well for 24 h. Then, the medium was removed and replaced with a fresh medium. The metallocompounds (G2Ru, RuCp and cisPt) at three different concentrations and 0.5% (v/v) DMSO (vehicle, control) were added. After 72 h, cells were detached with trypsin, centrifuged at 850 *g* and labeled with the mitochondrial membrane potential probe, JC-1 (1x, Biotium), for 15 min at 37°C. Then, cells were washed with PBS followed by centrifugation. The loss of mitochondrial membrane potential was examined by flow cytometry (Ex/Em: 510/527 nm for green monomeric dye and 585/590 nm for red aggregated dye).

3. Results and Discussion

3.1. Synthesis and characterization of the G2 ruthenium metallodendrimer

The G2Ru metallodendrimer was prepared following the previous work done by our group[314,364] in low yield (26%). As can be seen in Figure 54, the ^{1}H-NMR spectrum of the G2Ru metallodendrimer presented the characteristic signals of the compound. The signals around 7.0 and 7.5 ppm are characteristic of the aromatic protons from phosphines present in the ruthenium complex. The singlet at 4.44 ppm corresponds to the cyclopentadienyl protons from the metallic complex.

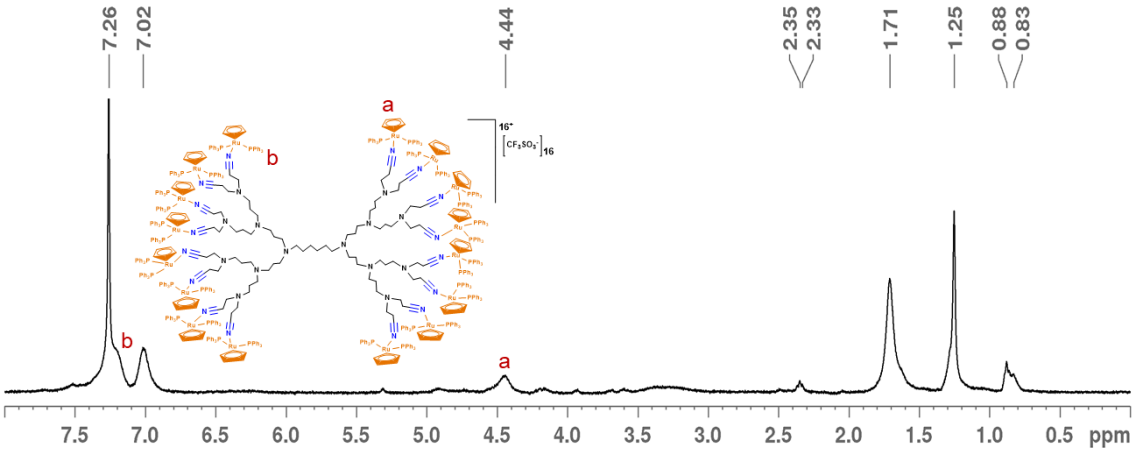

Figure 54. ^{1}H-NMR spectrum of the G2Ru metallodendrimer performed in $CDCl_3$.

In Figure 55, the ^{31}P-NMR spectrum of the metallodendrimer shows a singlet at 41.63 ppm from the phosphorous nucleus from the ruthenium complex. This indicates that the successful synthesis of the G2 ruthenium metallodendrimer was accomplished. The NMR phosphorous signal in all three metallodendrimers presents a singlet around 41 ppm, suggesting the equivalence of phosphorus atoms in the phosphine ligand, which appears, in this deuterated solvent at 38.83 ppm in the free RuCp complex.

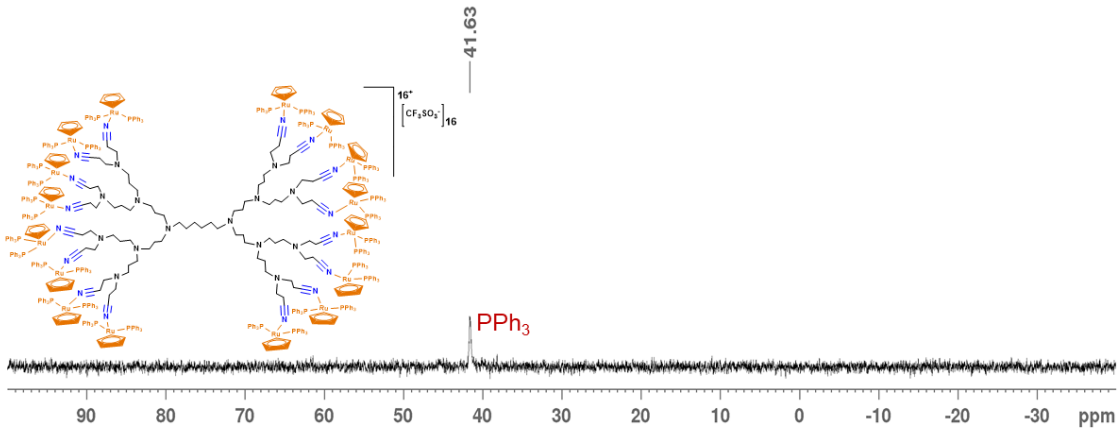

Figure 55. ^{31}P-NMR spectrum of the G2Ru metallodendrimer performed in $CDCl_3$.

All the metallodendrimers were characterized by FT-IR using KBr pellets, while the nitrile dendrimers were characterized using NaCl cells. The FT-IR spectra of the G2Ru metallodendrimers (see annex Figure A28) shifted the nitrile band C≡N stretch to higher wavelengths from 2248 cm^{-1} to 2370 cm^{-1}. This confirms the coordination of the RuCp complex to both nitrile dendrimers. The FT-IR spectra of the G0Ru and G1Ru metallodendrimers were previously discussed in the chapter 3.

The generation 0 to 2 ruthenium metallodendrimers were confirmed by the ESI$^+$ TOF-MS technique. The G2Ru metallodendrimer showed peaks with ruthenium at *m/z* = 1007.02 [M + 7($CF_3SO_3^-$) – 8(RuCp) – 5(C_5H_5) – 10(C_6H_6) + H]$^+$ and at *m/z* = 1009.03 [M + 7($CF_3SO_3^-$) – 8(RuCp) – 4(C_5H_5) – 2(C_6H_6) + 2(PPh_3)]$^+$ (see annex Figure A29).

The UV-Vis studies were performed to identify any evidence of the metal-ligand interaction as charge transfer bands concerning the delocalization of the electronic density between the ligand and the metal center. The absorption spectra were done using two solvents with different polarities, namely methanol (MeOH, polarity index: 5.1) and dichloromethane (DCM, polarity index: 3.1).[423] The UV-Vis spectra of the RuCp complex performed in MeOH presented a bathochromic effect, with a 40 nm shift from 207 nm to 247 nm for the RuCp complex in DCM (Figure 56). This redshift can be attributed to the n → π* transitions of the polar solvent displacement. The molar extinction coefficient (ε) is barely influenced by the solvent, with ε for MeOH an DCM corresponding to 2x10^4 to 3x10^4 $M^{-1}cm^{-1}$, respectively.

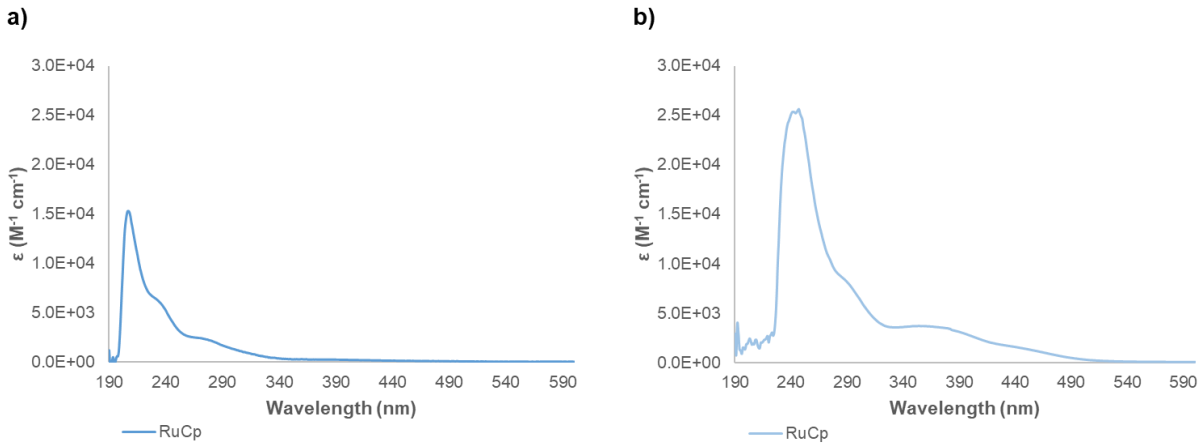

Figure 56. UV-Vis spectra of RuCp complex at 1x10^{-4} M: a) in MeOH and b) DCM.

For the ruthenium metallodendrimers, the UV-Vis spectra were performed in MeOH and in DCM as shown in Figure 57. The metallodendrimers presented a bathochromic effect with redshift n → π* transitions of 24 nm (G0Ru) and 27 nm (G1Ru) for MeOH and DCM, respectively. This trend was not observed in the case of the G2Ru metallodendrimer, where a slight difference of 2 nm was detected and was thus difficult to assign as a blue shift (*i.e.*, hypsochromic effect). As expected, forbidden d-d transitions were also observed in the metallodendrimers dissolved in MeOH and DCM. These transitions can be observed for G0Ru at 354 nm (MeOH) and 352 nm (DCM), G1Ru at 348 nm (MeOH) and 346 nm (DCM) and for G2Ru at 346 nm (MeOH) and 349 nm (DCM), as can be seen in Figure 57a and Figure 57b, respectively. A bathochromic effect was observed with no significant shifts of 5, 4 and 2 nm for G0Ru, G1Ru and G2Ru, when comparing the two solvents. The molar extinction coefficient is barely affected by the solvent for the G0Ru metallodendrimer (1 x 10^4 $M^{-1}cm^{-1}$ in both solvents) and the G2Ru metallodendrimer (6 x 10^4 and 5 x 10^4 $M^{-1}cm^{-1}$ for MeOH and DCM). In the case of the G1Ru

metallodendrimer, the molar extinction coefficient is 4 x 10^3 $M^{-1}cm^{-1}$ for MeOH and 3 x 10^4 $M^{-1}cm^{-1}$ for DCM.

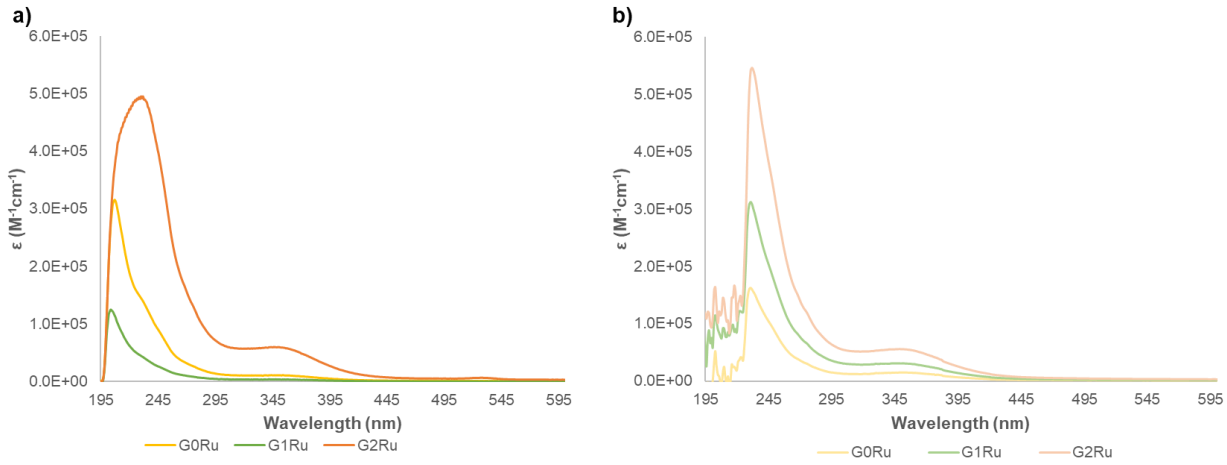

Figure 57. UV-Vis spectra of the ruthenium metallodendrimers (G0Ru, G1Ru, and G2Ru): a) 5 x 10^{-6} M in MeOH and b) 2.5 x 10^{-6} M in DCM.

3.2. Stability studies

The stability studies were carried out by the ^{1}H- and ^{31}P-NMR technique. The three metallodendrimers were dissolved in DMSO-d_6 at a concentration of 0.015 mg/µL, and the studies were first performed at 25°C and 37°C.

As can be seen in Figure 58 and Figure 59, the G0Ru metallodendrimer at 25°C presented new signals after 15 min, probably from the cyclopentadienyl (^{1}H-NMR) and the phosphines (^{31}P-NMR) from the free RuCp. These new signals increased with time indicating that the G0Ru metallodendrimer released the RuCp moiety in 48 hours.

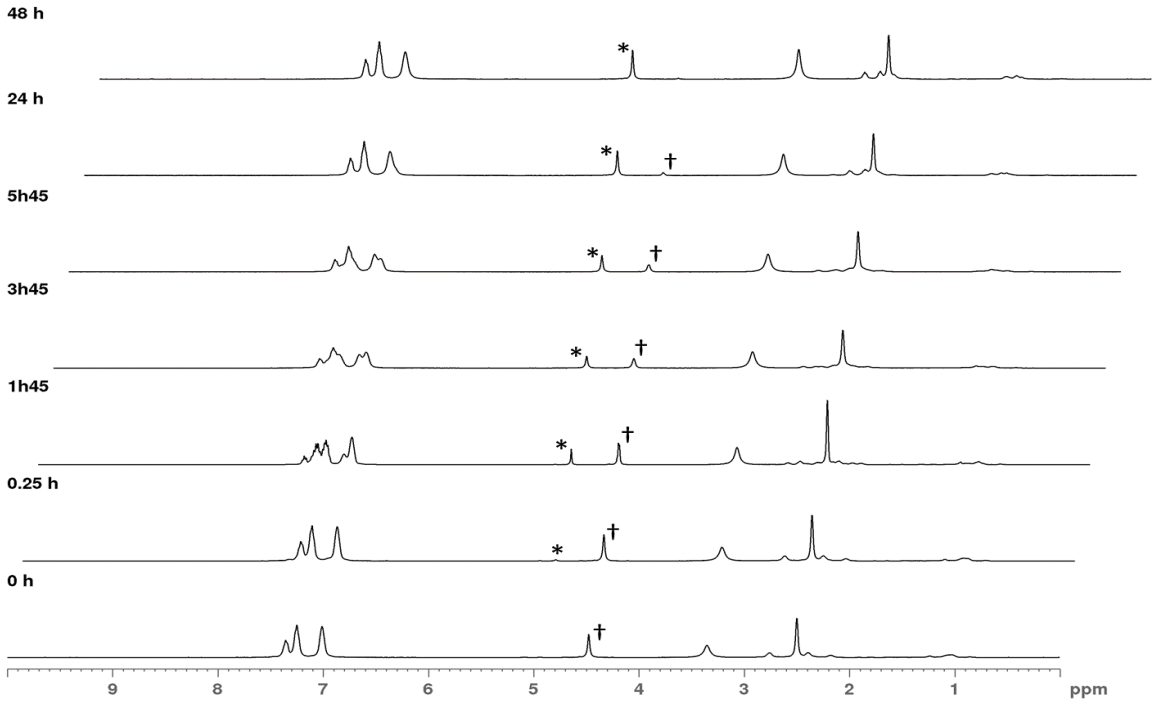

Figure 58. ^{1}H-NMR spectra of generation 0 of the ruthenium metallodendrimer. Stability studies were performed in DMSO-*d6* (probe temperature: 25°C) and the dendrimer solutions were kept at 25°C for a long time. † = proton signal from the cyclopentadienyl of the metallodendrimer, * = proton signal from the cyclopentadienyl of the RuCp complex.

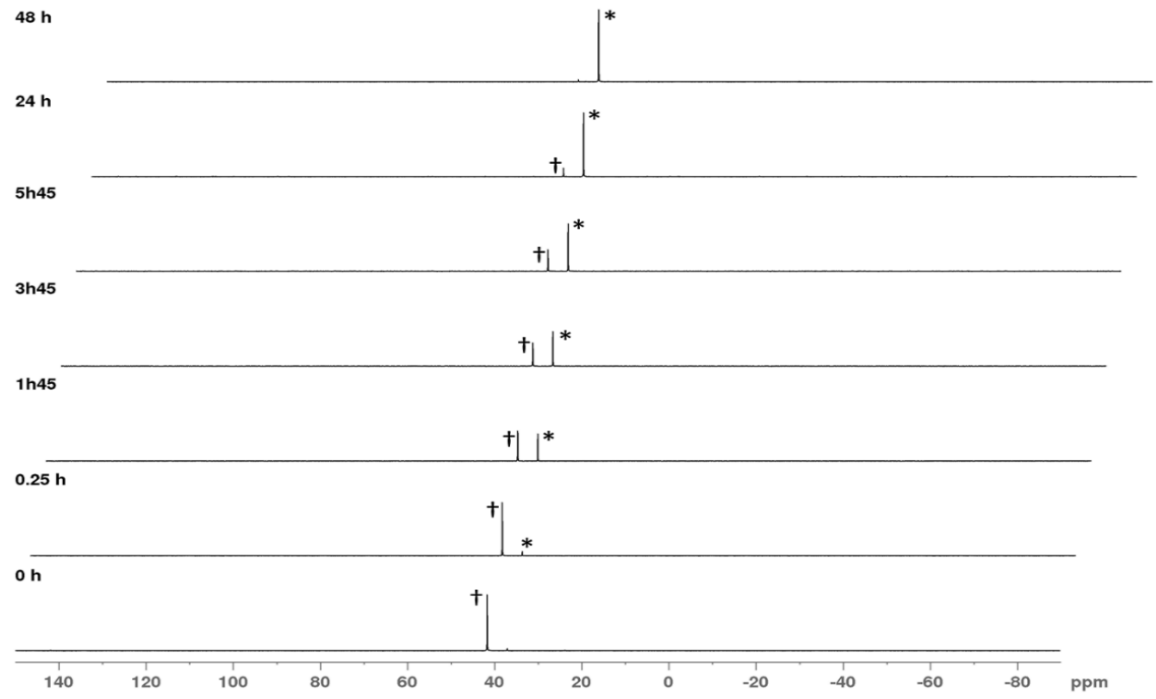

Figure 59. ^{31}P-NMR spectra of generation 0 of the ruthenium metallodendrimer. Stability studies were performed in DMSO-*d6* (probe temperature: 25°C) and the dendrimer solutions were kept at 25°C for a long time. † = phosphorous signal from the phosphines of the metallodendrimer, * = phosphorous signal from the phosphines of the RuCp complex.

Similar behavior was also observed when the stability studies were performed at 37°C (Figure 60 and Figure 61). The release of the ruthenium complex occured after 15 min, with the presence of a new signal from the aromatic protons of the cyclopentadienyl (^{1}H-NMR) and the phosphorus nucleus from the phosphines (^{31}P-NMR). After 48 h the ruthenium complex was almost released from the dendrimer. When comparing the stability studies performed at 25°C and 37°C, the release of the ruthenium complex from the dendrimer starts immediately at 37°C. In the meantime, this process was slower at 25°C, occurring after 15 min but becoming more evident after 1h45. We can conclude that for the G0Ru metallodendrimer, a controlled release of the RuCp complex is achieved at 25ºC after 48 h.

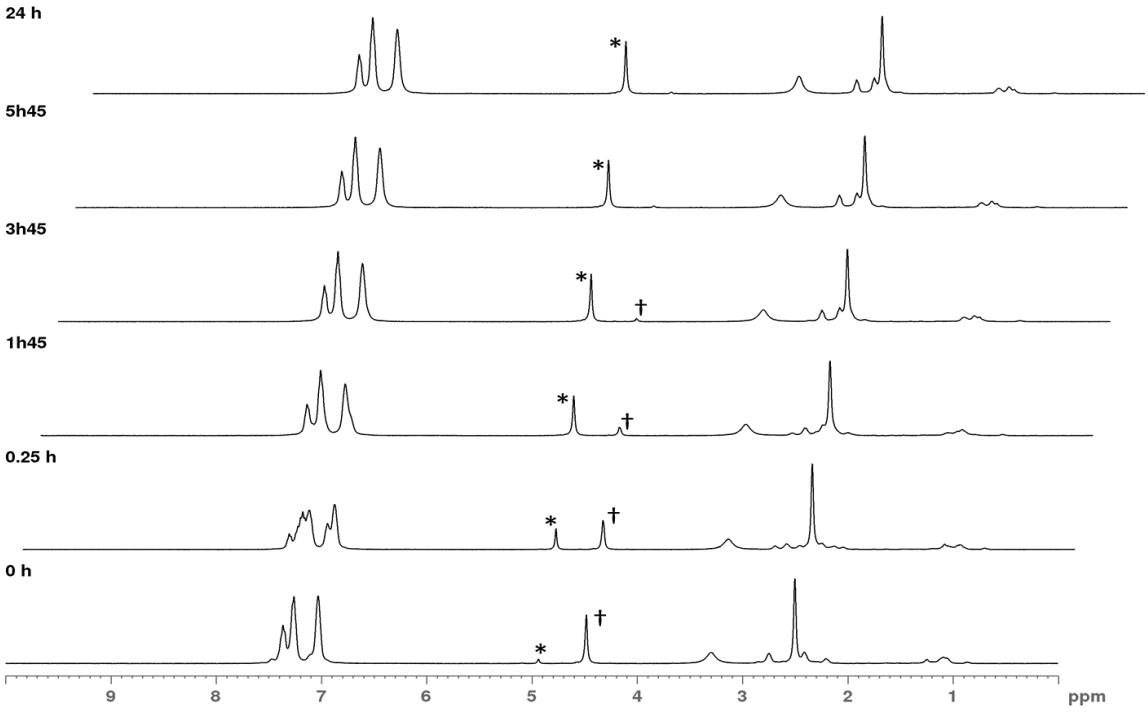

Figure 60. ^{1}H-NMR spectra of generation 0 of the ruthenium metallodendrimer. Stability studies were performed in DMSO-*d6* (probe temperature: 37°C) and the dendrimer solutions were kept at 37°C for a long time. † = proton signal from the cyclopentadienyl of the metallodendrimer, * = proton signal from the cyclopentadienyl of the RuCp complex.

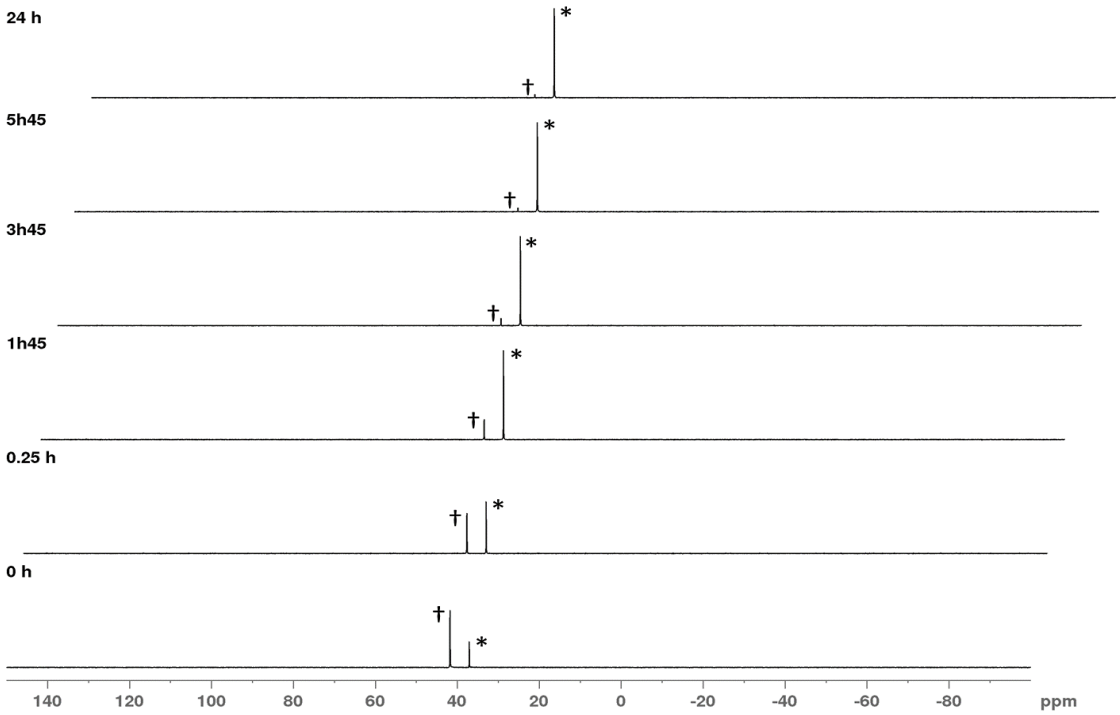

Figure 61. ^{31}P-NMR spectra of generation 0 of the ruthenium metallodendrimer. Stability studies were performed in DMSO-*d6* (probe temperature: 37°C) and the dendrimer solutions were kept at 37°C for a long time. † = phosphorous signal from the phosphines of the metallodendrimer, * = phosphorous signal from the phosphines of the RuCp complex.

The stability studies of the G1Ru and G2Ru metallodendrimers were also investigated. The ^{1}H-NMR and the ^{31}P-NMR (see annex, Figure A30 and Figure A31) of the G1Ru metallodendrimer at 25°C presented new signals of the cyclopentadienyl and the phosphines, respectively. The stability studies at 37°C of the G1Ru metallodendrimer (see annex, Figure A32 and Figure A33) presented an evident release of the ruthenium complex. This is supported by the presence of new signals from the aromatic protons from the cyclopentadienyl (^{1}H-NMR) and the phosphorus nucleus from the phosphines (^{31}P-NMR), suggesting the release of the RuCp complex from the metallodendrimer with time.

The stability studies performed at 25°C presented a slower release of the ruthenium complex from the G2 metallodendrimer, as represented in Figure A34 and Figure A35 (see annex). When compared with the stability experiments done at 37°C (see annex, Figure A36 and Figure A37), the release of the ruthenium complex from the dendrimer started right after it was placed in solution. Taking together both stability studies performed at 25°C and 37°C, and as observed for G0Ru, the release of the ruthenium complex was, as expected, faster at 37ºC than at 25°C.

The stability of the G0Ru metallodendrimer in solution at a low temperature was also conducted using ^{31}P-NMR. Briefly, a concentration of 0.011 mg/µL of the G0Ru metallodendrimer was prepared in $CDCl_3$ and the NMR probe was cooled down using liquid nitrogen. Since DMSO presents a freezing point at 19°C and the experiments could not be carried out at a low temperature (4°C) as planned, chloroform was used instead. As can be seen in Figure 62, the G0Ru metallodendrimer maintained its stability for

80 min (1h20min) at 4°C. A single signal of the phosphines in the phosphorus NMR spectra shows that this metallodendrimer does not release the RuCp complex for at least 1h20min in solution. This suggests that G0Ru keeps its structural integrity with time at lower temperatures. These preliminary results show that probably the metallodendrimer solution can be stored in refrigerated conditions without decomposition before their application.

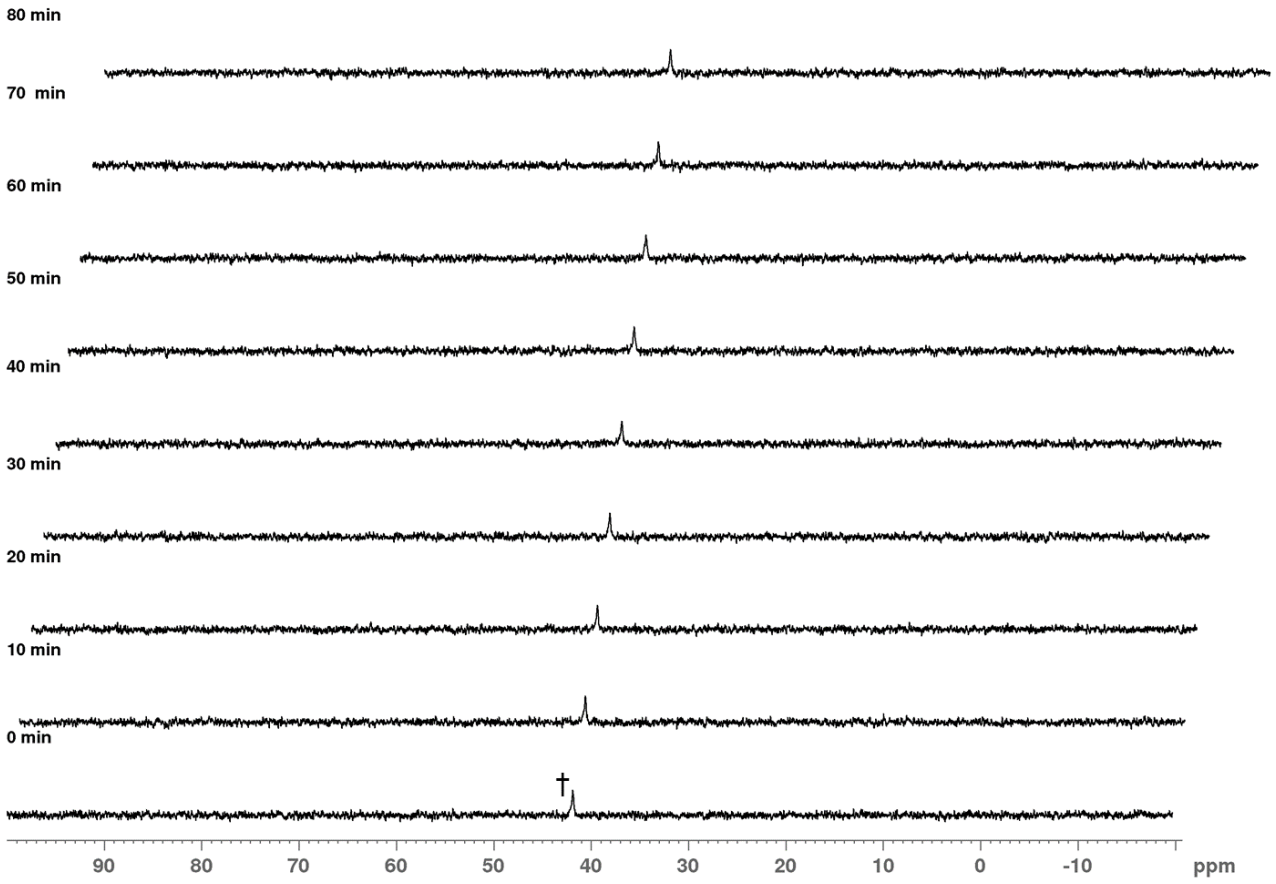

Figure 62. ^{31}P-NMR spectra of the G0Ru metallodendrimer. Stability studies were performed in $CDCl_3$ (probe temperature: 4°C). † = phosphorous signal from the phosphines of the metallodendrimer.

3.3. Cell viability assays

The metallodendrimers were tested against six cancer cell lines to assess their anticancer potential. The *in vitro* cytotoxicity of the G0Ru, G1Ru and G2Ru metallodendrimers were evaluated on the following cancer cell lines: A2780 (human ovarian carcinoma), A2780cisR (human ovarian carcinoma resistant to cisplatin), CAL-72 (human osteosarcoma), MCF-7 (human breast adenocarcinoma), Caco-2 (human colon adenocarcinoma), U-87 MG (human brain glioblastoma) and a non-cancer cell line (hMSCs) using the MTT assay. Cells were treated for 72 h with the metallodendrimers before the MTT assay. The results show that the metallodendrimers present anticancer activity at the low micro- to nanomolar concentration range (Table 6). The IC_{50} values confirm that the metallodendrimers are less toxic in the studied non-cancerogenic cell line presenting IC_{50} values higher than the one showed in the

cancer lines. The ruthenium metallodendrimers have shown excellent anticancer efficacy and generation dependence in these cancer cell lines. Increasing the metal centers per dendrimer also enhanced their toxicity. Cisplatin, which was used as a control, presented higher IC_{50} values in all cell lines tested when compared to the ruthenium-metallodendrimers. The metallocompounds showed to be less toxic in then non-cancer cell line, the hMSC, indicating that they present some selectivity towards cancer cell lines. The G2Ru metallodendrimer proved to be several times more efficient than cisplatin, with it being 4-fold (A2780), 4-fold (Caco-2), 9-fold (MCF-7), 11-fold (CAL-72), 18-fold (U-87MG), and 46-fold (A2780cisR) more cytotoxic than the well-known metallodrug. Our RuCp complex and metallodendrimers present lower IC_{50} values in the A2780 and MCF-7 tumor cells than other cyclopentadienyl Ru(II) compounds.[276,277]

Table 6. IC_{50} values of the metallodendrimers against A2780, A2780cisR, CAL-72, U-87MG, Caco-2, and MCF-7 cancer cell lines and hMSCs as a non-cancer cell line. Data are represented as mean ± SD of at least three independent experiments performed in triplicate.

Compound	M[a]	A2780 (IC_{50}, μM)	A2780cisR (IC_{50}, μM)	CAL-72 (IC_{50}, μM)	U-87MG (IC_{50}, μM)	Caco-2 (IC_{50}, μM)	MCF-7 (IC_{50}, μM)	hMSC (IC_{50}, μM)
cisplatin	1	0.26 ± 0.09	3.41 ± 0.7	1.19 ± 0.45	1.45 ± 0.8	0.37 ± 0.06	0.76 ± 0.16	>10
RuCp	1	0.46 ± 0.18	0.66 ± 0.13	0.61 ± 0.28	0.47 ± 0.16	0.59 ± 0.06	0.37 ± 0.03	3.89 ± 0.3
G0Ru	4	0.30 ± 0.03	0.26 ± 0.08	0.39 ± 0.06	0.36 ± 0.02	0.37 ± 0.04	0.33 ± 0.02	0.83 ± 0.07
G1Ru	8	0.15 ± 0.08	0.23 ± 0.07	0.30 ± 0.1	0.18 ± 0.04	0.26 ± 0.05	0.23 ± 0.05	0.83 ± 0.04
G2Ru	16	0.07 ± 0.01	0.07 ± 0.00	0.11± 0.05	0.08 ± 0.02	0.08 ± 0.01	0.09 ± 0.01	0.39 ± 0.3

[a] Metal centers

3.4. DNA binding studies

The interaction of the metallocompounds with DNA in the presence of different concentrations of CT-DNA was assessed by UV-Vis spectroscopy (see Figure 63). These ruthenium metallocompounds presented a hyperchromic effect, with a slight blue shift. When a hyperchromic effect is noticed, a non-covalent mode of binding to DNA by electrostatic binding occurs and indicates changes in the DNA conformation and structure.[424] The DNA binding constant (K_b) and the binding site size (s) were obtained by observing the changes in the absorbance of each metallocompound in the presence of DNA. The RuCp complex presented a K_b of 3.5 (± 0.02) x 10^{13} M^{-1} and $s = 2.3 \pm 0.0$. The coordination of the RuCp complex to the dendrimer increases the K_b and s values as follows: $K_b = 1.1$ (± 0.1) x 10^{14} M^{-1} and $s =$ 4.7 ± 0.0 for G0Ru; $K_b = 2.7$ (± 0.1) x 10^{14} M^{-1} and $s = 4.7 \pm 0.0$ for G1Ru; and $K_b = 2.1$ (± 0.6) x 10^{14} M^{-1} and $s = 9.4 \pm 0.0$ for G2Ru. These K_b values show a strong binding affinity of the metallodendrimers with DNA when compared to what is found in literature for cisplatin ($K_b =$ 5.7 (± 0.45) x 10^4 M^{-1}).[425] The

increase of the binding site size of these metallodendrimers reveals a concentration-dependent effect, with a higher concentration indicating asmaller binding site size. The binding strength by which these metallocompounds interact with DNA shows that these compounds strongly bind to DNA. This hyperchromic effect by the external contact of the CT-DNA with ruthenium (II) complexes indicates the mode of intercalation by electrostatic binding.[426,427] The *ΔG* energy of the prepared metallocompounds is shown in Table 7. The calculated *ΔG* energy values of the metallodendrimers and the RuCp complex indicate that the interaction of DNA with the metallocompounds each occur as an exothermic reaction with a favorable binding between both molecules.

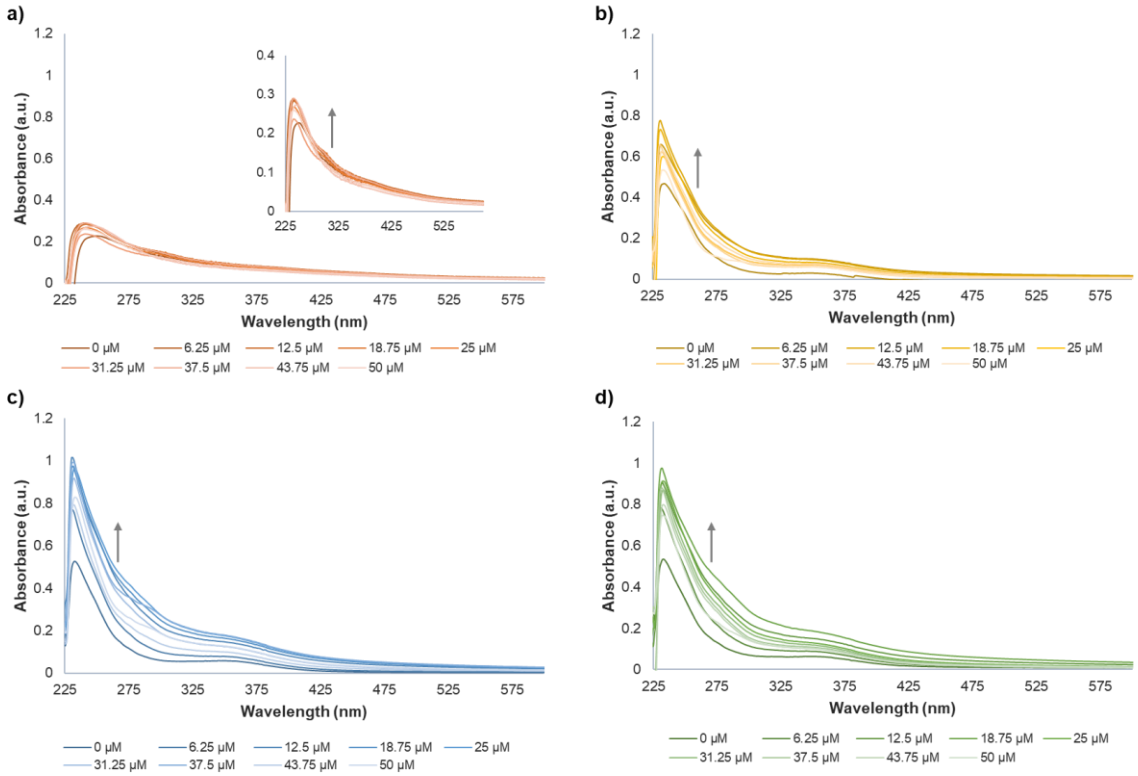

Figure 63. UV spectra of (a) RuCp complex, (b) G0Ru metallodendrimer, (c) G1Ru metallodendrimer and (d) G2Ru metallodendrimer in the absence and presence of increasing concentrations of CT-DNA. Solutions of the RuCp (6 µM), G0Ru (3 µM), G1Ru (3 µM) and G2Ru (1.5 µM) were incubated for 5 min at room temperature in 5 mM Tris-HCl buffer with 50 mM NaCl, pH 7.4. The arrows indicate the increasing absorbance with increasing concentration of CT-DNA.

Table 7. DNA binding constant (K_b), binding size site (*s*), and *ΔG* energy of the metallodendrimers and the RuCp complex. Data are represented as mean ± SD of two independent experiments.

Compound	K_b (M^{-1})	*s*	*ΔG* (kJ mol^{-1})
RuCp	3.5 (± 0.02) x 10^{13}	2.3 ± 0.00	-0.75 ± 0.00
G0Ru	1.1 (± 0.1) x 10^{14}	4.7 ± 2.8 x 10^{-3}	-0.79 ± 0.002
G1Ru	2.7 (± 0.1) x 10^{14}	4.7 ± 5.5 x 10^{-5}	-0.81 ± 0.001
G2Ru	2.1 (± 0.6) x 10^{14}	9.4 ± 2.2 x 10^{-4}	-0.80 ± 0.01

3.5. Hematotoxicity

Hemolysis is used to quantify the membrane disruption of red blood cells by measuring the release of hemoglobin.[428] Taking into consideration the cytotoxicity results in the tested cancer cell lines, all metallodendrimers were analyzed and their potential safety in the presence of human blood was verified, more specifically their toxicity towards red blood cells. As controls were used, water (positive control), PBS (negative control), and 0.5% DMSO (solvent control) for the metallodendrimer and RuCp. After 3 h incubation at 37°C, the metallodendrimers at the higher concentrations presented hemolysis. As can be seen in Figure 64, the G0Ru metallodendrimer presented less or similar toxicity at 0.1 µM (3.3 ± 0.9%) and 0.5 µM (3.8 ± 1.0%) when compared to cisplatin (cisPt) (3.6 ± 1.0% at both concentrations). The G0Ru and G1Ru metallodendrimers showed to be less than 5% toxic and safe up until 1 µM and 0.5 µM, respectively. In the case of the G2Ru metallodendrimer, no toxicity up to 0.5 µM was displayed. In general, all the metallodendrimers presented no toxicity at 0.1 µM, which is in agreement with the IC_{50} values of these metallocompounds. Our metallodendrimers are quite compatible with red blood cells and are safe at a nanomolar range. It is noteworthy that the hemolysis is related to the generation and concentration of the ruthenium-metallodendrimers.[317]

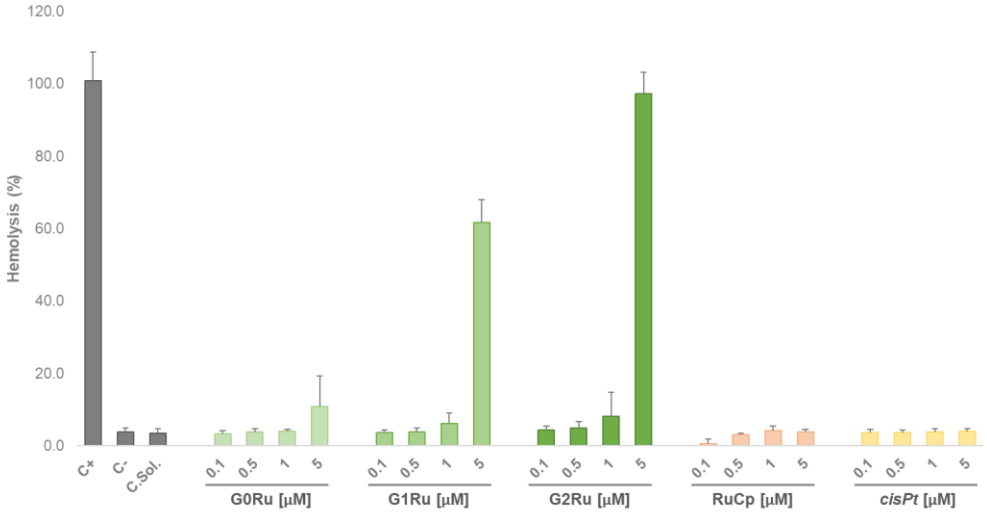

Figure 64. Hematotoxicity of RuCp, cisPt, and the prepared metallodendrimers. Healthy human blood was treated for 3 h with a concentration range of 0.1 µM to 5 µM of cisPt, RuCp and the metallodendrimers (G0Ru, G1Ru, and G2Ru). C+ is the positive control, C- is the negative control, and C. Sol. is the solvent control (0.5% DMSO). Data are represented as mean ± SD of at least three independent experiments performed in quadruplicate.

3.6. Apoptosis induction

Metal complexes have an important role in cell death. They bind to specific residues implicated in enzyme catalysis, which will change the cellular processes leading to cell death (apoptosis).[409] Chemotherapeutic drugs must provoke apoptotic stimuli in tumor cells, with this ability to induce apoptosis being a key factor in establishing drug efficacy.[429] The Annexin V eFluor kit is commonly used to study apoptosis induction. Phosphatidylserine (PS), which is mainly found in the inner plasma membrane, will

be detected by the Annexin V fluorescent label when it loses its asymmetric distribution and is in the exterior of the membrane.[294] To perform this experiment, MCF-7 cells were treated with the IC_{50} concentration of the metallocompounds for 72 h. According to the cytotoxicity studies and the results obtained for the MCF-7 cell line, the G2Ru metallodendrimer, RuCp and cisPt were examined for their capacity to induce apoptosis through double staining with Annexin V eFluor™ 450 and quantification by flow cytometry. To perform the assay, the IC_{50} concentration of each compound was used. The results presented in Figure 65 of the induced apoptosis show that G2Ru had 41.0 ± 1.8% of necrosis and 9.7 ± 2.4% of late-stage apoptosis. The controls, and the RuCp complex presented 33.7 ± 3.0% and 8.3 ± 2.3% and cisPt showed 42.1 ± 3.0% and 8.8 ± 1.5% of necrosis and late-stage apoptosis, respectively. These results indicate the existence of apoptotic cells characterized by the presence of PS on the outer membrane of the cells [294]. Our metallocompounds thus induced cells necrosis, which goes against what is normally found for ruthenium(II) complexes that induce apoptosis.[275,292,293]

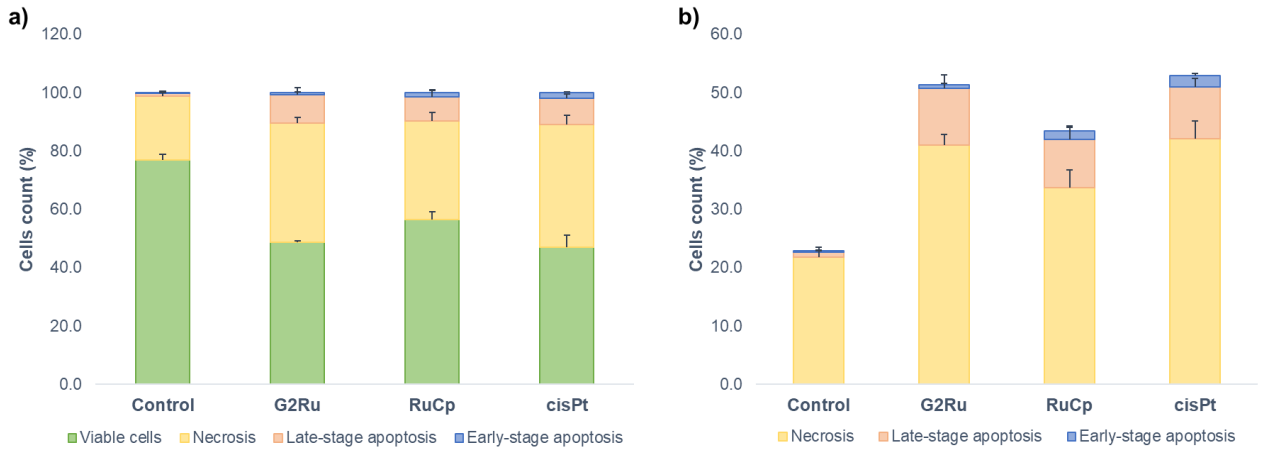

Figure 65. a) Evaluation and quantification of apoptosis and necrosis in MCF-7 cells by flow cytometry with annexin V/7-AAD. Cells were exposed to 0.5% DMSO (vehicle, control) and the IC_{50} of each metallocompound (G2Ru, RuCp and cisPt) for 72 h. Viable cells (Annexin V−/7AAD−), early apoptotic cells (Annexesin V+/7AAD-), late apoptotic cells (Annexesin V+/7AAD+) and necrotic cells (Annexin V-/7AAD+) were detected. b) Percentage of apoptosis in MCF-7 cells exposed to the metallocompounds. Data are expressed as mean ± SD of one experiment performed in triplicate.

3.7. Cell cycle analysis

Normal cell goes through the cell cycle in a regulated mannerbut cancer cells go through the same process with the cell dividing uncontrollably. Cell division has the purpose of replicating DNA to guarantee that the genetic material is replicated and evenly spread into two daughter cells.[281] To verify at which stage the metallocompounds were acting in the cell cycle, an assay was performed. The MCF-7 cells were treated with the IC_{50} concentration of each metallocompound for 72 h and analyzed by flow cytometry using DAPI labeling. As can be seen in Figure 66, the G2Ru metallodendrimer has an effect on cell cycle progression, more precisely in the G0/G1 phase, with 75% when compared to the control (60%) and to the other metallodrugs, RuCp (31%) and cisPt (60%). Since cell cycle arrest occurs in the G0 phase, the influence of the G2Ru metallodendrimer seems to inhibit cell growth affecting the

metabolic changes for normal cell division, as such, the G2Ru metallodendrimer presented a cytostatic effect in the MCF-7 cell line, which is in line with the results achieved by de la Mata.[430] Interestingly, the RuCp complex has an impact on the S phase responsible for DNA synthesis, with 48% of the cells in this phase. The other ruthenium polypyridyl complexes on the other hand were shown to act at the G0/G1 phase.[283,285,431]

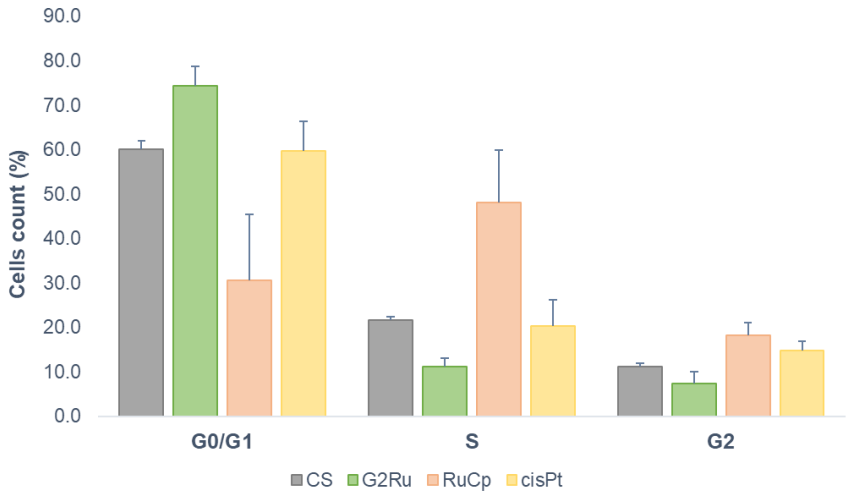

Figure 66. Percentage of MCF-7 cells in each phase of the cell cycle – G1/G0, S and G2 phases and analyzed by flow cytometry. Cells were exposed to a 0.5% (v/v) DMSO solution (vehicle control) or to the IC_{50} of each metallocompound for 72 h. Data are expressed as mean ± SD of one experiment performed in triplicate.

3.8. Reactive oxygen species (ROS) production

Transition metals, including Ru, accumulate in the mitochondria producing ROS. This characteristic causes free radicals in cancer cells and inactivates antioxidant proteins such as glutathione in an acidic microenvironment.[404] Cancer cells usually present high levels of ROS attributed to the mitochondrial DNA mutation as characteristic of genetic instability.[285] Metal complexes have been known for their capacity to induce high levels of oxidative stress and thus lead to cell death.[293,409] The growth-inhibitory effect is due to the increase and production of intracellular ROS, which has a significant role in the induction of apoptosis.[429,431] Therefore, MCF-7 cells were incubated with the IC_{50} concentration of each metallocompound for 72 h. Subsequently, cells were incubated with the CellROX® dye for 30 min before their quantification by flow cytometry. In Figure 67, the G2Ru metallodendrimer was able to induce intracellular ROS, as did cisPt and RuCp, which interestingly, contrasts with what is found in literature about ruthenium (II) complexes, such as Ru(cymene), Ru(arene) and Ru(polypyridyl), that induce low levels of ROS.[293,412,432]

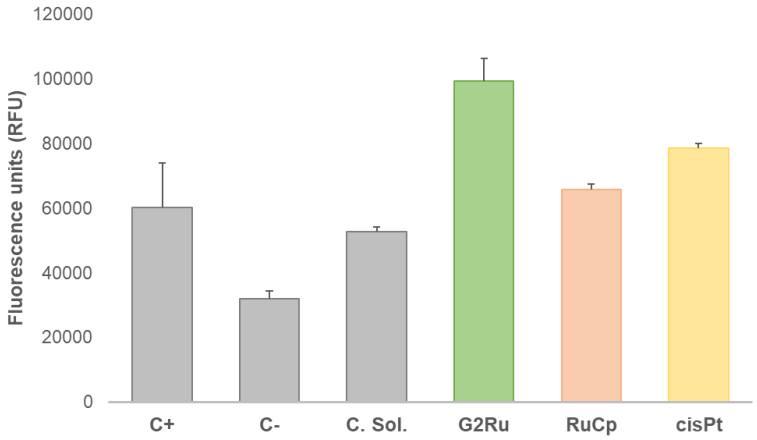

Figure 67. Reactive oxygen species (ROS) in the MCF-7 cell line were determined by flow cytometry. Cells were exposed to 0.5% (v/v) DMSO (vehicle control), hydrogen peroxide (H_2O_2, 50 µM, positive control), ascorbic acid (4 mM, negative control) and the metallocompounds, G2Ru, RuCp and cisPt at their IC_{50} concentration for 72 h. The data are represented as mean ± SD of one experiment performed in triplicate.

3.9. Mitochondrial membrane potential

The mitochondria have a relevant function associated with the intrinsic pathway of apoptosis, more particularly with the disruption and constant dissipation of the internal mitochondrial transmembrane potential ($\Delta\Psi_m$).[431,433,434] JC-1 (5,5′,6,6′-tetrachloro-1,1′,3,3′-tetraethylbenzimidazolylcarbocyanine iodide) is a lipophilic cationic dye that detects the loss of the mitochondrial membrane potential through the interaction with the negative charge of the mitochondria internal membrane and the subsequent accumulation in the matrix.[435] This assay evaluates mitochondrial dysfunction by quantifying the changes in the $\Delta\Psi_m$, through the formation of J aggregates shown by red fluorescence (590 nm) with high polarization (high $\Delta\Psi_m$). When the mitochondria are depolarized (low $\Delta\Psi_m$), the dye monomers are presented as green fluorescence (527 nm).[433,436] Therefore, different concentrations of the metallocompounds were added to MCF-7 cells for 72 h. Thereafter, cells were incubated with JC-1 and analyzed by flow cytometry to determine the *R* values.

Figure 68 shows the emission intensity of the red/green ratio (*R*) of JC-1, where a decrease in the ratio suggests a mitochondrial depolarization. From these results it is possible to conclude that the G2Ru metallodendrimer induced mitochondrial depolarization with an increasing concentration, suggesting that cell death happens by the intrinsic pathway of apoptosis.[437] On the other hand, RuCp and cisPt presented high polarization with increasing concentrations of both metallocompounds. The changes of *R* (ΔR) were determined and compared by using the following equation (ΔR = [($R_{1\mu M}$ – $R_{control}$)/$R_{control}$] x 100%) at 1 µM concentration between the metallocompounds.[437] The G2Ru metallodendrimer presented a ΔR of -67%, followed by cisPt with -18% and RuCp with 0.02%. Furthermore, the change of *R* (ΔR) of the G2Ru metallodendrimer showed that at a 1 µM concentration a superior $\Delta\Psi_m$ depolarization of the mitochondria occurred (-67%) relative to cisplatin -18%.

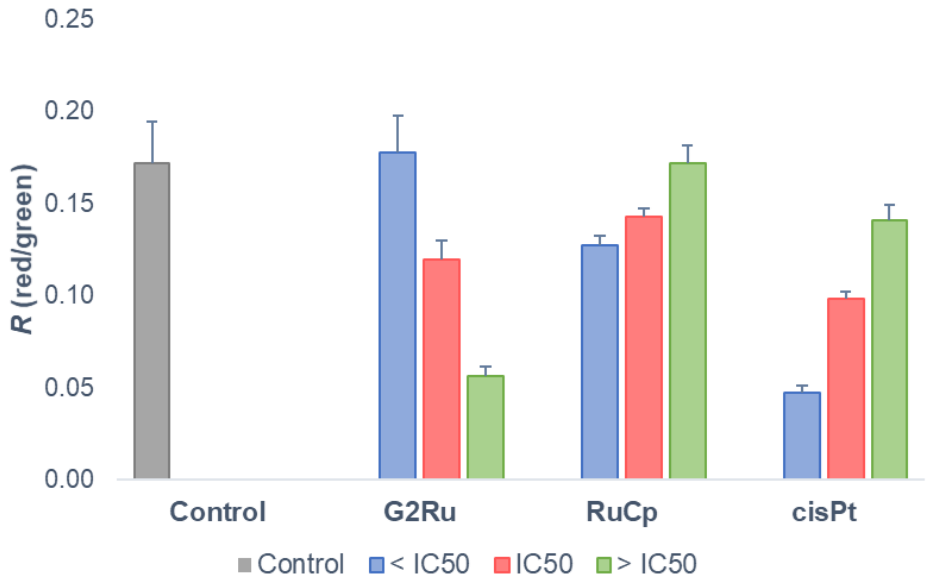

Figure 68. Ratio (*R* values) from the JC-1 assay using MCF-7 cells after 72 h incubation. Cells were exposed to a 0.5% (v/v) DMSO solution (vehicle control) or different concentrations of each metallocompound. Concentration for each compound: G2Ru metallodendrimer (0. 04 µM (<IC_{50}), 0.09 µM (IC_{50}), and 0.5 µM (>IC_{50})), for RuCp (0.2 µM (<IC_{50}), 0.4 µM (IC_{50}), and 0.8 µM (>IC_{50})), and cisPt (0.6 µM (<IC_{50}), 0.8 µM (IC_{50}), and 1 µM (>IC_{50})). Data are expressed as mean ± SD of one experiment performed in triplicate.

4. Conclusion

Three different generations of the poly(alkylidenamine)-based metallodendrimers were successfully functionalized with the $[Ru(\eta^5\text{-}C_5H_5)(PPh_3)_2]^+$ moiety and characterized. These ruthenium metallodendrimers were evaluated against six cancer cell lines and a non-tumorigenic cell line. The stability studies performed at two different temperatures showed that the RuCp moiety had a slower release from the nitrile dendrimer at 25°C. Experiments at 4°C revealed that these metallodendrimers were stable at low temperatures, suggesting that they can be stored at low temperatures before use. All three metallodendrimers presented excellent anticancer efficacy when compared to the well-known metallodrug cisplatin. The prepared metallocompounds were effective against a cisplatin-resistant cell line presenting 46-fold more toxicity than cisplatin, suggesting them as being a trustworthy alternative to drug-resistant tumors. A generation dependency in the cytotoxicity was observed, with the higher generations being more effective. The DNA binding studies revealed that our metallodendrimers binded to DNA non-covalently by electrostatic interactions. Also, our metallodendrimers presented a strong interaction with DNA when compared to other ruthenium (II) complexes and cisPt. The hemolysis assay using human blood demonstrated that our metallodendrimers present low toxicity towards red blood cells. The G2Ru metallodendrimer showed better IC_{50} values than RuCp and cisPt and it was selected to continue with other biological assays such as the ability to induce apoptosis, cell cycle analysis, ROS production and mitochondrial membrane potential. The results showed that the G2Ru metallodendrimer induced necrosis in a superior percentage, followed by late-apoptosis, contrary to what was found in the literature for the ruthenium(II) complexes.[275,293] The cell cycle experiment revealed that our G2Ru

metallodendrimer presented a cytostatic effect through the inhibition of cell growth, acting in the G0/G1 phase of the cell cycle. This metallodendrimer was able to induce ROS accumulation and also induce mitochondria depolarization, suggesting that cell death happens by the intrinsic pathway of apoptosis. In summary, the current work endorses additional experiments, such as *in vivo* studies that will confirm the use of these metallodendrimers as an anticancer drug alternative to cisplatin.

Chapter 5.

Novel poly(alkylidenamine) dendrimers functionalized with cisplatin as anticancer prodrugs

Chapter 5. Novel poly(alkylidenamine) dendrimers functionalized with cisplatin as anticancer prodrugs

1. Introduction

Since its approval by the FDA at the end of 1978,[250] cisplatin (*cis*-diamminedichloroplatinum(II)) and its analogs are currently the most widely used chemotherapeutic compounds to treat testicular, ovarian and non-small cell lung cancer.[249] Currently, these chemotherapeutics find application in a wide number of solid tumors such as head and neck, gastric, non-small cell lung, gallbladder, testicular, ovarian, breast and urinary bladder cancers.[251,252,438] However, cisplatin presents acute side effects such as toxicity, immunosuppression, and gastrointestinal disorders.[252,253,256,438,439] These considerable side effects are mainly due to the mechanism of resistance by cancer cells.[251,253,438] Three key mechanisms can lead to this acquired resistance: increased drug degradation and deactivation, reduced the uptake of the drug and enhanced the DNA repair of the damaged cell.[439] To overcome this drug resistance, cisplatin is used in combination therapy with other chemotherapeutic drugs, such as doxorubicin, 5-Fluorouracil, paclitaxel and gemcitabine.[247,440–442] The mechanism of action of cisplatin is caused by the lower chloride concentration of the intracellular environment relative to the extracellular environment, forming highly reactive species such as aquated cisplatin.[256,443,444] The reactivity and activation of cisplatin inside cells has been believed to happen by hydrolysis, which precedes toxicity.[443] Cisplatin can form coordinated intra- and inter-strand crosslinks with the guanine bases of DNA but only in the aquated form since it is more reactive, which is advantageous to cancer cells that cannot repair the DNA.[253,255,265,444] Due to its strong electrophilic ability, aquated cisplatin can interact with any nucleophile such as nitrogen donor atoms in the DNA residues,[265] resulting in the inhibition of transcription and causing apoptosis.[445]

Nanotechnology has explored approaches to deliver drugs and to avoid all the drawbacks associated with their toxicity. A great example is nanomaterials that have been used as transporters of molecules to overcome the drug limitations and improve their delivery and efficacy.[164,235,446,447] Dendrimers are exciting materials with unique properties to be used as drug delivery systems for biomedical applications, mainly due to their low polydispersity and particular architectures.[235,448] Nevertheless, dendrimers can present some undesirable toxicity associated with their physical and chemical properties.[448] Therefore, the functional terminal groups of dendrimers can improve their solubility and biocompatibility. The functionalization of dendrimers with platinum compounds showed that they improved the efficacy of the metallodrug transporting it into the cell.[448–450]

In this study, we present the synthesis of low generation anionic poly(alkylidenamine) dendrimers based on our previous work.[198,364] These generation 1 and 2 anionic dendrimers with carboxylate and sulfonate terminal groups were then functionalized with cisplatin. The prepared dendrimers and metallodendrimers were fully characterized by ^{1}H-, ^{13}C- and ^{195}Pt-NMR, MS and FT-IR techniques.

Thereafter, these dendrimers and metallodendrimers were tested against two cancer cell lines (MCF-7 and A2780) to evaluate their anticancer efficacy.

2. Materials and Methods

2.1. Materials

All reagents were used as received unless otherwise described. Sodium vinyl sulfonate was obtained from TCI. Methyl acrylate was obtained from Acros Organics. Sodium hydroxide was acquired from Fisher Scientific. Methanol was purchased from Fisher Chemical. Cisplatin was obtained from Acros Organics. Dialysis membranes (MWCO 100-500 Da, 500-1000 Da, and 3500 Da) were bought from SpectrumLabs.

2.2. Cisplatin aquation

The cisplatin aquation process was developed by using a published method by Nial J. Wheate.[450] Cisplatin (0.3 g; 0.8 mmol) was dissolved in 100 mL of ultrapure water. Silver nitrate (0.3 g; 1,7 mmol; 2 mol equiv.) in 6.5 mL of ultrapure water was added to the previous solution, protected from light, and stirred for 24 h. The resultant silver chloride (AgCl) precipitate was removed by centrifugation (1h30 at 15000 rpm) and by filtration through a 0.2 μm nylon filter. The final product was obtained after lyophilization (Scheme 6).

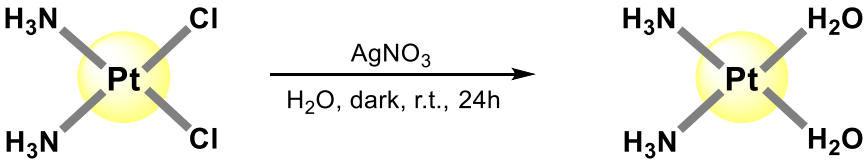

Scheme 6. Schematic representation of the synthesis of aquated cisplatin.

2.3. Synthesis of the platinum metallodendrimers

The carboxylate and sulfonate dendrimers were prepared according to the work published by our group.[198] Briefly, the nitrile poly(alkylidenamine) dendrimers were prepared as reported by us.[364] Then, the amine-terminated dendrimers were synthesized through the reduction of the nitrile groups into primary amines by the procedure developed by Marie-Christine Daniel *et al*.[369] The carboxylate and sulfonate dendrimers were acquired through Michael's addition reactions, following the method described by Francisco J. de la Mata *et al.*[366] The cisplatin metallodendrimers (Scheme 7) were prepared by adapting the method followed by Nial J. Wheate *et al.*[450]

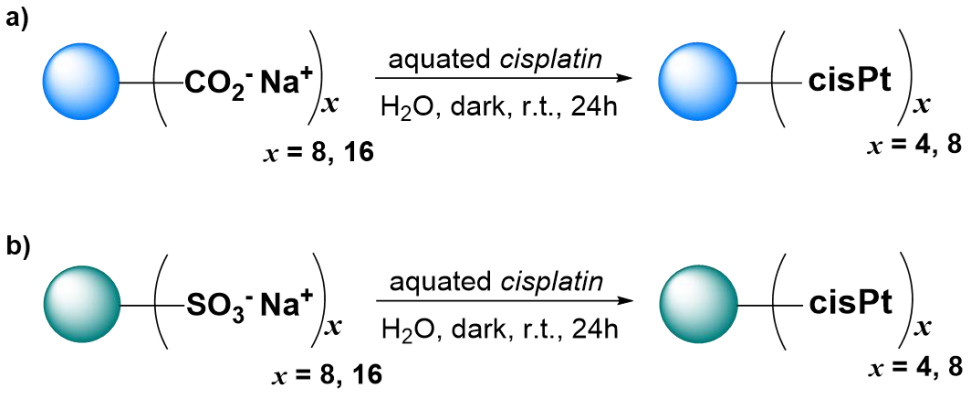

Scheme 7. Representation of the poly(alkylidenamine) metallodendrimers synthesis: a) preparation of the cisplatin carboxylate dendrimers; b) preparation of the cisplatin sulfonate dendrimers.

2.3.1. Synthesis and characterization of G1CPt metallodendrimer

Aquated cisplatin (0.1 g; 0.4 mmol) was dissolved in 100 mL of ultrapure water. Then, the G1C carboxylate dendrimer (0.1 g; 0.09 mmol) in 2 mL of ultrapure water was added to the previous solution. The reaction continued for 24 h, protected from light. The product was purified by dialysis (membrane MWCO 1 kDa) for 1 day, giving a dark brown solid after lyophilization with a 32% yield (0.054 g). ^{1}H-NMR (400 MHz, D_2O) δ = 3.36, 3.21, 2.63 (–C**H**$_2$CO$_2$Pt(NH$_3$)$_2$), 1.98, 1.71, 1.41 ppm. ^{13}C-NMR (100 MHz, D_2O) δ = 177.29 (–**C**H$_2$CO$_2$Pt(NH$_3$)$_2$), 56.92, 52.30, 50.27, 49.27, 30.09, 24.74, 22.77, 16.30 ppm. ^{195}Pt-NMR (86 MHz, D_2O) δ = -2121.21 ppm. FT-IR: ν = 2947 cm^{-1} (ν_{O-H}). TOF-MS (ESI-): *m/z* = 1019.46 [M – Pt(NH$_3$)$_2$ + H$_2$O].

2.3.2. Synthesis and characterization of G2CPt metallodendrimer

Aquated cisplatin (0.2 g; 0.9 mmol) was dissolved in 100 mL of ultrapure water. Afterwards, the G2C carboxylate dendrimer (0.3 g; 0.11 mmol) was added in 2 mL of ultrapure water and stirred for 24 h in the dark. The final product was purified by dialysis (membrane MWCO 3.5 kDa) for 1 day. The G2CPt metallodendrimer (Figure 69) was lyophilized and obtained as a dark brown solid with a yield of 15% (0.063 g). ^{1}H-NMR (400 MHz, D_2O) δ = 3.36, 3.21, 2.63 (–C**H**$_2$CO$_2$Pt(NH$_3$)$_2$), 1.98, 1.71, 1.41 ppm. ^{13}C-NMR (100 MHz, D_2O) δ = 177.23 (–**C**H$_2$CO$_2$Pt(NH$_3$)$_2$), 52.18, 50.30, 49.43, 43.94, 30.14, 25.23, 22.66, 19.74 ppm. ^{195}Pt-NMR (86 MHz, D_2O) δ = -2123.96 ppm. FT-IR: ν = 2959 cm^{-1} (ν_{O-H}), 1726 cm^{-1} ($\nu_{C=O}$). TOF-MS (ESI-): *m/z* = 2160.35 [M – (Pt(NH$_3$)$_2$)$_6$ – C$_8$H$_{12}$NO$_4$ + H].

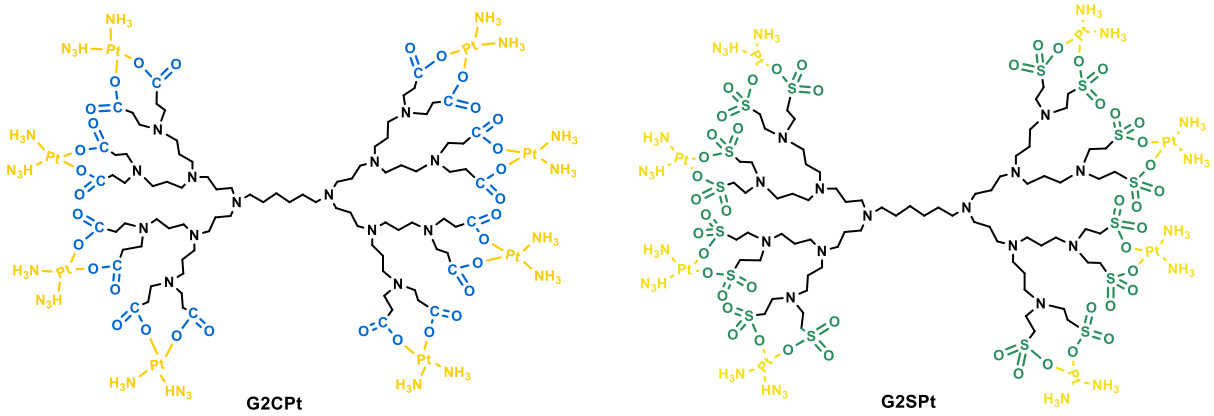

Figure 69. Schematic representation of the bidentate generation 2 platinum metallodendrimers (G2CPt and G2SPt) with 8 cisplatin molecules in each dendrimer.

2.3.3. Synthesis and characterization of G1SPt metallodendrimer

Aquated cisplatin (0.1 g; 0.5 mmol) was dissolved in 100 mL of ultrapure water. To this solution, the G1S sulfonate dendrimer (0.2 g; 0.11 mmol) in 2 mL of ultrapure water was added and the reaction continued for 24 h in the dark. After this, the product was purified by dialysis (membrane MWCO 2 kDa) for 1 day. A brown sticky solid was obtained after lyophilization with a 62% yield (0.144 g). ^{1}H-NMR (400 MHz, D_2O) δ = 3.48, 3.30, 3.21 (–C**H**$_2$SO$_3$Pt(NH$_3$)$_2$), 3.05, 2.72, 2.02 – 1.47 ppm. ^{13}C-NMR (100 MHz, D_2O) δ = 57.16, 52.35, 49.87 (–**C**H$_2$SO$_3$Pt(NH$_3$)$_2$), 48.75, 45.14, 35.70, 24.72, 21.63, 20.08 ppm. ^{195}Pt-NMR (86 MHz, D_2O) δ = -2046.20 ppm. FT-IR: ν = 1196 cm^{-1} ($\nu_{S=O}$), 1041 cm^{-1} ($\nu_{S=O}$). TOF-MS (ESI-): *m/z* = m/z = 1938.93 [M – Pt(NH$_3$)$_2$ – 2H].

2.3.4. Synthesis and characterization of G2SPt metallodendrimer

Aquated cisplatin (0.2 g; 0.6 mmol) was dissolved in 100 mL of ultrapure water. The G2S sulfonate dendrimer (0.2 g; 0.07 mmol) in 2 mL of ultrapure water was added to the previous solution and stirred for 24 h, protected from light. The product was purified by dialysis (membrane MWCO 3.5 kDa) for 1 day. The product was obtained with a yield of 39% (0.119 g) as a brown sticky solid after lyophilization (Figure 69). ^{1}H-NMR (400 MHz, D_2O) δ = 3.48, 3.30, 3.21 (–C**H**$_2$SO$_3$Pt(NH$_3$)$_2$), 3.05, 2.72, 2.02 – 1.47 ppm. ^{13}C-NMR (100 MHz, D_2O) δ = 52.36, 49.73, 47.59, 46.26 (–**C**H$_2$SO$_3$Pt(NH$_3$)$_2$), 42.71, 25.03, 22.89 ppm. ^{195}Pt-NMR (86 MHz, D_2O) δ = -2273.67 ppm. FT-IR: ν = 1195 cm^{-1} ($\nu_{S=O}$), 1044 cm^{-1} ($\nu_{S=O}$). TOF-MS (ESI-): *m/z* = 1916.95 [M – C$_{40}$H$_{96}$N$_{23}$O$_2$4Pt$_4$S$_8$ – Pt(NH$_3$)$_2$ + H].

2.4. Biological assays

2.4.1. Cell viability assays

The anticancer activity of the platinum-dendrimers was assessed against two cancer cell lines A2780 (human ovarian carcinoma) and MCF-7 (human breast adenocarcinoma) using the MTT assay. Cells were cultured in 96-well plates at a density of 5 x 10^3 cells/well with RPMI medium supplemented with 10% FBS and 1% antibiotic-antimycotic for 24h, incubated at 37°C and 5% CO_2. Later, the cells were treated with the platinum metallodendrimers, G1CPt, G2CPt, G1SPt and G2SPt, the anionic terminated dendrimers, G1C, G2C, G1S and G2S, and as well as cisPt (positive control), at a range concentration of 0.01 µM to 10 µM. After 72 h of incubation, cell viability was quantified by the analysis of the metabolic activity of the cells in culture by the MTT assay. In brief, the cell culture medium was substituted with cell culture medium containing MTT (0.5 mg/mL). Then, the medium with MTT was removed and the formazan crystals were dissolved in DMSO. The absorbance at 550 nm was measured using a microplate reader.

3. Results and discussion

3.1. Synthesis and characterization of the platinum metallodendrimers

In the preparation of the platinum metallodendrimers, the aquation of cisplatin was necessary to activate the part of the drug molecule for dendrimer complexation.[450] Therefore, the *bis*-aquated cisplatin was first prepared by reaction of cisplatin with silver nitrate that worked as a chloride abstractor. After that, the two generations (G1 and G2) of the poly(alkylidenamine) dendrimer were coordinated to the aquated cisplatin through a bidentate form with two different terminal groups, namely carboxylate and sulfonate.

Their synthesis was obtained with low to reasonable yields of 32% (G1CPt), 15% (G2CPt), 62% (G1SPt), and 39% (G2SPt). All platinum metallodendrimers were fully characterized by NMR and FT-IR spectroscopies and mass spectrometry (MS). The metallodendrimers were characterized by the ^{1}H-, ^{13}C- and ^{195}Pt-NMR techniques. Potassium tetrachloroplatinate(II) was used as an external reference for the Pt nucleus experiments. For the other NMR experiments (^{1}H), the signal of the deuterated solvent (D_2O) was used as an internal reference. As can be seen, Figure 70, shows the expected ^{1}H-NMR spectrum of the G1CPt metallodendrimer. The characteristic signals of the metallocompound core are present at 1.46, 1.75 and 3.22 ppm. At 2.25 ppm in the amine region of the NMR spectrum, the characteristic signal corresponding to the amines of the cisplatin moiety can be seen. The multiplet at 2.65 – 2.67 ppm corresponds to the protons near the carboxylic acid.

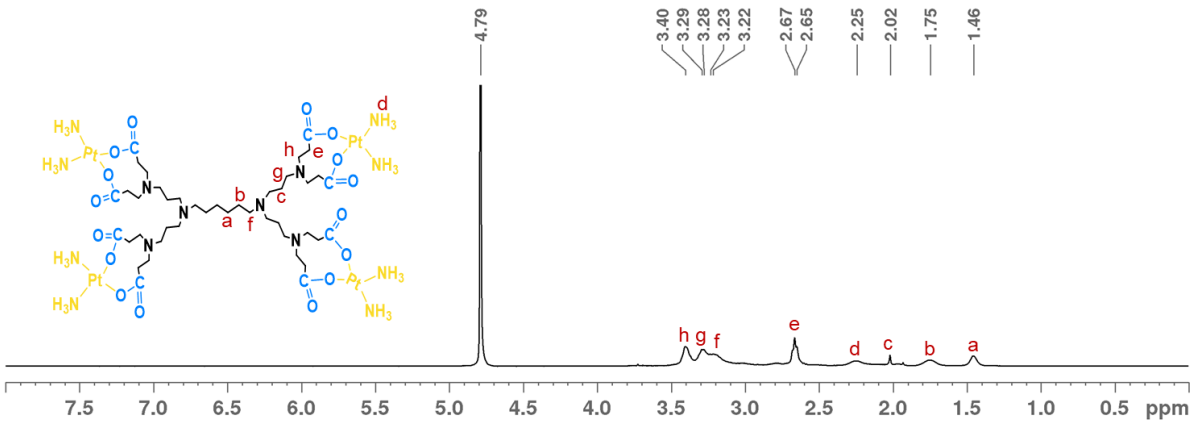

Figure 70. ^{1}H-NMR spectrum of generation 1 of the carboxylate platinum metallodendrimer (G1CPt) performed in D_2O.

The ^{13}C-NMR spectrum of the G1CPt metallodendrimer presents the characteristic spectrum of the compound (Figure 71). At 22.72, 24.86 and 52.53 ppm are the signals of the dendrimer core. The carbon located next to the carboxylic acid is represented at 29.97 ppm. At 177.34 ppm it is possible to observe the signal of the carboxylic acid, slightly shifted downfield when compared with the carboxylic acid of the pristine carboxylate dendrimer (180 ppm). Therefore, it can be concluded that the coordination of the carboxylate dendrimer and cisplatin was successfully obtained.

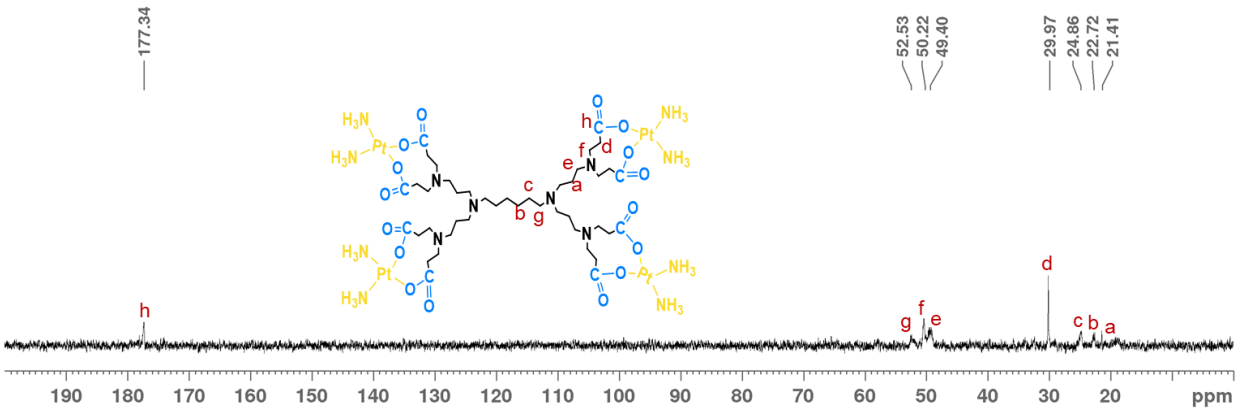

Figure 71. ^{13}C-NMR spectrum of generation 1 of the carboxylate platinum metallodendrimer (G1CPt) performed in D_2O.

The ^{195}Pt-NMR spectrum of the G1CPt metallodendrimer can be seen in Figure 72. The coordination of cisplatin to the carboxylate dendrimer in a bidentate form was accomplished, with the signal at -2121.21 ppm. The signal intensity is low due to the sensitivity of the NMR equipment to this nucleus as other studies can confirm.[451] This signal is characteristic of the bidentate form, which confirms that the synthesis was successfully achieved with the coordination of 4 cisplatin molecules to generation 1 of the carboxylate dendrimer.

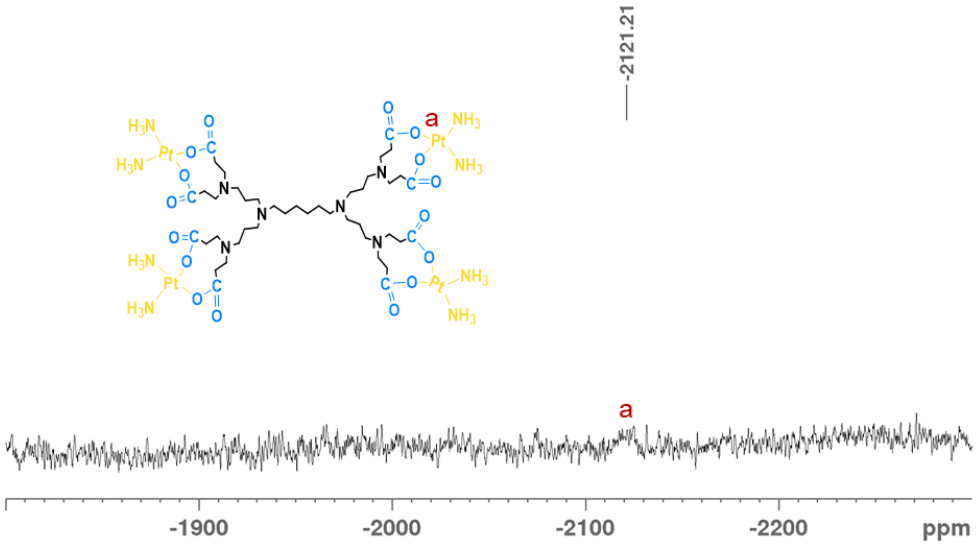

Figure 72. ^{195}Pt-NMR spectrum of generation 1 of the carboxylate platinum metallodendrimer (G1CPt) performed in D_2O with K_2PtCl_4 as an external reference.

Generation 2 of the carboxylate metallodendrimer (G2CPt) presented the expected signals using NMR techniques. In Figure 73, the most prominent signals of the dendrimer core are presented at 1.44 and 1.74 ppm. The protons near the carboxylic acid can be observed at 2.66 ppm.

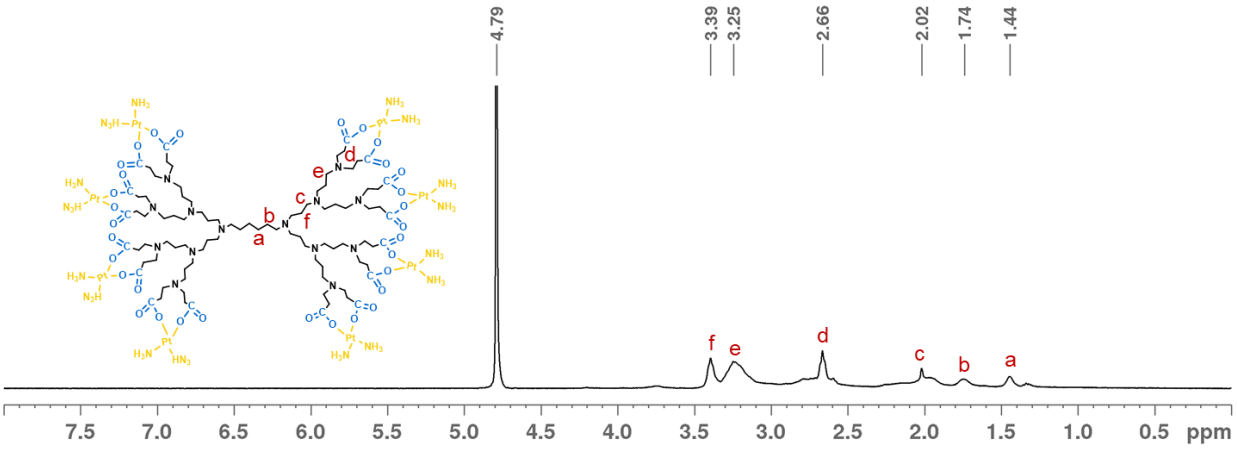

Figure 73. ^{1}H-NMR spectrum of generation 2 of the carboxylate platinum metallodendrimer (G2CPt) done in D_2O.

The ^{13}C-NMR spectrum of the G2CPt metallodendrimer displayed the typical signals of the compound (Figure 74). At 177.34 ppm is the carbon of the carboxylic acid bonded to the platinum center, which shifted from 178.68 ppm of the carboxylic acid from the carboxylate dendrimer (see annex Figure A10). A slight shift is also observed in the carbon placed next to the carboxylic acid from 31.68 to 29.97 ppm in the G2CPt metallodendrimer.

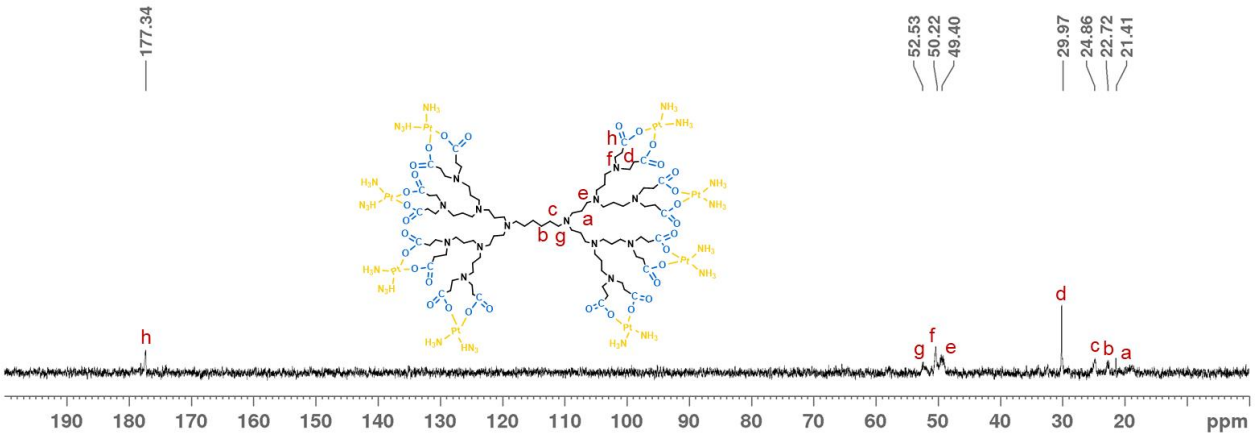

Figure 74. ^{13}C-NMR spectrum of generation 2 of the carboxylate platinum metallodendrimer (G2CPt) performed in D_2O.

The mode of functionalization of cisplatin to generation 2 of the carboxylate dendrimer was confirmed by the ^{195}Pt-NMR technique (Figure 75). The expected signal at -2123.96 ppm suggests that the synthesis was accomplished with 8 cisplatin moieties in a bidentate form located at the surface of generation 2 of the carboxylate dendrimer.

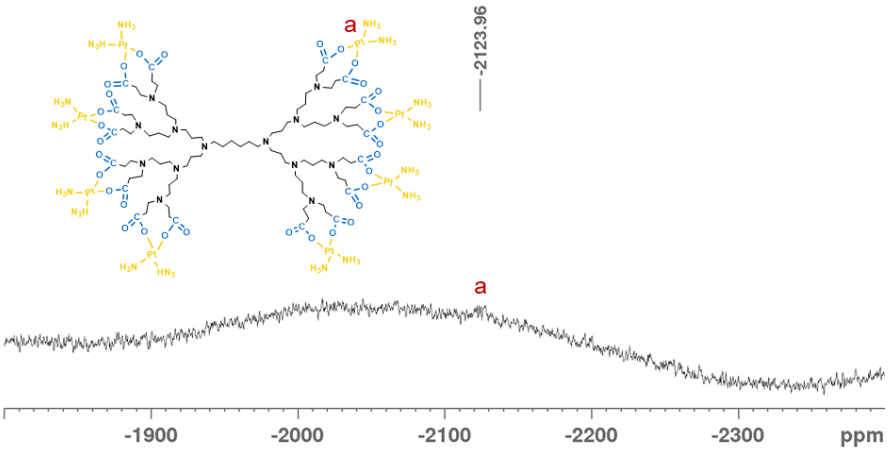

Figure 75. ^{195}Pt-NMR spectrum of generation 2 of the carboxylate platinum metallodendrimer (G2CPt) done in D_2O with K_2PtCl_4 as an external reference.

The G1 and G2 sulfonate dendrimers were also prepared and characterized. The expected ^{1}H-NMR spectrum of generation 1 of the sulfonate metallodendrimer presented the expected signals for the compound (see annex Figure A38). The dendrimer core signals are presented at 1.48 and 1.78 ppm. The signal of the amines present in the cisplatin moiety can be seen at 2.18 ppm. As for the ^{13}C-NMR spectrum of the G1SPt metallodendrimer, the expected signals of the compound were observed. The dendrimer core signals can be found at 20.08, 22.83, and 57.16 ppm. Other relevant signals can be observed at

45.14, 48.75, 49.87 and 52.35 ppm (see annex Figure A39). The ^{195}Pt-NMR spectrum of the G1SPt metallodendrimer suggests that the synthesis was accomplished in a bidentate form (see annex Figure A40). The signal at -2046.20 ppm confirms that the sulfonate dendrimer was successfully coordinated with cisplatin.

Generation 2 of the sulfonate platinum metallodendrimer presented the characteristic signals of the proton NMR spectrum (see annex Figure A41). The signals at 1.48 and 1.77 ppm can be attributed to the dendrimer core, while those at 1.96 – 2.03 ppm can be seen as the signal of the amines present in the cisplatin moiety. The G2SPt metallodendrimer was also characterized by ^{13}C-NMR and presented the expected signals of the compound (see annex Figure A42). The ^{195}Pt-NMR spectrum of the G2SPt metallodendrimer exhibited a signal at -2273.67 ppm which suggests the coordination of the sulfonate dendrimer with *bis*-aquated cisplatin (Figure A43).

Taken together, the NMR results for the carboxylate platinum metallodendrimers revealed a slight shift towards the downfield of 3 ppm (G1C) and 1 ppm (G2C) in the carboxylic region of the carbon NMR in both generations with cisplatin complexed in the bidentate form to the bare dendrimers. For the sulfonate platinum metallodendrimers, no significant changes were observed in the proton and carbon NMR. Globally, the results show that the carboxylate and sulfonate dendrimers were fully functionalized with cisplatin in the bidentate form.

For further characterization, FT-IR analysis of the platinum metallodendrimers was performed using KBr pellets. Figure 76 shows the comparison of both spectra of the G1C and the G1CPt compounds. The characteristic bands of these compounds showed no relative difference of the O-H stretch band at 2946 (G1C dendrimer) and 2947 cm^{-1} (G1CPt metallodendrimer), indicating the coordination of the dendrimers to cisplatin. The G2CPt FT-IR spectrum also presented a slight shift of the O-H stretch to 2959 cm^{-1} from 2954 cm^{-1} of the G2C dendrimer (see annexes Figure A44). The C=O stretch of the carboxylic acid was observed in the G2C dendrimer (1727 cm^{-1}) and the G2CPt metallodendrimer (1726 cm^{-1}). For the sulfonate dendrimers, signals in the sulfoxide and sulfonate regions were observed. The sulfoxide stretch (S=O) band was shifted to a lower wavelength from 1045 cm^{-1} for G1S to 1041 cm^{-1} for the G1SPt metallodendrimer (Figure 77). In the sulfonate region, no significant shifts were observed for the G1S dendrimer (1195 cm^{-1}) and the G1SPt metallodendrimer (1196 cm^{-1}). The sulfoxide and sulfonate stretches were also detected in generation 2 of the sulfonate dendrimer and metallodendrimer with bands at 1044 cm^{-1} (G2S) and 1042 cm^{-1} (G2SPt) and 1188 cm^{-1} (G2S) to 1195 cm^{-1} (G2SPt), respectively (see annex Figure A45). These findings suggest the coordination of the sulfonate dendrimers with the cisplatin moiety.

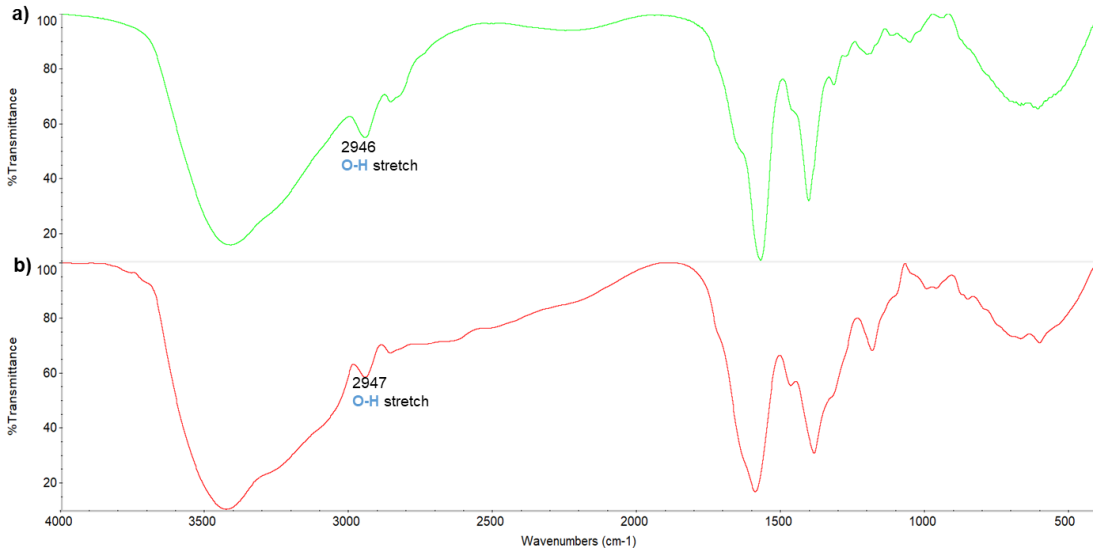

Figure 76. FT-IR spectra of the a) G1C carboxylate dendrimer and b) G1CPt metallodendrimer (in KBr pellets).

Figure 77. FT-IR spectra of the a) G1S sulfonate dendrimer and b) G1SPt metallodendrimer (in KBr pellets).

TOF-MS analysis was used to confirm the synthesis of the prepared platinum metallodendrimers. The G1CPt metallodendrimer was verified with a loss of one cisplatin molecule by the presence of a peak at *m/z* = 1019.46 [M – $Pt(NH_3)_2$ + H_2O] (Figure 78). The partial G2CPt metallodendrimer was found at *m/z* = 2160.35 [M – $(Pt(NH_3)_2)_6$ – $C_8H_{12}NO_4$ + H], due to the fragmentation of the molecule (see annex Figure A46). The G1SPt metallodendrimer was found with three cisplatin molecules with *m/z* = 1938.93 [M – $Pt(NH_3)_2$ – 2H] (Figure 79). For the G2SPt metallodendrimer with *m/z* = 1916.95 [M – $C_{40}H_{96}N_2O_{24}Pt_4S_8$ – $Pt(NH_3)_2$ + H], only half of the molecule was observed due to its large size easily fragmented (annex Figure A47).

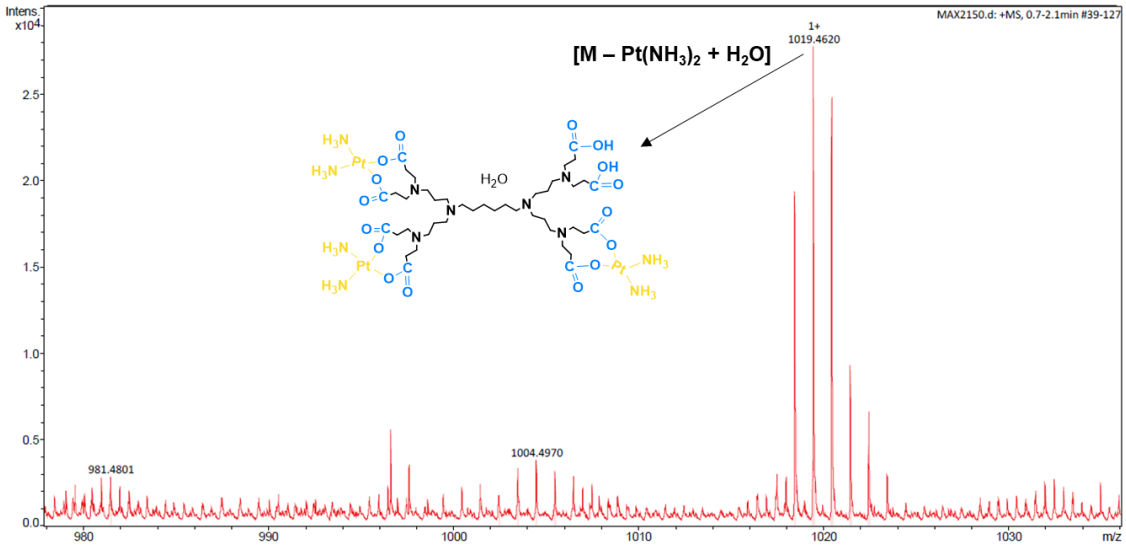

Figure 78. MS Q-TOF (ESI-) mass spectrum of the G1CPt metallodendrimer.

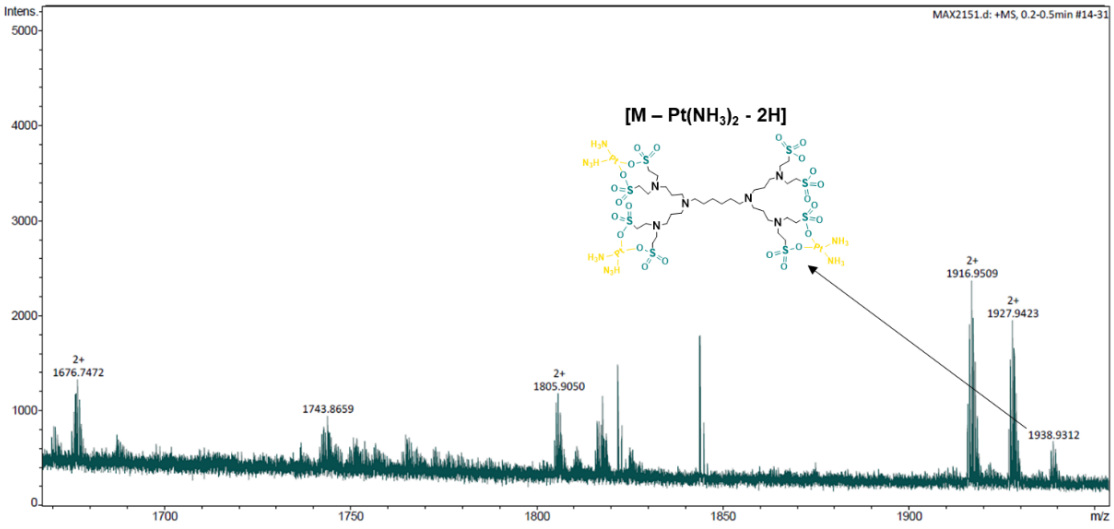

Figure 79. MS Q-TOF (ESI-) mass spectrum of the G1SPt metallodendrimer.

The cisplatin metallodendrimers were also characterized by elemental analysis (EA). However, due to the high hygroscopicity of these compounds, the errors were beyond what is considered acceptable and for this reason the data are not presented.

3.2. Cell viability assays

The evaluation of the potential of the platinum metallodendrimers potential as anticancer drugs was carried out using two cancer cell lines, namely the MCF-7 and A2780 cell lines. Cells were exposed to the metallodendrimers for 72 h, and cell viability was determined through the MTT assay. The preliminary results of the cytotoxicity assay are described below. The anionic dendrimers and cisplatin were used as controls. As can be observed in Figure 80, the carboxylate dendrimers and the metallodendrimers presented anticancer activity in the A2780 cell line. The cisplatin metallodendrimers showed a generation dependent toxicity in these cancer cell lines. However, the same did not happen with the sulfonate dendrimers, where generation 1 of the metallodendrimers presented to be more cytotoxic than generation 2 (Figure 81). In the MCF-7 cells, the G2CPt carboxylate metallodendrimer only showed anticancer activity at 10 μM (annex Figure A48). For the sulfonate dendrimers, only the G1SPt metallodendrimer presented toxicity at 10 μM (annex Figure A49). Interestingly, the G2SPt metallodendrimer did not show any anticancer activity at the higher concentration tested.

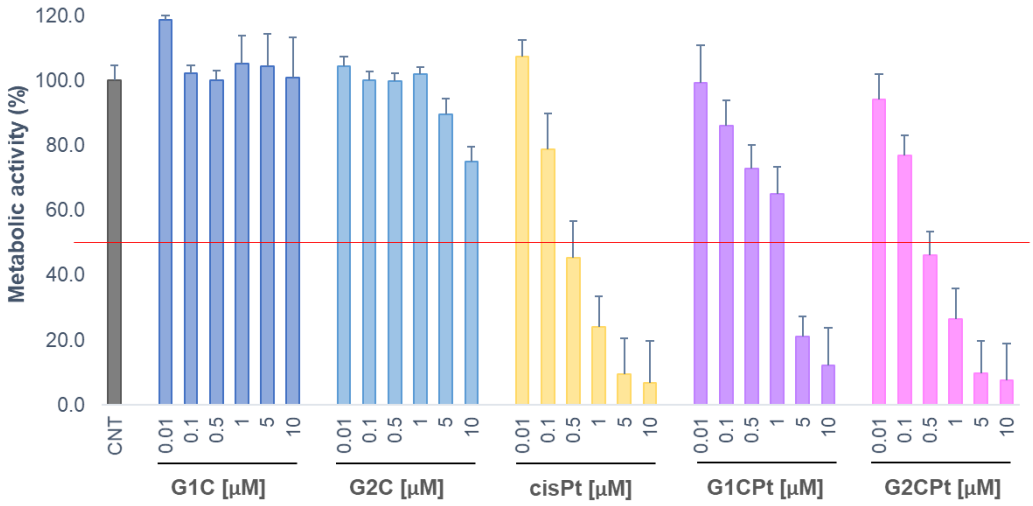

Figure 80. Viability studies of the metallodendrimers in A2780 cells. Cells were treated for 72 h with a concentration range of 0.01 μM to 10 μM of the carboxylate dendrimers (G1C and G2C), cisPt and the metallodendrimers (G1CPt and G2CPt). The metabolic activity is represented against the control. Data are represented as mean ± SD of one independent experiment performed in triplicate.

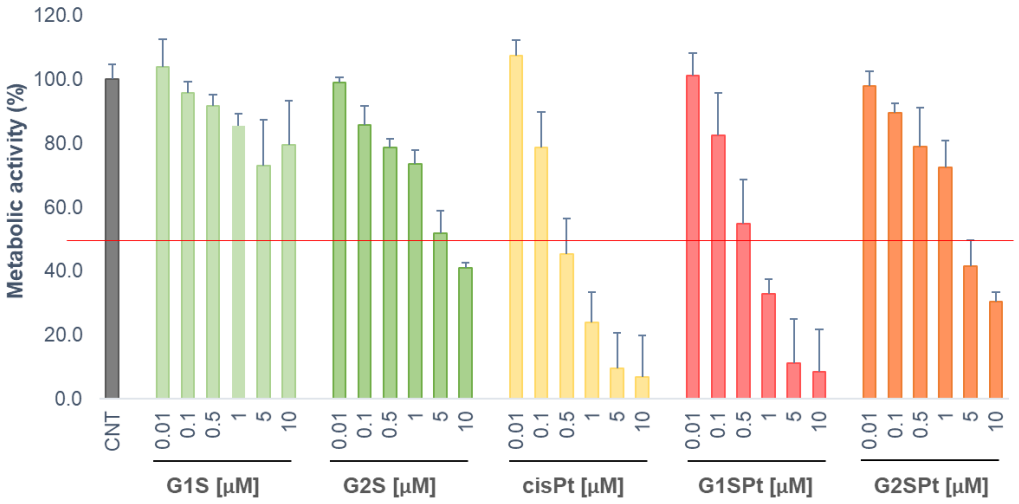

Figure 81. Viability studies of the metallodendrimers in A2780 cells. Cells were treated for 72 h with a concentration range of 0.01 μM to 10 μM of the sulfonate dendrimers (G1S and G2S), cisplatin (cisPt) and the metallodendrimers (G1SPt and G2SPt). The metabolic activity is represented against the control. Data are represented as mean ± SD of one independent experiment performed in triplicate.

In Table 8, the preliminary IC_{50} values for the cisplatin metallodendrimers in the A2780 and the MCF-7 cancer cell lines are presented. The IC_{50} values confirm that the metallodendrimers are more selective towards the A2780 cell line relative to MCF-7 cells. These results are in accordance with the expected findings for cisplatin compounds that are generally used to treat ovarian cancer.[452,453] Nevertheless, it is important to emphasize that these results are from one experimentt and another two independent experiments will be performed to corroborate this anticancer activity.

Table 8. The preliminary IC_{50} values of the platinum metallodendrimers towards the A2780 and MCF-7 cancer cell lines. Data are represented as the mean of one independent experiment performed in triplicate.

Compound	Metal centers	A2780 (IC_{50}, μM)	MCF-7 (IC_{50}, μM)
cisplatin	1	0.4	4.2
G1CPt	4	2.4	>10
G2CPt	8	0.4	7.6
G1SPt	4	0.6	7.0
G2SPt	8	3.9	>10

4. Conclusion

We can conclude that we have successfully metallodendrimers with cisplatin attached in a bidentate form on the surface. To the best of our knowledge, we have prepared the first poly(alkylidenamine)-based dendrimers with carboxylate and sulfonate terminal groups with cisplatin in the bidentate form to be potentially used as anticancer drugs. Previous studies have shown just the functionalization or the entrapment of cisplatin using PAMAM dendrimers.[450,454,455] Cisplatin can be coordinated either in a mono- or bidentate manner, linked to the dendrimer with a single bond or two bonds, respectively, in which the bis-aquated cisplatin coordination should increase the retention of the drug.[450] Therefore, aquated cisplatin was prepared to coordinate with the anionic dendrimers in a bidentate form. The prepared carboxylate and sulfonate metallodendrimers, after characterization by the NMR, FT-IR and MS techniques, were then evaluated against two cancer cell lines (A2780 and MCF-7). The preliminary results of the cytotoxicity assays showed that our metallodendrimers presented toxicity similar to cisplatin towards the A2780 cell line in the micromolar concentration range. The similarity of the cytotoxicity results of our dendrimers with cisplatin can probably be due to the fact that these poly(alkylidenamine) dendrimers belong to a group of dendrimers with reduced toxicity compared to the cationic dendrimers that are more toxic. However, additional studies are necessary, such as the study of the stability of these compounds, the evaluation of the anticancer activity against cisplatin-resistant cancer cell lines and other cancer and non-cancerous cell lines. The toxicity towards red blood cells as well as DNA binding studies to assess the mechanism of action of these metallodendrimers is also needed to complement the biological assays. The ability to induce apoptosis, the accumulation of reactive oxygen species (ROS) and the cell cycle can be also evaluated. These additional experiments are necessary to confirm if these metallodendrimers can be used as a promising drug with fewer side effects than the free drug.

Chapter 6.

Conclusions and Future Perspectives

Chapter 6. Conclusions and Future Perspectives

In summary, these poly(alkylidenamine)-based dendrimers are versatile nanoplatforms for biomedical applications, specifically for antiviral and anticancer therapeutics. They can be easily prepared with different terminal groups, such as nitrile, amine, carboxylate and sulfonate, depending on the final application. For instance, the nitrile and amine dendrimers were prepared to be used as building blocks to increase the dendrimer generation. Moreover, these nitrile and amine dendrimers can be used as sites for metal coordination. The anionic dendrimers, with carboxylate and sulfonate terminal groups, presented less toxicity, improved solubility, improved metal coordination and can inhibit HIV infection.

In chapter 2, we presented a new family of anionic poly(alkylidenamine) dendrimers with improved antiviral activity against HIV-1 infection. First, second and third generation dendrimers with of carboxylate (G1C, G2C and G3C) and sulfonate (G1S, G2S and G3S) terminal groups were prepared and fully characterized by ^{1}H- and ^{13}C-NMR, FT-IR, MS and zeta potential techniques. Stability studies with the G1C and G1S dendrimers were conducted and they were revealed to be stable in an aqueous solution for more than one year and a half. The six prepared dendrimers were evaluated for their cytotoxicity using the TZM.bl cell line to find a nontoxic concentration for the antiviral inhibition experiments and for the analysis of the mechanism of action. Our results demonstrated that these anionic dendrimers were cytocompatible and that the first generation of both dendrimers (G1C and G1S) presented antiviral activity against R5-HIV-1_{NLAD8} and X4-HIV-$1_{NL4.3}$. The mechanism of action experiments showed that the G1C and G1S dendrimers were clearly acting on the viral particles and blocking the entry of the virus into the host cell. Moreover, these dendrimers were tested at different pH values, and the results showed that they preserved their inhibitory effect. The *in vivo* assays were performed using BALB/c mice through a vaginal irritation experiment. Our dendrimers were demonstrated to be safe for topical administration with no inflammation or irritation. The G1C and G1S dendrimers have proved to be excellent candidates to prevent new HIV-1 infections and to create an efficient microbicide.

In chapter 3, generation 0 to 2 of nitrile poly(alkylidenamine) dendrimers and generation 0 and 1 of the metallodendrimers functionalized with ruthenium moieties ($[Ru(\eta^5\text{-}C_5H_5)(PPh_3)_2]^+$) were prepared. Their anti-HIV-1 activity was evaluated towards two viruses, R5-HIV-$1_{NLAD8,}$ and X4-HIV-$1_{NL4.3}$. These dendrimers and metallodendrimers were entirely characterized by ^{1}H-, ^{13}C-, and ^{31}P-NMR, MS, FT-IR and EA techniques. Generation 0 and 1 of the nitrile dendrimers showed no toxicity at the tested concentrations and the G2CN dendrimer revealed no toxicity up to 10 µM. The RuCp complex and the G0Ru and G1Ru metallodendrimers showed toxicity from 1 µM up to 25 µM. The antiviral assays revealed that the nitrile dendrimers and the metallocompounds presented no anti-HIV-1 activity against HIV-1 infection.

In chapter 4, the preparation of generation 2 of the poly(alkylidenamine)-based metallodendrimer functionalized with ruthenium moieties ($[Ru(\eta^5\text{-}C_5H_5)(PPh_3)_2]^+$) is described. This G2Ru metallodendrimer was entirely characterized by ^{1}H-, ^{13}C-, and ^{31}P-NMR, MS and FT-IR techniques. The G0Ru, G1Ru and G2Ru metallodendrimers were studied for their stability using NMR techniques at 4°C, 25°C, and 37°C. The results revealed that these metallodendrimers were more stable at low temperatures. Afterward, they were tested in several cancer cell lines and a non-cancer cell line to assess their anticancer activity. The cytotoxicity results indicated a generation impact with increasing toxicity in higher generations, as well as an exceptional anticancer activity of the ruthenium metallodendrimers when compared to cisplatin. The DNA binding experiments using CT-DNA showed a strong interaction between our metallodendrimers and DNA when compared to the well-known metallodrug cisplatin. Their capacity for disruption of the cell membrane was evaluated using red blood cells from human blood. The hemolysis experiment showed toxicity of these metallodendrimers at low concentrations. For further assays, the G2Ru metallodendrimer was used to evaluate its apoptosis-inducing ability, cell cycle analysis, accumulation of ROS and the mitochondrial membrane potential. The G2Ru metallodendrimer presented higher necrosis and late-apoptosis ability, which relates to the results from the mitochondrial potential that showed a mitochondria depolarization indicating that cell death occurs through apoptosis. The ROS assay revealed that the G2Ru metallodendrimer was able to induce the production of ROS. The G2Ru metallodendrimer displayed a cytostatic effect, acting in the G0/G1 phase, more precisely in the inhibition of cell growth, as revealed by the cell cycle experiment. The prepared metallodendrimers presented promising outcomes as metallodrugs when compared to other ruthenium metallodendrimers found in the literature.[85,317,319] Taken together, these metallodendrimers can be considered as good candidates to be used as anticancer metallodrug.

In chapter 5, we prepared poly(alkylidenamine) dendrimers with cisplatin in the bidentate form. These metallodendrimers were prepared by adding *bis*-aquated cisplatin to the carboxylate (G1C and G2C) and sulfonate (G1S and G2S) terminal groups of the dendrimers. They were characterized by NMR, MS and FT-IR techniques. Then, these metallodendrimers were tested in two cancer cell lines. They presented anticancer activity in the A2780 (ovarian carcinoma) cancer cell line. The carboxylate metallodendrimers presented to be more effective against the ovarian cancer cell line.

Concluding, all dendrimers and metallodendrimers presented promising outcomes when used as antiviral or anticancer agents. Furthermore, they can be considered as new nanotherapeutics against diseases such as HIV infection and cancer.

As future perspectives, other experiments are ongoing with the anionic poly(alkylidenamine) dendrimers, such as the evaluation of these dendrimers in combination with other antiretrovirals drugs in

the market, to verify the total inhibition against HIV-1 infection; and additional *in vivo* studies will be performed.

For the ruthenium metallodendrimers, additional studies should be performed, such as transferrin binding studies that could help to determine the mechanism of action of these compounds. Also, *in vivo* assays are currently underway in China to evaluate the toxicity, the tolerant dose and the pharmacokinetics of these potential metallodrugs.

For the cisplatin metallodendrimers, further cytotoxicity studies will be performed in other cancer cell lines. Hemotoxicity will also be done using human blood. Other experiments, including DNA binding, apoptosis and cell cycle analysis, will also be evaluated.

References

References

(1) Nikalje, A. P. Nanotechnology and Its Applications in Medicine. *Med Chem (Los Angeles)* **2015**, *5*, 81–89. https://doi.org/10.4172/2161-0444.1000247.

(2) Leon, L.; Chung, E. J.; Rinaldi, C. A Brief History of Nanotechnology and Introduction to Nanoparticles for Biomedical Applications. In *Nanoparticles for Biomedical Applications: Fundamental Concepts, Biological Interactions and Clinical Applications Micro and Nano Technologies*; Chung, E. J., Leon, L., Rinaldi, C., Eds.; Elsevier Inc., 2020; pp 1–4. https://doi.org/10.1016/B978-0-12-816662-8.00001-1.

(3) Ramos, A. P.; Cruz, M. A. E.; Tovani, C. B.; Ciancaglini, P. Biomedical Applications of Nanotechnology. *Biophys Rev* **2017**, *9*, 79–89. https://doi.org/10.1007/s12551-016-0246-2.

(4) Nobile, S.; Nobile, L. Nanotechnology for Biomedical Applications: Recent Advances in Neurosciences and Bone Tissue Engineering. *Polym Eng Sci* **2017**, 644–650. https://doi.org/10.1002/pen.

(5) Myung, J. H.; Tam, K. A.; Hong, S. Dendritic Nanomaterials for Therapeutic and Diagnostic Applications. In *Biomedical Engineering: Frontier Research and Converging Technologies*; Jo, H., Jun, H.-W., Shin, J., Lee, S., Eds.; Springer International Publishing, 2016; pp 41–75. https://doi.org/10.1007/978-3-319-21813-7_3.

(6) Berzelius, J. J. Isomerie, Unterscheidung von Damit Analogen Verhältnissen. *Jahres-Bericht* **1833**, *12*, 63–67.

(7) Jensen, W. B. The Origin of the Polymer Concept. *J Chem Educ* **2008**, *85*, 624–625. https://doi.org/10.1021/ed085p624.

(8) Staudinger, H. Über Polymerization. *Berichte der Dtsch Chem Gesellschaft (A B Ser* **1920**, *53*, 1073–1085. https://doi.org/10.1002/cber.19200530627.

(9) Staudinger, H. The Nobel Prize in Chemistry 1953 https://www.nobelprize.org/prizes/chemistry/1953/summary/ (accessed Apr 19, 2020).

(10) Flory, P. J. Molecular Size Distribution in Three Dimensional Polymers. I. Gelation. *J Am Chem Soc* **1941**, *63*, 3083–3090. https://doi.org/10.1021/ja01856a061.

(11) Flory, P. J. Molecular Size Distribution in Three Dimensional Polymers. II. Trifunctional Branching Units. *J Am Chem Soc* **1941**, *63*, 3091–3096. https://doi.org/10.1021/ja01856a062.

(12) Flory, P. J. Molecular Size Distribution in Three Dimensional Polymers. III. Tetrafunctional Branching Units. *J Am Chem Soc* **1941**, *63*, 3096–3100. https://doi.org/10.1021/ja01856a063.

(13) Flory, P. J.; Rehner, J. Statistical Mechanics of Cross-Linked Polymer Networks I. Rubberlike Elasticity. *J Chem Phys* **1943**, *11*, 512–520. https://doi.org/10.1063/1.1723791.

(14) Flory, P. J. The Nobel Prize in Chemistry 1974 https://www.nobelprize.org/prizes/chemistry/1974/summary/ (accessed Apr 19, 2020).

(15) Mignani, S.; Rodrigues, J.; Tomas, H.; Zablocka, M.; Shi, X.; Caminade, A.-M.; Majoral, J.-P. Dendrimers in Combination with Natural Products and Analogues as Anti-Cancer Agents. *Chem*

Soc Rev **2018**, *47*, 514–532. https://doi.org/10.1039/c7cs00550d.

(16) Janaszewska, A.; Lazniewska, J.; Trzepiński, P.; Marcinkowska, M.; Klajnert-Maculewicz, B. Cytotoxicity of Dendrimers. *Biomolecules* **2019**, *9*, 330–352. https://doi.org/10.3390/biom9080330.

(17) Buhleier, E.; Wehner, W.; Vögtle, F. "Cascade"- and "Nonskid-Chain-like" Synthesis of Molecular Cavity Topologies. *Synthesis (Stuttg)* **1978**, *1978*, 155–158. https://doi.org/10.1055/s-1978-24702.

(18) Tomalia, D. A.; Baker, H.; Dewald, J.; Hall, M.; Kallos, G.; Martin, S.; Roeck, J.; Ryder, J.; Smith, P. A New Class of Polymers: Starburst-Dendritic Macromolecules. *Polym J* **1985**, *17*, 117–132. https://doi.org/10.1295/polymj.17.117.

(19) Tomalia, D. A.; Baker, H.; Hall, M.; Kallos, G.; Martin, S.; Roeck, J.; Ryder, J.; Smith, P. Dendritic Macromolecules: Synthesis of Starburst Dendrimers. *Macromolecules* **1986**, *19*, 2466–2468. https://doi.org/10.1021/ma00163a029.

(20) Newkome, G. R.; Yao, Z.; Baker, G. R.; Gupta, V. K. Cascade Molecules: A New Approach to Micelles. A [27]-Arborol. *J Org Chem* **1985**, *50*, 2003–2004. https://doi.org/10.1021/jo00211a052.

(21) Newkome, G. R.; Yao, Z.; Baker, G. R.; Gupta, V. K.; Russo, P. S.; Saunders, M. J. Cascade Molecules: Synthesis and Characterization of a Benzene[9]3-Arborol. *J Am Chem Soc* **1986**, *108*, 849–850. https://doi.org/10.1021/ja00264a054.

(22) Sowinska, M.; Urbanczyk-Lipkowska, Z. Advances in the Chemistry of Dendrimers. *New J Chem* **2014**, *38*, 2168–2203. https://doi.org/10.1039/c3nj01239e.

(23) Noriega-Luna, B.; Godínez, L. A.; Rodríguez, F. J.; Rodríguez, A.; Zaldívar-Lelo De Larrea, G.; Sosa-Ferreyra, C. F.; Mercado-Curiel, R. F.; Manríquez, J.; Bustos, E. Applications of Dendrimers in Drug Delivery Agents, Diagnosis, Therapy, and Detection. *J Nanomater* **2014**, *2014*, 1–19. https://doi.org/10.1155/2014/507273.

(24) Singh, A. P.; Biswas, A.; Shukla, A.; Maiti, P. Targeted Therapy in Chronic Diseases Using Nanomaterial-Based Drug Delivery Vehicles. *Signal Transduct Target Ther* **2019**, *4*, 33–53. https://doi.org/10.1038/s41392-019-0068-3.

(25) Cai, H.; Li, K.; Li, J.; Wen, S.; Chen, Q.; Shen, M.; Zheng, L.; Zhang, G.; Shi, X. Dendrimer-Assisted Formation of Fe3O4/Au Nanocomposite Particles for Targeted Dual Mode CT/MR Imaging of Tumors. *Small* **2015**, *11*, 4584–4593. https://doi.org/10.1002/smll.201500856.

(26) Hill, E. E.; Kim, J. K.; Jung, Y.; Neeley, C. K.; Pienta, K. J.; Taichman, R. S.; Nor, J. E.; Baker, J. R.; Krebsbach, P. H. Integrin Alpha V Beta 3 Targeted Dendrimer-Rapamycin Conjugate Reduces Fibroblast-Mediated Prostate Tumor Progression and Metastasis. *J Cell Biochem* **2018**, *119*, 8074–8083. https://doi.org/10.1002/jcb.26727.

(27) Ondarse-Alvarez, D.; Kömürlü, S.; Roitberg, A. E.; Pierdominici-Sottile, G.; Tretiak, S.; Fernandez-Alberti, S.; Kleiman, V. D. Ultrafast Electronic Energy Relaxation in a Conjugated Dendrimer Leading to Inter-Branch Energy Redistribution. *Phys Chem Chem Phys* **2016**, *18*, 25080–25089. https://doi.org/10.1039/c6cp04448d.

(28) Liu, X.; He, B.; Xu, Z.; Yin, M.; Yang, W.; Zhang, H.; Cao, J.; Shen, J. A Functionalized Fluorescent Dendrimer as a Pesticide Nanocarrier: Application in Pest Control. *Nanoscale* **2015**, *7*, 445–449. https://doi.org/10.1039/c4nr05733c.

(29) Gajjar, D.; Patel, R.; Patel, H.; Patel, P. M. Removal of Heavy Metal Ions from Water by Hydroxyl Terminated Triazine-Based Dendrimer. *Desalin Water Treat* **2015**, *55*, 1209–1219. https://doi.org/10.1080/19443994.2014.922446.

(30) Amariei, G.; Santiago-Morales, J.; Boltes, K.; Letón, P.; Iriepa, I.; Moraleda, I.; Fernández-Alba, A. R.; Rosal, R. Dendrimer-Functionalized Electrospun Nanofibres as Dual-Action Water Treatment Membranes. *Sci Total Environ* **2017**, *601–602*, 732–740. https://doi.org/10.1016/j.scitotenv.2017.05.243.

(31) Mekelburger, H.-B.; Jaworek, W.; Vögtle, F. Dendrimers, Arborols, and Cascade Molecules: Breakthrough into Generations of New Materials. *Angew Chem Int Ed Engl* **1992**, *31*, 1571–1576. https://doi.org/10.1002/anie.199215711.

(32) Hawker, C. J.; Fréchet, J. M. J. Preparation of Polymers with Controlled Molecular Architecture. A New Convergent Approach to Dendritic Macromolecules. *J Am Chem Soc* **1990**, *112*, 7638–7647. https://doi.org/10.1021/ja00177a027.

(33) Augustus, E. N.; Allen, E. T.; Nimibofa, A.; Donbebe, W. A Review of Synthesis, Characterization and Applications of Functionalized Dendrimers. *Am J Polym Sci* **2017**, *7*, 8–14. https://doi.org/10.5923/j.ajps.20170701.02.

(34) Gupta, V.; Nayak, S. K. Dendrimers: A Review on Synthetic Approaches. *J Appl Pharm Sci* **2015**, *5*, 117–122. https://doi.org/10.7324/JAPS.2015.50321.

(35) McMahon, M. T.; Bulte, J. W. M. Two Decades of Dendrimers as Versatile MRI Agents: A Tale with and without Metals. *Wiley Interdiscip Rev Nanomedicine Nanobiotechnology* **2018**, *10*, 1–17. https://doi.org/10.1002/wnan.1496.

(36) Maraval, V.; Pyzowski, J.; Caminade, A.-M.; Majoral, J.-P. “Lego” Chemistry for the Straightforward Synthesis of Dendrimers. *J Org Chem* **2003**, *68*, 6043–6046. https://doi.org/10.1021/jo0344438.

(37) Lallana, E.; Fernandez-Trillo, F.; Sousa-Herves, A.; Riguera, R.; Fernandez-Megia, E. Click Chemistry with Polymers, Dendrimers, and Hydrogels for Drug Delivery. *Pharm Res* **2012**, *29*, 1134–1142. https://doi.org/10.1007/s11095-012-0683-y.

(38) Sherje, A. P.; Jadhav, M.; Dravyakar, B. R.; Kadam, D. Dendrimers: A Versatile Nanocarrier for Drug Delivery and Targeting. *Int J Pharm* **2018**, *548*, 707–720. https://doi.org/10.1016/j.ijpharm.2018.07.030.

(39) Mendes, L. P.; Pan, J.; Torchilin, V. P. Dendrimers as Nanocarriers for Nucleic Acid and Drug Delivery in Cancer Therapy. *Molecules* **2017**, *22*, 1401–1421. https://doi.org/10.3390/molecules22091401.

(40) Nanjwade, B. K.; Bechra, H. M.; Derkar, G. K.; Manvi, F. V; Nanjwade, V. K. Dendrimers: Emerging Polymers for Drug-Delivery Systems. *Eur J Pharm Sci* **2009**, *38*, 185–196.

https://doi.org/10.1016/j.ejps.2009.07.008.

(41) Bosman, A. W.; Janssen, H. M.; Meijer, E. W. About Dendrimers: Structure, Physical Properties, and Applications. *Chem Rev* **1999**, *99*, 1665–1688. https://doi.org/10.1021/cr970069y.

(42) Kesharwani, P.; Iyer, A. K. Recent Advances in Dendrimer-Based Nanovectors for Tumor-Targeted Drug and Gene Delivery. *Drug Discov Today* **2015**, *20* (5), 536–547. https://doi.org/10.1016/j.drudis.2014.12.012.

(43) Mignani, S.; Rodrigues, J.; Tomas, H.; Roy, R.; Shi, X.; Majoral, J.-P. Bench-to-Bedside Translation of Dendrimers: Reality or Utopia? A Concise Analysis. *Adv Drug Deliver Rev* **2017**, *136–137*, 73–81. https://doi.org/10.1016/j.addr.2017.11.007.

(44) Klajnert, B.; Bryszewska, M. Dendrimers: Properties and Applications. *Acta Biochim Pol* **2001**, *48*, 199–208. https://doi.org/10.1016/B978-0-444-53349-4.00162-X.

(45) Selin, M.; Peltonen, L.; Hirvonen, J.; Bimbo, L. M. Dendrimers and Their Supramolecular Nanostructures for Biomedical Applications. *J Drug Deliv Sci Technol* **2016**, *34*, 10–20. https://doi.org/10.1016/j.jddst.2016.02.008.

(46) Kannan, R. M.; Nance, E.; Kannan, S.; Tomalia, D. A. Emerging Concepts in Dendrimer-Based Nanomedicine: From Design Principles to Clinical Applications. *J Intern Med* **2014**, *276*, 579–617. https://doi.org/10.1111/joim.12280.

(47) Santos, A.; Veiga, F.; Figueiras, A. Dendrimers as Pharmaceutical Excipients: Synthesis, Properties, Toxicity and Biomedical Applications. *Materials (Basel)* **2020**, *13*, 65–95. https://doi.org/10.3390/ma13010065.

(48) Lee, C. C.; Mackay, J. A.; Fréchet, J. M. J.; Szoka, F. C. Designing Dendrimers for Biological Applications. *Nat Biotechnol* **2005**, *23*, 1517–1526. https://doi.org/10.1038/nbt1171.

(49) Mintzer, M. A.; Grinstaff, M. W. Biomedical Applications of Dendrimers: A Tutorial. *Chem Soc Rev* **2011**, *40*, 173–190. https://doi.org/10.1039/B901839P.

(50) Das, N.; Sharma, P. A.; Seth, A.; Maheshwari, R.; Tekade, M.; Shrivastava, S. K.; Tekade, R. K. An Overview of Dendrimers and Their Biomedical Applications. In *Dendrimers for Drug Delivery*; Sharma, A. K., Keservani, R. K., Eds.; Apple Academic Press, 2018; pp 114–183. https://doi.org/10.1201/b22463.

(51) Pooja, D.; Sistla, R.; Kulhari, H. Dendrimer-Drug Conjugates: Synthesis Strategies, Stability and Application in Anticancer Drug Delivery. In *Design of Nanostructures for Theranostics Applications*; Elsevier Inc., 2018; pp 277–303. https://doi.org/10.1016/B978-0-12-813669-0.00007-5.

(52) Wagner, A. M.; Spencer, D. S.; Peppas, N. A. Advanced Architectures in the Design of Responsive Polymers for Cancer Nanomedicine. *J Appl Polym Sci* **2018**, *135*, 46154–46170. https://doi.org/10.1002/APP.46154.

(53) Safari, H.; Lee, J. K.; Eniola-adefeso, O. Effects of Shape, Rigidity, Size, and Flow on Targeting. In *Nanoparticles for Biomedical Applications: Fundamental Concepts, Biological Interactions and Clinical Applications Micro and Nano Technologies*; Chung, E. J., Leon, L., Rinaldi, C., Eds.;

Elsevier Inc., 2020; pp 55–66. https://doi.org/10.1016/B978-0-12-816662-8.00005-9.

(54) Navya, P. N.; Kaphle, A.; Srinivas, S. P.; Bhargava, S. K.; Rotello, V. M.; Daima, H. K. Current Trends and Challenges in Cancer Management and Therapy Using Designer Nanomaterials. *Nano Converg* **2019**, *6*, 23–52. https://doi.org/10.1186/s40580-019-0193-2.

(55) Abbasi, E.; Aval, S. F.; Akbarzadeh, A.; Milani, M.; Nasrabadi, H. T.; Joo, S. W.; Hanifehpour, Y.; Nejati-Koshki, K.; Pashaei-Asl, R. Dendrimers: Synthesis, Applications, and Properties. *Nanoscale Res Lett* **2014**, *9*, 247–256. https://doi.org/10.1186/1556-276X-9-247.

(56) Gupta, U.; Agashe, H. B.; Asthana, A.; Jain, N. K. Dendrimers: Novel Polymeric Nanoarchitectures for Solubility Enhancement. *Biomacromolecules* **2006**, *7*, 649–658. https://doi.org/10.1021/bm050802s.

(57) Kumar, P. S.; Datta, M. S.; Kumar, D. M.; Kumar, T. V.; Kr, V. K.; C, D. R. Dendrimers in Drug Delivery, Diagnosis and Therapy: Basics and Potential Applications. *J Drug Deliv Ther* **2016**, *6*, 67–92. https://doi.org/10.22270/jddt.v6i1.1190.

(58) Choudhary, S.; Gupta, L.; Rani, S.; Dave, K.; Gupta, U. Impact of Dendrimers on Solubility of Hydrophobic Drug Molecules. *Front Pharmacol* **2017**, *8*, 261–283. https://doi.org/10.3389/fphar.2017.00261.

(59) Bodewein, L.; Schmelter, F.; Di Fiore, S.; Hollert, H.; Fischer, R.; Fenske, M. Differences in Toxicity of Anionic and Cationic PAMAM and PPI Dendrimers in Zebrafish Embryos and Cancer Cell Lines. *Toxicol Appl Pharm* **2016**, *305*, 83–92. https://doi.org/10.1016/j.taap.2016.06.008.

(60) Witvrouw, M.; Fikkert, V.; Pluymers, W.; Matthews, B.; Mardel, K.; Schols, D.; Raff, J.; Debyser, Z.; De Clercq, E.; Holan, G.; et al. Polyanionic (i.e., Polysulfonate) Dendrimers Can Inhibit the Replication of Human Immunodeficiency Virus by Interfering with Both Virus Adsorption and Later Steps (Reverse Transcriptase/Integrase) in the Virus Replicative Cycle. *Mol Pharmacol* **2000**, *58*, 1100–1108. https://doi.org/10.1124/mol.58.5.1100.

(61) García-Gallego, S.; Rodríguez, J. S.; Jiménez, J. L.; Cangiotti, M.; Ottaviani, M. F.; Muñoz-Fernández, M. Á.; Gómez, R.; de la Mata, F. J. Polyanionic N-Donor Ligands as Chelating Agents in Transition Metal Complexes: Synthesis, Structural Characterization and Antiviral Properties against HIV. *Dalton Trans* **2012**, *41*, 6488–6499. https://doi.org/10.1039/c2dt12247b.

(62) Córdoba, E. V.; Arnaiz, E.; Relloso, M.; Sánchez-Torres, C.; García, F.; Pérez-Álvarez, L.; Gómez, R.; de la Mata, F. J.; Pion, M.; Muñoz-Fernández, M. Á. Development of Sulphated and Naphthylsulphonated Carbosilane Dendrimers as Topical Microbicides to Prevent HIV-1 Sexual Transmission. *AIDS* **2013**, *27*, 1219–1229. https://doi.org/10.1097/QAD.0b013e32835f2b7a.

(63) Arnáiz, E.; Doucede, L. I.; García-Gallego, S.; Urbiola, K.; Gómez, R.; Tros De Ilarduya, C.; De La Mata, F. J. Synthesis of Cationic Carbosilane Dendrimers via Click Chemistry and Their Use as Effective Carriers for DNA Transfection into Cancerous Cells. *Mol Pharm* **2012**, *9*, 433–447. https://doi.org/10.1021/mp200542j.

(64) Fuentes-Paniagua, E.; Hernández-Ros, J. M.; Sánchez-Milla, M.; Camero, M. A.; Maly, M.; Pérez-Serrano, J.; Copa-Patiño, J. L.; Sánchez-Nieves, J.; Soliveri, J.; Gómez, R.; et al. Carbosilane

Cationic Dendrimers Synthesized by Thiol-Ene Click Chemistry and Their Use as Antibacterial Agents. *RSC Adv* **2014**, *4*, 1256–1265. https://doi.org/10.1039/c3ra45408h.

(65) Tong, N. A. N.; Nguyen, T. H.; Nguyen, D. H.; Nguyen, C. K.; Tran, N. Q. Preparation of the Cationic Dendrimer-Based Hydrogels for Controlled Heparin Release. *J Macromol Sci Part A Pure Appl Chem* **2015**, *52*, 830–837. https://doi.org/10.1080/10601325.2015.1067043.

(66) Chen, W.; Li, W.; Xu, K.; Li, M.; Dai, L.; Shen, X.; Hu, Y.; Cai, K. Functionalizing Titanium Surface with PAMAM Dendrimer and Human BMP2 Gene via Layer-by-Layer Assembly for Enhanced Osteogenesis. *J Biomed Mater Res - Part A* **2018**, *106*, 706–717. https://doi.org/10.1002/jbm.a.36273.

(67) Ghaffari, M.; Dehghan, G.; Abedi-Gaballu, F.; Kashanian, S.; Baradaran, B.; Ezzati Nazhad Dolatabadi, J.; Losic, D. Surface Functionalized Dendrimers as Controlled-Release Delivery Nanosystems for Tumor Targeting. *Eur J Pharm Sci* **2018**, *122*, 311–330. https://doi.org/10.1016/j.ejps.2018.07.020.

(68) Ambekar, R. S.; Choudhary, M.; Kandasubramanian, B. Recent Advances in Dendrimer-Based Nanoplatform for Cancer Treatment: A Review. *Eur Polym J* **2020**, *126*, 109546. https://doi.org/10.1016/j.eurpolymj.2020.109546.

(69) Ciolkowski, M.; Petersen, J. F.; Ficker, M.; Janaszewska, A.; Christensen, J. B.; Klajnert, B.; Bryszewska, M. Surface Modification of PAMAM Dendrimer Improves Its Biocompatibility. *Nanomed-Nanotechnol* **2012**, *8*, 815–817. https://doi.org/10.1016/j.nano.2012.03.009.

(70) Paleos, C. M.; Tsiourvas, D.; Sideratou, Z.; Tziveleka, L. A. Drug Delivery Using Multifunctional Dendrimers and Hyperbranched Polymers. *Expert Opin Drug Deliv* **2010**, *7*, 1387–1398. https://doi.org/10.1517/17425247.2010.534981.

(71) Mignani, S.; Rodrigues, J.; Roy, R.; Shi, X.; Ceña, V.; Kazzouli, S. El; Majoral, J.-P. Exploration of Biomedical Dendrimer Space Based on In-Vivo Physicochemical Parameters: Key Factor Analysis (Part 2). *Drug Discov Today* **2019**, *24*, 1184–1192. https://doi.org/10.1016/j.drudis.2019.03.001.

(72) Hurst, M. N.; DeLong, R. K. Spectral signature analysis of surface functionalized nanoparticles https://www.moleculardevices.com/en/assets/app-note/br/spectral-signature-analysis-of-surface-functionalized-nanoparticles#gref (accessed Jun 5, 2020).

(73) Mulder, A.; Huskens, J.; Reinhoudt, D. N. Multivalency in Supramolecular Chemistry and Nanofabrication. *Org Biomol Chem* **2004**, *2*, 3409–3424. https://doi.org/10.1039/b413971b.

(74) Levine, P. M.; Carberry, T. P.; Holub, J. M.; Kirshenbaum, K. Crafting Precise Multivalent Architectures. *Med Chem Commun* **2013**, *4*, 493–509. https://doi.org/10.1039/c2md20338c.

(75) Rolland, O.; Turrin, C.-O.; Caminade, A.-M.; Majoral, J.-P. Dendrimers and Nanomedicine: Multivalency in Action. *New J Chem* **2009**, *33*, 1809–1824. https://doi.org/10.1039/b901054h.

(76) Sharma, P.; Garg, S. Pure Drug and Polymer Based Nanotechnologies for the Improved Solubility, Stability, Bioavailability and Targeting of Anti-HIV Drugs. *Adv Drug Deliver Rev* **2010**, *62*, 491–502. https://doi.org/10.1016/j.addr.2009.11.019.

(77) Tjandra, K. C.; Thordarson, P. Multivalency in Drug Delivery-When Is It Too Much of a Good

Thing? *Bioconjug Chem* **2019**, *30*, 503–514. https://doi.org/10.1021/acs.bioconjchem.8b00804.

(78) Caminade, A.-M. Phosphorus Dendrimers for Nanomedicine. *Chem Commun* **2017**, *53*, 9830–9838. https://doi.org/10.1039/c7cc04949h.

(79) de Araújo, R. V.; da Silva Santos, S.; Ferreira, E. I.; Giarolla, J. New Advances in General Biomedical Applications of PAMAM Dendrimers. *Molecules* **2018**, *23*, 2849–2875. https://doi.org/10.3390/molecules23112849.

(80) Rasines, B.; Sánchez-Nieves, J.; Maiolo, M.; Maly, M.; Chonco, L.; Jiménez, J. L.; Muñoz-Fernández, M. Á.; de la Mata, F. J.; Gómez, R. Synthesis, Structure and Molecular Modelling of Anionic Carbosilane Dendrimers. *Dalton Trans* **2012**, *41*, 12733–12748. https://doi.org/10.1039/c2dt31099f.

(81) Chonco, L.; Pion, M.; Vacas, E.; Rasines, B.; Maly, M.; Serramía, M. J.; López-Fernández, L.; De La Mata, J.; Alvarez, S.; Gómez, R.; et al. Carbosilane Dendrimer Nanotechnology Outlines of the Broad HIV Blocker Profile. *J Control Release* **2012**, *161*, 949–958. https://doi.org/10.1016/j.jconrel.2012.04.050.

(82) Gillies, E. R. Glycodendrimers and Their Biological Applications. In *Engineered Carbohydrate-Based Materials for Biomedical Applications: Polymers, Surfaces, Dendrimers, Nanoparticles, and Hydrogels*; Narain, R., Ed.; John Wiley & Sons, Inc., 2010; pp 261–305. https://doi.org/10.1002/9780470944349.ch7.

(83) Feliu, N.; Walter, M. V.; Montañez, M. I.; Kunzmann, A.; Hult, A.; Nyström, A.; Malkoch, M.; Fadeel, B. Stability and Biocompatibility of a Library of Polyester Dendrimers in Comparison to Polyamidoamine Dendrimers. *Biomaterials* **2012**, *33*, 1970–1981. https://doi.org/10.1016/j.biomaterials.2011.11.054.

(84) Restani, R. B.; Morgado, P. I.; Ribeiro, M. P.; Correia, I. J.; Aguiar-Ricardo, A.; Bonifácio, V. D. B. Biocompatible Polyurea Dendrimers with PH-Dependent Fluorescence. *Angew Chemie - Int Ed* **2012**, *51*, 5162–5165. https://doi.org/10.1002/anie.201200362.

(85) Govender, P.; Renfrew, A. K.; Clavel, C. M.; Dyson, P. J.; Therrien, B.; Smith, G. S. Antiproliferative Activity of Chelating N,O- and N,N-Ruthenium(II) Arene Functionalised Poly(Propyleneimine) Dendrimer Scaffolds. *Dalton Trans* **2011**, *40*, 1158–1167. https://doi.org/10.1039/c0dt00761g.

(86) Vaidya, A.; Jain, S.; Pathak, K.; Pathak, D. Dendrimers: Nanosized Multifunctional Platform for Drug Delivery. *Drug Deliv Lett* **2017**, *8*, 3–19. https://doi.org/10.2174/2210303107666171109112523.

(87) Medina, S. H.; El-Sayed, M. E. H. Dendrimers as Carriers for Delivery of Chemotherapeutic Agents. *Chem Rev* **2009**, *109*, 3141–3157. https://doi.org/10.1021/cr900174j.

(88) Ramalingam, K.; Castro, R.; Pires, P.; Shi, X.; Rodrigues, J.; Xiao, S.; Tomás, H. Gene Delivery Using Dendrimer/PDNA Complexes Immobilized in Electrospun Fibers Using the Layer-by-Layer Technique. *RSC Adv* **2016**, *6*, 97116–97128. https://doi.org/10.1039/c6ra22444j.

(89) Yoyen-Ermis, D.; Ozturk-Atar, K.; Kursunel, M. A.; Aydin, C.; Ozkazanc, D.; Gurbuz, M. U.; Uner,

A.; Tulu, M.; Calis, S.; Esendagli, G. Tumor-Induced Myeloid Cells Are Reduced by Gemcitabine-Loaded PAMAM Dendrimers Decorated with Anti-Flt1 Antibody. *Mol Pharm* **2018**, *15*, 1526–1533. https://doi.org/10.1021/acs.molpharmaceut.7b01075.

(90) Serri, A.; Mahboubi, A.; Zarghi, A.; Moghimi, H. R. PAMAM-Dendrimer Enhanced Antibacterial Effect of Vancomycin Hydrochloride against Gram-Negative Bacteria. *J Pharm Pharm Sci* **2019**, *22*, 10–21. https://doi.org/10.18433/jpps29659.

(91) de Brabander-van den Berg, E. M. M.; Meijer, E. W. Poly(Propylene Imine) Dendrimers: Large-Scale Synthesis by Hetereogeneously Catalyzed Hydrogenations. *Angew Chemie Int Ed English* **1993**, *32*, 1308–1311. https://doi.org/10.1002/anie.199313081.

(92) Kaur, D.; Jain, K.; Mehra, N. K.; Kesharwani, P.; Jain, N. K.; Kumar, N. A Review on Comparative Study of PPI and PAMAM Dendrimers. *J Nanopart Res* **2016**, *18*, 1–14. https://doi.org/10.1007/s11051-016-3423-0.

(93) García-Gallego, S.; Franci, G.; Falanga, A.; Gómez, R.; Folliero, V.; Galdiero, S.; de la Mata, F. J.; Galdiero, M. Function Oriented Molecular Design: Dendrimers as Novel Antimicrobials. *Molecules* **2017**, *22*, 1–29. https://doi.org/10.3390/molecules22101581.

(94) Szulc, A.; Pulaski, L.; Appelhans, D.; Voit, B.; Klajnert-Maculewicz, B. Sugar-Modified Poly(Propylene Imine) Dendrimers as Drug Delivery Agents for Cytarabine to Overcome Drug Resistance. *Int J Pharm* **2016**, *513*, 572–583. https://doi.org/10.1016/j.ijpharm.2016.09.063.

(95) Bosch, P.; Staneva, D.; Vasileva-Tonkova, E.; Grozdanov, P.; Nikolova, I.; Kukeva, R.; Stoyanova, R.; Grabchev, I. New Poly (Propylene Imine) Dendrimer Modified with Acridine and Its Cu(II) Complex: Synthesis, Characterization and Antimicrobial Activity. *Materials (Basel)* **2019**, *12*, 3020–3033. https://doi.org/10.3390/ma12183020.

(96) Hadjichristidis, N.; Guyot, A.; Fetters, L. J. Star-Branched Polymers. 1. The Synthesis of Star Polyisoprenes Using Octa- and Dodecachlorosilanes as Linking Agents. *Macromolecules* **1978**, *11*, 668–672. https://doi.org/10.1021/ma60064a010.

(97) Uchida, H.; Kabe, Y.; Yoshino, K.; Kawamata, A.; Tsumuraya, T.; Masamune, S. General Strategy for the Systematic Synthesis of Oligosiloxanes. Silicone Dendrimers. *J Am Chem Soc* **1990**, *112*, 7077–7079. https://doi.org/10.1021/ja00175a062.

(98) Morikawa, A.; Kakimoto, M.; Imai, Y. Synthesis and Characterization of New Polysiloxane Starburst Polymer. *Macromolecules* **1991**, *24*, 3469–3474. https://doi.org/10.1021/ma00012a001.

(99) Frey, H.; Schlenk, C. Silicon-Based Dendrimers. In *Dendrimers II - Architecture, Nanostructure and Supramolecular Chemistry*; Vogtle, F., Ed.; Springer-Verlag Berlin Heidelberg, 2000; pp 69–129. https://doi.org/10.1007/3-540-46577-4.

(100) Herma, R.; Wrobel, D.; Liegertová, M.; Müllerová, M.; Strašák, T.; Maly, M.; Semerádtová, A.; Štofik, M.; Appelhans, D.; Maly, J. Carbosilane Dendrimers with Phosphonium Terminal Groups Are Low Toxic Non-Viral Transfection Vectors for SiRNA Cell Delivery. *Int J Pharm* **2019**, *562*, 51–65. https://doi.org/10.1016/j.ijpharm.2019.03.018.

(101) Sánchez-Milla, M.; Muñoz-Moreno, L.; Sánchez-Nieves, J.; Malý, M.; Gómez, R.; Carmena, M. J.;

De La Mata, F. J. Anticancer Activity of Dendriplexes against Advanced Prostate Cancer from Protumoral Peptides and Cationic Carbosilane Dendrimers. *Biomacromolecules* **2019**, *20*, 1224–1234. https://doi.org/10.1021/acs.biomac.8b01632.

(102) Lambert, J. B.; Pflug, J. L.; Stern, C. L. Synthesis and Structure of a Dendritic Polysilane. *Angew Chem Int Ed Engl* **1995**, *34*, 98–99. https://doi.org/10.1002/anie.199500981.

(103) Hu, J.; Son, D. Y. Carbosilazane Dendrimers - Synthesis and Preliminary Characterization Studies. *Macromolecules* **1998**, *31*, 8644–8646. https://doi.org/10.1021/ma9808934.

(104) Kemmitt, T.; Henderson, W. Dendrimeric Silatrane Wedges. *J Chem Soc - Perkin Trans 1* **1997**, 729–739. https://doi.org/10.1039/a605135i.

(105) Roy, R.; Zanini, D.; Meunier, S. J.; Romanowska, A. Solid-Phase Synthesis of Dendritic Sialoside Inhibitors of Influenza A Virus Haemagglutinin. *J Chem Soc Chem Commun* **1993**, 1869–1872. https://doi.org/10.1039/C39930001869.

(106) Li, Y.; Cheng, Y.; Xu, T. Design, Synthesis and Potent Pharmaceutical Applications of Glycodendrimers: A Mini Review. *Curr Drug Discov Technol* **2007**, *4*, 246–254. https://doi.org/10.2174/157016307783220503.

(107) Jain, K.; Kesharwani, P.; Gupta, U.; Jain, N. K. Dendrimer Toxicity: Let's Meet the Challenge. *Int J Pharm* **2010**, *394*, 122–142. https://doi.org/10.1016/j.ijpharm.2010.04.027.

(108) Shiao, T. C.; Roy, R. Glycodendrimers as Functional Antigens and Antitumor Vaccines. *New J Chem* **2012**, *36*, 324–339. https://doi.org/10.1039/c2nj20873c.

(109) Roy, R.; Shiao, T. C.; Rittenhouse-Olson, K. Glycodendrimers: Versatile Tools for Nanotechnology. *Brazilian J Pharm Sci* **2013**, *49*, 85–108. https://doi.org/10.1590/S1984-82502013000700008.

(110) Han, S.; Kanamoto, T.; Nakashima, H.; Yoshida, T. Synthesis of a New Amphiphilic Glycodendrimer with Antiviral Functionality. *Carbohydr Polym* **2012**, *90*, 1061–1068. https://doi.org/10.1016/j.carbpol.2012.06.044.

(111) Duinkerken, S.; Horrevorts, S. K.; Kalay, H.; Ambrosini, M.; Rutte, L.; de Gruijl, T. D.; Garcia-Vallejo, J. J.; van Kooyk, Y. Glyco-Dendrimers as Intradermal Anti-Tumor Vaccine Targeting Multiple Skin DC Subsets. *Theranostics* **2019**, *9*, 5797–5809. https://doi.org/10.7150/thno.35059.

(112) Rengan, K.; Engel, R. The Synthesis of Phosphonium Cascade Molecules. *J Chem Soc Perkin Trans 1* **1991**, 987–990. https://doi.org/10.1039/P19910000987.

(113) Launay, N.; Caminade, A.; Lahana, R.; Majoral, J. A General Synthetic Strategy for Neutral Phosphorus-Containing Dendrimers. *Angew Chemie Int Ed English* **1994**, *33*, 1589–1592. https://doi.org/10.1002/anie.199415891.

(114) Pedziwiatr-Werbicka, E.; Milowska, K.; Dzmitruk, V.; Ionov, M.; Shcharbin, D.; Bryszewska, M. Dendrimers and Hyperbranched Structures for Biomedical Applications. *Eur Polym J* **2019**, *119*, 61–73. https://doi.org/10.1016/j.eurpolymj.2019.07.013.

(115) Shcharbin, D.; Shcharbina, N.; Pedziwiatr-Werbicka, E.; de la Mata, J.; Gomez-Ramirez, R.; Mignani, S.; Kulchitsky, V. A.; Muñoz-Fernández, M.-A.; Caminade, A.-M.; Majoral, J.-P.; et al.

Phosphorus Dendrimers as Vectors for Gene Therapy in Cancer. In *Phosphorous Dendrimers in Biology and Nanomedicine: Syntheses, Characterization, and Properties*; Caminade, A.-M., Majoral, J.-P., Turrin, C.-O., Eds.; Pan Stanford Publishing Pte. Ltd., 2018; pp 228–243. https://doi.org/10.1201/9781315110851.

(116) Qiu, J.; Hameau, A.; Shi, X.; Mignani, S.; Majoral, J.; Caminade, A. Fluorescent Phosphorus Dendrimers: Towards Material and Biological Applications. *Chempluschem* **2019**, *84*, 1070–1080. https://doi.org/10.1002/cplu.201900337.

(117) Ihnatsyeu-Kachan, A.; Dzmitruk, V.; Apartsin, E.; Krasheninina, O.; Ionov, M.; Loznikova, S.; Venyaminova, A.; Miłowska, K.; Shcharbin, D.; Mignani, S.; et al. Multi-Target Inhibition of Cancer Cell Growth by SiRNA Cocktails and 5-Fluorouracil Using Effective Piperidine-Terminated Phosphorus Dendrimers. *Colloids and Interfaces* **2017**, *1*, 6–23. https://doi.org/10.3390/colloids1010006.

(118) Li, A.; Fan, Y.; Cao, X.; Chen, L.; Wang, L.; Alves, C. S.; Mignani, S.; Majoral, J. P.; Tomás, H.; Shi, X. Morpholino-Functionalized Phosphorus Dendrimers for Precision Regenerative Medicine: Osteogenic Differentiation of Mesenchymal Stem Cells. *Nanoscale* **2019**, *11*, 17230–17234. https://doi.org/10.1039/c9nr06410a.

(119) Hawker, C. J.; Fréchet, J. M. J. Monodispersed Dendritic Polyesters with Removable Chain Ends: A Versatile Approach to Globular Macromolecules with Chemically Reversible Polarities. *J Chem Soc Perkin Trans 1* **1992**, 2459–2469. https://doi.org/10.1039/p19920002459.

(120) Ihre, H.; Hult, A.; Söderlind, E. Synthesis, Characterization, and 1H NMR Self-Diffusion Studies of Dendritic Aliphatic Polyesters Based on 2,2-Bis(Hydroxymethyl)Propionic Acid and 1,1,1-Tris(Hydroxyphenyl)Ethane. *J Am Chem Soc* **1996**, *118*, 6388–6395. https://doi.org/10.1021/ja954171t.

(121) Huang, D.; Wu, D. Biodegradable Dendrimers for Drug Delivery. *Mater Sci Eng C* **2018**, *90*, 713–727. https://doi.org/10.1016/j.msec.2018.03.002.

(122) Leiro, V.; Garcia, J. P.; Tomás, H.; Pêgo, A. P. The Present and the Future of Degradable Dendrimers and Derivatives in Theranostics. *Bioconjug Chem* **2015**, *26*, 1185–1197. https://doi.org/10.1021/bc5006224.

(123) Stenström, P.; Manzanares, D.; Zhang, Y.; Ceña, V.; Malkoch, M. Evaluation of Amino-Functional Polyester Dendrimers Based on Bis-MPA as Nonviral Vectors for SiRNA Delivery. *Molecules* **2018**, *23* (8). https://doi.org/10.3390/molecules23082028.

(124) Alfei, S.; Castellaro, S. Synthesis and Characterization of Polyester-Based Dendrimers Containing Peripheral Arginine or Mixed Amino Acids as Potential Vectors for Gene and Drug Delivery. *Macromol Res* **2017**, *25*, 1172–1186. https://doi.org/10.1007/s13233-017-5160-3.

(125) Leiro, V.; Garcia, J. P.; Moreno, P. M. D.; Spencer, A. P.; Fernandez-Villamarin, M.; Riguera, R.; Fernandez-Megia, E.; Pêgo, A. P. Biodegradable PEG-Dendritic Block Copolymers: Synthesis and Biofunctionality Assessment as Vectors of SiRNA. *J Mater Chem B* **2017**, *5*, 4901–4917. https://doi.org/10.1039/c7tb00279c.

(126) Gothwal, A.; Malik, S.; Gupta, U.; Jain, N. K. 11 - Toxicity and Biocompatibility Aspects of Dendrimers. In *Pharmaceutical Applications of Dendrimers*; Elsevier Inc., 2020; pp 251–274. https://doi.org/10.1016/B978-0-12-814527-2.00011-1.

(127) Restani, R. B.; Conde, J.; Baptista, P. V.; Cidade, M. T.; Bragança, A. M.; Morgado, J.; Correia, I. J.; Aguiar-Ricardo, A.; Bonifácio, V. D. B. Polyurea Dendrimer for Efficient Cytosolic SiRNA Delivery. *RSC Adv* **2014**, *4*, 54872–54878. https://doi.org/10.1039/c4ra09603g.

(128) Santos, I.; Ramos, C.; Mendes, C.; Sequeira, C. O.; Tomé, C. S.; Fernandes, D. G. H.; Mota, P.; Pires, R. F.; Urso, D.; Hipólito, A.; et al. Targeting Glutathione and Cystathionine β-Synthase in Ovarian Cancer Treatment by Selenium–chrysin Polyurea Dendrimer Nanoformulation. *Nutrients* **2019**, *11*, 2523–2545. https://doi.org/10.3390/nu11102523.

(129) Denti, G.; Serroni, S.; Campagna, S.; Ricevuto, V.; Balzani, V. Directional Energy Transfer in a Luminescent Tetranuclear Ru(II) Polypyridine Complex That Contains Two Different Types of Bridging Ligands. *Inorg Chim Acta* **1991**, *182*, 127–129. https://doi.org/10.1016/S0020-1693(00)90144-0.

(130) Denti, G.; Campagna, S.; Serroni, S.; Ciano, M.; Balzani, V. Decanuclear Homo-and Heterometallic Polypyridine Complexes: Syntheses, Absorption Spectra, Luminescence, Electrochemical Oxidation, and Intercomponent Energy Transfer. *J Am Chem Soc* **1992**, *114*, 2944–2950. https://doi.org/10.1021/ja00034a029.

(131) Newkome, G. R.; Moorefield, C. N.; Baker, G. R.; Saunders, M. J.; Grossman, S. H. Unimolecular Micelles. *Angew Chemie Int Ed English* **1991**, *30*, 1178–1180. https://doi.org/10.1002/anie.199111781.

(132) Newkome, G. R.; Cardullo, F.; Constable, E. C.; Moorefield, C. N.; Thompson, A. M. W. C. Metallomicellanols: Incorporation of Ruthenium(II)-2,2′: 6′,2″-Terpyridine Triads into Cascade Polymers. *J Chem Soc Chem Commun* **1993**, No. 11, 925–927. https://doi.org/10.1039/C39930000925.

(133) Xu, L.; Chen, L.-J.; Yang, H.-B. Recent Progress in the Construction of Cavity-Cored Supramolecular Metallodendrimers via Coordination-Driven Self-Assembly. *Chem Commun* **2014**, *50*, 5156–5170. https://doi.org/10.1039/c3cc47484d.

(134) Valério, C.; Alonso, E.; Ruiz, J.; Blais, J.-C.; Astruc, D. A Polycationic Metallodendrimer with 24 $[Fe(\eta^5\text{-}C_5Me_5)(\eta^6\text{-N-Alkylaniline})]^+$ Termini That Recognizes Chloride and Bromide Anions. *Angew Chem Int Ed* **1999**, *38*, 1747–1751. https://doi.org/10.1002/(SICI)1521-3773(19990614)38:12<1747::AID-ANIE1747>3.0.CO;2-G.

(135) Huck, W. T. S.; Prins, L. J.; Fokkens, R. H.; Nibbering, N. M. M.; Van Veggel, F. C. J. M.; Reinhoudt, D. N. Convergent and Divergent Noncovalent Synthesis of Metallodendrimers. *J Am Chem Soc* **1998**, *120*, 6240–6246. https://doi.org/10.1021/ja974031e.

(136) Ornelas, C.; Ruiz Aranzaes, J.; Cloutet, E.; Alves, S.; Astruc, D. Click Assembly of 1,2,3-Triazole-Linked Dendrimers, Including Ferrocenyl Dendrimers, Which Sense Both Oxo Anions and Metal Cations. *Angew Chemie - Int Ed* **2007**, *46*, 872–877. https://doi.org/10.1002/anie.200602858.

(137) Hwang, S.-H.; Shreiner, C. D.; Moorefield, C. N.; Newkome, G. R. Recent Progress and Applications for Metallodendrimers. *New J Chem* **2007**, *31*, 1192–1217. https://doi.org/10.1039/b612656c.

(138) Manen, H.-J.; van Veggel, F. C. J. M.; Reinhoudt, D. N. Non-Covalent Synthesis of Metallodendrimers. In *Dendrimers IV. Metal Coordination, Self Assembly, Catalysis*; Vögtle, F., Schalley, C. A., Eds.; Springer, 2001; pp 121–162. https://doi.org/10.1016/s0022-328x(00)88472-7.

(139) Govender, P.; Therrien, B.; Smith, G. S. Bio-Metallodendrimers - Emerging Strategies in Metal-Based Drug Design. *Eur J Inorg Chem* **2012**, *2012*, 2853–2862. https://doi.org/10.1002/ejic.201200161.

(140) Zheng, W.; Alkorta, I.; Yang, D.; Wan, L.; Zhao, M.; Elguero, J. Synthesis and Structural Characterization of 1,2,4-Diazaphospholide Complexes of Titanium(IV) and Titanium(III). *Inorg Chem* **2011**, *50*, 12408–12410. https://doi.org/10.1021/ic2021066.

(141) Tang, Y.-H.; Huang, A. Y.-T.; Chen, P.-Y.; Chen, H.-T.; Kao, C.-L. Metallodendrimers and Dendrimer Nanocomposites. *Curr Pharm Des* **2011**, *17*, 2308–2330. https://doi.org/10.2174/138161211797052367.

(142) Alam, M. A.; Jahan, A.; Khan, M. W. A Review on Dendrimers and Metallodendrimers, the Important Compounds as Catalyst in Material Chemistry. *Adv Mater* **2017**, *6*, 52–56. https://doi.org/10.11648/j.am.20170605.11.

(143) Chen, L.; Mignani, S.; Caminade, A.-M.; Majoral, J.-P. Metal-Based Phosphorus Dendrimers as Novel Nanotherapeutic Strategies to Tackle Cancers: A Concise Overview. *WIREs Nanomed Nanobiotechnol.* **2019**, e1577–e1588. https://doi.org/10.1002/wnan.1577.

(144) Kazzouli, S. El; Brahmi, N. El; Mignani, S.; Bousmina, M.; Zablocka, M.; Majoral, J.-P. From Metallodrugs to Metallodendrimers for Nanotherapy in Oncology: A Concise Overview. *Curr Med Chem* **2012**, *19*, 4995–5010. https://doi.org/10.2174/0929867311209024995.

(145) Viñas, C.; Teixidor, F.; Núñez, R. Boron Clusters-Based Metallodendrimers Metallodendrimers. *Inorg Chim Acta* **2014**, *409*, 12–25. https://doi.org/10.1016/j.ica.2013.05.038.

(146) Martin, M.; Manea, F.; Fiammengo, R.; Prins, L. J.; Pasquato, L.; Scrimin, P. Metallodendrimers as Transphosphorylation Catalysts. *J Am Chem Soc* **2007**, *129*, 6982–6983. https://doi.org/10.1021/ja070980o.

(147) Makhubela, B. C. E.; Jardine, A. M.; Westman, G.; Smith, G. S. Hydroformylation of 1-Octene Using Low-Generation Rh(I) Metallodendritic Catalysts Based on a Tris-2-(2-Pyridyliminoethyl)Amine Scaffold. *Dalton Trans* **2012**, *41*, 10715–10723. https://doi.org/10.1039/c2dt30856h.

(148) Ruggi, A.; Beekman, C.; Wasserberg, D.; Subramaniam, V.; Reinhoudt, D. N.; Van Leeuwen, F. W. B.; Velders, A. H. Dendritic Ruthenium(II)-Based Dyes Tuneable for Diagnostic or Therapeutic Applications. *Chem-Eur J* **2011**, *17*, 464–467. https://doi.org/10.1002/chem.201002514.

(149) Wang, H.; Yuan, Y.; Zhuo, Y.; Chai, Y.; Yuan, R. Sensitive Electrochemiluminescence

Immunosensor for Detection of N-Acetyl-β-D-Glucosaminidase Based on a “Light-Switch” Molecule Combined with DNA Dendrimer. *Anal Chem* **2016**, *88*, 5797–5803. https://doi.org/10.1021/acs.analchem.6b00357.

(150) Li, S.; Liu, C.; Han, B.; Luo, J.; Yin, G. An Electrochemiluminescence Aptasensor Switch for Aldicarb Recognition via Ruthenium Complex-Modified Dendrimers on Multiwalled Carbon Nanotubes. *Microchim Acta* **2017**, *184*, 1669–1675. https://doi.org/10.1007/s00604-017-2177-4.

(151) Llamazares, C.; del Olmo, N. S.; Ortega, P.; Gómez, R.; Soliveri, J.; de la Mata, F. J.; García-Gallego, S.; Copa-Patiño, J. L. Antibacterial Effect of Carbosilane Metallodendrimers in Planktonic Cells of Gram-Positive and Gram-Negative Bacteria and Staphylococcus Aureus Biofilm. *Biomolecules* **2019**, *9*, 405–415. https://doi.org/10.3390/biom9090405.

(152) Giffard, D.; Fischer-Fodor, E.; Vlad, C.; Achimas-Cadariu, P.; Smith, G. S. Synthesis and Antitumour Evaluation of Mono- and Multinuclear [2+1] Tricarbonylrhenium(I) Complexes. *Eur J Med Chem* **2018**, *157*, 773–781. https://doi.org/10.1016/j.ejmech.2018.08.011.

(153) Gano, L.; Pinheiro, T.; Matos, A. P.; Tortosa, F.; Jorge, T. F.; Gonçalves, M. S.; Martins, M.; Morais, T. S.; Valente, A.; Tomaz, A. I.; et al. Antitumour and Toxicity Evaluation of a Ru(II)-Cyclopentadienyl Complex in a Prostate Cancer Model by Imaging Tools. *Anticancer Agents Med Chem* **2019**, *19*, 1–14. https://doi.org/10.2174/1871520619666190318152726.

(154) Wani, W. A.; Prashar, S.; Shreaz, S.; Gómez-Ruiz, S. Nanostructured Materials Functionalized with Metal Complexes: In Search of Alternatives for Administering Anticancer Metallodrugs. *Coordin Chem Rev* **2016**, *312*, 67–98. https://doi.org/10.1016/j.ccr.2016.01.001.

(155) Kaminskas, L. M.; Boyd, B. J.; Porter, C. J. H. Dendrimer Pharmacokinetics: The Effect of Size, Structure and Surface Characteristics on ADME Properties. *Nanomedicine* **2011**, *6*, 1063–1084. https://doi.org/10.2217/nnm.11.173.

(156) Yellepeddi, V. K.; Ghandehari, H. Pharmacokinetics of Oral Therapeutics Delivered by Dendrimer-Based Carriers. *Expert Opin Drug Deliv* **2019**, *16*, 1–11. https://doi.org/10.1080/17425247.2019.1656607.

(157) Guo, H.; Mackay, J. A. A Pharmacokinetics Primer for Preclinical Nanomedicine Research. In *Nanoparticles for Biomedical Applications: Fundamental Concepts, Biological Interactions and Clinical Applications Micro and Nano Technologies*; Chung, E. J., Leon, L., Rinaldi, C., Eds.; Elsevier Inc., 2020; pp 109–128. https://doi.org/10.1016/B978-0-12-816662-8.00008-4.

(158) Zolnik, B. S.; Sadrieh, N. Regulatory Perspective on the Importance of ADME Assessment of Nanoscale Material Containing Drugs. *Adv Drug Deliver Rev* **2009**, *61*, 422–427. https://doi.org/10.1016/j.addr.2009.03.006.

(159) Wijagkanalan, W.; Kawakami, S.; Hashida, M. Designing Dendrimers for Drug Delivery and Imaging: Pharmacokinetic Considerations. *Pharm Res* **2011**, *28*, 1500–1519. https://doi.org/10.1007/s11095-010-0339-8.

(160) Jurj, A.; Braicu, C.; Pop, L.-A.; Tomuleasa, C.; Gherman, C. D.; Berindan-Neagoe, I. The New Era of Nanotechnology, an Alternative to Change Cancer Treatment. *Drug Des Devel Ther* **2017**, *11*,

2871–2890. https://doi.org/10.2147/DDDT.S142337.

(161) Wolinsky, J. B.; Grinstaff, M. W. Therapeutic and Diagnostic Applications of Dendrimers for Cancer Treatment. *Adv Drug Deliver Rev* **2008**, *60*, 1037–1055. https://doi.org/10.1016/j.addr.2008.02.012.

(162) Kesharwani, P.; Tekade, R. K.; Jain, N. K. Generation Dependent Cancer Targeting Potential of Poly(Propyleneimine) Dendrimer. *Biomaterials* **2014**, *35*, 5539–5548. https://doi.org/10.1016/j.biomaterials.2014.03.064.

(163) Wu, L.-P.; Ficker, M.; Christensen, J. B.; Trohopoulos, P. N.; Moghimi, S. M. Dendrimers in Medicine: Therapeutic Concepts and Pharmaceutical Challenges. *Bioconjug Chem* **2015**, *26*, 1198–1211. https://doi.org/10.1021/acs.bioconjchem.5b00031.

(164) Yellepeddi, V. K.; Vangara, K. K.; Palakurthi, S. Poly(Amido)Amine (PAMAM) Dendrimer-Cisplatin Complexes for Chemotherapy of Cisplatin-Resistant Ovarian Cancer Cells. *J Nanopart Res* **2013**, *15*, 1897–1911. https://doi.org/10.1007/s11051-013-1897-6.

(165) Caminade, A.-M.; Turrin, C. O. Dendrimers for Drug Delivery. *J Mater Chem B* **2014**, *2*, 4055–4066. https://doi.org/10.1039/c4tb00171k.

(166) Singh, J.; Jain, K.; Mehra, N. K.; Jain, N. K. Dendrimers in Anticancer Drug Delivery: Mechanism of Interaction of Drug and Dendrimers. *Artif Cells, Nanomedicine Biotechnol* **2016**, *44*, 1626–1634. https://doi.org/10.3109/21691401.2015.1129625.

(167) Abedi-Gaballu, F.; Dehghan, G.; Ghaffari, M.; Yekta, R.; Abbaspour-Ravasjani, S.; Baradaran, B.; Ezzati Nazhad Dolatabadi, J.; Hamblin, M. R. PAMAM Dendrimers as Efficient Drug and Gene Delivery Nanosystems for Cancer Therapy. *Appl Mater Today* **2018**, *12*, 177–190. https://doi.org/10.1016/j.apmt.2018.05.002.

(168) Chauhan, A. S. Dendrimers for Drug Delivery. *Molecules* **2018**, *23*, 938–946. https://doi.org/10.3390/molecules23040938.

(169) Sk, U. H.; Kojima, C. Dendrimers for Theranostic Applications. *Biomol Concepts* **2015**, *6*, 205–217. https://doi.org/10.1515/bmc-2015-0012.

(170) Singh, L.; Kruger, H. G.; Maguire, G. E. M.; Govender, T.; Parboosing, R. The Role of Nanotechnology in the Treatment of Viral Infections. *Ther Adv Infect Dis* **2017**, *4*, 105–131. https://doi.org/10.1177/2049936117713593.

(171) Mehendale, R.; Joshi, M.; Patravale, V. Nanomedicines for Treatment of Viral Diseases. *Crit Rev Ther Drug Carrier Syst* **2013**, *30*, 1–49. https://doi.org/10.1615/CritRevTherDrugCarrierSyst.2013005469.

(172) Lai, C.-C.; Shih, T.-P.; Ko, W.-C.; Tang, H.-J.; Hsueh, P.-R. Severe Acute Respiratory Syndrome Coronavirus 2 (SARS-CoV-2) and Coronavirus Disease-2019 (COVID-19): The Epidemic and the Challenges. *Int J Antimicrob Agents* **2020**, *55*, 105924. https://doi.org/10.1016/j.ijantimicag.2020.105924.

(173) University, J. H. COVID-19 Dashboard by the Center for Systems Science and Engineering (CSSE) at Jonh Hopkins University https://coronavirus.jhu.edu/map.html (accessed Jul 29, 2020).

(174) UNAIDS. Global HIV & AIDS statistics — 2020 fact sheet https://www.unaids.org/en/resources/fact-sheet (accessed Jul 28, 2020).

(175) Boyapalle, S.; Mohapatra, S.; Mohapatra, S. Nanotechnology Applications to HIV Vaccines and Microbicides. *J Glob Infect Dis* **2012**, *4*, 62–68. https://doi.org/10.4103/0974-777X.93764.

(176) Liu, Y.; Chen, C. Role of Nanotechnology in HIV/AIDS Vaccine Development. *Adv Drug Deliver Rev* **2016**, *103*, 76–89. https://doi.org/10.1016/j.addr.2016.02.010.

(177) Kumar, L.; Verma, S.; Prasad, D. N.; Bhardwaj, A.; Vaidya, B.; Jain, A. K. Nanotechnology: A Magic Bullet for HIV AIDS Treatment. *Artif Cells, Nanomedicine Biotechnol* **2015**, *43*, 71–86. https://doi.org/10.3109/21691401.2014.883400.

(178) Barré-Sinoussi, F.; Chermann, J. C.; Rey, F.; Nugeyre, M. T.; Chamaret, S.; Gruest, J.; Dauguet, C.; Axler-Blin, C.; Vézinet-Brun, F.; Rouzioux, C.; et al. Isolation of a T-Lymphotropic Retrovirus from a Patient at Risk for Acquired Immune Deficiency Syndrome (AIDS). *Science* **1983**, *220*, 868–871. https://doi.org/10.1126/science.6189183.

(179) Gallo, R. C.; Sarin, P. S.; Gelmann, E. P.; Robert-Guroff, M.; Richardson, E.; Kalyanaraman, V. S.; Mann, D.; Sidhu, G. D.; Stahl, R. E.; Zolla-Pazner, S.; et al. Isolation of Human T-Cell Leukemia Virus in Acquired Immune Deficiency Syndrome (AIDS). *Science* **1983**, *220*, 865–867. https://doi.org/10.1126/science.6601823.

(180) Popovic, M.; Sarngadharan, M. G.; Read, E.; Gallo, R. C. Detection, Isolation, and Continuous Production of Cytopathic Retroviruses (HTLV-III) from Patients with AIDS and Pre-AIDS. *Science* **1984**, *224*, 497–500. https://doi.org/10.1126/science.6200935.

(181) Montagnier, L. Historical Essay: A History of HIV Discovery. *Science* **2002**, *298*, 1727–1728. https://doi.org/10.1126/science.1079027.

(182) Gallo, R. C. Historical Essay: The Early Years of HIV/AIDS. *Science* **2002**, *298*, 1728–1730. https://doi.org/10.1126/science.1078050.

(183) Gallo, R. C.; Montagnier, L. Historical Essay: Prospects for the Future. *Science* **2002**, *298* (5599), 1730–1731. https://doi.org/10.1126/science.1079864.

(184) Cao, S.; Woodrow, K. A. Nanotechnology Approaches to Eradicating HIV Reservoirs. *Eur J Pharm Biopharm* **2019**, *138*, 48–63. https://doi.org/10.1016/j.ejpb.2018.06.002.

(185) Parboosing, R.; Maguire, G. E. M.; Govender, P.; Kruger, H. G. Nanotechnology and the Treatment of HIV Infection. *Viruses* **2012**, *4*, 488–520. https://doi.org/10.3390/v4040488.

(186) Mhlwatika, Z.; Aderibigbe, B. A. Application of Dendrimers for the Treatment of Infectious Diseases. *Molecules* **2018**, *23*, 2205–2236. https://doi.org/10.3390/molecules23092205.

(187) Coutinho, C.; Sarmento, B.; das Neves, J. Targeted Microbicides for Preventing Sexual HIV Transmission. *J Control Release* **2017**, *266*, 119–128. https://doi.org/10.1016/j.jconrel.2017.09.030.

(188) Nandy, B.; Saurabh, S.; Sahoo, A. K.; Dixit, N. M.; Maiti, P. K. The SPL7013 Dendrimer Destabilizes the HIV-1 Gp120–CD4 Complex. *Nanoscale* **2015**, *7*, 18628–18641. https://doi.org/10.1039/C5NR04632G.

(189) Bronshtein, T.; Toledano, N.; Danino, D.; Pollack, S.; MacHluf, M. Cell Derived Liposomes Expressing CCR5 as a New Targeted Drug-Delivery System for HIV Infected Cells. *J Control Release* **2011**, *151*, 139–148. https://doi.org/10.1016/j.jconrel.2011.02.023.

(190) Chan, D. C.; Kim, P. S. HIV Entry and Its Inhibition. *Cell* **1998**, *93*, 681–684. https://doi.org/10.1016/S0092-8674(00)81430-0.

(191) Yavuz, B.; Morgan, J. L.; Showalter, L.; Horng, K. R.; Dandekar, S.; Herrera, C.; LiWang, P.; Kaplan, D. L. Pharmaceutical Approaches to HIV Treatment and Prevention. *Adv Ther* **2018**, *1* (Yavuz), 1800054–1800080. https://doi.org/10.1002/adtp.201800054.

(192) Roy, U.; Rodríguez, J.; Barber, P.; Sarmento, B.; Nair, M. The Potential of HIV-1 Nanotherapeutics: From in Vitro Studies to Clinical Trials. *Nanomedicine* **2015**, *10*, 3597–3609. https://doi.org/10.2217/nnm.15.160.

(193) Sepúlveda-Crespo, D.; Ceña-Díez, R.; Jiménez, J. L.; Muñoz-Fernández, M. Á. Mechanistic Studies of Viral Entry: An Overview of Dendrimer-Based Microbicides As Entry Inhibitors Against Both HIV and HSV-2 Overlapped Infections. *Med Res Rev* **2017**, *37*, 149–179. https://doi.org/10.1002/med.21405.

(194) Fasting, C.; Schalley, C. A.; Weber, M.; Seitz, O.; Hecht, S.; Koksch, B.; Dernedde, J.; Graf, C.; Knapp, E. W.; Haag, R. Multivalency as a Chemical Organization and Action Principle. *Angew Chemie - Int Ed* **2012**, *51*, 10472–10498. https://doi.org/10.1002/anie.201201114.

(195) Briz, V.; Serramia, M. J.; Madrid, R.; Hameau, A.; Caminade, A.-M.; Majoral, J.-P.; Muñoz-Fernández, M. A. Validation of a Generation 4 Phosphorus-Containing Polycationic Dendrimer for Gene Delivery Against HIV-1. *Curr Med Chem* **2012**, *19*, 5044–5051. https://doi.org/10.2174/0929867311209025044.

(196) Bon, I.; Lembo, D.; Rusnati, M.; Clò, A.; Morini, S.; Miserocchi, A.; Bugatti, A.; Grigolon, S.; Musumeci, G.; Landolfo, S.; et al. Peptide-Derivatized SB105-A10 Dendrimer Inhibits the Infectivity of R5 and X4 HIV-1 Strains in Primary PBMCs and Cervicovaginal Histocultures. *PLOS One* **2013**, *8*, 1–13. https://doi.org/10.1371/journal.pone.0076482.

(197) Ceña-Diez, R.; García-Broncano, P.; de la Mata, F. J.; Gómez, R.; Resino, S.; Muñoz-Fernández, M. Á. G2-S16 Dendrimer as a Candidate for a Microbicide to Prevent HIV-1 Infection in Women. *Nanoscale* **2017**, *9*, 9732–9742. https://doi.org/10.1039/c7nr03034g.

(198) Maciel, D.; Guerrero-Beltrán, C.; Ceña-Diez, R.; Tomás, H.; Muñoz-Fernández, M. Á.; Rodrigues, J. New Anionic Poly(Alkylideneamine) Dendrimers as Microbicide Agents against HIV-1 Infection. *Nanoscale* **2019**, *11*, 9679–9690. https://doi.org/10.1039/c9nr00303g.

(199) Donalisio, M.; Quaranta, P.; Chiuppesi, F.; Pistello, M.; Cagno, V.; Cavalli, R.; Volante, M.; Bugatti, A.; Rusnati, M.; Ranucci, E.; et al. The AGMA1 Poly(Amidoamine) Inhibits the Infectivity of Herpes Simplex Virus in Cell Lines, in Human Cervicovaginal Histocultures, and in Vaginally Infected Mice. *Biomaterials* **2016**, *85*, 40–53. https://doi.org/10.1016/j.biomaterials.2016.01.055.

(200) Ceña-Diez, R.; Martin-Moreno, A.; de la Mata, F. J.; Gómez-Ramirez, R.; Muñoz, E.; Ardoy, M.; Muñoz-Fernández, M. Á. G1-S4 or G2-S16 Carbosilane Dendrimer in Combination with Platycodin

D as a Promising Vaginal Microbicide Candidate with Contraceptive Activity. *Int J Nanomed* **2019**, *14*, 2371–2381. https://doi.org/10.2147/IJN.S188495.

(201) Donalisio, M.; Rusnati, M.; Cagno, V.; Civra, A.; Bugatti, A.; Giuliani, A.; Pirri, G.; Volante, M.; Papotti, M.; Landolfo, S.; et al. Inhibition of Human Respiratory Syncytial Virus Infectivity by a Dendrimeric Heparan Sulfate-Binding Peptide. *Antimicrob Agents Ch* **2012**, *56*, 5278–5288. https://doi.org/10.1128/AAC.00771-12.

(202) Muñoz, A.; Sigwalt, D.; Illescas, B. M.; Luczkowiak, J.; Rodríguez-Pérez, L.; Nierengarten, I.; Holler, M.; Remy, J. S.; Buffet, K.; Vincent, S. P.; et al. Synthesis of Giant Globular Multivalent Glycofullerenes as Potent Inhibitors in a Model of Ebola Virus Infection. *Nat Chem* **2016**, *8*, 50–57. https://doi.org/10.1038/nchem.2387.

(203) Chahal, J. S.; Khan, O. F.; Cooper, C. L.; McPartlan, J. S.; Tsosie, J. K.; Tilley, L. D.; Sidik, S. M.; Lourido, S.; Langer, R.; Bavari, S.; et al. Dendrimer-RNA Nanoparticles Generate Protective Immunity against Lethal Ebola, H1N1 Influenza, and Toxoplasma Gondii Challenges with a Single Dose. *Proc Natl Acad Sci U S A* **2016**, *113*, E4133–E4142. https://doi.org/10.1073/pnas.1600299113.

(204) Illescas, B. M.; Rojo, J.; Delgado, R.; Martín, N. Multivalent Glycosylated Nanostructures To Inhibit Ebola Virus Infection. *J Am Chem Soc* **2017**, *139* (17), 6018–6025. https://doi.org/10.1021/jacs.7b01683.

(205) Bahadoran, A.; Ebrahimi, M.; Yeap, S. K.; Safi, N.; Moeini, H.; Hair-Bejo, M.; Hussein, M. Z.; Omar, A. R. Induction of a Robust Immune Response against Avian Influenza Virus Following Transdermal Inoculation with H5-DNA Vaccine Formulated in Modified Dendrimer-Based Delivery System in Mouse Model. *Int J Nanomed* **2017**, *12*, 8573–8585. https://doi.org/10.2147/IJN.S139126.

(206) Lee, J.; Lee, S.; Kwon, Y. E.; Kim, Y. J.; Choi, J. S. Gene Delivery by PAMAM Dendrimer Conjugated with the Nuclear Localization Signal Peptide Derived from Influenza B Virus Nucleoprotein. *Macromol Res* **2019**, *27*, 360–368. https://doi.org/10.1007/s13233-019-7057-9.

(207) Borges, A. R.; Schengrund, C.-L. Dendrimers and Antivirals: A Review. *Curr Drug Targets Infect Disord* **2005**, *5*, 247–254. https://doi.org/10.2174/1568005054880127.

(208) Starpharma. SPL7013 shows significant activity against SARS-CoV-2 (coronavirus) https://www.starpharma.com/news/473 (accessed May 13, 2020).

(209) FDA. Antiretroviral drugs used in the treatment of HIV infection https://www.fda.gov/patients/hiv-treatment/antiretroviral-drugs-used-treatment-hiv-infection (accessed Nov 6, 2019).

(210) Pirrone, V.; Thakkar, N.; Jacobson, J. M.; Wigdahl, B.; Krebs, F. C. Combinatorial Approaches to the Prevention and Treatment of HIV-1 Infection. *Antimicrob Agents Ch* **2011**, *55*, 1831–1842. https://doi.org/10.1128/AAC.00976-10.

(211) Córdoba, E. V.; Arnáiz, E.; De La Mata, F. J.; Gómez, R.; Leal, M.; Pion, M.; Muñoz-Fernández, M. Á. Synergistic Activity of Carbosilane Dendrimers in Combination with Maraviroc against HIV in Vitro. *AIDS* **2013**, *27*, 2053–2058. https://doi.org/10.1097/QAD.0b013e328361fa4a.

(212) Sepúlveda-Crespo, D.; Sánchez-Rodríguez, J.; Serramía, M. J.; Gómez, R.; De La Mata, F. J.; Jiménez, J. L.; Muñoz-Fernández, M. Á. Triple Combination of Carbosilane Dendrimers, Tenofovir and Maraviroc as Potential Microbicide to Prevent HIV-1 Sexual Transmission. *Nanomedicine* **2015**, *10*, 899–914. https://doi.org/10.2217/nnm.14.79.

(213) Boskey, E.; Olender, S. What is cART? https://www.verywellhealth.com/what-is-cart-p2-3132623 (accessed Apr 14, 2020).

(214) Starpharma. VivaGel® for Bacterial Vaginosis https://starpharma.com/vivagel_bv (accessed Nov 5, 2019).

(215) Blanzat, M.; Turrin, C.-O.; Aubertin, A.-M.; Couturier-Vidal, C.; Caminade, A.-M.; Majoral, J.-P.; Rico-Lattes, I.; Lattes, A. Dendritic Catanionic Assemblies: In Vitro Anti-HIV Activity of Phosphorus-Containing Dendrimers Bearing Galβ1cer Analogues. *ChemBioChem* **2005**, *6*, 2207–2213. https://doi.org/10.1002/cbic.200500203.

(216) Moreno, S.; Sepúlveda-Crespo, D.; de la Mata, F. J.; Gómez, R.; Muñoz-Fernández, M. Á. New Anionic Carbosilane Dendrons Functionalized with a DO3A Ligand at the Focal Point for the Prevention of HIV-1 Infection. *Antivir Res* **2017**, *146*, 54–64. https://doi.org/10.1016/j.antiviral.2017.08.009.

(217) Guerrero-Beltrán, C.; Ceña-Diez, R.; Sepúlveda-Crespo, D.; De La Mata, J.; Gómez, R.; Leal, M.; Muñoz-Fernández, M. A.; Jiménez, J. L. Carbosilane Dendrons with Fatty Acids at the Core as a New Potential Microbicide against HSV-2/HIV-1 Co-Infection. *Nanoscale* **2017**, *9* (44), 17263–17273. https://doi.org/10.1039/c7nr05859d.

(218) García-Gallego, S.; Díaz, L.; Jiménez, J. L.; Gómez, R.; de la Mata, F. J.; Muñoz-Fernández, M. Á. HIV-1 Antiviral Behavior of Anionic PPI Metallo-Dendrimers with EDA Core. *Eur J Med Chem* **2015**, *98*, 139–148. https://doi.org/10.1016/j.ejmech.2015.05.026.

(219) Rivero-Buceta, E.; Doyagüez, E. G.; Colomer, I.; Quesada, E.; Mathys, L.; Noppen, S.; Liekens, S.; Camarasa, M. J.; Pérez-Pérez, M. J.; Balzarini, J.; et al. Tryptophan Dendrimers That Inhibit HIV Replication, Prevent Virus Entry and Bind to the HIV Envelope Glycoproteins Gp120 and Gp41. *Eur J Med Chem* **2015**, *106*, 34–43. https://doi.org/10.1016/j.ejmech.2015.10.031.

(220) World Health Organisation (WHO). Cancer https://www.who.int/news-room/fact-sheets/detail/cancer (accessed Oct 25, 2019).

(221) Commission, E. ECIS - European Cancer Information System https://ecis.jrc.ec.europa.eu/index.php (accessed Oct 28, 2019).

(222) Miller, K. D.; Nogueira, L.; Mariotto, A. B.; Rowland, J. H.; Yabroff, K. R.; Alfano, C. M.; Jemal, A.; Kramer, J. L.; Siegel, R. L. Cancer Treatment and Survivorship Statistics, 2019. *CA Cancer J Clin* **2019**, *0*, 1–23. https://doi.org/10.3322/caac.21565.

(223) Siegel, R. L.; Miller, K. D.; Jemal, A. Cancer Statistics, 2020. *CA Cancer J Clin* **2020**, *70*, 7–30. https://doi.org/10.3322/caac.21590.

(224) (NIH), N. C. R. What is cancer? https://www.cancer.gov/about-cancer/understanding/what-is-cancer (accessed Oct 25, 2019).

(225) Vasan, N.; Baselga, J.; Hyman, D. M. A View on Drug Resistance in Cancer. *Nature* **2019**, *575*, 299–309. https://doi.org/10.1038/s41586-019-1730-1.

(226) Caracciolo, G.; Vali, H.; Moore, A.; Mahmoudi, M. Challenges in Molecular Diagnostic Research in Cancer Nanotechnology. *Nano Today* **2019**, *27*, 6–10. https://doi.org/10.1016/j.nantod.2019.06.001.

(227) Bidram, E.; Esmaeili, Y.; Ranji-burachaloo, H.; Al-zaubai, N.; Zarrabi, A.; Stewart, A.; Dunstan, D. E. Journal of Drug Delivery Science and Technology A Concise Review on Cancer Treatment Methods and Delivery Systems. *J Drug Deliv Sci Technol* **2019**, No. October, 101350. https://doi.org/10.1016/j.jddst.2019.101350.

(228) Kim, H.; Kwak, G.; Kim, K.; Yoon, H. Y.; Kwon, I. C. Theranostic Designs of Biomaterials for Precision Medicine in Cancer Therapy. *Biomaterials* **2019**, *213*, 119207–119223. https://doi.org/10.1016/j.biomaterials.2019.05.018.

(229) Alessio, E. Thirty Years of the Drug Candidate NAMI-A and the Myths in the Field of Ruthenium Anticancer Compounds: A Personal Perspective. *Eur J Inorg Chem* **2017**, *2017*, 1549–1560. https://doi.org/10.1002/ejic.201600986.

(230) Bhattarai, P.; Hameed, S.; Dai, Z. Recent Advances in Anti-Angiogenic Nanomedicines for Cancer Therapy. *Nanoscale* **2018**, *10*, 5393–5423. https://doi.org/10.1039/c7nr09612g.

(231) Mukherjee, S. Recent Progress toward Antiangiogenesis Application of Nanomedicine in Cancer Therapy. *Futur Sci OA* **2018**, *4*, 9–12. https://doi.org/10.4155/fsoa-2018-0051.

(232) Chen, Q.; Chen, M.; Liu, Z. Local Biomaterials-Assisted Cancer Immunotherapy to Trigger Systemic Antitumor Responses. *Chem Soc Rev* **2019**. https://doi.org/10.1039/c9cs00271e.

(233) Nam, J.; Son, S.; Park, K. S.; Zou, W.; Shea, L. D.; Moon, J. J. Cancer Nanomedicine for Combination Cancer Immunotherapy. *Nat Rev Mater* **2019**, *4*, 398–414. https://doi.org/10.1038/s41578-019-0108-1.

(234) Boca, S.; Gulei, D.; Andreea, A.; Anca, Z.; Lorand, O.; Adrian, M.; Tigu, B. Nanoscale Delivery Systems for MicroRNAs in Cancer Therapy. *Cell Mol Life Sci* **2019**. https://doi.org/10.1007/s00018-019-03317-9.

(235) Duan, X.; He, C.; Kron, S. J.; Lin, W. Nanoparticle Formulations of Cisplatin for Cancer Therapy. *Wiley Interdiscip Rev Nanomedicine Nanobiotechnology* **2016**, *8*, 776–791. https://doi.org/10.1002/wnan.1390.

(236) Cheng, Y.; Zhao, L.; Li, Y.; Xu, T. Design of Biocompatible Dendrimers for Cancer Diagnosis and Therapy: Current Status and Future Perspectives. *Chem Soc Rev* **2011**, *40*, 2673–2703. https://doi.org/10.1039/c0cs00097c.

(237) Barry, N. P. E.; Sadler, P. J. 100 Years of Metal Coordination Chemistry: From Alfred Werner to Anticancer Metallodrugs. *Pure Appl Chem* **2014**, *86*, 1897–1910. https://doi.org/10.1515/pac-2014-0504.

(238) Lawrance, G. A. Chapter 3. Complexes. In *Introduction to Coordination Chemistry*; John Wiley & Sons, Ltd, 2010; pp 41–82. https://doi.org/10.1002/9780470687123.

(239) Yoshinari, N.; Konno, T. Chapter 8. Coordination Molecular Technology. In *Molecular Technology: Synthesis Innovation*; Yamamoto, H., Kato, T., Eds.; Wiley-VCH Verlag GmbH & Co. KGaA, 2019; Vol. 4, pp 199–229. https://doi.org/10.1002/9783527823987.vol4_c8.

(240) Trudu, F.; Amato, F.; Vaňhara, P.; Pivetta, T.; Peña-Méndez, E. M.; Havel, J. Coordination Compounds in Cancer: Past, Present and Perspectives. *J Appl Biomed* **2015**, *13*, 79–103. https://doi.org/10.1016/j.jab.2015.03.003.

(241) Caminade, A.-M.; Ouali, A.; Laurent, R.; Turrin, C. O.; Majoral, J.-P. Coordination Chemistry with Phosphorus Dendrimers. Applications as Catalysts, for Materials, and in Biology. *Coordin Chem Rev* **2016**, *308*, 478–497. https://doi.org/10.1016/j.ccr.2015.06.007.

(242) Thota, S.; Rodrigues, D. A.; Crans, D. C.; Barreiro, E. J. Ru(II) Compounds: Next-Generation Anticancer Metallotherapeutics? *J Med Chem* **2018**, *61*, 5805–5821. https://doi.org/10.1021/acs.jmedchem.7b01689.

(243) McQuitty, R. J. Metal-Based Drugs. *Sci Prog* **2014**, *97*, 1–19. https://doi.org/10.3184/003685014x13898980185076.

(244) Peyrone, M. Ueber Die Einwirkung Des Ammoniaks Auf Platinchlorür [On the Action of Ammonia on Platinum Chloride]. *Ann der Chemie und Pharm* **1877**, *51*, 1–29. https://doi.org/10.1002/jlac.18440510102.

(245) Rosenberg, B.; VanCamp, L.; Krigas, T. Inhibition of Cell Division in Escherichia Coli by Electrolysis Products from a Platinum Electrode. *Nature* **1965**, *205*, 698–699. https://doi.org/10.1038/205698a0.

(246) Rosenberg, B.; VanCamp, L.; Trosko, J. E.; Mansour, V. H. Platinum Compounds: A New Class of Potent Antitumour Agents. *Nature* **1969**, *222*, 385–386. https://doi.org/10.1038/222385a0.

(247) Dasari, S.; Bernard Tchounwou, P. Cisplatin in Cancer Therapy: Molecular Mechanisms of Action. *Eur J Pharmacol* **2014**, *740*, 364–378. https://doi.org/10.1016/j.ejphar.2014.07.025.

(248) Ghosh, S. Cisplatin: The First Metal Based Anticancer Drug. *Bioorg Chem* **2019**, *88*, 102925. https://doi.org/10.1016/j.bioorg.2019.102925.

(249) Fennell, D. A.; Summers, Y.; Cadranel, J.; Benepal, T.; Christoph, D. C.; Lal, R.; Das, M.; Maxwell, F.; Visseren-Grul, C.; Ferry, D. Cisplatin in the Modern Era: The Backbone of First-Line Chemotherapy for Non-Small Cell Lung Cancer. *Cancer Treat Rev* **2016**, *44*, 42–50. https://doi.org/10.1016/j.ctrv.2016.01.003.

(250) FDA Oncology Tools. Food and Drug Administration. Approval Summary for cisplatin for Metastatic ovarian tumors https://web.archive.org/web/20080208232952/http:/www.accessdata.fda.gov/scripts/cder/onctools/summary.cfm?ID=73 (accessed Mar 10, 2020).

(251) Amable, L. Cisplatin Resistance and Opportunities for Precision Medicine. *Pharmacol Res* **2016**, *106*, 27–36. https://doi.org/10.1016/j.phrs.2016.01.001.

(252) Armstrong-Gordon, E.; Gnjidic, D.; McLachlan, A. J.; Hosseini, B.; Grant, A.; Beale, P. J.; Wheate, N. J. Patterns of Platinum Drug Use in an Acute Care Setting: A Retrospective Study. *J Cancer*

Res Clin Oncol **2018**, *144*, 1561–1568. https://doi.org/10.1007/s00432-018-2669-6.

(253) Martinho, N.; Santos, T. C. B.; Florindo, H. F.; Silva, L. C. Cisplatin-Membrane Interactions and Their Influence on Platinum Complexes Activity and Toxicity. *Front Physiol* **2019**, *9*, 1–15. https://doi.org/10.3389/fphys.2018.01898.

(254) Palermo, G.; Magistrato, A.; Riedel, T.; von Erlach, T.; Davey, C. A.; Dyson, P. J.; Rothlisberger, U. Fighting Cancer with Transition Metal Complexes: From Naked DNA to Protein and Chromatin Targeting Strategies. *ChemMedChem* **2016**, *11*, 1199–1210. https://doi.org/10.1002/cmdc.201500478.

(255) Deo, K. M.; Ang, D. L.; McGhie, B.; Rajamanickam, A.; Dhiman, A.; Khoury, A.; Holland, J.; Bjelosevic, A.; Pages, B.; Gordon, C.; et al. Platinum Coordination Compounds with Potent Anticancer Activity. *Coordin Chem Rev* **2018**, *375*, 148–163. https://doi.org/10.1016/j.ccr.2017.11.014.

(256) Karasawa, T.; Steyger, P. S. An Integrated View of Cisplatin-Induced Nephrotoxicity and Ototoxicity. *Toxicol Lett* **2015**, *237*, 219–227. https://doi.org/10.1016/j.toxlet.2015.06.012.

(257) Wheate, N. J.; Walker, S.; Craig, G. E.; Oun, R. The Status of Platinum Anticancer Drugs in the Clinic and in Clinical Trials. *Dalton Trans* **2010**, *39*, 8113–8127. https://doi.org/10.1039/c0dt00292e.

(258) Florea, A. M.; Büsselberg, D. Cisplatin as an Anti-Tumor Drug: Cellular Mechanisms of Activity, Drug Resistance and Induced Side Effects. *Cancers (Basel)* **2011**, *3*, 1351–1371. https://doi.org/10.3390/cancers3011351.

(259) Coverdale, J.; Laroiya-McCarron, T.; Romero-Canelón, I. Designing Ruthenium Anticancer Drugs: What Have We Learnt from the Key Drug Candidates? *Inorganics* **2019**, *7*, 31–45. https://doi.org/10.3390/inorganics7030031.

(260) Kartalou, M.; Essigmann, J. M. Mechanisms of Resistance to Cisplatin. *Mutat Res* **2001**, *478*, 23–43. https://doi.org/10.1016/S0027-5107(01)00141-5.

(261) Dilruba, S.; Kalayda, G. V. Platinum-Based Drugs: Past, Present and Future. *Cancer Chemother Pharmacol* **2016**, *77*, 1103–1124. https://doi.org/10.1007/s00280-016-2976-z.

(262) Kalayda, G. V.; Wagner, C. H.; Jaehde, U. Relevance of Copper Transporter 1 for Cisplatin Resistance in Human Ovarian Carcinoma Cells. *J Inorg Biochem* **2012**, *116*, 1–10. https://doi.org/10.1016/j.jinorgbio.2012.07.010.

(263) Galluzzi, L.; Senovilla, L.; Vitale, I.; Michels, J.; Martins, I.; Kepp, O.; Castedo, M.; Kroemer, G. Molecular Mechanisms of Cisplatin Resistance. *Oncogene* **2012**, *31*, 1869–1883. https://doi.org/10.1038/onc.2011.384.

(264) Alderden, R. A.; Hall, M. D.; Hambley, T. W. The Discovery and Development of Cisplatin. *J Chem Educ* **2006**, *83*, 728–734. https://doi.org/10.1021/ed083p728.

(265) Brabec, V.; Hrabina, O.; Kasparkova, J. Cytotoxic Platinum Coordination Compounds. DNA Binding Agents. *Coordin Chem Rev* **2017**, *351*, 2–31. https://doi.org/10.1016/j.ccr.2017.04.013.

(266) Roner, M. R.; Carraher Jr., C. E. Cisplatin Derivatives as Antiviral Agents. In *Inorganic and*

Organometallic Macromolecules: Design and Applications; Abd-El-Aziz, A. S., Carraher Jr., C. E., Pittman Jr, C. U., Zeldin, M., Eds.; Springer, 2008; pp 193–223.

(267) Davies, M. S.; Berners-Price, S. J.; Hambley, T. W. Slowing of Cisplatin Aquation in the Presence of DNA but Not in the Presence of Phosphate: Improved Understanding of Sequence Selectivity and the Roles of Monoaquated and Diaquated Species in the Binding of Cisplatin to DNA. *Inorg Chem* **2000**, *39*, 5603–5613. https://doi.org/10.1021/ic000847w.

(268) Ivanov, A. I.; Christodoulou, J.; Parkinson, J. A.; Barnham, K. J.; Tucker, A.; Woodrow, J.; Sadler, P. J. Cisplatin Binding Sites on Human Albumin. *J Biol Chem* **1998**, *273*, 14721–14730. https://doi.org/10.1074/jbc.273.24.14721.

(269) Chu, G. Cellular Responses to Cisplatin. The Roles of DNA-Binding Proteins and DNA Repair. *J Biol Chem* **1994**, *269*, 787–790.

(270) Gullo, J. J.; Litterst, C. L.; Maguire, P. J.; Sikic, B. I.; Hoth, D. F.; Woolley, P. V. Pharmacokinetics and Protein Binding of Cis-Dichlorodiammine Platinum (II) Administered as a One Hour or as a Twenty Hour Infusion. *Cancer Chemother Pharmacol* **1980**, *5*, 21–26. https://doi.org/10.1007/BF00578558.

(271) Lazarević, T.; Rilak, A.; Bugarčić, Ž. D. Platinum, Palladium, Gold and Ruthenium Complexes as Anticancer Agents: Current Clinical Uses, Cytotoxicity Studies and Future Perspectives. *Eur J Med Chem* **2017**, *142*, 8–31. https://doi.org/10.1016/j.ejmech.2017.04.007.

(272) Southam, H. M.; Butler, J. A.; Chapman, J. A.; Poole, R. K. The Microbiology of Ruthenium Complexes. *Adv Microb Physiol* **2017**, *71*, 1–96. https://doi.org/10.1016/bs.ampbs.2017.03.001.

(273) Lin, K.; Zhao, Z.-Z.; Bo, H.-B.; Hao, X.-J.; Wang, J.-Q. Applications of Ruthenium Complex in Tumor Diagnosis and Therapy. *Front Pharmacol* **2018**, *9*, 1–10. https://doi.org/10.3389/fphar.2018.01323.

(274) Pal, M.; Nandi, U.; Mukherjee, D. Detailed Account on Activation Mechanisms of Ruthenium Coordination Complexes and Their Role as Antineoplastic Agents. *Eur J Med Chem* **2018**, *150*, 419–445. https://doi.org/10.1016/j.ejmech.2018.03.015.

(275) Moreno, V.; Font-Bardia, M.; Calvet, T.; Lorenzo, J.; Avilés, F. X.; Garcia, M. H.; Morais, T. S.; Valente, A.; Robalo, M. P. DNA Interaction and Cytotoxicity Studies of New Ruthenium(II) Cyclopentadienyl Derivative Complexes Containing Heteroaromatic Ligands. *J Inorg Biochem* **2011**, *105*, 241–249. https://doi.org/10.1016/j.jinorgbio.2010.10.009.

(276) Valente, A.; Garcia, M. H.; Marques, F.; Miao, Y.; Rousseau, C.; Zinck, P. First Polymer "Ruthenium-Cyclopentadienyl" Complex as Potential Anticancer Agent. *J Inorg Biochem* **2013**, *127*, 79–81. https://doi.org/10.1016/j.jinorgbio.2013.07.002.

(277) Arce, E. R.; Sarniguet, C.; Moraes, T. S.; Vieites, M.; Tomaz, A. I.; Medeiros, A.; Comini, M. A.; Varela, J.; Cerecetto, H.; González, M.; et al. A New Ruthenium Cyclopentadienyl Azole Compound with Activity on Tumor Cell Lines and Trypanosomatid Parasites. *J Coord Chem* **2015**, *68*, 2923–2937. https://doi.org/10.1080/00958972.2015.1062480.

(278) Florindo, P. R.; Pereira, D. M.; Borralho, P. M.; Rodrigues, C. M. P.; Piedade, M. F. M.; Fernandes,

A. C. Cyclopentadienyl-Ruthenium(II) and Iron(II) Organometallic Compounds with Carbohydrate Derivative Ligands as Good Colorectal Anticancer Agents. *J Med Chem* **2015**, *58*, 4339–4347. https://doi.org/10.1021/acs.jmedchem.5b00403.

(279) Malumbres, M.; Barbacid, M. Cell Cycle, CDKs and Cancer: A Changing Paradigm. *Nat Rev Cancer* **2009**, *9*, 153–166. https://doi.org/10.1038/nrc2602.

(280) Otto, T.; Sicinski, P. Cell Cycle Proteins as Promising Targets in Cancer Therapy. *Nat Rev Cancer* **2017**, *17*, 93–115. https://doi.org/10.1038/nrc.2016.138.

(281) Sherr, C. J.; Bartek, J. Cell Cycle–Targeted Cancer Therapies. *Annu Rev Cancer Biol* **2017**, *1*, 41–57. https://doi.org/10.1146/annurev-cancerbio-040716-075628.

(282) Williams, G. H.; Stoeber, K. The Cell Cycle and Cancer. *J Pathol* **2012**, *226*, 352–364. https://doi.org/10.1002/path.3022.

(283) Lai, S.-H.; Li, W.; Wang, X.-Z.; Zhang, C.; Zeng, C.-C.; Tang, B.; Wan, D.; Liu, Y.-J. Apoptosis, Autophagy, Cell Cycle Arrest, Cell Invasion and BSA-Binding Studies: In Vitro of Ruthenium(II) Polypyridyl Complexes. *RSC Adv* **2016**, *6*, 63143–63155. https://doi.org/10.1039/c6ra11391e.

(284) Li, M.; Lai, L.; Zhao, Z.; Chen, T. Aquation Is a Crucial Activation Step for Anticancer Action of Ruthenium(II) Polypyridyl Complexes to Trigger Cancer Cell Apoptosis. *Chem - An Asian J* **2016**, *11*, 310–320. https://doi.org/10.1002/asia.201501048.

(285) Qasim Warraich, M.; Ghion, A.; Perdisatt, L.; O'Neill, L.; Casey, A.; O'Connor, C. In Vitro Cytotoxicity, Cellular Uptake, Reactive Oxygen Species and Cell Cycle Arrest Studies of Novel Ruthenium(II) Polypyridyl Complexes towards A549 Lung Cancer Cell Line. *Drug Chem Toxicol* **2019**, *0*, 1–11. https://doi.org/10.1080/01480545.2019.1589492.

(286) Brabec, V.; Kasparkova, J. Ruthenium Coordination Compounds of Biological and Biomedical Significance. DNA Binding Agents. *Coordin Chem Rev* **2018**, *376*, 75–94. https://doi.org/10.1016/j.ccr.2018.07.012.

(287) Romerosa, A.; Campos-Malpartida, T.; Lidrissi, C.; Saoud, M.; Serrano-Ruiz, M.; Peruzzini, M.; Garrido-Cárdenas, J. A.; García-Maroto, F. Synthesis, Characterization, and DNA Binding of New Water-Soluble Cyclopentadienyl Ruthenium(II) Complexes Incorporating Phosphines. *Inorg Chem* **2006**, *45*, 1289–1298.

(288) Clarke, M. J.; Zhu, F.; Frasca, D. R. Non-Platinum Chemotherapeutic Metallopharmaceuticals. *Chem Rev* **1999**, *99*, 2511–2533. https://doi.org/10.1021/cr9804238.

(289) Florindo, P. R.; Pereira, D. M.; Borralho, P. M.; Costa, P. J.; Piedade, M. F. M.; Rodrigues, C. M. P.; Fernandes, A. C. New $[(\eta^5\text{-}C_5H_5)Ru(N–N)(PPh_3)][PF_6]$ Compounds: Colon Anticancer Activity and GLUT-Mediated Cellular Uptake of Carbohydrate-Appended Complexes. *Dalton Trans* **2016**, *45*, 11926–11930. https://doi.org/10.1039/c6dt01571a.

(290) Licona, C.; Spaety, M.-E.; Capuozzo, A.; Ali, M.; Santamaria, R.; Armant, O.; Delalande, F.; Van Dorsselaer, A.; Cianferani, S.; Spencer, J.; et al. A Ruthenium Anticancer Compound Interacts with Histones and Impacts Differently on Epigenetic and Death Pathways Compared to Cisplatin. *Oncotarget* **2017**, *8*, 2568–2584. https://doi.org/10.18632/oncotarget.13711.

(291) Oliveira, K. M.; Liany, L. D.; Corrêa, R. S.; Deflon, V. M.; Cominetti, M. R.; Batista, A. A. Selective Ru(II)/Lawsone Complexes Inhibiting Tumor Cell Growth by Apoptosis. *J Inorg Biochem* **2017**, *176*, 66–76. https://doi.org/10.1016/j.jinorgbio.2017.08.019.

(292) Pettinari, R.; Marchetti, F.; Petrini, A.; Pettinari, C.; Lupidi, G.; Fernández, B.; Diéguez, A. R.; Santoni, G.; Nabissi, M. Ruthenium(II)-Arene Complexes with Dibenzoylmethane Induce Apoptotic Cell Death in Multiple Myeloma Cell Lines. *Inorg Chim Acta* **2017**, *454*, 139–148. https://doi.org/10.1016/j.ica.2016.04.031.

(293) Lenis-Rojas, O. A.; Robalo, M. P.; Tomaz, A. I.; Carvalho, A.; Fernandes, A. R.; Marques, F.; Folgueira, M.; Yánez, J.; Vázquez-García, D.; López Torres, M.; et al. Ru II (*p*-Cymene) Compounds as Effective and Selective Anticancer Candidates with No Toxicity in Vivo. *Inorg Chem* **2018**, *57*, 13150–13166. https://doi.org/10.1021/acs.inorgchem.8b01270.

(294) Ramírez-Rivera, S.; Pizarro, S.; Gallardo, M.; Gajardo, F.; Delgadillo, A.; De La Fuente-Ortega, E.; MacDonnell, F. M.; Bernal, G. Anticancer Activity of Two Novel Ruthenium Compounds in Gastric Cancer Cells. *Life Sci* **2018**, *213*, 57–65. https://doi.org/10.1016/j.lfs.2018.10.024.

(295) Alessio, E.; Messori, L. NAMI-A and KP1019/1339, Two Iconic Ruthenium Anticancer Drug Candidates Face-to-Face: A Case Story in Medicinal Inorganic Chemistry. *Molecules* **2019**, *24*, 1995–2015. https://doi.org/10.3390/molecules24101995.

(296) Sava, G.; Pacor, S.; Bergamo, A.; Cocchietto, M.; Mestroni, G.; Alessio, E. Effects of Ruthenium Complexes on Experimental Tumors: Irrelevance of Cytotoxicity for Metastasis Inhibition. *Chem Biol Interact* **1995**, *95*, 109–126. https://doi.org/10.1016/0009-2797(94)03350-1.

(297) Pluim, D.; Van Waardenburg, R. C. A. M.; Beijnen, J. H.; Schellens, J. H. M. Cytotoxicity of the Organic Ruthenium Anticancer Drug Nami-A Is Correlated with DNA Binding in Four Different Human Tumor Cell Lines. *Cancer Chemother Pharmacol* **2004**, *54*, 71–78. https://doi.org/10.1007/s00280-004-0773-6.

(298) Pillozzi, S.; Gasparoli, L.; Stefanini, M.; Ristori, M.; D'Amico, M.; Alessio, E.; Scaletti, F.; Becchetti, A.; Arcangeli, A.; Messori, L. NAMI-A Is Highly Cytotoxic toward Leukaemia Cell Lines: Evidence of Inhibition of KCa 3.1 Channels. *Dalton Trans* **2014**, *43*, 12150–12155. https://doi.org/10.1039/c4dt01356e.

(299) Sava, G.; Capozzi, I.; Clerici, K.; Gagliardi, G.; Alessio, E.; Mestroni, G. Pharmacological Control of Lung Metastases of Solid Tumours by a Novel Ruthenium Complex. *Clin Exp Metastasis* **1998**, *16*, 371–379. https://doi.org/10.1023/A:1006521715400.

(300) Gava, B.; Zorzet, S.; Spessotto, P.; Cocchietto, M.; Sava, G. Inhibition of B16 Melanoma Metastases with the Ruthenium Complex Imidazolium. *J Pharmacol Exp Ther* **2006**, *317*, 284–291. https://doi.org/10.1124/jpet.105.095141.

(301) Coluccia, M.; Sava, G.; Salerno, G.; Bergamo, A.; Pacor, S.; Mestroni, G.; Alessio, E. Efficacy of 5-FU Combined to Na[Trans-$RuCl_4$(DMSO)Lm], a Novel Selective Antimetastic Agent, on the Survival Time of Mice with P388 Leukemia, P388/DDP Subline and MCa Mammary Carcinoma. *Met Based Drugs* **1995**, *2*, 195–199. https://doi.org/10.1155/MBD.1995.195.

(302) Leijen, S.; Burgers, S. A.; Baas, P.; Pluim, D.; Tibben, M.; Van Werkhoven, E.; Alessio, E.; Sava, G.; Beijnen, J. H.; Schellens, J. H. M. Phase I/II Study with Ruthenium Compound NAMI-A and Gemcitabine in Patients with Non-Small Cell Lung Cancer after First Line Therapy. *Invest New Drugs* **2015**, *33* (1), 201–214. https://doi.org/10.1007/s10637-014-0179-1.

(303) Rademaker-Lakhai, J. M.; Van Den Bongard, D.; Pluim, D.; Beijnen, J. H.; Schellens, J. H. M. A Phase I and Pharmacological Study with Imidazolium-*trans*-DMSO-imidazole-tetrachlororuthenate, a Novel Ruthenium Anticancer Agent. *Clin Cancer Res* **2004**, *10*, 3717–3727. https://doi.org/10.1158/1078-0432.CCR-03-0746.

(304) Adams, M.; Hanif, M.; Hartinger, C. G. Ruthenium Anticancer Agents — From Cisplatin Analogues to Rational Drug Design. In *Encyclopedia of Inorganic and Bioinorganic Chemistry*; John Wiley & Sons, Ltd, 2017; pp 1–21. https://doi.org/10.1002/9781119951438.eibc2500.

(305) Heffeter, P.; Pongratz, M.; Steiner, E.; Chiba, P.; Jakupec, M. A.; Elbling, L.; Marian, B.; Körner, W.; Sevelda, F.; Micksche, M.; et al. Intrinsic and Acquired Forms of Resistance against the Anticancer Ruthenium Compound KP1019 [Indazolium *trans*-[tetrachlorobis(1*H*-indazole)ruthenate (III)] (FFC14A). *J Pharmacol Exp Ther* **2005**, *312*, 281–289. https://doi.org/10.1124/jpet.104.073395.

(306) Clinicaltrials.gov. Dose Escalation Study of NKP-1339 to Treat Advanced Solid Tumors https://clinicaltrials.gov/ct2/show/NCT01415297?term=NKP-1339&rank=1 (accessed Nov 15, 2019).

(307) Burris, H. A.; Bakewell, S.; Bendell, J. C.; Infante, J.; Jones, S. F.; Spigel, D. R.; Weiss, G. J.; Ramanathan, R. K.; Ogden, A.; Von Hoff, D. Safety and Activity of IT-139, a Ruthenium-Based Compound, in Patients with Advanced Solid Tumours: A First-in-Human, Open-Label, Dose-Escalation Phase i Study with Expansion Cohort. *ESMO Open* **2016**, *1*, e000154–e000161. https://doi.org/10.1136/esmoopen-2016-000154.

(308) Morris, R. E.; Aird, R. E.; Del Socorro Murdoch, P.; Chen, H.; Cummings, J.; Hughes, N. D.; Parsons, S.; Parkin, A.; Boyd, G.; Jodrell, D. I.; et al. Inhibition of Cancer Cell Growth by Ruthenium(II) Arene Complexes. *J Med Chem* **2001**, *44*, 3616–3621. https://doi.org/10.1021/jm010051m.

(309) Bergamo, A.; Masi, A.; Peacock, A. F. A.; Habtemariam, A.; Sadler, P. J.; Sava, G. In Vivo Tumour and Metastasis Reduction and in Vitro Effects on Invasion Assays of the Ruthenium RM175 and Osmium AFAP51 Organometallics in the Mammary Cancer Model. *J Inorg Biochem* **2010**, *104*, 79–86. https://doi.org/10.1016/j.jinorgbio.2009.10.005.

(310) Guichard, S. M.; Else, R.; Reid, E.; Zeitlin, B.; Aird, R.; Muir, M.; Dodds, M.; Fiebig, H.; Sadler, P. J.; Jodrell, D. I. Anti-Tumour Activity in Non-Small Cell Lung Cancer Models and Toxicity Profiles for Novel Ruthenium(II) Based Organo-Metallic Compounds. *Biochem Pharmacol* **2006**, *71*, 408–415. https://doi.org/10.1016/j.bcp.2005.10.053.

(311) Aird, R. E.; Cummings, J.; Ritchie, A. A.; Muir, M.; Morris, R. E.; Chen, H.; Sadler, P. J.; Jodrell, D. I. In Vitro and in Vivo Activity and Cross Resistance Profiles of Novel Ruthenium (II)

Organometallic Arene Complexes in Human Ovarian Cancer. *Br J Cancer* **2002**, *86*, 1652–1657. https://doi.org/10.1038/sj.bjc.6600290.

(312) Scolaro, C.; Bergamo, A.; Brescacin, L.; Delfino, R.; Cocchietto, M.; Laurenczy, G.; Geldbach, T. J.; Sava, G.; Dyson, P. J. In Vitro and in Vivo Evaluation of Ruthenium(II)-Arene PTA Complexes. *J Med Chem* **2005**, *48*, 4161–4171. https://doi.org/10.1021/jm050015d.

(313) Weiss, A.; Berndsen, R. H.; Dubois, M.; Müller, C.; Schibli, R.; Griffioen, A. W.; Dyson, P. J.; Nowak-Sliwinska, P. In Vivo Anti-Tumor Activity of the Organometallic Ruthenium(II)-Arene Complex [Ru(η^6-*p*-Cymene)Cl_2(Pta)] (RAPTA-C) in Human Ovarian and Colorectal Carcinomas. *Chem Sci* **2014**, *5*, 4742–4748. https://doi.org/10.1039/c4sc01255k.

(314) Gouveia, M.; Figueira, J.; Jardim, M. G.; Castro, R.; Tomás, H.; Rissanen, K.; Rodrigues, J. Poly(Alkylidenimine) Dendrimers Functionalized with the Organometallic Moiety [Ru(η^5-C_5H_5)$(PPh_3)_2$]$^+$ as Promising Drugs against Cisplatin-Resistant Cancer Cells and Human Mesenchymal Stem Cells. *Molecules* **2018**, *23*, 1471–1488. https://doi.org/10.3390/molecules23061471.

(315) Govender, P.; Riedel, T.; Dyson, P. J.; Smith, G. S. Higher Generation Cationic N,N-Ruthenium(II)-Ethylene-Glycol-Derived Metallodendrimers: Synthesis, Characterization and Cytotoxicity. *J Organomet Chem* **2015**, *799–800*, 38–44. https://doi.org/10.1016/j.jorganchem.2015.09.003.

(316) Maroto-Díaz, M.; Elie, B. T.; Gómez-Sal, P.; Pérez-Serrano, J.; Gómez, R.; Contel, M.; de la Mata, F. J. Synthesis and Anticancer Activity of Carbosilane Metallodendrimers Based on Arene Ruthenium(II) Complexes. *Dalton Trans* **2016**, *45*, 7049–7066. https://doi.org/10.1039/C6DT00465B.

(317) Michlewska, S.; Ionov, M.; Shcharbin, D.; Maroto-Díaz, M.; Ramirez, R. G.; de la Mata, F. J.; Bryszewska, M. Ruthenium Metallodendrimers with Anticancer Potential in an Acute Promyelocytic Leukemia Cell Line (HL60). *Eur Polym J* **2017**, *87*, 39–47. https://doi.org/10.1016/j.eurpolymj.2016.12.011.

(318) Michlewska, S.; Ionov, M.; Maroto-Díaz, M.; Szwed, A.; Ihnatsyeu-Kachan, A.; Loznikova, S.; Shcharbin, D.; Maly, M.; Ramirez, R. G.; de la Mata, F. J.; et al. Ruthenium Dendrimers as Carriers for Anticancer SiRNA. *J Inorg Biochem* **2018**, *181*, 18–27. https://doi.org/10.1016/j.jinorgbio.2018.01.001.

(319) del Olmo, N. S.; Bajo, A.; Ionov, M.; Garcia-Gallego, S.; Bryszewskz, M.; Gómez, R.; Ortega, P.; de la Mata, F. J. Cyclopentadienyl Ruthenium(II) Carbosilane Metallodendrimers as a Promising Treatment against Advanced Prostate Cancer. *Eur J Med Chem* **2020**, *199*, 112414. https://doi.org/10.1016/j.ejmech.2020.112414.

(320) Pêgo, A. P.; Leiro, V.; Megia, E. F.; Vega, R. R. Biodegradable Dendritic Structure, Methods and Uses Thereof. WO 2017/203437 Al, 2017.

(321) Poupot, M.; Poupot, R.; Fournie, J.-J.; Portevin, D.; Fruchon, S.; Davignon, J.-L.; Turrin, C.-O.; Caminade, A.-M.; Majoral, J.-P.; Rolland, O. Phosphorylated Dendrimers as Antiinflammatory Drugs. US 10,106,565 B2, 2018.

(322) Majoral, J.; Meunier, B.; Caminade, A.; Loup, C.; Zanta-Boussif, M.-A. Phosphorus-Containing Dendrimers as Transfection Agents. WO 01/38335 A1, 2001.

(323) Trevisiol, E.; Leclaire, J.; Pratviel, G.; Caminade, A.; Francois, J.; Majoral, J.; Meunier, B. Solid Supports Functionalised with Phosphorus Dendrimers, Method for Preparing Same and Uses Thereof. US 7,517,538 B2, 2009.

(324) Majoral, J.; Caminade, A.; Jacqueline, J.; Fournie, J.-J.; Griffe, L.; Poupot-Marsan, M.; Poupot, R.; Turrin, C.-O. Use of Dendrimers to Stimulate Cell Growth. US 8,815,834 B2, 2014.

(325) Spataro, G.; Malecaze, F.; Turrin, C. O.; Soler, V.; Duhayon, C.; Elena, P. P.; Majoral, J. P.; Caminade, A. M. Designing Dendrimers for Ocular Drug Delivery. *Eur J Med Chem* **2010**, *45*, 326–334. https://doi.org/10.1016/j.ejmech.2009.10.017.

(326) Wolfram, J.; Ferrari, M. Clinical Cancer Nanomedicine. *Nano Today* **2019**, *25*, 85–98. https://doi.org/10.1016/j.nantod.2019.02.005.

(327) Starpharma. US FDA requests further data for VivaGel BV approval https://starpharma.com/news/story/us-fda-requests-further-data-for-vivagel-bv-approval (accessed May 10, 2020).

(328) Starpharma. Regulatory progress for VivaGel BV in the US https://starpharma.com/news/story/regulatory-progress-for-vivagel-bv-in-the-us (accessed May 10, 2020).

(329) Chauhan, A.; Patil, C.; Jain, P.; Kulhari, H. Dendrimer-Based Marketed Formulations and Miscellaneous Applications in Cosmetics, Veterinary, and Agriculture. In *Pharmaceutical Applications of Dendrimers*; Elsevier Inc., 2020; pp 325–334. https://doi.org/10.1016/b978-0-12-814527-2.00014-7.

(330) Bénéteau-Burnat, B.; Baudin, B.; Vaubourdolle, M. Evaluation of Stratus® CS Stat Fluorimetric Analyser for Measurement of Cardiac Markers Troponin I (CTnl), Creatine Kinase MB (CK-MB), and Myoglobin. *J Clin Lab Anal* **2001**, *15*, 314–318. https://doi.org/10.1002/jcla.1043.

(331) SiemensHealthineersGlobal. Stratus® CS 200 Acute Care™ Troponin Analyzer https://www.siemens-healthineers.com/cardiac/cardiac-systems/stratus-cs-acute-care (accessed Jan 14, 2020).

(332) Akhtar, S.; Chandrasekhar, B.; Attur, S.; Yousif, M. H. M.; Benter, I. F. On the Nanotoxicity of PAMAM Dendrimers: Superfect® Stimulates the EGFR-ERK1/2 Signal Transduction Pathway via an Oxidative Stress-Dependent Mechanism in HEK 293 Cells. *Int J Pharm* **2013**, *448*, 239–246. https://doi.org/10.1016/j.ijpharm.2013.03.039.

(333) Liu, H.; Wang, H.; Yang, W.; Cheng, Y. Disulfide Cross-Linked Low Generation Dendrimers with High Gene Transfection Efficacy, Low Cytotoxicity, and Low Cost. *J Am Chem Soc* **2012**, *134*, 17680–17687. https://doi.org/10.1021/ja307290j.

(334) Chiribiri, A.; Kelle, S.; Götze, S.; Kriatselis, C.; Thouet, T.; Tangcharoen, T.; Paetsch, I.; Schnackenburg, B.; Fleck, E.; Nagel, E. Visualization of the Cardiac Venous System Using Cardiac Magnetic Resonance. *Am J Cardiol* **2008**, *101*, 407–412.

https://doi.org/10.1016/j.amjcard.2007.08.049.

(335) invivoContrast. Gadomer 17 http://www.invivocontrast.com/gadomer_17 (accessed Jan 15, 2020).

(336) Spangler, B. D.; Spangler, C. W. Biosensors Utilizing Dendrimer-Immobilized Ligands and There Use Thereof. US Patent 7,138,121 B2, 2006.

(337) Spangler, C. W.; Spangler, B. D.; Tarter, E. S.; Suo, Z. Design and Synthesis of Dendritic Tethers for the Immobilization of Antibodies for the Detection of Class a Bioterror Pathogens. In *Antiterrorism and Homeland Defense*; Reynolds, J. G., Lawson, G. E., Koester, C. J., Eds.; ACS, 2007; Vol. 980, pp 159–174. https://doi.org/10.1021/bk-2007-0980.ch010.

(338) Clinicaltrials.gov. A Study to Evaluate the Safety, Tolerability, and Pharmacokinetics of OP-101 After Intravenous Administration in Healthy Volunteers https://clinicaltrials.gov/ct2/show/NCT03500627?term=dendrimer&draw=2&rank=1 (accessed Nov 5, 2019).

(339) Orpheris. Our lead product, OP-101, specifically targets reactive microglia and reactive astrocytes in the CNS, delivering a potent anti-inflammatory and anti-oxidant payload to the activated cells http://orpheris.com/pipeline/op101.php (accessed Nov 5, 2019).

(340) AdrenoleukodystrophyNews. OP-101 https://adrenoleukodystrophynews.com/op-101/ (accessed Nov 5, 2019).

(341) Starpharma. DEP™ docetaxel Summary and Commercial Opportunity https://starpharma.com/drug_delivery/dep_docetaxel (accessed Nov 5, 2019).

(342) Starpharma. DEP® cabazitaxel https://starpharma.com/drug_delivery/dep_cabazitaxel (accessed Nov 5, 2019).

(343) Starpharma. DEP® irinotecan https://starpharma.com/drug_delivery/dep_irinotecan (accessed Nov 5, 2019).

(344) Moura, L. I. F.; Malfanti, A.; Peres, C.; Matos, A. I.; Guegain, E.; Sainz, V.; Zloh, M.; Vicent, M. J.; Florindo, H. F. Functionalized Branched Polymers: Promising Immunomodulatory Tools for the Treatment of Cancer and Immune Disorders. *Mater Horizons* **2019**. https://doi.org/10.1039/c9mh00628a.

(345) Clinicaltrials.gov. Treatment of Non-responding to Conventional Therapy Inoperable Liver Cancers by in Situ Introduction of ImDendrim (ImDendrim) https://clinicaltrials.gov/ct2/show/NCT03255343?term=dendrimer&draw=2&rank=2 (accessed Jan 19, 2020).

(346) Yang, G.; Sadeg, N.; Belhadj-Tahar, H. New Potential In Situ Anticancer Agent Derived from [^{188}Re]Rhenium Nitro-Imidazole Ligand Loaded 5th Generation Poly-L-Lysine Dendrimer for Treatment of Transplanted Human Liver Carcinoma in Nude Mice. *Drug Des Open Access* **2017**, *6*, 144–150. https://doi.org/10.4172/2169-0138.1000144.

(347) Teeraananchai, S.; Kerr, S. J.; Amin, J.; Ruxrungtham, K.; Law, M. G. Life Expectancy of HIV-Positive People after Starting Combination Antiretroviral Therapy: A Meta-Analysis. *HIV Med*

2017, *18*, 256–266. https://doi.org/10.1111/hiv.12421.

(348) De Cock, K. M.; Jaffe, H. W.; Curran, J. W. The Evolving Epidemiology of HIV/AIDS. *AIDS* **2012**, *26*, 1205–1213. https://doi.org/10.1097/QAD.0b013e328354622a.

(349) Baeten, J. M.; Palanee-Phillips, T.; Brown, E. R.; Schwartz, K.; Soto-Torres, L. E.; Govender, V.; Mgodi, N. M.; Kiweewa, F. M.; Nair, G.; Mhlanga, F.; et al. Use of a Vaginal Ring Containing Dapivirine for HIV-1 Prevention in Women. *Obstet Gynecol Surv* **2016**, *71*, 466–468. https://doi.org/10.1056/NEJMoa1506110.

(350) Nel, A.; van Niekerk, N.; Kapiga, S.; Bekker, L.-G.; Gama, C.; Gill, K.; Kamali, A.; Kotze, P.; Louw, C.; Mabude, Z.; et al. Safety and Efficacy of a Dapivirine Vaginal Ring for HIV Prevention in Women. *N Engl J Med* **2016**, *375*, 2133–2143. https://doi.org/10.1056/NEJMoa1602046.

(351) Jiménez, J. L.; Pion, M.; de la Mata, F. J.; Gomez, R.; Muñoz, E.; Leal, M.; Muñoz-Fernández, M. Á. Dendrimers as Topical Microbicides with Activity against HIV. *New J Chem* **2012**, *36*, 299–309. https://doi.org/10.1039/C1NJ20396G.

(352) Gupta, S. K. N. Clinical Use of Vaginal or Rectally Applied Microbicides in Patients Suffering from HIV/AIDS. *HIV AIDS* **2013**, *5*, 295–307. https://doi.org/10.2147/HIV.S39164.

(353) Garcia-Vallejo, J. J.; Koning, N.; Ambrosini, M.; Kalay, H.; Vuist, I.; Sarrami-Forooshani, R.; Geijtenbeek, T. B. H.; van Kooyk, Y. Glycodendrimers Prevent HIV Transmission via DC-SIGN on Dendritic Cells. *Int Immunol* **2013**, *25*, 221–234. https://doi.org/10.1093/intimm/dxs115.

(354) Antimisiaris, S. G.; Mourtas, S. Recent Advances on Anti-HIV Vaginal Delivery Systems Development. *Adv Drug Deliver Rev* **2015**, *92*, 123–145. https://doi.org/10.1016/j.addr.2015.03.015.

(355) Notario-Pérez, F.; Ruiz-Caro, R.; Veiga-Ochoa, M. D. Historical Development of Vaginal Microbicides to Prevent Sexual Transmission of HIV in Women: From Past Failures to Future Hopes. *Drug Des Devel Ther* **2017**, *11*, 1767–1787. https://doi.org/10.2147/DDDT.S133170.

(356) Vacas-Córdoba, E.; Maly, M.; De la Mata, F. J.; Gómez, R.; Pion, M.; Muñoz-Fernández, M. Á. Antiviral Mechanism of Polyanionic Carbosilane Dendrimers against HIV-I. *Int J Nanomed* **2016**, *11*, 1281–1294. https://doi.org/10.2147/IJN.S96352.

(357) Telwatte, S.; Moore, K.; Johnson, A.; Tyssen, D.; Sterjovski, J.; Aldunate, M.; Gorry, P. R.; Ramsland, P. A.; Lewis, G. R.; Paull, J. R. A.; et al. Virucidal Activity of the Dendrimer Microbicide SPL7013 against HIV-1. *Antivir Res* **2011**, *90*, 195–199. https://doi.org/10.1016/j.antiviral.2011.03.186.

(358) McCarthy, T. D.; Karellas, P.; Henderson, S. A.; Giannis, M.; O'Keefe, D. F.; Heery, G.; Paull, J. R. A.; Matthews, B. R.; Holan, G. Dendrimers as Drugs: Discovery and Preclinical and Clinical Development of Dendrimer-Based Microbicides for HIV and STI Prevention. *Mol Pharm* **2005**, *2*, 312–318. https://doi.org/10.1021/mp050023q.

(359) Rupp, R.; Rosenthal, S. L.; Stanberry, L. R. VivaGel™ (SPL7013 Gel): A Candidate Dendrimer – Microbicide for the Prevention of HIV and HSV Infection. *Int J Nanomed* **2007**, *2*, 561–566.

(360) Tyssen, D.; Henderson, S. A.; Johnson, A.; Sterjovski, J.; Moore, K.; La, J.; Zanin, M.; Sonza, S.;

Karellas, P.; Giannis, M. P.; et al. Structure Activity Relationship of Dendrimer Microbicides with Dual Action Antiviral Activity. *PLOS One* **2010**, *5*, 1–15. https://doi.org/10.1371/journal.pone.0012309.

(361) Cohen, C. R.; Brown, J.; Moscicki, A. B.; Bukusi, E. A.; Paull, J. R. A.; Price, C. F.; Shiboski, S. A Phase I Randomized Placebo Controlled Trial of the Safety of 3% SPL7013 Gel (VivaGel®) in Healthy Young Women Administered Twice Daily for 14 Days. *PLOS One* **2011**, *6*, 1–9. https://doi.org/10.1371/journal.pone.0016258.

(362) Moscicki, A.-B.; Kaul, R.; Yifei, M. A.; Scott, M. E.; Daud, I. I.; Bukusi, E. A.; Shiboski, S.; Rebbapragada, A.; Huibner, S.; Cohen, C. R. Measurement of Mucosal Biomarkers in a Phase 1 Trial of Intravaginal 3% Starpharma LTD 7013 Gel (VivaGel) to Assess Expanded Safety. *J Acquir Immune Defic Syndr* **2012**, *59*, 134–140. https://doi.org/10.1097/QAI.0b013e31823f2aeb.

(363) Sepúlveda-Crespo, D.; Serramía, M. J.; Tager, A. M.; Vrbanac, V.; Gómez, R.; De La Mata, F. J.; Jiménez, J. L.; Muñoz-Fernández, M. Á. Prevention Vaginally of HIV-1 Transmission in Humanized BLT Mice and Mode of Antiviral Action of Polyanionic Carbosilane Dendrimer G2-S16. *Nanomed-Nanotechnol* **2015**, *11*, 1299–1308. https://doi.org/10.1016/j.nano.2015.04.013.

(364) Jardim, M. G.; Rissanen, K.; Rodrigues, J. Preparation and Characterization of Novel Poly(Alkylidenamine) Nitrile Ruthenium Metallodendrimers. *Eur J Inorg Chem* **2010**, *2010*, 1729–1735. https://doi.org/10.1002/ejic.200901187.

(365) Rodrigues, J.; Jardim, M. G.; Figueira, J.; Gouveia, M.; Tomás, H.; Rissanen, K. Poly(Alkylidenamines) Dendrimers as Scaffolds for the Preparation of Low-Generation Ruthenium Based Metallodendrimers. *New J Chem* **2011**, *35*, 1938. https://doi.org/10.1039/c1nj20364a.

(366) García-Gallego, S.; Cangiotti, M.; Fiorani, L.; Fattori, A.; Muñoz-Fernández, M. Á.; Gomez, R.; Ottaviani, M. F.; de la Mata, F. J. Anionic Sulfonated and Carboxylated PPI Dendrimers with the EDA Core: Synthesis and Characterization of Selective Metal Complexing Agents. *Dalton Trans* **2013**, *42*, 5874–5889. https://doi.org/10.1039/c3dt32870h.

(367) Nedeva, I.; Koripelly, G.; Caballero, D.; Chièze, L.; Guichard, B.; Romain, B.; Pencreach, E.; Lehn, J.-M.; Carlier, M.-F.; Riveline, D. Synthetic Polyamines Promote Rapid Lamellipodial Growth by Regulating Actin Dynamics. *Nat Commun* **2013**, *4*, 1–11. https://doi.org/10.1038/ncomms3165.

(368) Sarzotti-Kelsoe, M.; Bailer, R. T.; Turk, E.; Lin, C.; Bilska, M.; Greene, K. M.; Gao, H.; Todd, C. A.; Ozaki, D. A.; Seaman, M. S.; et al. Optimization and Validation of the TZM-Bl Assay for Standardized Assessments of Neutralizing Antibodies against HIV-1. *J Immunol Methods* **2014**, *409*, 131–146. https://doi.org/10.1016/j.jim.2013.11.022.

(369) Pan, H.; Grow, M. E.; Wilson, O.; Daniel, M.-C. A New Poly(Propylene Imine) Dendron as Potential Convenient Building-Block in the Construction of Multifunctional Systems. *Tetrahedron* **2013**, *69*, 2799–2806. https://doi.org/10.1016/j.tet.2013.01.070.

(370) Lazniewska, J.; Milowska, K.; Gabryelak, T. Dendrimers — Revolutionary Drugs for Infectious Diseases. *Wiley Interdiscip Rev Nanomed Nanobiotechnol* **2012**, *4*, 469–491. https://doi.org/10.1002/wnan.1181.

(371) Guerrero-Beltran, C.; Rodriguez-Izquierdo, I.; Serramia, M. J.; Araya-Durán, I.; Márquez-Miranda, V.; Gómez, R.; de la Mata, F. J.; Leal, M.; González-Nilo, F.; Muñoz-Fernández, M. Á. Anionic Carbosilane Dendrimers Destabilize the GP120-CD4 Complex Blocking HIV-1 Entry and Cell to Cell Fusion. *Bioconjug Chem* **2018**, *29*, 1584–1594. https://doi.org/10.1021/acs.bioconjchem.8b00106.

(372) AIDSinfo. Enfuvirtide https://aidsinfo.nih.gov/drugs/306/enfuvirtide/0/patient (accessed May 13, 2020).

(373) Drugbank. Enfuvirtide https://www.drugbank.ca/drugs/DB00109 (accessed May 13, 2020).

(374) Drugbank. Tenofovir disoproxil https://www.drugbank.ca/drugs/DB00300 (accessed May 13, 2020).

(375) AIDSinfo. Tenofovir Disoproxil Fumarate https://aidsinfo.nih.gov/drugs/290/tenofovir-disoproxil-fumarate/0/patient (accessed May 13, 2020).

(376) AIDSinfo. Raltegravir https://aidsinfo.nih.gov/drugs/420/raltegravir/0/patient (accessed May 13, 2020).

(377) Sawyer, J. R. Raltegravir http://www.antimicrobe.org/d98.asp (accessed May 13, 2020).

(378) Pirrone, V.; Wigdahl, B.; Krebs, F. C. The Rise and Fall of Polyanionic Inhibitors of the Human Immunodeficiency Virus Type 1. *Antivir Res* **2011**, *90*, 168–182. https://doi.org/10.1016/j.antiviral.2011.03.176.

(379) Ceña-Diez, R.; Vacas-Córdoba, E.; García-Broncano, P.; de la Mata, F. J.; Gómez, R.; Maly, M.; Muñoz-Fernández, M. Á. Prevention of Vaginal and Rectal Herpes Simplex Virus Type 2 Transmission in Mice: Mechanism of Antiviral Action. *Int J Nanomed* **2016**, *11*, 2147–2162. https://doi.org/10.2147/IJN.S95301.

(380) Hill, M. A. Estrous Cycle https://embryology.med.unsw.edu.au/embryology/index.php/Estrous_Cycle (accessed May 13, 2020).

(381) Mjos, K. D.; Orvig, C. Metallodrugs in Medicinal Inorganic Chemistry. *Chem Rev* **2014**, *114*, 4540–4563. https://doi.org/10.1021/cr400460s.

(382) Romero-Canelón, I.; Sadler, P. J. Systems Approach to Metal-Based Pharmacology. *Proc Natl Acad Sci U S A* **2015**, *112*, 4187–4188. https://doi.org/10.1073/pnas.1503858112.

(383) Wang, Y.; Astruc, D.; Abd-El-Aziz, A. S. Metallopolymers for Advanced Sustainable Applications. *Chem Soc Rev* **2019**, *48*, 558–636. https://doi.org/10.1039/c7cs00656j.

(384) Parveen, S.; Hanif, M.; Movassaghi, S.; Sullivan, M.; Kubanik, M.; Shaheen, M. A.; Söhnel, T.; Jamieson, S. M. F.; Hartinger, C. G. Cationic Ru(η^6-*p*-Cymene) Complexes of 3-hydroxy-4-pyr(id)ones: Lipophilic Triphenylphoshine as Co-Ligand Is Key to Highly Stable and Cytotoxic Anticancer Agents. *Eur J Inorg Chem* **2017**, 1721–1727. https://doi.org/10.1111/febs.13334.

(385) Makhubela, B. C. E.; Meyer, M.; Smith, G. S. Evaluation of Trimetallic Ru(II)- and Os(II)-Arene Complexes as Potential Anticancer Agents. *J Organomet Chem* **2014**, *772–773*, 229–241. https://doi.org/10.1016/j.jorganchem.2014.08.034.

(386) Delgado, R. A.; Galdámez, A.; Villena, J.; Reveco, P. G.; Thomet, F. A. Synthesis, Characterization and in Vitro Biological Evaluation of [Ru(η^6-arene)(*N,N*)Cl]PF_6 compounds Using the Natural Products Arenes Methylisoeugenol and Anethole. *J Organomet Chem* **2015**, *782*, 131–137. https://doi.org/10.1016/j.jorganchem.2014.09.005.

(387) Hadda, T. Ben; Akkurt, M.; Baba, M. F.; Daoudi, M.; Bennani, B.; Kerbal, A.; Chohan, Z. H. Anti-Tubercular Activity of Ruthenium (II) Complexes with Polypyridines. *J Enzyme Inhib Med Chem* **2009**, *24*, 457–463. https://doi.org/10.1080/14756360802188628.

(388) de Oliveira, L. P.; Carneiro, Z. A.; Ribeiro, C. M.; Lima, M. F.; Paixão, D. A.; Pivatto, M.; de Souza, M. V. N.; Teixeira, L. R.; Lopes, C. D.; de Albuquerque, S.; et al. Three New Platinum Complexes Containing Fluoroquinolones and DMSO: Cytotoxicity and Evaluation against Drug-Resistant Tuberculosis. *J Inorg Biochem* **2018**, *183*, 77–83. https://doi.org/10.1016/j.jinorgbio.2018.03.010.

(389) Yufanyi, D. M.; Abbo, H. S.; Titinchi, S. J. J.; Neville, T. Platinum(II) and Ruthenium(II) Complexes in Medicine: Antimycobacterial and Anti-HIV Activities. *Coordin Chem Rev* **2020**, *414*, 213285. https://doi.org/10.1016/j.ccr.2020.213285.

(390) Mishra, L.; Singh, A. K.; Trigun, S. K.; Singh, S. K.; Pandey, S. M. Anti-HIV and Cytotoxic Ruthenium(II) Complexes Containing Flavones: Biochemical Evaluation in Mice. *Indian J Exp Biol* **2004**, *42*, 660–666.

(391) Wong, E. L.-M.; Sun, R. W.-Y.; Chung, N. P.-Y.; Lin, C.-L. S.; Zhu, N.; Che, C.-M. A Mixed-Valent Ruthenium-Oxo Oxalato Cluster $Na_7[Ru_4(\mu_3\text{-}O)_4(C_2O_4)_6]$ with Potent Anti-HIV Activities. *J Am Chem Soc* **2006**, *128*, 4938–4939. https://doi.org/10.1021/ja057883k.

(392) Carcelli, M.; Bacchi, A.; Pelagatti, P.; Rispoli, G.; Rogolino, D.; Sanchez, T. W.; Sechi, M.; Neamati, N. Ruthenium Arene Complexes as HIV-1 Integrase Strand Transfer Inhibitors. *J Inorg Biochem* **2013**, *118*, 74–82. https://doi.org/10.1016/j.jinorgbio.2012.09.021.

(393) Al-Masoudi, W. A.; Al-Masoudi, N. A.; Weibert, B.; Winter, R. Synthesis, X-Ray Structure, in Vitro HIV and Kinesin Eg5 Inhibition Activities of New Arene Ruthenium Complexes of Pyrimidine Analogs. *J Coord Chem* **2017**, *70*, 2061–2073. https://doi.org/10.1080/00958972.2017.1334259.

(394) Al-Masoudi, W. A.; Al-Masoudi, N. A. A Ruthenium Complexes of Monastrol and Its Pyrimidine Analogues: Synthesis and Biological Properties. *Phosphorus, Sulfur Silicon Relat Elem* **2019**, *194*, 1020–1027. https://doi.org/10.1080/10426507.2019.1597362.

(395) De Clercq, E. Antiviral Metal Complexes. *Met Based Drugs* **1997**, *4*, 173–192. https://doi.org/10.1155/MBD.1997.173.

(396) Galán, M.; Sánchez-Rodríguez, J.; Cangiotti, M.; García-Gallego, S.; Jiménez, J. L.; Gómez, R.; Ottaviani, M. F.; Muñoz-Fernández, M. Á.; de la Mata, F. J. Antiviral Properties Against HIV of Water Soluble Copper Carbosilane Dendrimers and Their EPR Characterization. *Curr Med Chem* **2012**, *19*, 4984–4994. https://doi.org/10.2174/0929867311209024984.

(397) Dias, A. R.; Garcia, M. H.; Rodrigues, J. C.; Green, M. L. H.; Kuebler, S. M. Synthesis and Characterization of η^5-monocyclopentadienyl (*p*-nitrobenzonitrile)ruthenium(II) Salts: Second Harmonic Generation Powder Efficiencies. *J Organomet Chem* **1994**, *475*, 241–245.

https://doi.org/10.1016/0022-328X(94)84028-8.

(398) Bruce, M. I.; Windsor, N. J. Cyclopentadienyl-Ruthenium and -Osmium Chemistry. IV* Convenient High-Yield Synthesis of Some Cyclopentadienyl Ruthenium or -Osmium Tertiary Phosphine Halide Complexes. *Aust J Chem* **1977**, *30* (43), 1601–1604. https://doi.org/10.1002/chin.197743313.

(399) Sirois, S.; Sing, T.; Chou, K.-C. HIV-1 Gp120 V3 Loop for Structure-Based Drug Design. *Curr Protein Pept Sci* **2005**, *6*, 413–422. https://doi.org/10.2174/138920305774329359.

(400) Harrop, H. A.; Coombe, D. R.; Rider, C. C. Heparin Specifically Inhibits Binding of V3 Loop Antibodies to HIV-1 Gp120, an Effect Potentiated by CD4 Binding. *AIDS* **1994**, *8*, 183–192. https://doi.org/10.1097/00002030-199402000-00005.

(401) Gianvincenzo, P. Di; Calvo, J.; Perez, S.; Álvarez, A.; Bedoya, L. M.; Alcamí, J.; Penadés, S. Negatively Charged Glyconanoparticles Modulate and Stabilize the Secondary Structures of a Gp120 V3 Loop Peptide: Toward Fully Synthetic HIV Vaccine Candidates. *Bioconjug Chem* **2015**, *26*, 755–765. https://doi.org/10.1021/acs.bioconjchem.5b00077.

(402) Pal, M.; Nandi, U.; Mukherjee, D. Detailed Account on Activation Mechanisms of Ruthenium Coordination Complexes and Their Role as Antineoplastic Agents. *Eur J Med Chem* **2018**, *150*, 419–445. https://doi.org/10.1016/j.ejmech.2018.03.015.

(403) Thangavel, P.; Viswanath, B.; Kim, S. Recent Developments in the Nanostructured Materials Functionalized with Ruthenium Complexes for Targeted Drug Delivery to Tumors. *Int J Nanomed* **2017**, *12*, 2749–2758. https://doi.org/10.2147/IJN.S131304.

(404) Purushothaman, B.; Arumugam, P.; Ju, H.; Kulsi, G.; Samson, A. A. S.; Song, J. M. Novel Ruthenium(II) Triazine Complex $[Ru(bdpta)(tpy)]^{2+}$ Co-Targeting Drug Resistant GRP78 and Subcellular Organelles in Cancer Stem Cells. *Eur J Med Chem* **2018**, *156*, 747–759. https://doi.org/10.1016/j.ejmech.2018.07.048.

(405) Pettinari, R.; Marchetti, F.; Petrini, A.; Pettinari, C.; Lupidi, G.; Smoleński, P.; Scopelliti, R.; Riedel, T.; Dyson, P. J. From Sunscreen to Anticancer Agent: Ruthenium(II) Arene Avobenzone Complexes Display Potent Anticancer Activity. *Organometallics* **2016**, *35*, 3734–3742. https://doi.org/10.1021/acs.organomet.6b00694.

(406) Liu, P.; Wu, B.-Y.; Liu, J.; Dai, Y.-C.; Wang, Y.-J.; Wang, K.-Z. DNA Binding and Photocleavage Properties, Cellular Uptake and Localization, and in-Vitro Cytotoxicity of Dinuclear Ruthenium(II) Complexes with Varying Lengths in Bridging Alkyl Linkers. *Inorg Chem* **2016**, *55*, 1412–1422. https://doi.org/10.1021/acs.inorgchem.5b01934.

(407) Dragutan, I.; Dragutan, V.; Demonceau, A. Editorial of Special Issue Ruthenium Complex: The Expanding Chemistry of the Ruthenium Complexes. *Molecules* **2015**, *20*, 17244–17274. https://doi.org/10.3390/molecules200917244.

(408) Aderibigbe, B. A. Polymeric Prodrugs Containing Metal-Based Anticancer Drugs. *J Inorg Organomet Polym Mater* **2015**, *25*, 339–353. https://doi.org/10.1007/s10904-015-0220-7.

(409) Ndagi, U.; Mhlongo, N.; Soliman, M. E. Metal Complexes in Cancer Therapy - an Update from Drug Design Perspective. *Drug Des Devel Ther* **2017**, *11*, 599–616.

https://doi.org/10.2147/DDDT.S119488.

(410) Alessio, E.; Messori, L. The Deceptively Similar Ruthenium(III) Drug Candidates KP1019 and NAMI-A Have Different Actions. What Did We Learn in the Past 30 Years? *Met Ions Life Sci* **2018**, *18*, 141–170. https://doi.org/10.1515/9783110470734-005.

(411) Grabchev, I.; Staneva, D.; Vasileva-Tonkova, E.; Alexandrova, R.; Cangiotti, M.; Fattori, A.; Ottaviani, M. F. Antimicrobial and Anticancer Activity of New Poly(Propyleneamine) Metallodendrimers. *J Polym Res* **2017**, *24*, 1–11. https://doi.org/10.1007/s10965-017-1387-0.

(412) Pernar, M.; Kokan, Z.; Kralj, J.; Glasovac, Z.; Tumir, L.-M.; Piantanida, I.; Eljuga, D.; Turel, I.; Brozovic, A.; Kirin, S. I. Organometallic Ruthenium(II)-Arene Complexes with Triphenylphosphine Amino Acid Bioconjugates: Synthesis, Characterization and Biological Properties. *Bioorg Chem* **2019**, *87*, 432–446. https://doi.org/10.1016/j.bioorg.2019.03.048.

(413) Ruiz, M. C.; Kljun, J.; Turel, I.; Di Virgilio, A. L.; León, I. E. Comparative Antitumor Studies of Organoruthenium Complexes with 8-Hydroxyquinolines on 2D and 3D Cell Models of Bone, Lung and Breast Cancer. *Metallomics* **2019**, *11*, 666–675. https://doi.org/10.1039/c8mt00369f.

(414) Morais, T. S.; Santos, F. C.; Jorge, T. F.; Côrte-Real, L.; Madeira, P. J. A.; Marques, F.; Robalo, M. P.; Matos, A.; Santos, I.; Garcia, M. H. New Water-Soluble Ruthenium(II) Cytotoxic Complex: Biological Activity and Cellular Distribution. *J Inorg Biochem* **2014**, *130*, 1–14. https://doi.org/10.1016/j.jinorgbio.2013.09.013.

(415) Gilbert, J. D.; Wilkinson, G. New Complexes of Ruthenium(II) with Triphenylphosphine and Other Ligands. *J Chem Soc A* **1969**, 1749–1753. https://doi.org/10.1039/J19690001749.

(416) Blackmore, T.; Bruce, M. I.; Stone, F. G. A. Some New π-Cyclopentadienylruthenium Complexes. *J Chem Soc A* **1971**, 2376–2382. https://doi.org/10.1039/J19710002376.

(417) Gupta, A.; Dubey, S.; Mishra, M. Unique Structures, Properties and Applications of Dendrimers. *J Drug Deliv Ther* **2019**, *8*, 328–339. https://doi.org/10.22270/jddt.v8i6-s.2083.

(418) Mignani, S.; Rodrigues, J.; Tomas, H.; Caminade, A.-M.; Laurent, R.; Shi, X.; Majoral, J.-P. Recent Therapeutic Applications of the Theranostic Principle with Dendrimers in Oncology. *Sci China Mater* **2018**, *61*, 1367–1386. https://doi.org/10.1007/s40843-018-9244-5.

(419) Ventola, C. L. Progress in Nanomedicine: Approved and Investigational Nanodrugs. *P T* **2017**, *42*, 742–755.

(420) Smith, G. S.; Therrien, B. Targeted and Multifunctional Arene Ruthenium Chemotherapeutics. *Dalton Trans* **2011**, *40*, 10793–10800. https://doi.org/10.1039/c1dt11007a.

(421) Carter, M. T.; Rodriguez, M.; Bard, A. J. Voltammetric Studies of the Interaction of Metal Chelates with DNA. 2. Tris-Chelated Complexes of Cobalt(III) and Iron(II) with 1, 10-Phenanthroline and 2, 2'-Bipyridine. *J Am Chem Soc* **1989**, *111*, 8901–8911. https://doi.org/10.1021/ja00206a020.

(422) Ju, C.-C.; Zhang, A.-G.; Yuan, C.-L.; Zhao, X.-L.; Wang, K.-Z. The Interesting DNA-Binding Properties of Three Novel Dinuclear Ru(II) Complexes with Varied Lengths of Flexible Bridges. *J Inorg Biochem* **2011**, *105*, 435–443. https://doi.org/10.1016/j.jinorgbio.2010.12.004.

(423) Snyder, L. R. Classification of the Solvent Properties of Common Liquids. *J Chromatogr A* **1974**,

92, 223–230. https://doi.org/10.1016/S0021-9673(00)85732-5.

(424) Sirajuddin, M.; Ali, S.; Badshah, A. Drug-DNA Interactions and Their Study by UV-Visible, Fluorescence Spectroscopies and Cyclic Voltametry. *J Photochem Photobiol B Biol* **2013**, *124*, 1–19. https://doi.org/10.1016/j.jphotobiol.2013.03.013.

(425) N'Soukpoé-Kossi, C. N.; Descôteaux, C.; Asselin, É.; Tajmir-Riahi, H. A.; Bérubé, G. DNA Interaction with Novel Antitumor Estradiol-Platinum(II) Hybrid Molecule: A Comparative Study with Cisplatin Drug. *DNA Cell Biol* **2008**, *27*, 101–107. https://doi.org/10.1089/dna.2007.0669.

(426) Lu, X. L.; Zhang, L.; Lou, J. D.; Yan, J.; Nong, P. S.; Chen, X. H.; Yang, J. J.; Gao, M. Synthesis, Characterization and DNA Binding Studies of Two Cyclopentadienyl Ruthenium(II) Complexes with Amino Acid Ligands. *Transit Met Chem* **2010**, *35*, 513–519. https://doi.org/10.1007/s11243-010-9357-y.

(427) Devagi, G.; Dallemer, F.; Kalaivani, P.; Prabhakaran, R. Organometallic Ruthenium(II) Complexes Containing NS Donor Schiff Bases: Synthesis, Structure, Electrochemistry, DNA/BSA Binding, DNA Cleavage, Radical Scavenging and Antibacterial Activities. *J Organomet Chem* **2018**, *854*, 1–14. https://doi.org/10.1016/j.jorganchem.2017.10.036.

(428) Fandzloch, M.; Jaromin, A.; Zaremba-Czogalla, M.; Wojtczak, A.; Lewińska, A.; Sitkowski, J.; Wiśniewska, J.; Łakomska, I.; Gubernator, J. Nanoencapsulation of a Ruthenium(II) Complex with Triazolopyrimidine in Liposomes as a Tool for Improving Its Anticancer Activity against Melanoma Cell Lines. *Dalton Trans* **2020**, *49*, 1207–1219. https://doi.org/10.1039/c9dt03464a.

(429) Li, W.; Jiang, G. Bin; Yao, J. H.; Wang, X. Z.; Wang, J.; Han, B. J.; Xie, Y. Y.; Lin, G. J.; Huang, H. L.; Liu, Y. J. Ruthenium(II) Complexes: DNA-Binding, Cytotoxicity, Apoptosis, Cellular Localization, Cell Cycle Arrest, Reactive Oxygen Species, Mitochondrial Membrane Potential and Western Blot Analysis. *J Photochem Photobiol B Biol* **2014**, *140*, 94–104. https://doi.org/10.1016/j.jphotobiol.2014.07.011.

(430) Maroto-Diaz, M.; Sanz del Olmo, N.; Muñoz-Moreno, L.; Bajo, A. M.; Carmena, M. J.; Gómez, R.; García-Gallego, S.; de la Mata, F. J. In Vitro and in Vivo Evaluation of First-Generation Carbosilane Arene Ru(II)-Metallodendrimers in Advanced Prostate Cancer. *Eur Polym J* **2019**, *113* (January), 229–235. https://doi.org/10.1016/j.eurpolymj.2019.01.047.

(431) Huang, H. L.; Tang, B.; Yi, Q. Y.; Wan, D.; Yang, L. L.; Liu, Y. J. Synthesis, DNA-Binding, Molecular Docking and Cytotoxic Activity in Vitro Evaluation of Ruthenium(II) Complexes. *Transit Met Chem* **2019**, *44* (1), 11–24. https://doi.org/10.1007/s11243-018-0264-y.

(432) Liang, Z.-H.; Wang, Y.-N.; Xiong, Z.-W.; Chen, X.-Y.; Tong, L. Studies of the Anticancer Activities of Ruthenium (II) Polypyridyl Complexes toward Human Hepatocellular Carcinoma BEL-7402 Cells. *Transit Met Chem* **2019**, *2*, 1–10. https://doi.org/10.1007/s11243-019-00315-5.

(433) Kroemer, G.; Galluzzi, L.; Brenner, C. Mitochondrial Membrane Permeabilization in Cell Death. *Physiol Rev* **2007**, *87*, 99–163. https://doi.org/10.1152/physrev.00013.2006.

(434) Zorova, L. D.; Popkov, V. A.; Plotnikov, E. Y.; Silachev, D. N.; Pevzner, I. B.; Jankauskas, S. S.; Babenko, V. A.; Zorov, S. D.; Balakireva, A. V.; Juhaszova, M.; et al. Mitochondrial Membrane

Potential. *Anal Biochem* **2018**, *552*, 50–59. https://doi.org/10.1016/j.ab.2017.07.009.

(435) Lemasters, J. J.; Ramshesh, V. K. Imaging of Mitochondrial Polarization and Depolarization with Cationic Fluorophores. *Methods Cell Biol* **2007**, *80*, 283–295. https://doi.org/10.1016/S0091-679X(06)80014-2.

(436) Qian, C.; Wang, J.-Q.; Song, C.-L.; Wang, L.-L.; Ji, L.-N.; Chao, H. The Induction of Mitochondria-Mediated Apoptosis in Cancer Cells by Ruthenium(II) Asymmetric Complexes. *Metallomics* **2013**, *5*, 844–854. https://doi.org/10.1039/c3mt20270d.

(437) Peña, B.; Saha, S.; Barhoumi, R.; Burghardt, R. C.; Dunbar, K. R. Ruthenium(II)-Polypyridyl Compounds with π-Extended Nitrogen Donor Ligands Induce Apoptosis in Human Lung Adenocarcinoma (A549) Cells by Triggering Caspase-3/7 Pathway. *Inorg Chem* **2018**, *57*, 12777–12786. https://doi.org/10.1021/acs.inorgchem.8b01988.

(438) Ferreira, J. A.; Peixoto, A.; Neves, M.; Gaiteiro, C.; Reis, C. A.; Assaraf, Y. G.; Santos, L. L. Mechanisms of Cisplatin Resistance and Targeting of Cancer Stem Cells: Adding Glycosylation to the Equation. *Drug Resist Update* **2016**, *24*, 34–54. https://doi.org/10.1016/j.drup.2015.11.003.

(439) Oun, R.; Moussa, Y. E.; Wheate, N. J. The Side Effects of Platinum-Based Chemotherapy Drugs: A Review for Chemists. *Dalton Trans* **2018**, *47*, 6645–6653. https://doi.org/10.1039/c8dt00838h.

(440) Clinicaltrials.gov. Preoperative Trial of Sorafenib in Combination With Cisplatin Followed by Paclitaxel for Early Stage Breast Cancer https://clinicaltrials.gov/ct2/show/NCT01194869?term=cisplatin&cond=cancer&draw=5&rank=34 (accessed Jul 1, 2020).

(441) Clinicaltrials.gov. A Trial of Gemcitabine, Infusional 5-Fluorouracil and Cisplatin for Advanced Pancreatic and Biliary Cancers https://clinicaltrials.gov/ct2/show/NCT01661114?term=cisplatin&cond=cancer&draw=2&rank=8 (accessed Jul 1, 2020).

(442) Clinicaltrials.gov. Adjuvant Chemotherapy With Docetaxel, Capecitabine and Cisplatin in Patients With Advanced Gastric Cancer: Adjuvant DXP https://clinicaltrials.gov/ct2/show/NCT00976976?term=cisplatin&cond=cancer&draw=3&rank=17 (accessed Jul 1, 2020).

(443) Berners-Price, S. J.; Ronconi, L.; Sadler, P. J. Insights into the Mechanism of Action of Platinum Anticancer Drugs from Multinuclear NMR Spectroscopy. *Prog Nucl Magn Reson Spectrosc* **2006**, *49*, 65–98. https://doi.org/10.1016/j.pnmrs.2006.05.002.

(444) Jing, X.; Song, W.; Chen, X.; Xiao, H.; Zhou, D.; Yan, L.; Ding, J.; Dempsey, E. M.; Huang, Y.; Qi, R.; et al. Recent Progress in Polymer-Based Platinum Drug Delivery Systems. *Prog Polym Sci* **2018**, *87*, 70–106. https://doi.org/10.1016/j.progpolymsci.2018.07.004.

(445) Hanif, M.; Hartinger, C. G. Anticancer Metallodrugs: Where Is the next Cisplatin? *Future Med Chem* **2018**, *10*, 615–617. https://doi.org/10.4155/fmc-2017-0317.

(446) Liu, Z.; Wang, H.; Feng, L.; Chen, M.; Dong, Z.; Chen, Q.; Gao, M.; Tao, D. Cisplatin-Prodrug-Constructed Liposomes as a Versatile Theranostic Nanoplatform for Bimodal Imaging Guided

Combination Cancer Therapy. *Adv Funct Mater* **2016**, *26*, 2207–2217. https://doi.org/10.1002/adfm.201504899.

(447) Zhu, Y. H.; Sun, C. Y.; Shen, S.; Khan, M. I. U.; Zhao, Y. Y.; Liu, Y.; Wang, Y. C.; Wang, J. A Micellar Cisplatin Prodrug Simultaneously Eliminates Both Cancer Cells and Cancer Stem Cells in Lung Cancer. *Biomater Sci* **2017**, *5* (8), 1612–1621. https://doi.org/10.1039/c7bm00278e.

(448) Haririan, I.; Alavidjeh, M. S.; Khorramizadeh, M. R.; Ardestani, M. S.; Ghane, Z. Z.; Namazi, H. Anionic Linear-Globular Dendrimer-*cis*-platinum (II) Conjugates Promote Cytotoxicity in Vitro against Different Cancer Cell Lines. *Int J Nanomed* **2010**, *5*, 63–75.

(449) Sommerfeld, N. S.; Hejl, M.; Klose, M. H. M.; Schreiber-Brynzak, E.; Bileck, A.; Meier, S. M.; Gerner, C.; Jakupec, M. A.; Galanski, M.; Keppler, B. K. Low-Generation Polyamidoamine Dendrimers as Drug Carriers for Platinum(IV) Complexes. *Eur J Inorg Chem* **2017**, *2017*, 1713–1720. https://doi.org/10.1002/ejic.201601205.

(450) Kirkpatrick, G. J.; Plumb, J. A.; Sutcliffe, O. B.; Flint, D. J.; Wheate, N. J. Evaluation of Anionic Half Generation 3.5–6.5 Poly(Amidoamine) Dendrimers as Delivery Vehicles for the Active Component of the Anticancer Drug Cisplatin. *J Inorg Biochem* **2011**, *105*, 1115–1122. https://doi.org/10.1016/j.jinorgbio.2011.05.017.

(451) Ferrari, E.; Grandi, R.; Lazzari, S.; Marverti, G.; Rossi, M. C.; Saladini, M. ^{1}H, ^{13}C, ^{195}Pt NMR Study on Platinum(II) Interaction with Sulphur Containing Amadori Compounds. *Polyhedron* **2007**, *26*, 4045–4052. https://doi.org/10.1016/j.poly.2007.05.001.

(452) Bergamini, A.; Pisano, C.; Di Napoli, M.; Arenare, L.; Della Pepa, C.; Tambaro, R.; Facchini, G.; Gargiulo, P.; Rossetti, S.; Mangili, G.; et al. Cisplatin Can Be Safely Administered to Ovarian Cancer Patients with Hypersensitivity to Carboplatin. *Gynecol Oncol* **2017**, *144*, 72–76. https://doi.org/10.1016/j.ygyno.2016.10.023.

(453) Grabosch, S.; Bulatovic, M.; Zeng, F.; Ma, T.; Zhang, L.; Ross, M.; Brozick, J.; Fang, Y.; Tseng, G.; Kim, E.; et al. Cisplatin-Induced Immune Modulation in Ovarian Cancer Mouse Models with Distinct Inflammation Profiles. *Oncogene* **2019**, *38*, 2380–2393. https://doi.org/10.1038/s41388-018-0581-9.

(454) Kulhari, H.; Pooja, D.; Singh, M. K.; Chauhan, A. S. Optimization of Carboxylate-Terminated Poly(Amidoamine) Dendrimer-Mediated Cisplatin Formulation. *Drug Dev Ind Pharm* **2015**, *41*, 232–238. https://doi.org/10.3109/03639045.2013.858735.

(455) Nguyen, H.; Nguyen, N. H.; Tran, N. Q.; Nguyen, C. K. Improved Method for Preparing Cisplatin-Dendrimer Nanocomplex and Its Behavior Against NCI-H460 Lung Cancer Cell. *J Nanosci Nanotechnol* **2015**, *15*, 4106–4110. https://doi.org/10.1166/jnn.2015.9808.

Annex

Annex

A.1. General experimental procedures

A.1.1. Solvents and reactions

All reactions were carried out under an inert atmosphere (nitrogen or argon), using basic Schlenk techniques. For the reactions and purifications performed under an inert atmosphere, the solvents were degassed under nitrogen flow. Dry dichloromethane, ethyl ether, n-hexane and tetrahydrofuran, were used pre-dried using a mBRAUN MB SPS-800 solvent purification system.

A.1.2. Synthesis of the amine-terminated dendrimers

A.1.2.1. Synthesis of G1NH_2

The G0CN dendrimer (9.7 g, 29.6 mmol) was dissolved in 100 mL of anhydrous tetrahydrofuran (THF) under nitrogen. Borane dimethyl sulfide complex (56.1 mL, 591.8 mmol, 5 equiv. per nitrile group) was added to the previous mixture using a syringe. The reaction was stirred at room temperature for 2 days. Methanol extra-dry was added slowly at 0ºC until it was not observed any bubbling or reaction, followed by solvent removed under reduced pressure. Fresh methanol extra-dry (120 mL) was added to the residual white paste and heated to reflux overnight. After cooling to room temperature, the solvent was removed under vacuum. The oily product was taken up in water (20 mL) and washed with diethyl ether (5 x 20 mL), hexane (5 x 20 mL), and ethyl acetate (2 x 20 mL), and dry under vacuum to get a slightly golden oil an 84% yield (8.5 g). ^{1}H-NMR (400 MHz, D_2O) $\delta =$ 1.30, 1.47, 1.67 – 1.69, 1.97 (–$CH_2N\mathbf{H}_2$), 2.51 – 2.58 (–$C\mathbf{H}_2NH_2$), 2.73 ppm ^{13}C-NMR (100 MHz, D_2O) $\delta =$ 22.98, 24.53, 26.06, 38.30 (–$\mathbf{C}H_2NH_2$), 49.93, 52.62 ppm.

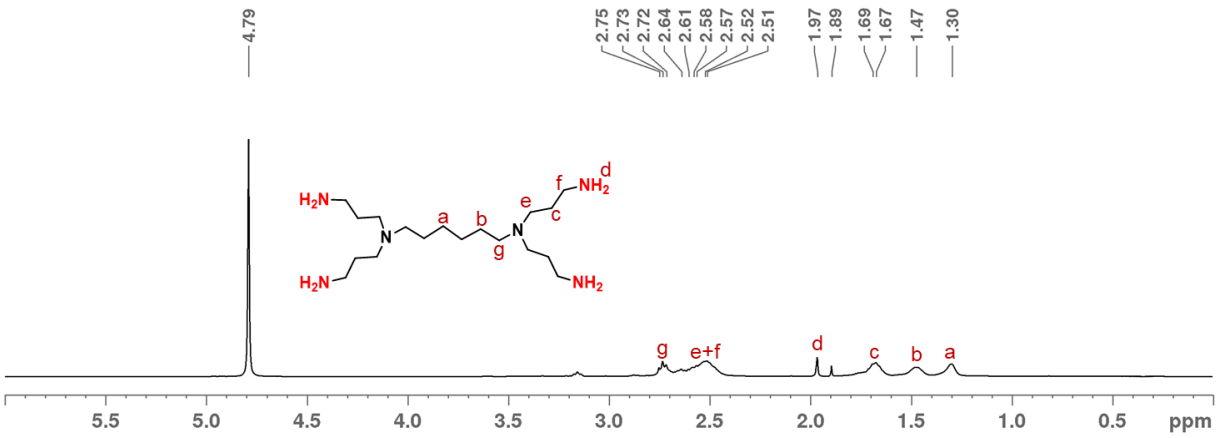

Figure A1. ^{1}H-NMR spectrum of generation 0 of the amine dendrimer G0NH_2 in D_2O.

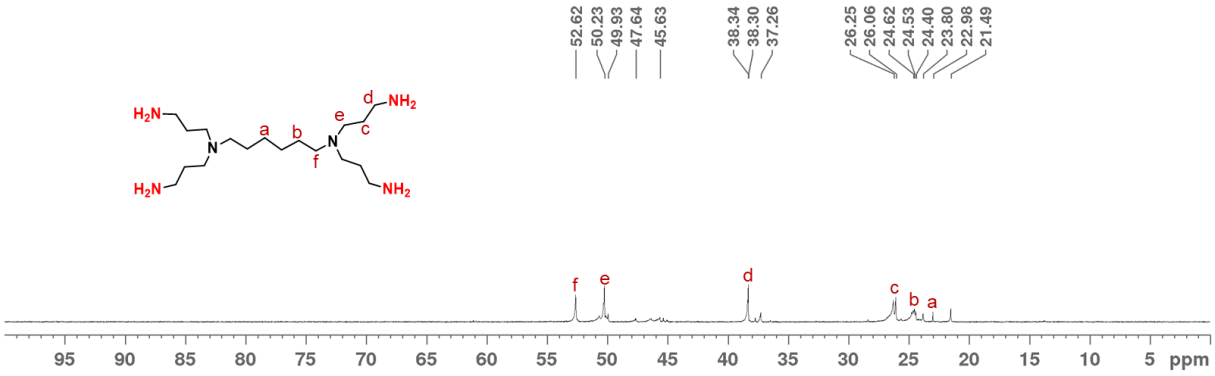

Figure A2. ^{13}C-NMR spectrum of generation 0 of the amine dendrimer G0NH$_2$ in D$_2$O.

A.1.2.2. Synthesis of G2NH$_2$

The G1CN dendrimer (5.1 g, 6.7 mmol) was dissolved in 100 mL of anhydrous THF under nitrogen. Borane dimethyl sulfide complex (25.4 mL, 267.5 mmol, 5 equiv. per nitrile group) was added to the previous mixture using a syringe. The reaction was stirred at room temperature for 3 days. Methanol extra-dry was added slowly at 0ºC until it was not observed any bubbling or reaction, followed by solvent removed under reduced pressure. Fresh methanol extra-dry (120 mL) was added to the residual white paste and heated to reflux overnight. After cooling to room temperature, the solvent was removed under reduced pressure. The oily product was taken up in water (20 mL) and washed with diethyl ether (5 x 20 mL), hexane (5 x 20 mL), and ethyl acetate (2 x 20 mL), and dry under vacuum to get a transparent oil 63% yield (3.4 g). ^{1}H-NMR (400 MHz, D$_2$O) δ = 1.17, 1.26, 1.45, 1.69, 1.87 (–CH$_2$N**H**$_2$), 2.49 – 2.51 (–C**H**$_2$NH$_2$), 2.77 ppm. ^{13}C-NMR (100 MHz, D$_2$O) δ = 22.96, 24.67, 25.45, 26.30, 38.06 (–**C**H$_2$NH$_2$), 49.95, 50.62, 52.59 ppm.

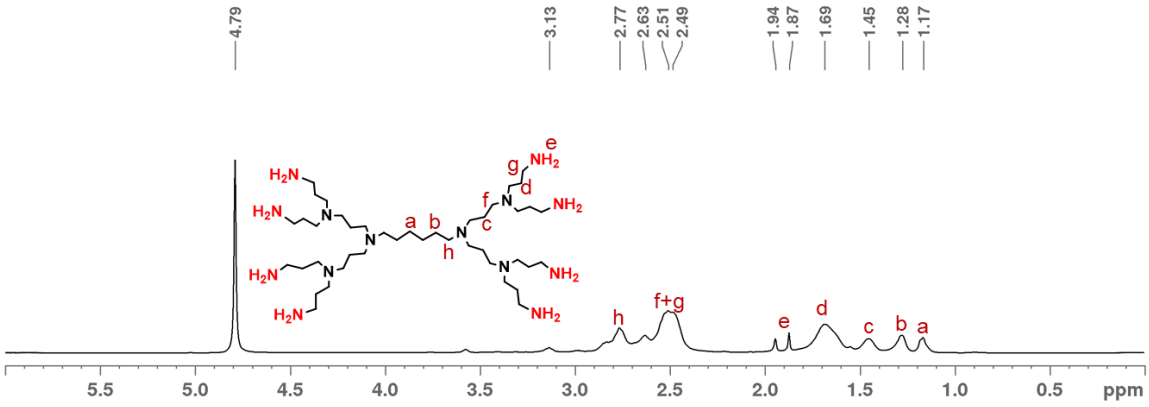

Figure A3. ^{1}H-NMR spectrum of generation 1 of the amine dendrimer G1NH$_2$ in D$_2$O.

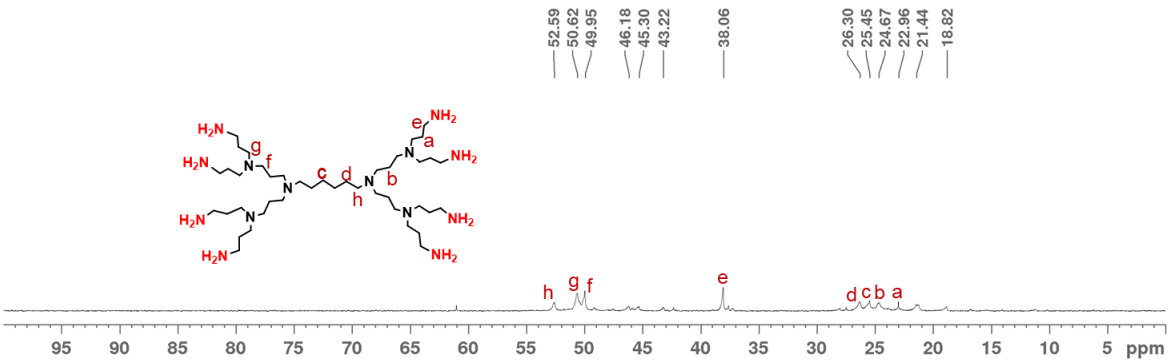

Figure A4. ^{13}C-NMR spectrum of generation 1 of the amine dendrimer G1NH$_2$ in D$_2$O.

A.1.2.3. Synthesis of G3NH$_2$

The G2CN dendrimer (2.5 g, 3.2 mmol) was dissolved in 80 mL of anhydrous tetrahydrofuran (THF) under nitrogen. Borane dimethyl sulfide complex (24.3 mL, 256.4 mmol, 5 equiv. per nitrile group) was added to the previous mixture using a syringe. The reaction was stirred at room temperature for 48 h. Methanol extra-dry was added slowly at 0ºC until it was not observed any bubbling or reaction, followed by solvent removed under reduced pressure. Fresh methanol extra-dry (80 mL) was added to the residual white paste and heated to reflux overnight. After cooling to room temperature, the solvent was removed under vacuum. The oily product was taken up in water (10 mL) and washed with diethyl ether (5 x 10 mL), hexane (5 x 10 mL), and ethyl acetate (2 x 10 mL), and dry under vacuum to get a slightly golden oil an 15% yield (0.8 g). ^{1}H-NMR (400 MHz, D$_2$O) δ = 1.41, 1.59, 1.74 – 1.84, 1.97 (–CH$_2$N**H**$_2$), 2.62 – 2.74 (–C**H**$_2$NH$_2$), 3.08 ppm. ^{13}C-NMR (100 MHz, D$_2$O) δ = 21.74, 23.96, 27.55, 38.34 (–**C**H$_2$NH$_2$), 49.97, 51.00 ppm.

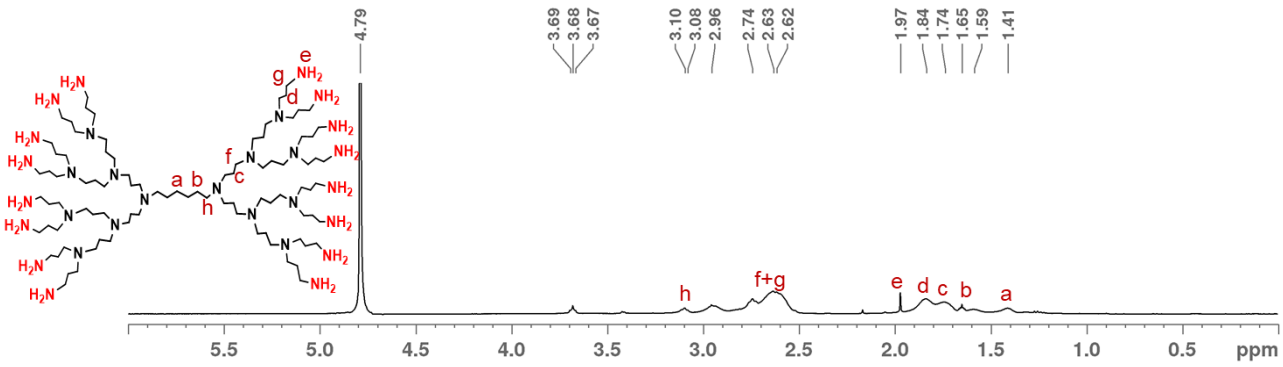

Figure A5. ^{1}H-NMR spectrum of generation 3 of the amine dendrimer G3NH$_2$ in D$_2$O.

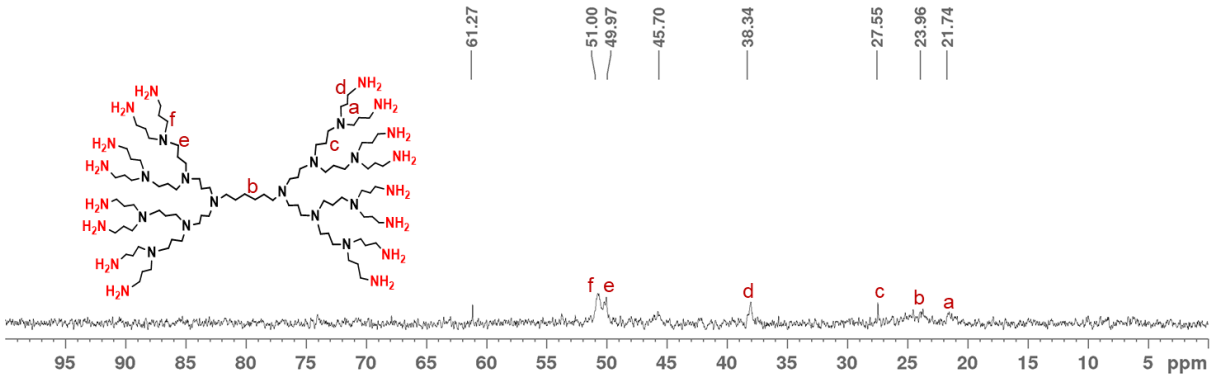

Figure A6. ^{13}C-NMR spectrum of generation 3 of the amine dendrimer G3NH$_2$ in D_2O.

A.1.3. Preparation of starting material [Ru(η^5-C_5H_5)(PPh_3)$_2$Cl] complex

Triphenylphosphine (14.9 g, 56.8 mmol) in 200 mL absolute ethanol was refluxed for 20 min, $RuCl_3$ (3.6 g, 17 mmol) dissolved in 80 mL of absolute ethanol was dropped into the previous solution, and cyclopentadiene (15 mL, 183.7 mmol) was added to the mixture. The reaction mixture was refluxed at 85ºC for 2h. After it cooled, the suspension was filtered still at a warm temperature, and the orange precipitate was washed with cool ethanol (3 x 25 mL), distilled water (3 x 25 mL), ethanol (3 x 25 mL), and diethyl ether (3 x 25 mL). Then the solid was dried under reduced pressure to obtain the orange microcrystals ([Ru(η^5-C_5H_5)(PPh_3)$_2$Cl]) with a 63% yield (7.9 g). The filtered orange solution was kept in the freezer to crystalize. ^{1}H-NMR (400 MHz, $CDCl_3$) δ = 1.29, 1.60, 4.14 (–C_5**H**$_5$), 7.16 – 7.41 (–PPh_3). ^{31}P-NMR (161 MHz, $CDCl_3$) δ = 38.83 (**P**Ph_3) ppm.

The ruthenium complex was characterized by NMR, using ^{1}H and ^{31}P techniques. In Figure A7, the ^{1}H spectrum of the compound presents the expected spectrum of the metallocomplex, with the characteristics signals 1.29 (s), 1.60 (s), 4.14 (s), 7.16 (t), 7.60 (m), and 7.41 (t) ppm, suggesting that the synthesis was accomplished.

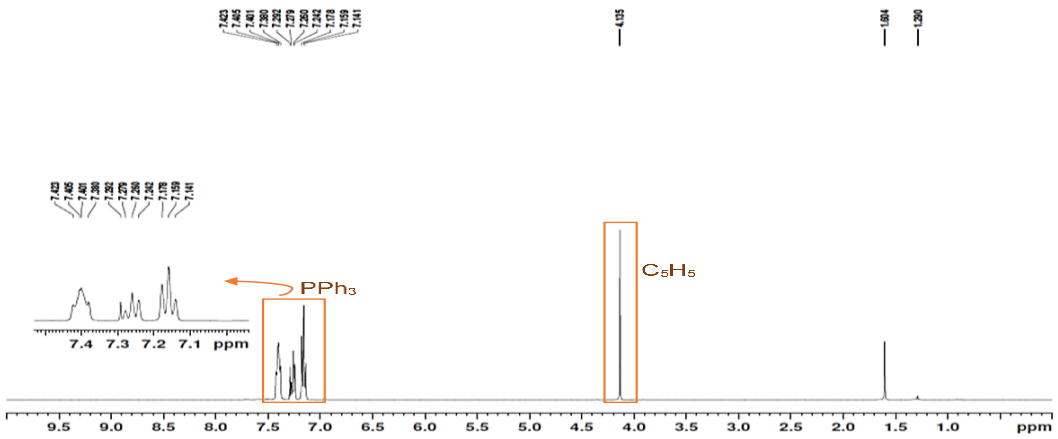

Figure A7. ^{1}H-NMR spectrum of the ruthenium metallocomplex [Ru(η^5-C_5H_5)(PPh_3)$_2$Cl] in $CDCl_3$.

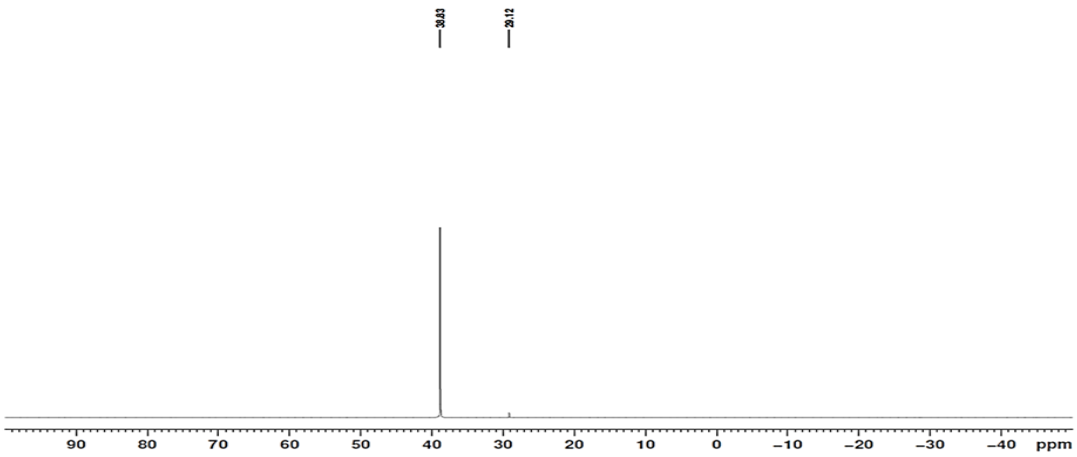

Figure A8. ^{31}P-NMR spectrum of the metallocomplex [Ru(η^5-C_5H_5)(PPh_3)$_2$Cl] in $CDCl_3$.

A.2. Characterization techniques

A.2.1. Nuclear Magnetic Resonance (NMR)

Nuclear Magnetic Resonance (NMR) spectroscopy was performed using a Bruker Avance II+ 400 equipment with a probe temperature at 4°C, 25°C and at 37°C. NMR spectra ^{1}H, ^{13}C, ^{31}P, and ^{195}Pt plots were obtained and treated using a Bruker® Topspin 3.6.1 software. Potassium tetrachloroplatinate(II) (K_2PtCl_4, Sigma-Aldrich) was used as an external reference for ^{195}Pt chemical shifts. The experiment carried out at 4°C, was used a liquid nitrogen circulator to cool down the probe and to maintain the low temperature.

A.2.2. Fourier Transformed Infrared (FT-IR)

Fourier Transform Infrared (FT-IR) spectroscopy was carried out with a Spectrum Two™ spectrometer from PerkinElmer through the normal NaCl cells or KBr pellets in the range of 400 - 4000 cm^{-1}.

A.2.3. Mass Spectrometry (MS)

Mass spectrometry (MS) analysis was obtained by a high-resolution mass spectrometer, with electrospray ionization technique, in positive or negative mode, by QTOF hybrid analyzer model MAXIS II from Bruker, and by a MALDI ionization technique with a ULTRAFLEX III TOF TOF equipment from Bruker. MS analyses were performed by the Mass Spectrometry Unit at Interdepartmental Investigation Service (SIdI), located at *Universidad Autónoma de Madrid* (Madrid, Spain).

A.2.4. Elemental Analysis (EA)

Elemental analyses were carried out by LECO-CHNS 932 equipment. EA analyses were performed by the Elemental Analysis Unit at Interdepartmental Investigation Service (SIdI), located at *Universidad Autónoma de Madrid* (Madrid, Spain).

A.2.5. Zeta Potential

Zeta potential was measured by Zetasizer Nano ZS (Malvern Instruments, UK) at 25 °C with disposable folded capillary cells (DTS1060C, Malvern).

A.2.6. UV-Vis spectroscopy

Ultraviolet-visible (UV-Vis) spectroscopy was recorded with a Cintra 40 UV−Vis spectrophotometer (GBC) or with a Lambda25 spectrophotometer from PerkinElmer. All measurements were performed with 1 cm path quartz cuvettes in a wavelength range of 190-800 nm.

A.2.7. Microplate reader

Cell viability and the luciferase activity were measured by a microplate reader (Synergy 2 Multi-Detection Microplate Reader, BioTek Instruments, Inc.) and by using a VICTOR^3 Multilabel from PerkinElmer.

A.2.8. Flow cytometry

Flow cytometry analysis was carried out by Flow Cytometer NovoCyte® 3000 + NovoSampler® Pro (ACEA Bioscience), with the acquisition of 10000 events per sample, and the collected data were treated with NovoExpress™ Flow Cytometer Software.

A.3. Chapter 2. New poly(alkylidenamine) dendrimers as a microbicide against HIV-1 infection

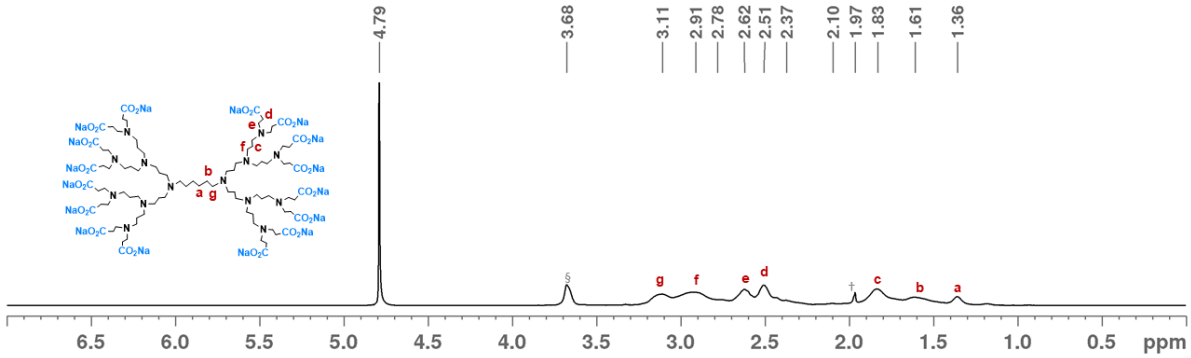

Figure A9. ^{1}H-NMR spectrum of the carboxylate dendrimer G2C in D_2O. (§ = diethyl ether, † = ethyl acetate).

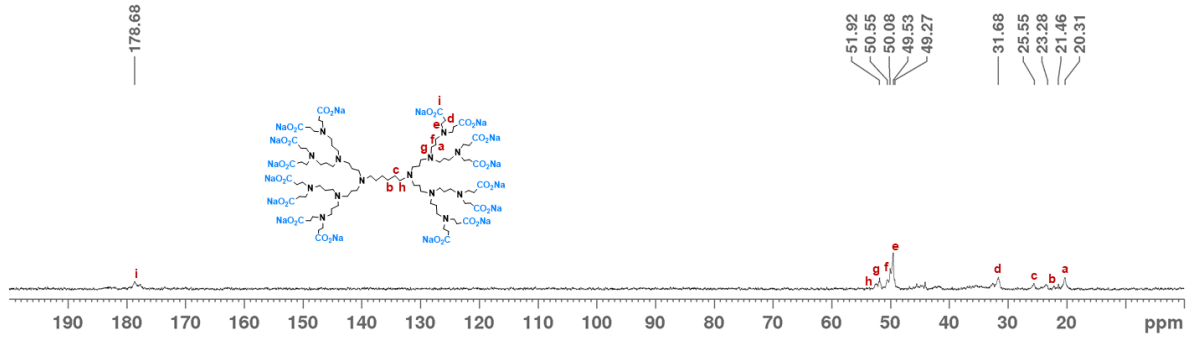

Figure A10. ^{13}C-NMR spectrum of the carboxylate dendrimer G2C in D_2O.

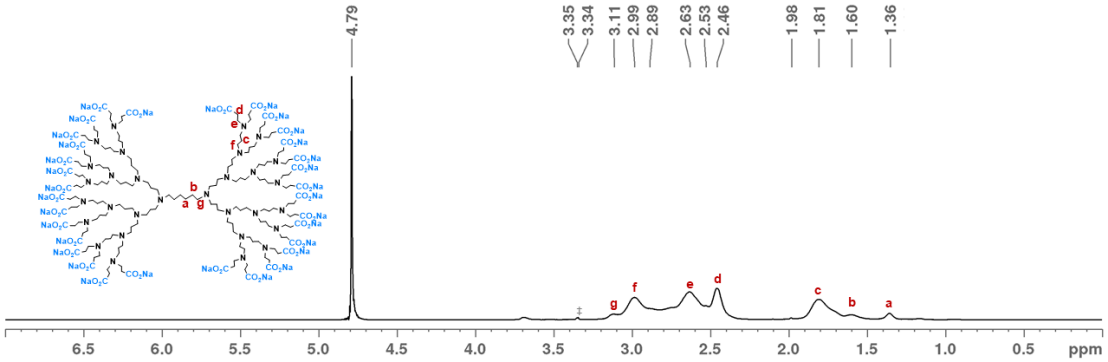

Figure A11. ^{1}H-NMR spectrum of the carboxylate dendrimer G3C in D_2O. (‡ = methanol).

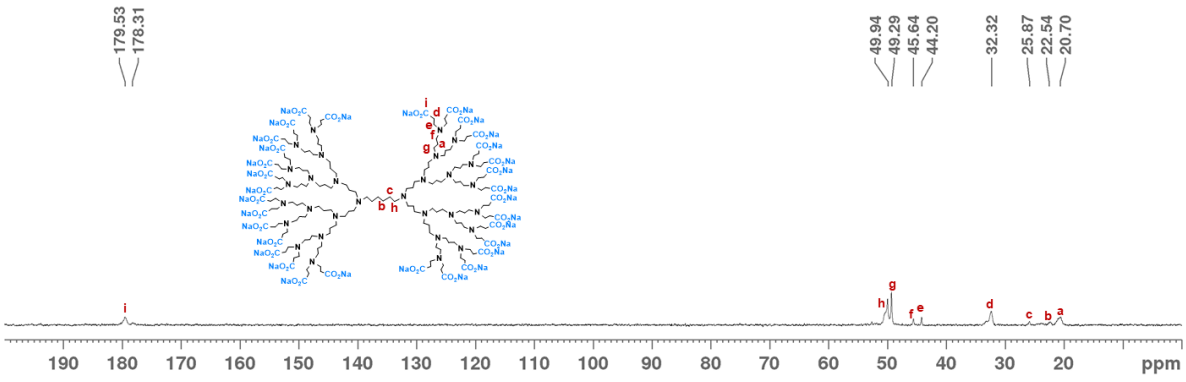

Figure A12. ^{13}C-NMR spectrum of the carboxylate dendrimer G3C in D_2O.

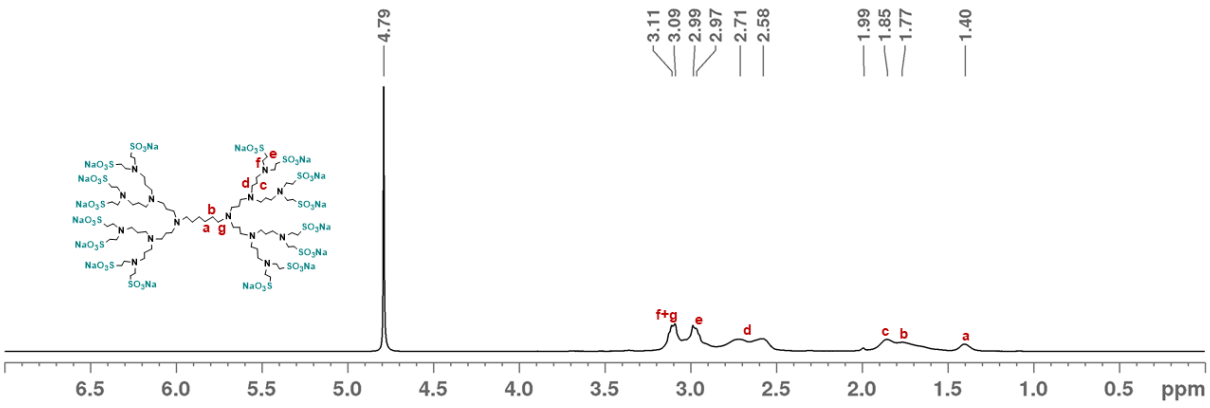

Figure A13. ^{1}H-NMR spectrum of the sulfonate dendrimer G2S in D_2O.

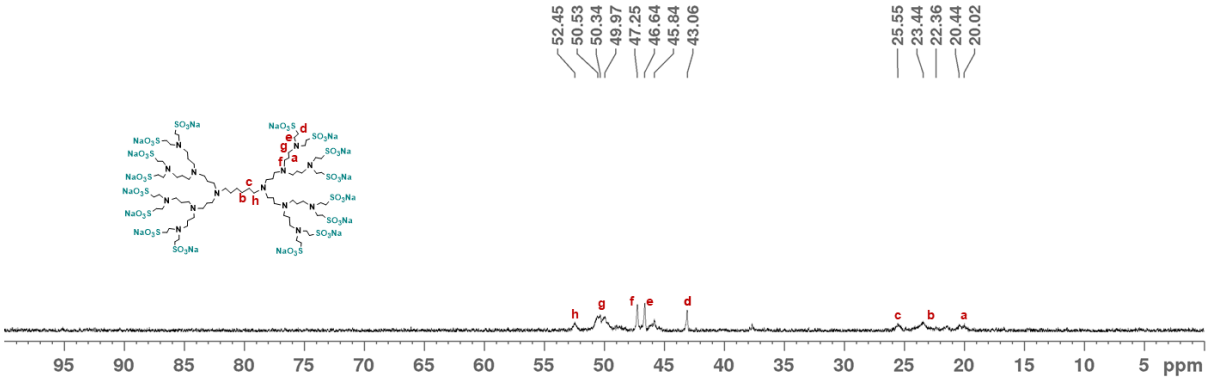

Figure A14. ^{13}C-NMR spectrum of the sulfonate dendrimer G2S in D_2O.

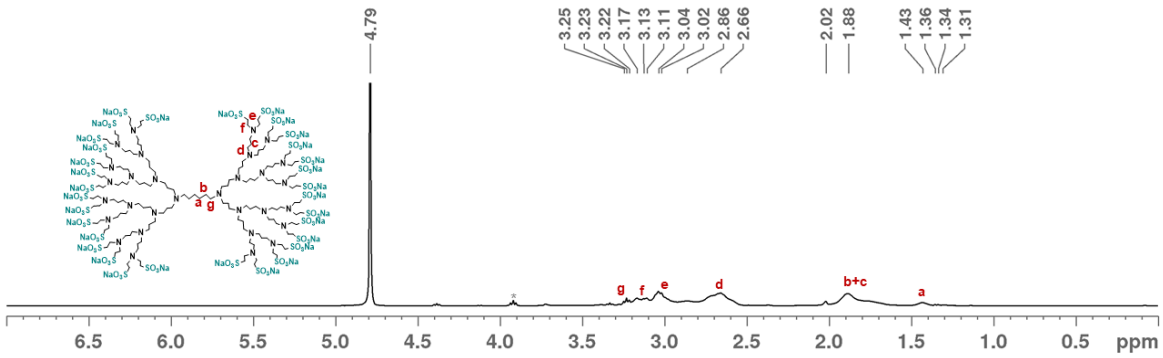

Figure A15. ^{1}H-NMR spectrum of the sulfonate dendrimer G3S in D_2O. (* = tetrahydrofuran).

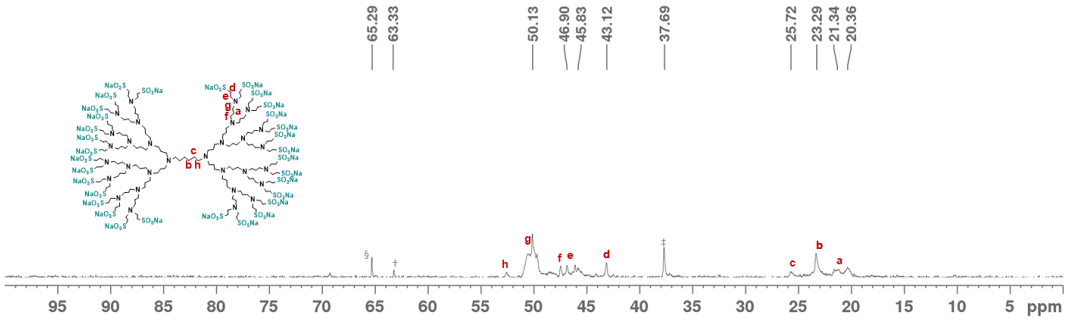

Figure A16. ^{13}C-NMR spectrum of the sulfonate dendrimer G3S in D_2O. (‡ = amine-terminated dendrimer, § = diethyl ether, † = ethyl acetate).

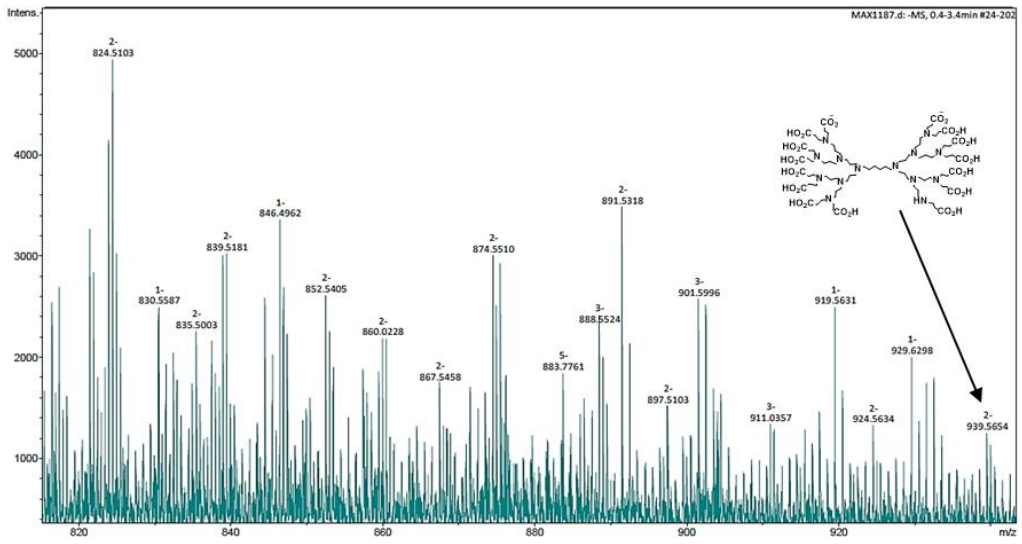

Figure A17. HRMS Q-TOF (ESI-) mass spectrum of the G2C dendrimer.

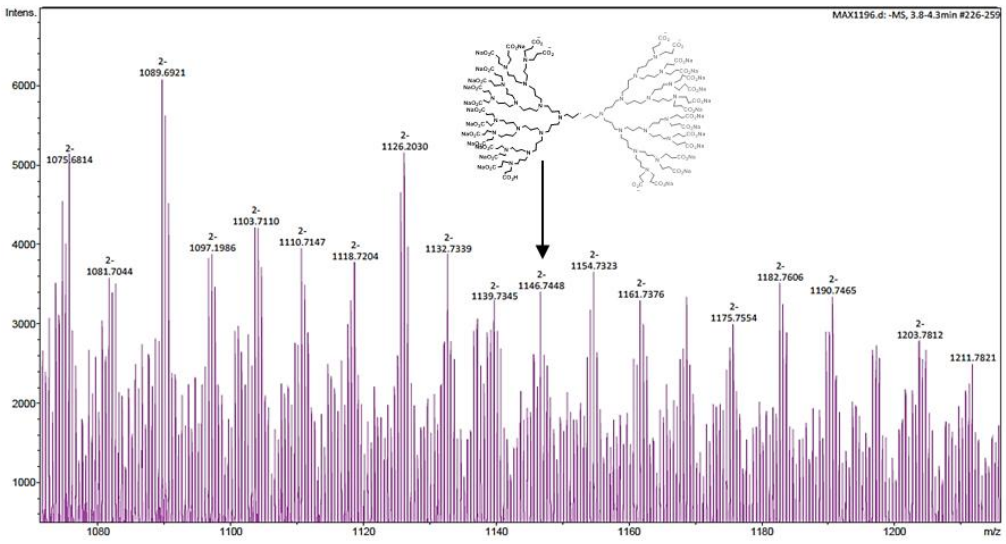

Figure A18. HRMS Q-TOF (ESI-) mass spectrum of the G3C dendrimer.

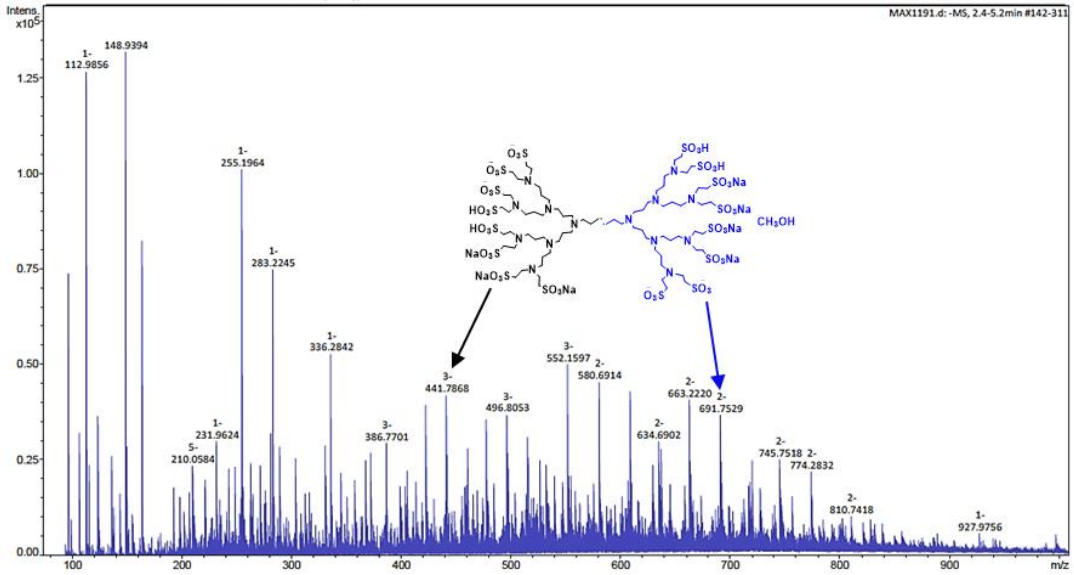

Figure A19. HRMS Q-TOF (ESI-) mass spectrum of the G2S dendrimer.

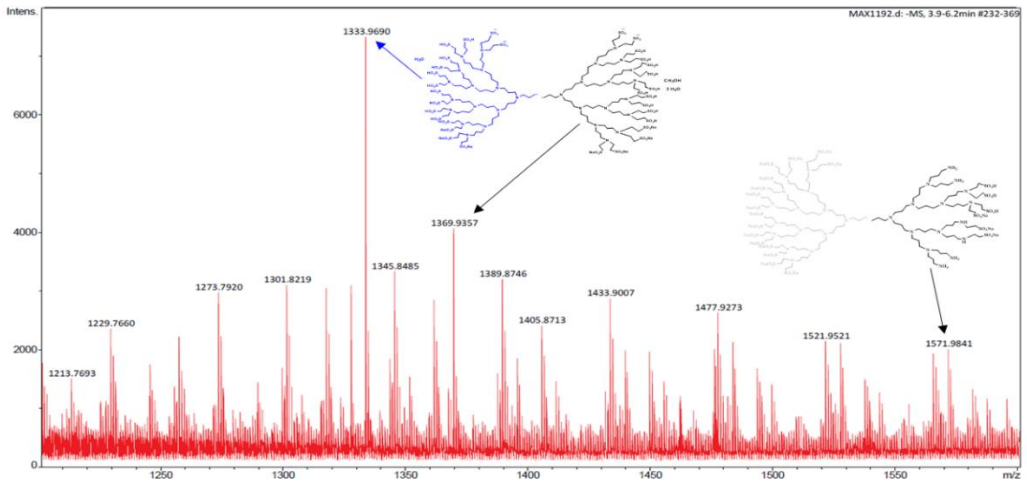

Figure A20. HRMS Q-TOF (ESI-) mass spectrum of the G3S dendrimer.

A.4. Chapter 3. The behavior of low generation dendrimers coordinated with [Ru(η5-C5H5)(PPh3)2]+ moieties against HIV-1 infection

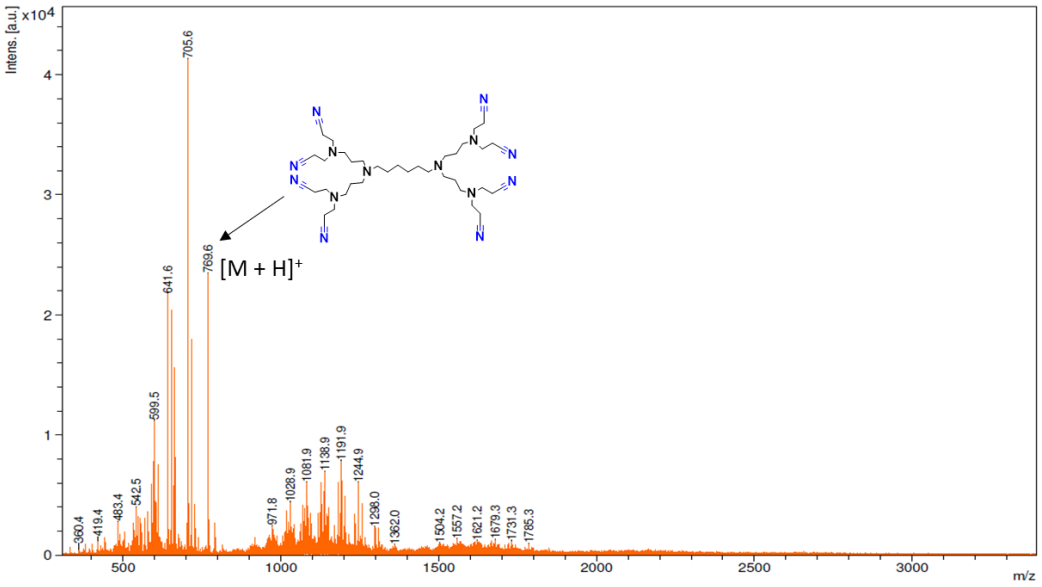

Figure A21. Mass spectrum of G1CN nitrile dendrimer.

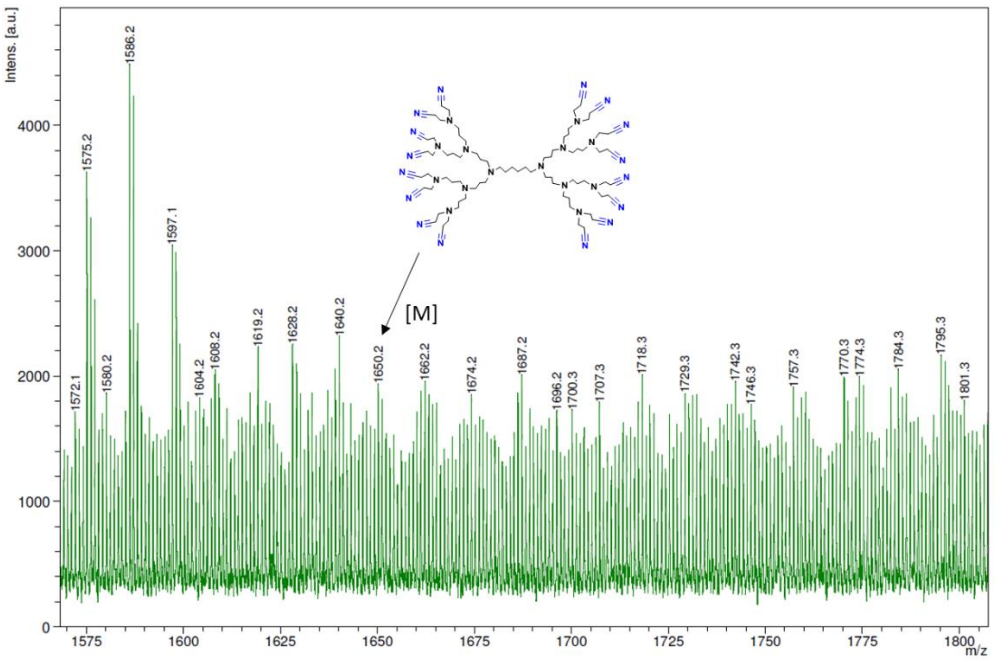

Figure A22. Mass spectrum of G2CN nitrile dendrimer.

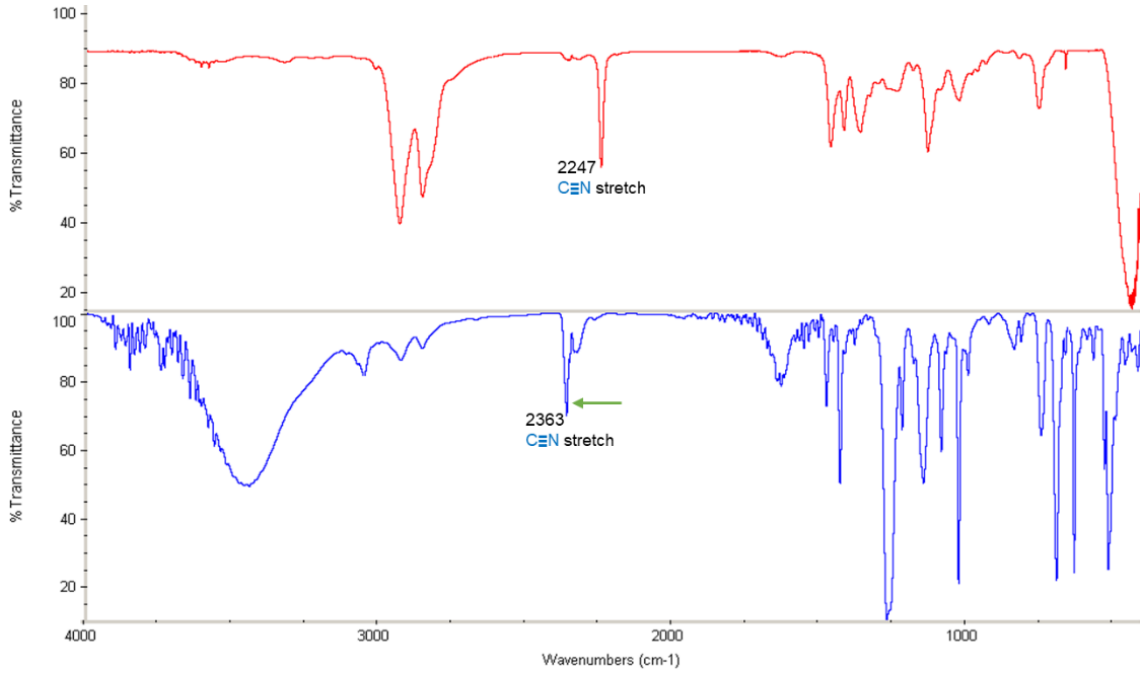

Figure A23. FT-IR spectra of the G0CN dendrimer (above) and G0Ru metallodendrimer (below). G0CN was performed using NaCl cells and G0Ru in KBr pellets.

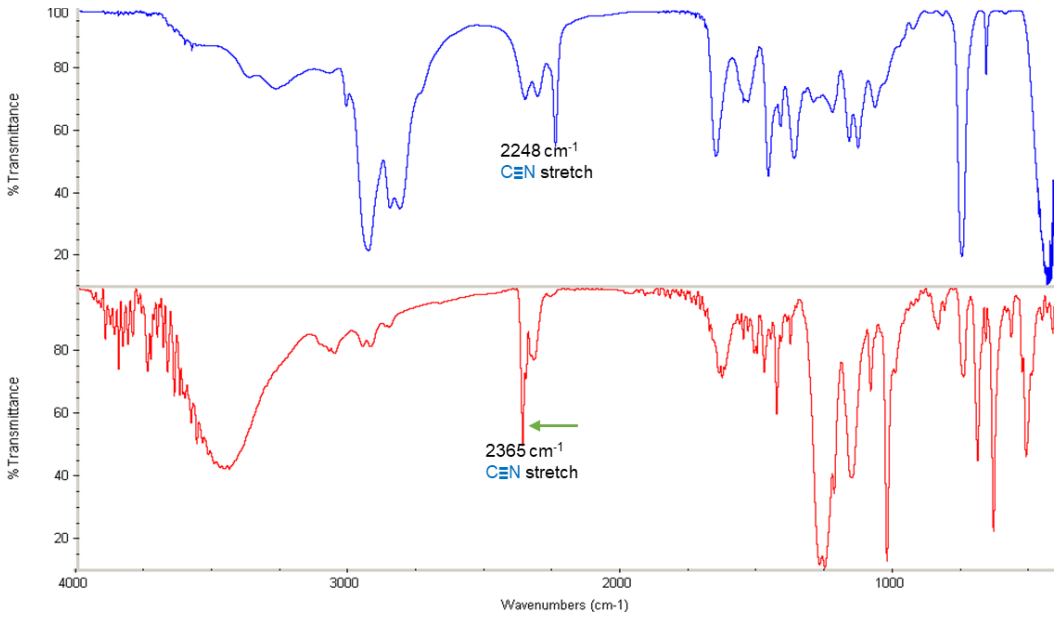

Figure A24. FT-IR spectra of the G1CN dendrimer (above) and G1Ru metallodendrimer (below). G1CN was performed in the NaCl cells and G1Ru in KBr pellets.

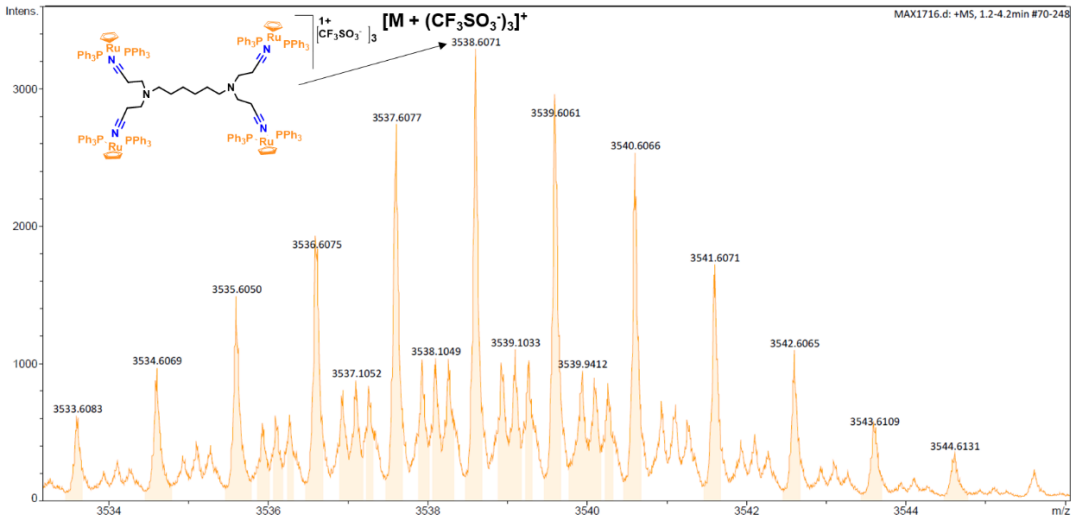

Figure A25. Mass spectrum of G0Ru metallodendrimer.

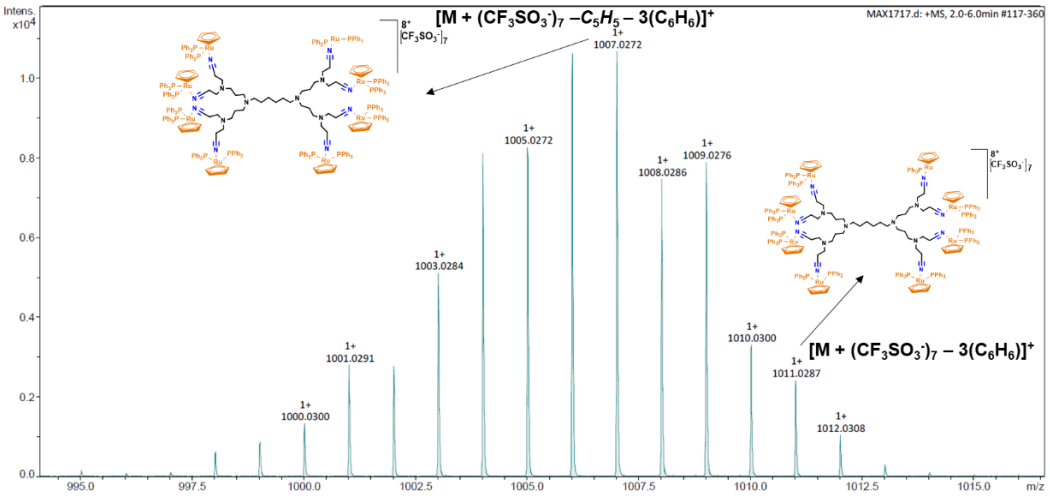

Figure A26. Mass spectrum of G1Ru metallodendrimer.

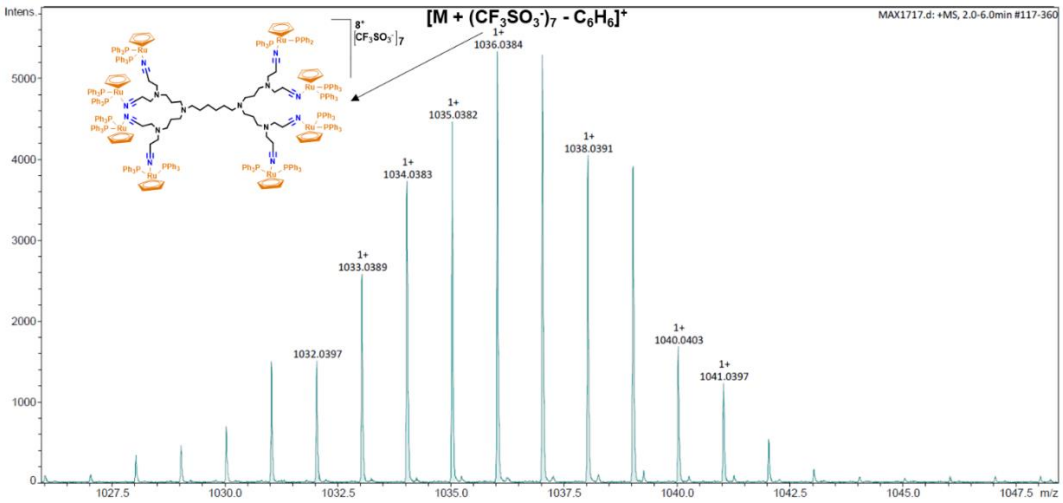

Figure A27. Mass spectrum of G1Ru metallodendrimer.

A.5. Chapter 4. Ruthenium-based metallodendrimers as promising anticancer drugs

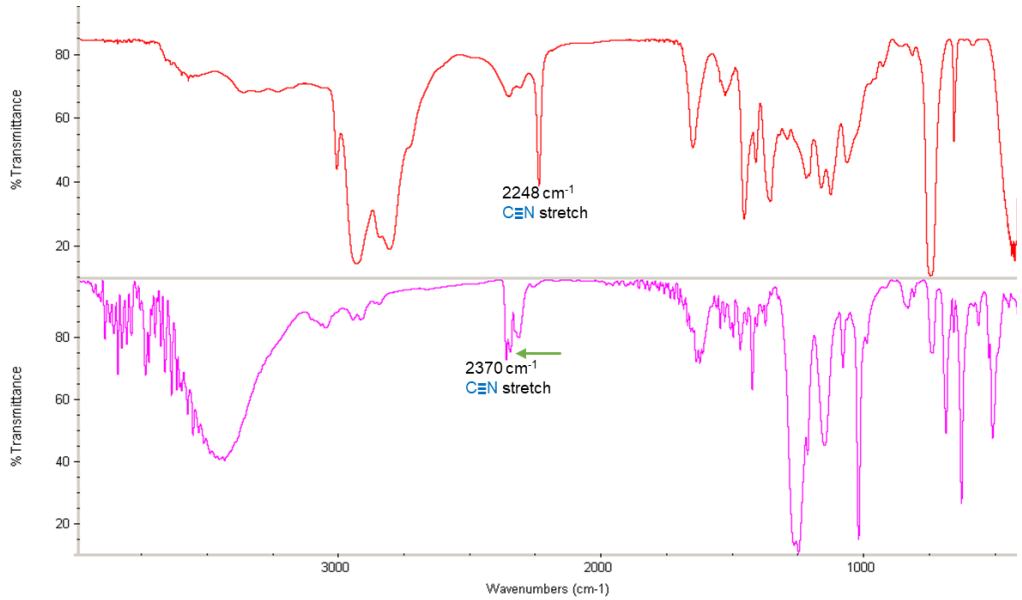

Figure A28. FT-IR spectra of the G2CN dendrimer (above) and G2Ru metallodendrimer (below). G2CN was performed in the NaCl cells and G2Ru in KBr pellets.

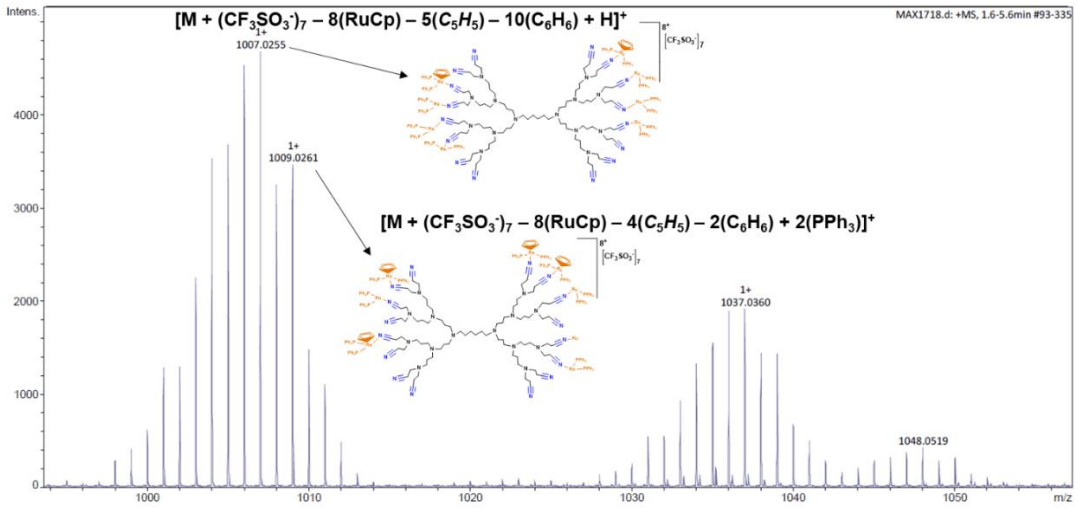

Figure A29. Mass spectrum of G2Ru metallodendrimer.

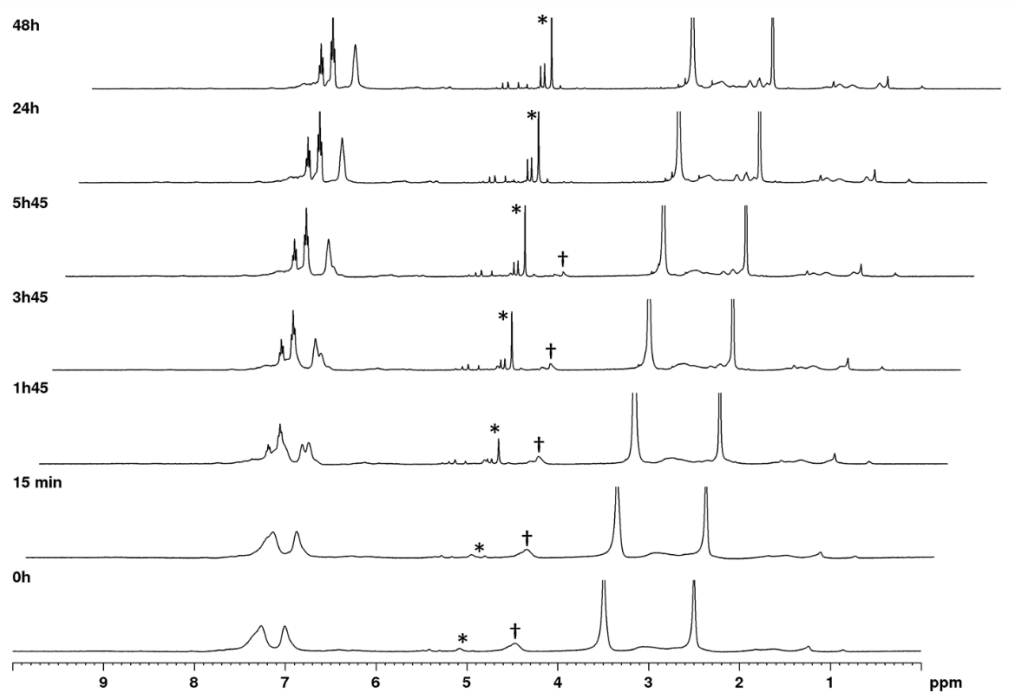

Figure A30. ^{1}H-NMR spectra of generation 1 of the ruthenium metallodendrimer. Stability studies were performed in DMSO-*d6* (probe temperature: 25ºC), and the dendrimer's solutions were kept at 25ºC along time. † = cyclopentadienyl signal of the metallodendrimer, * = cyclopentadienyl signal of the RuCp complex.

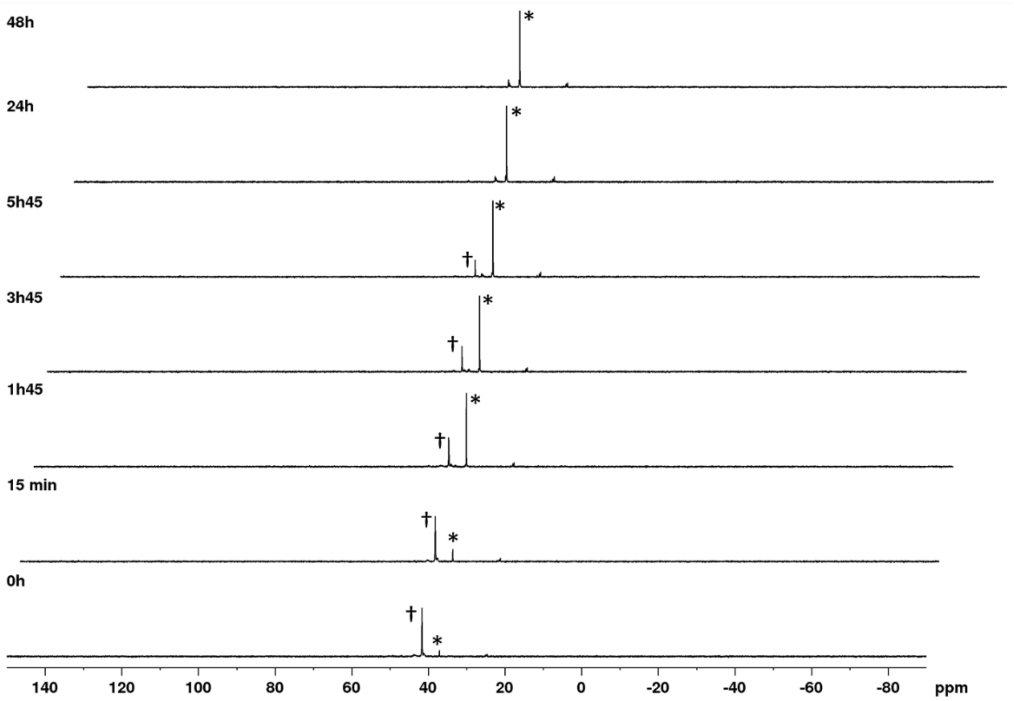

Figure A31. ^{31}P-NMR spectra of generation 1 of the ruthenium metallodendrimer. Stability studies were performed in DMSO-*d6* (probe temperature: 25ºC), and the dendrimer's solutions were kept at 25ºC along time. † = phosphines signal of the metallodendrimer, * = phosphines signal of the RuCp complex.

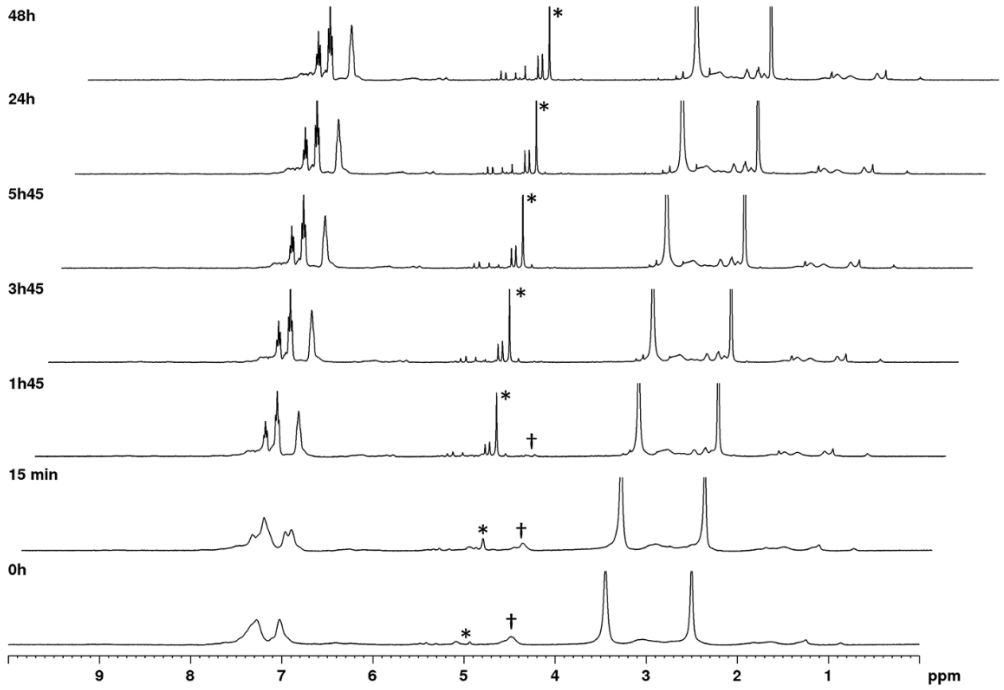

Figure A32. ^{1}H-NMR spectra of generation 1 of the ruthenium metallodendrimer. Stability studies were performed in DMSO-*d6* (probe temperature: 37ºC), and the dendrimer's solutions were kept at 37ºC along time. † = cyclopentadienyl signal of the metallodendrimer, * = cyclopentadienyl signal of the RuCp complex.

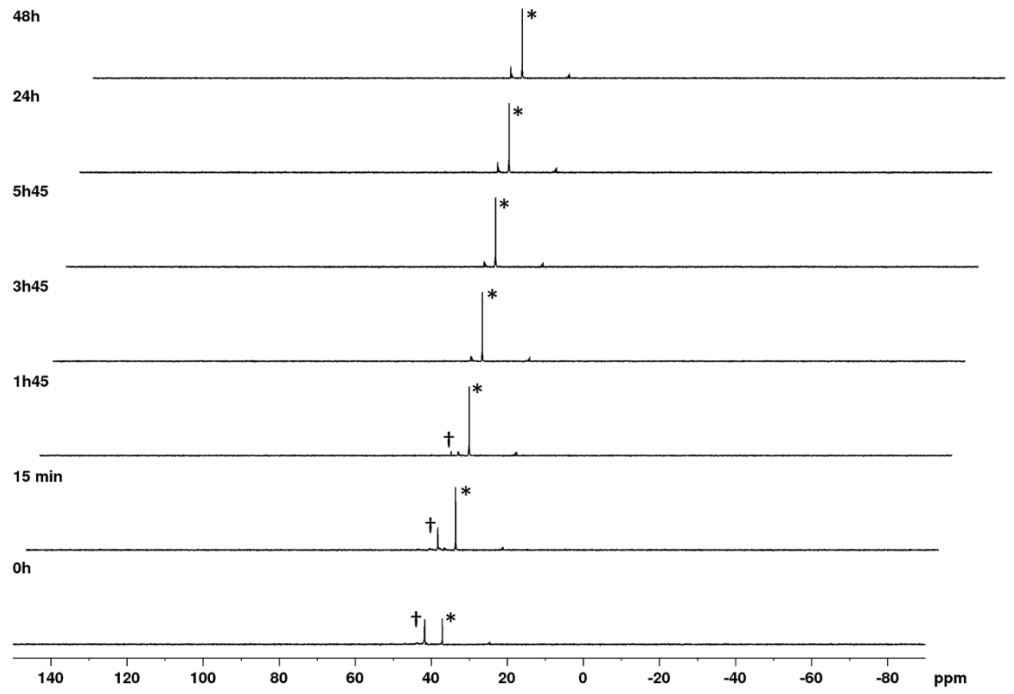

Figure A33. ^{31}P-NMR spectra of generation 1 of the ruthenium metallodendrimer. Stability studies were performed in DMSO-*d6* (probe temperature: 37ºC), and the dendrimer's solutions were kept at 37ºC along time. † = phosphines signal of the metallodendrimer, * = phosphines signal of the RuCp complex.

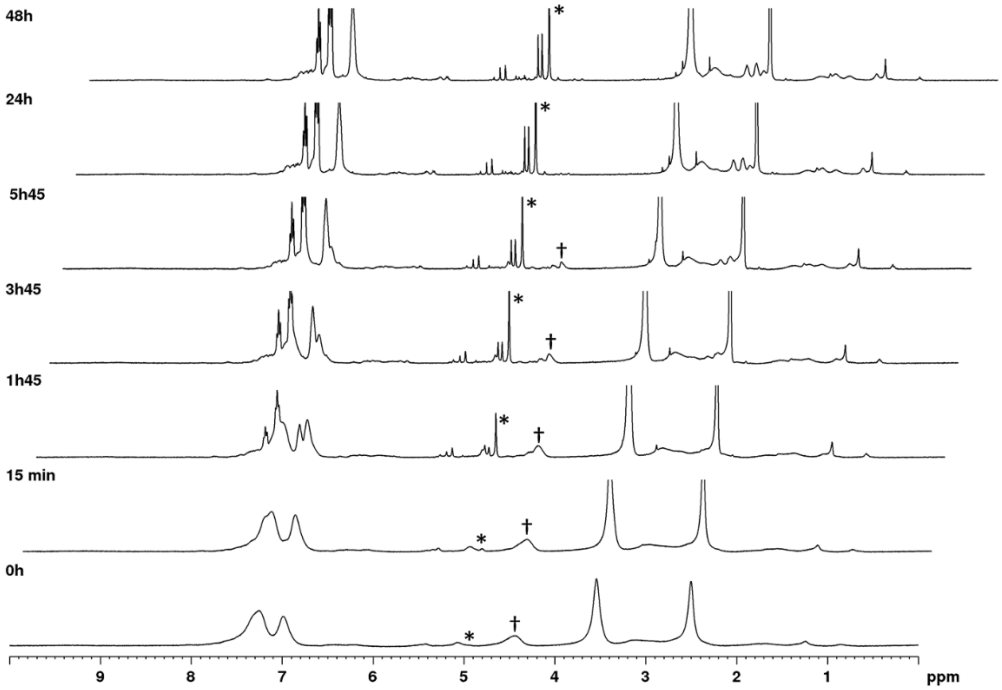

Figure A34. ^{1}H-NMR spectra of generation 2 of the ruthenium metallodendrimer. Stability studies were performed in DMSO-*d6* (probe temperature: 25ºC), and the dendrimer's solutions were kept at 25ºC along time. † = cyclopentadienyl signal of the metallodendrimer, * = cyclopentadienyl signal of the RuCp complex.

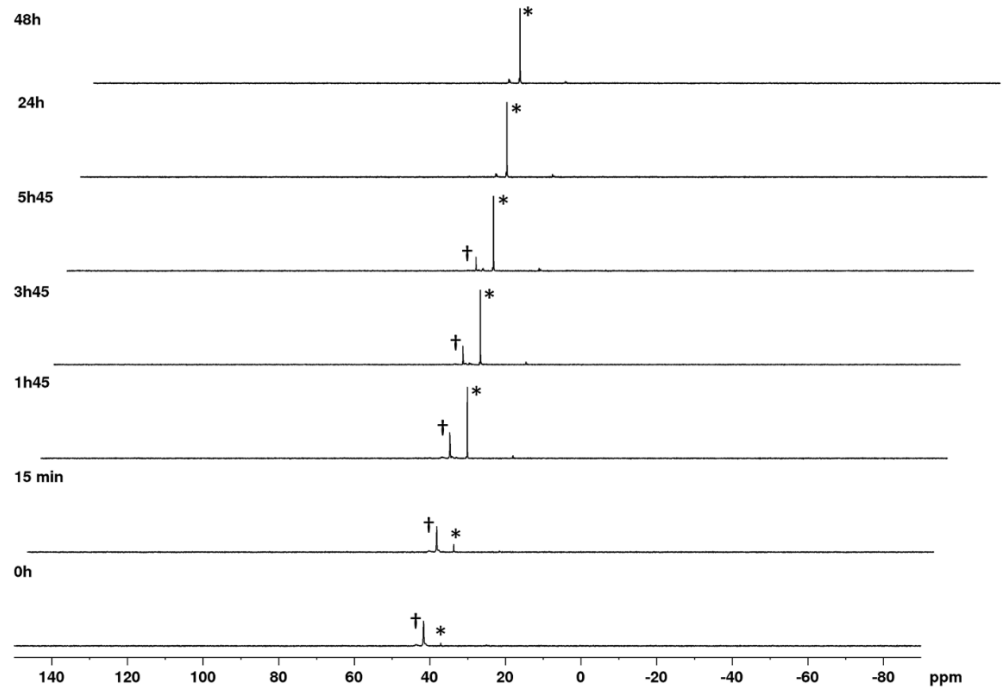

Figure A35. ^{31}P-NMR spectra of generation 2 of the ruthenium metallodendrimer. Stability studies were performed in DMSO-*d6* (probe temperature: 25ºC), and the dendrimer's solutions were kept at 25ºC along time. † = phosphines signal of the metallodendrimer, * = phosphines signal of the RuCp complex.

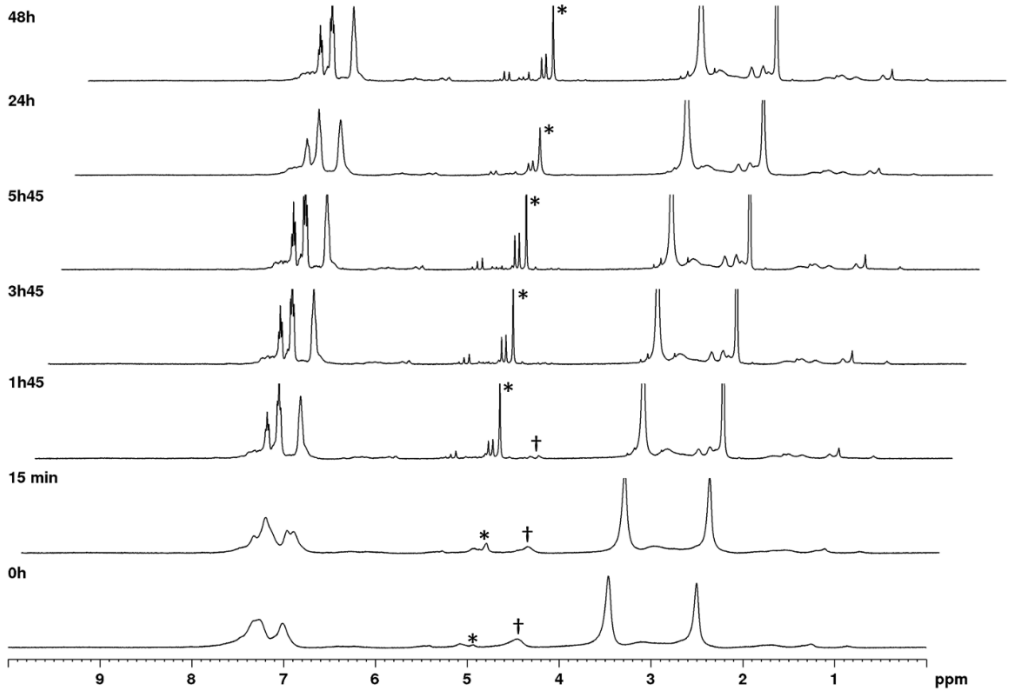

Figure A36. ^{1}H-NMR spectra of generation 2 of the ruthenium metallodendrimer. Stability studies were performed in DMSO-*d6* (probe temperature: 37ºC), and the dendrimer's solutions were kept at 37ºC along time. † = cyclopentadienyl signal of the metallodendrimer, * = cyclopentadienyl signal of the RuCp complex.

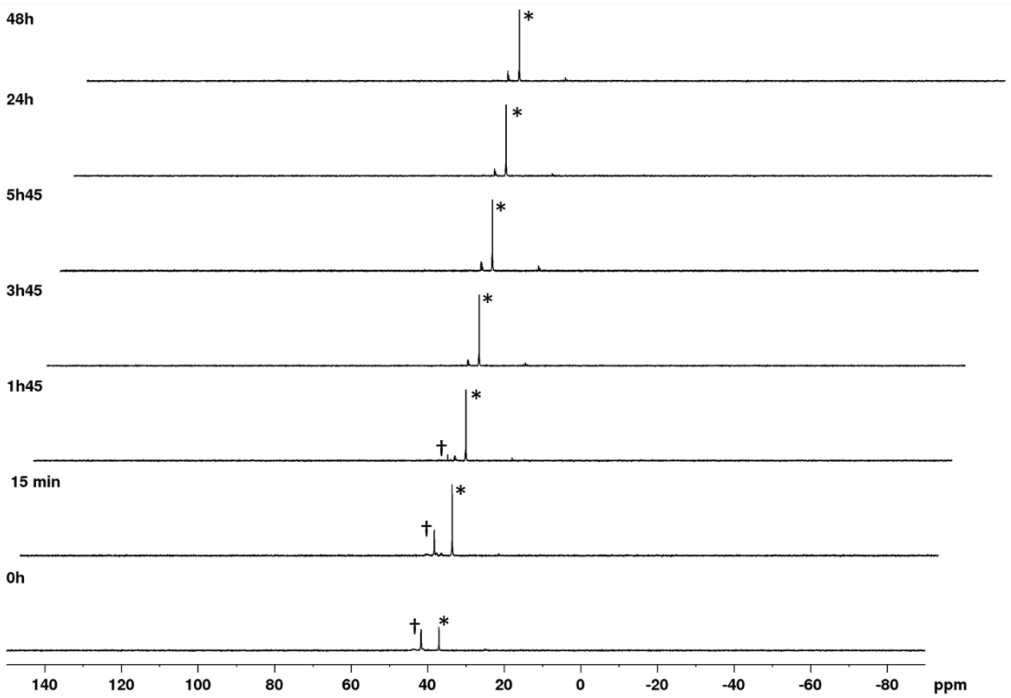

Figure A37. ^{31}P-NMR spectra of generation 2 of the ruthenium metallodendrimer. Stability studies were performed in DMSO-*d6* (probe temperature: 37ºC), and the dendrimer's solutions were kept at 37ºC along time. † = phosphines signal of the metallodendrimer, * = phosphines signal of the RuCp complex.

A.6. Chapter 4. Novel poly(alkylidenamine) dendrimers functionalized with *cisplatin* as anticancer prodrugs

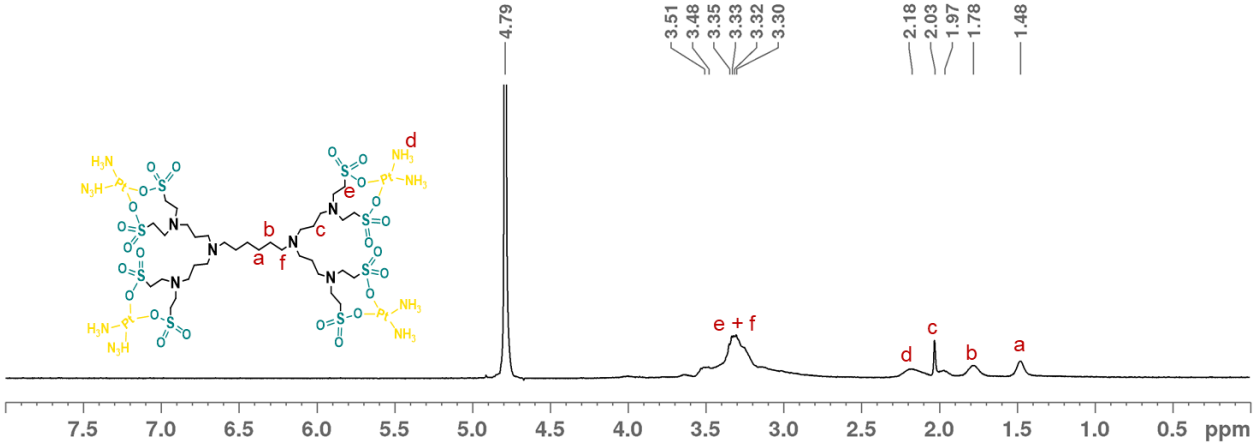

Figure A38. ^{1}H-NMR spectrum of generation 1 of the sulfonate platinum metallodendrimer performed in D_2O.

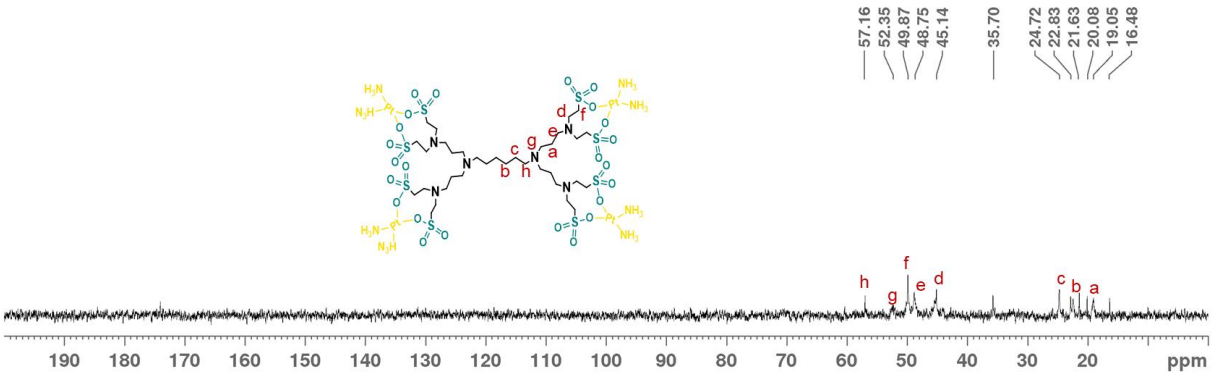

Figure A39. ^{13}C-NMR spectrum of generation 1 of the sulfonate platinum (G1SPt) metallodendrimer performed in D_2O.

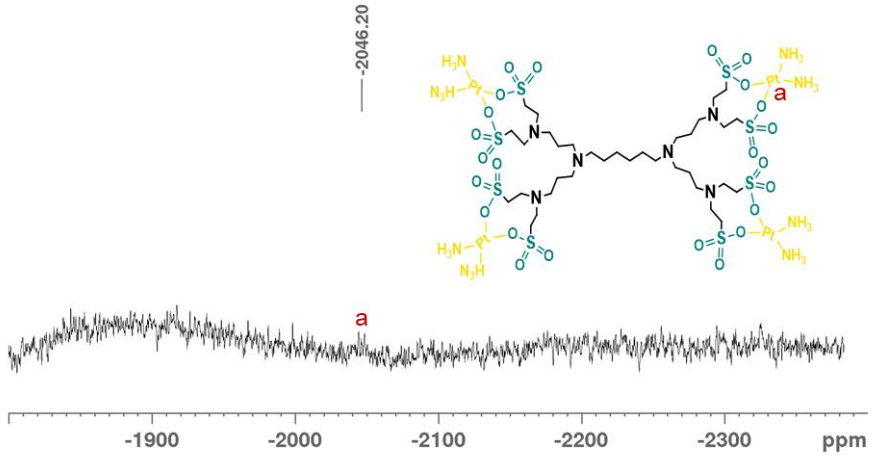

Figure A40. ^{195}Pt-NMR spectrum of generation 1 of the sulfonate platinum metallodendrimer (G1SPt) performed in D_2O with K_2PtCl_4 as an external reference

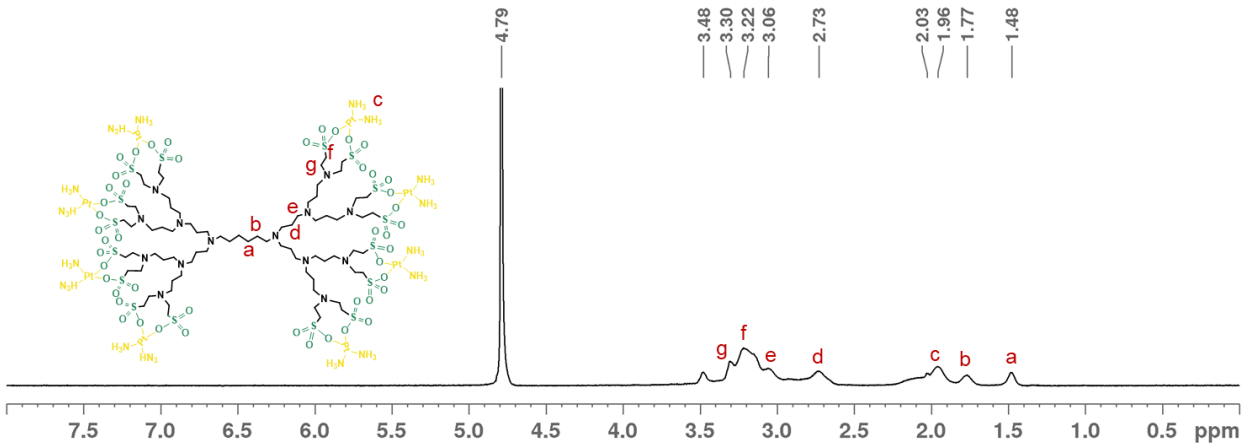

Figure A41. ^{1}H-NMR spectrum of generation 2 of the sulfonate platinum metallodendrimer (G2SPt) performed in D_2O.

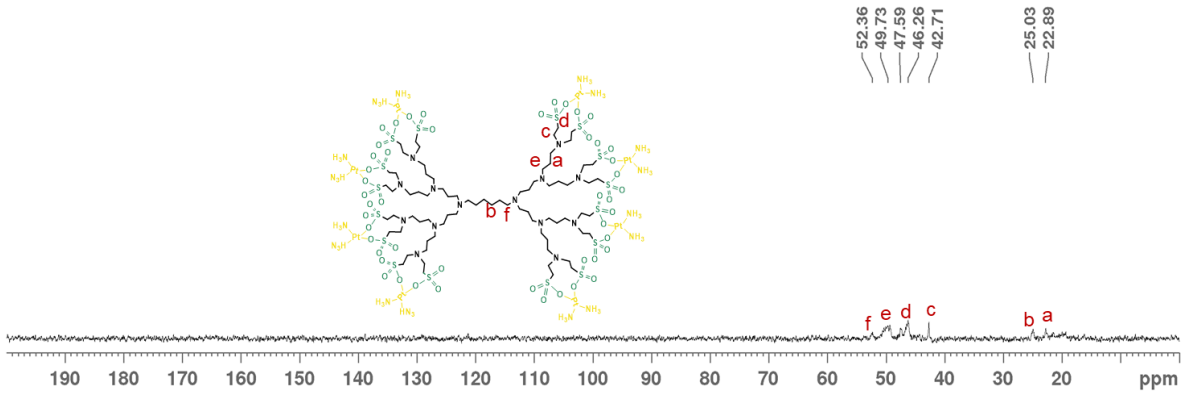

Figure A42. ^{13}C-NMR spectrum of generation 2 of the sulfonate platinum (G2SPt) metallodendrimer performed in D_2O.

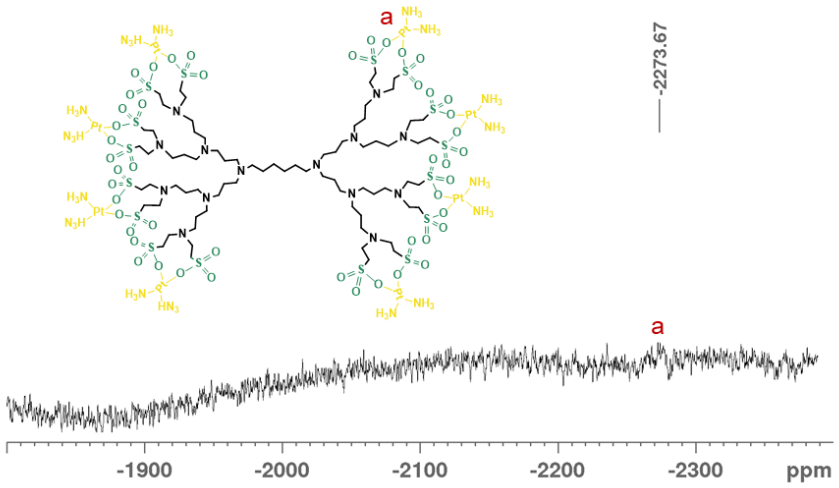

Figure A43. ^{195}Pt-NMR spectrum of generation 2 of the sulfonate platinum metallodendrimer (G2SPt) performed in D_2O with K_2PtCl_4 as an external reference.

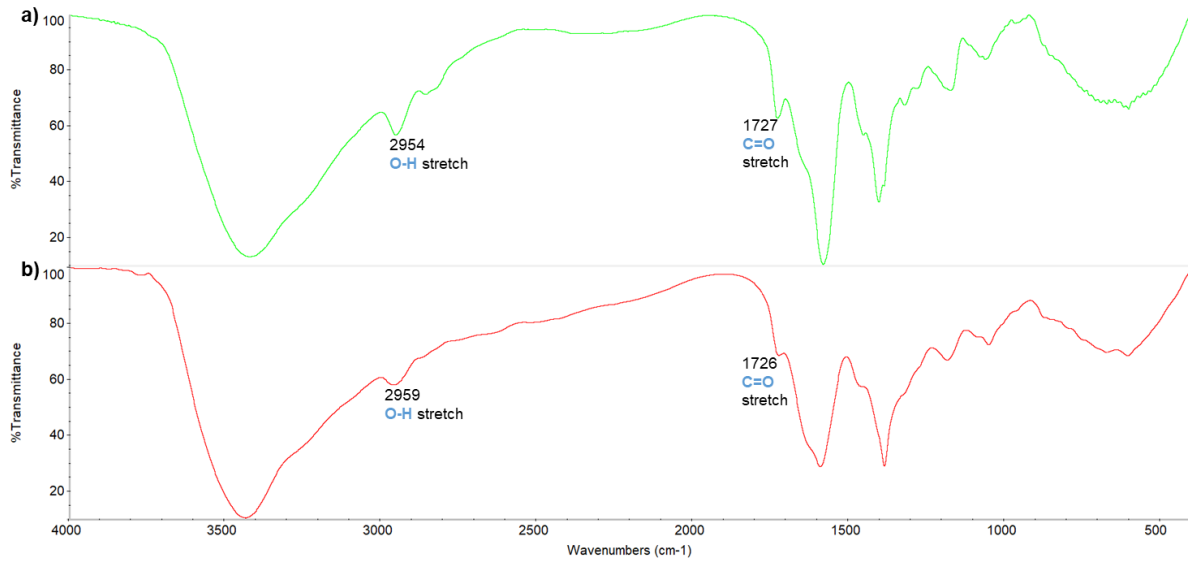

Figure A44. FT-IR spectra of the a) G2C carboxylate dendrimer and b) G2CPt metallodendrimer. The sample preparation was done using KBr pellets.

Figure A45. FT-IR spectra of the a) G2S carboxylate dendrimer and b) G2SPt metallodendrimer. The sample preparation was done using KBr pellets.

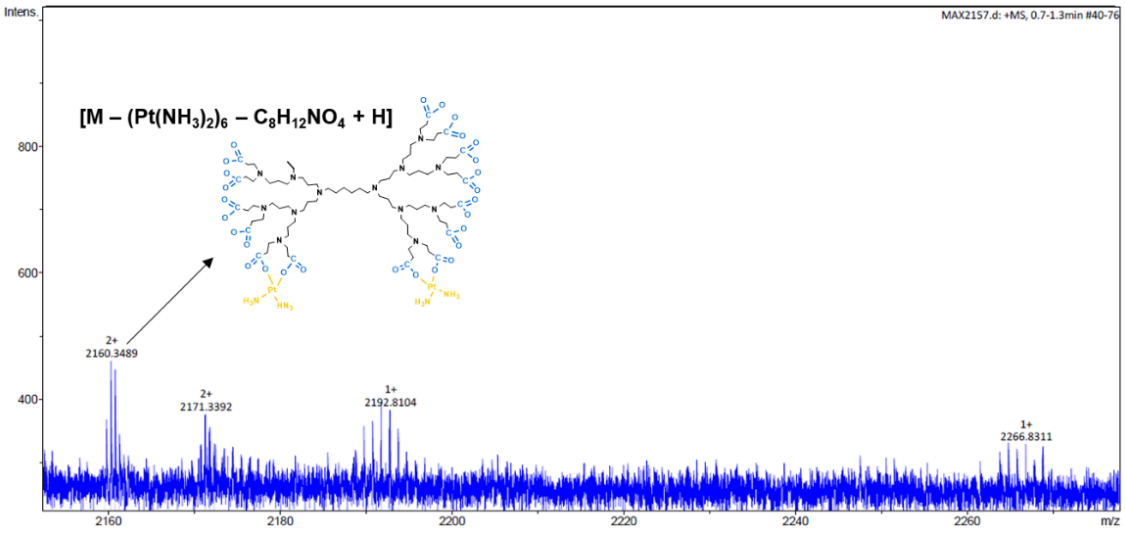

Figure A46. Mass spectrum of G2CPt metallodendrimer.

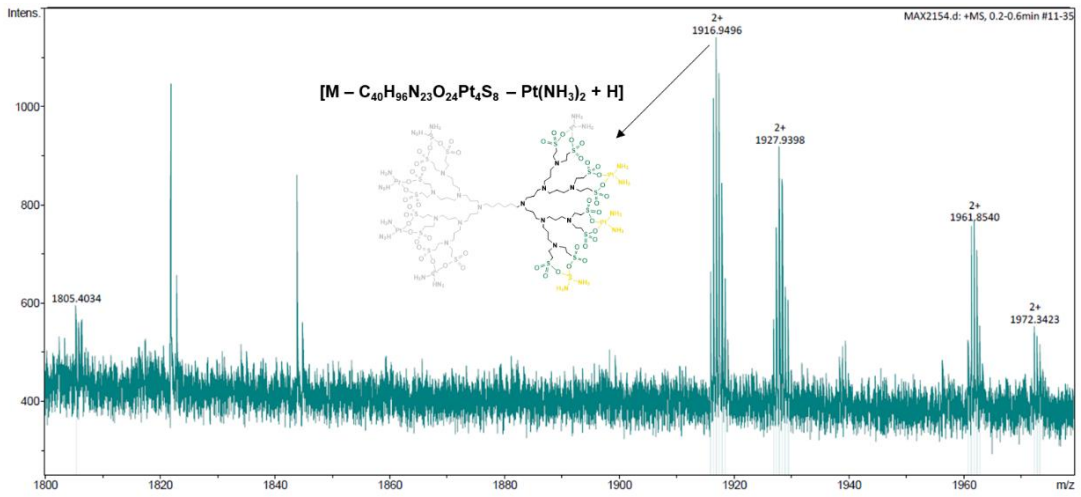

Figure A47. Mass spectrum of G2SPt metallodendrimer.

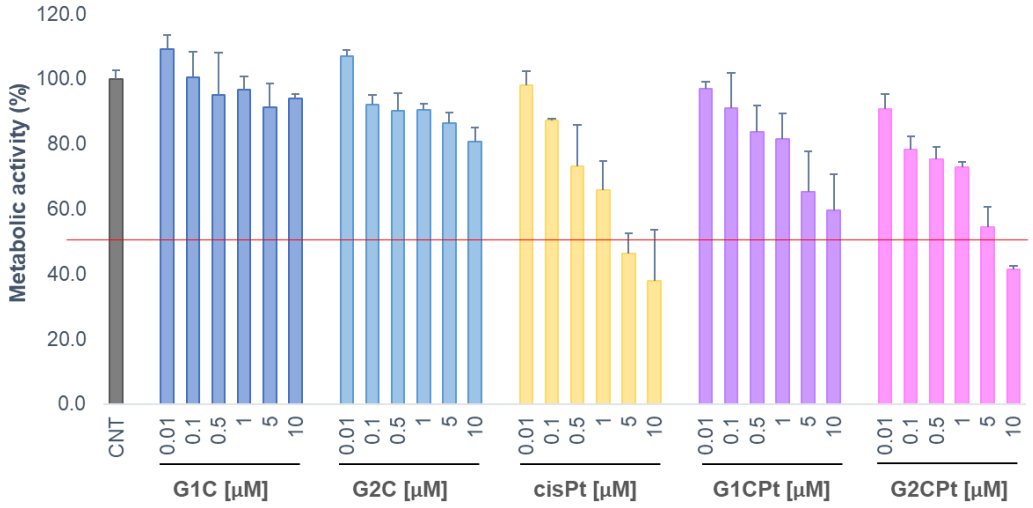

Figure A48. Viability studies of metallodendrimers on MCF-7 cells. Cells were treated for 72 h with a concentration range of 0.01 µM to 10 µM of the carboxylate dendrimers (G1C and G2C), cisplatin (cisPt), and the metallodendrimers (G1CPt and G2CPt). The metabolic activity is represented against the control. Data are represented as mean ± SD of one independent experiment performed in triplicate.

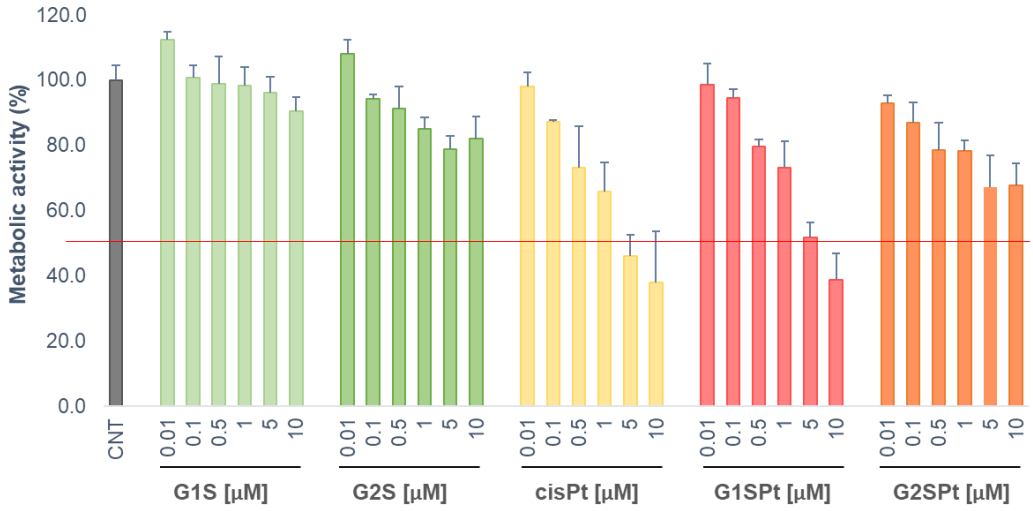

Figure A49. Viability studies of metallodendrimers on MCF-7 cells. Cells were treated for 72 h with a concentration range of 0.01 µM to 10 µM of the sulfonate dendrimers (G1S and G2S), cisplatin (cisPt), and the metallodendrimers (G1SPt and G2SPt). The metabolic activity is represented against the control. Data are represented as mean ± SD of one independent experiment performed in triplicate.

This thesis was written using Microsoft Word Office 365, font Arial (font size 28, 26, 12, 11, 10.5, and 9), generally with line spacing of 1.5 lines. For data process and treatment were also used the following software from Microsoft Office 365: Excel (data and graph processing), PowerPoint (images process and processing), ChemDraw Professional 15.0 (images and structures drawing), Topspin® 3.6.1 (software for NMR data processing from BRUKER), OMNIC™ (software for FT-IR data processing), Microsoft Paint version 1903 (images drawing), GraphPad Prism v.5.0 software (statistics and data processing), Mendeley version 1.19 (references).

FCT Fundação para a Ciência e a Tecnologia
MINISTÉRIO DA CIÊNCIA, TECNOLOGIA E ENSINO SUPERIOR

PhD Grant SFRH/BD/102123/2014 (DM)
CQM Strategic Projects: UID/QUI/00674/2013, UID/QUI/00674/2015, UID/QUI/00674/2019
CQM Base Fund - UIDB/00674/2020
Programmatic Fund - UIDP/00674/2020

PROEQUIPRAM (M1420-01-0145-FEDER-000008)
M1420-01-0145-FEDER-000005 - CQM+
(Madeira 14-20 Program)

CYTED 214RT0482

Cofinanciado por:

A Nossa Universidade

Colégio dos Jesuítas
Rua dos Ferreiros - 9000-082, Funchal

Tel: +351 291 209400
Fax: +351 291 209410
Email: gabinetedareitoria@uma.pt